BAW-10154P
November 1982

B&W's SMALL-BREAK LOCA ECCS EVALUATION MODEL

B&W PROPRIETARY

Please Send Copy of XA to PDR

XA

Babcock & Wilcox
a McDermott company

Copy No. 044

BAW-10154P
Topical Report
November 1982

B&W's SMALL-BREAK LOCA ECCS EVALUATION MODEL

by

N. K. Savani
J. R. Paljug
R. J. Schomaker

BABCOCK & WILCOX
Power Generation Group
Utility Power Generation Division
P. O. Box 1260
Lynchburg, Virginia 24505

ACKNOWLEDGMENTS

The authors wish to credit the production of this report to a number of other individuals who participated in creating the material and concepts. The work of J. C. Seals, M. Bostoni, P. T. Poole, D. J. Roesch, L. K. Nicholson, M. R. Eberl, M. Ferguson, J. H. Arthur, D. Mulvihill, and C. Ogureck is acknowledged. Recognition is also accorded to R. C. Jones, whose work forms an integral portion of this report.

The authors also acknowledge the contributions and cooperation of members of Computer Services, Analysis Technology, Technical Reports, and Central Reproduction.

Babcock & Wilcox
Utility Power Generation Division
Lynchburg, Virginia

Topical Report BAW-10154
November 1982

B&W's Small-Break LOCA ECCS Evaluation Model

N. K. Savani, J. R. Paljug, R. J. Schomaker

Key Words: ECCS, LOCA, Model, CRAFT, REFLOOD, THETA, CONTEMPT, QUENCH, FOAM

ABSTRACT

The generic model for evaluating the performance of emergency core cooling systems following a small-break loss-of-coolant accident for all B&W nuclear steam systems is developed and compared with the required and acceptable features contained in Appendix K of the Code of Federal Regulations, Part 50 (10 CFR 50). This report describes the small-break evaluation model as it has been modified with regard to Item II.K.3.30 of NUREG-0737, and demonstrates that it conforms to Appendix K.

CONTENTS

		Page
1.	INTRODUCTION	1-1
2.	BACKGROUND	2-1
3.	OVERVIEW OF 10 CFR 50.46	3-1
4.	DEFINITION OF MODEL	4-1
5.	SMALL BREAK EVALUATION MODEL	5-1
	5.1. Model Applicability	5-1
	5.2. Code Relationships	5-2
	5.3. Evaluation Model Features	5-3
	5.3.1. Heat Sources	5-3
	5.3.2. Reactor System Hydrodynamics	5-5
	5.3.3. Heat Transfer and Thermal Analysis	5-9
	5.3.4. Cladding Rupture	5-10
	5.4. Compliance	5-12
	5.5. Response to Requirements of NUREG-0737, Section II.K.3.30	5-16
	5.5.1. Concerns in NUREG-0565	5-16
	5.5.2. Concerns in NUREG-0623	5-22
	5.5.3. Concern Raised at December 16, 1980, Meeting	5-23
	5.6. Summary and Conclusions	5-23
6.	MAXIMUM HYDROGEN GENERATION, COOLABLE GEOMETRY, AND LONG-TERM COOLING	6-1
	6.1. Maximum Hydrogen Generation	6-1
	6.2. Coolable Geometry	6-1
	6.3. Long-Term Cooling	6-1
	6.4. Boric Acid Concentration	6-2
7.	REQUIRED DOCUMENTATION	7-1
8.	REFERENCES	8-1
	APPENDIXES	
	A – Comparison of SB Core Heat Transfer Model to ORNL SBLOCA Heat Transfer Tests	A-1
	B – Leak Discharge Model	B-1
	C – Surge Line Modeling	C-1
	D – Evaluation and Justification of the B&W ECCS Injection Model	D-1

CONTENTS (Cont'd)

Page

E – Noding Sensitivity Studies for 177-FA Lowered-Loop Plants E-1
F – Noding Sensitivity Studies for 177-FA Raised-Loop Plants F-1
G – B&W's Natural Circulation Test Prediction of Semiscale Test S-NC-2 . . . . . G-1
H – B&W's Plant Prediction H-1
I – Noding Sensitivity Studies for 205-FA Plants . . . . . Later*

List of Tables

Table

1-1 Category Classifications 1-2
A-1. Results of FOAM Analysis A-8
A-2. Results of ORNL Analysis A-9
A-3. Comparison of FOAM to ORNL A-10
B-1. Flow Rates Vs Time of CFT Actuation and Minimum Core Mixture Level B-17
D-1. Control Volume Size Study D-10
E-1. Sequence of Events for Previous SBLOCA Analysis E-11
E-2. Sequence of Events for Upgraded SBLOCA Analysis E-12
E-3. SBLOCA Event Sequence and Timing Predicted by Revised Base Case and Detailed Hot Leg Models E-12
F-1. Comparison of Key Events in Former and New Models F-11
F-2. Comparison of Key Events in Single-Node and Four-Node Hot Leg Models F-11
G-1. Nodal Description G-13
H-1. Summary of Natural Circulation Tests H-13
H-2. Node and Path Identification, CRAFT2 Model H-14

List of Figures

Figure

5-1. Small Break Analysis Code Interface 5-24
A-1. Partial Assembly A-11
A-2. Classification of THTF Bundle 3 Fuel Rod Simulators A-12
A-3. Fuel Rod Elevation Diagram for ORNL Test A-13
A-4. Test C A-14
A-5. Test D A-15
A-6. Test E A-16
A-7. Test F A-17
A-8. Test G A-18

*To be supplied December 1, 1982.

Figures (Cont'd)

Figure		Page
A-9.	Test H	A-19
A-10.	Radiation HTC to Degree of Superheat	A-20
A-11.	Flow Rate Effect on Heat Transfer	A-21
A-12.	Typical Core Shape Skewed Toward Core Exit	A-22
A-13.	Comparison of Dittus-Boelter Correlation to Data	A-23
B-1.	Comparison of Mass Flow Ratios Calculated Using Two Critical Flow Models and the Bernoulli Mass Flux Expression	B-18
B-2.	Comparison of Critical Pressures Calculated Using Five Critical Flow Models With Measured Throat Pressures	B-19
B-3.	Ratios of Measured Break Mass Flow Rates to Critical Mass Flow Rates Calculated Using Five Critical Flow Models	B-20
B-4.	Discharge of Saturated Water Through Orifices Nozzles and Pipes	B-21
B-5.	Discharge Coefficient Required for Orifice Equation	B-22
B-6.	Discharge Coefficient Required for Modified Zaloudek Equation	B-23
B-7.	Pressure Vs Time for 177-FA Lowered-Loop Break Spectrum at RC Pump Discharge Using Orifice Equation for Subcooled Discharge	B-24
B-8.	Mixture Height Vs Time for 177-FA Lowered-Loop Break Spectrum at RC Pump Discharge Using Orifice Equation for Subcooled Discharge	B-25
B-9.	Pressure Vs Time for 177-FA Lowered-Loop Break Spectrum at RC Pump Discharge Using Modified Zaloudek Subcooled Discharge Model	B-26
B-10.	Mixture Height Vs Time for 177-FA Lowered-Loop Break Spectrum At RC Pump Discharge Using Modified Zaloudek Subcooled Discharge Model	B-27
B-11.	Ratios of Measured Break Mass Flow Rates to Critical Mass Flow Rates Calculated Using Five Critical Flow Models	B-28
B-12.	Comparison of Critical Flow Models With Data	B-29
B-13.	Effect of Throat Length to Throat Diameter Ratio on Calculated Flow Multiplier for HEM	B-30
B-14.	Leak Quality for 0.07-ft^2 Break	B-30
B-15.	Ratio of HEM to Moody Critical Flow Predictions	B-31
B-16.	Comparison of Integrated Leak Flow Vs Time for 177-FA Lowered-Loop Break at RC Pump Discharge	B-32
B-17.	Comparison of Pressure Versus Time for 177-FA Lowered-Loop Break at RC Pump Discharge	B-33
B-18.	Comparison of Core Mixture Level for 177-FA Lowered-Loop Break at RC Pump Discharge	B-34
B-19.	Comparison of Best Estimate Pressure Prediction and Evaluation Model Results	B-35
B-20.	Comparison of Best Estimate Mixture Height Prediction and Evaluation Model Results	B-36
B-21.	Comparison of Best Estimate Pressure Prediction and Evaluation Model Results	B-37
B-22.	Comparison of Best Estimate Mixture Height Prediction and Evaluation Model Results	B-38

Figures (Cont'd)

Figure		Page
C-1.	Typical B&W Surge Line Arrangement	C-8
C-2.	Typical B&W Surge Line Arrangement Along With Rising Surge Line From Hot Leg to the Pressurizer	C-9
C-3.	Effect of Steam/Liquid Stratification and Slip in Different Surge Line Designs	C-10
C-4.	B&W Surge Line With Watertrap	C-11
D-1.	Safety Injection Location Studies Westinghouse 4-Loop PWR 4 Inch Break	D-11
D-2.	Safety Injection Location Studies Westinghouse 4-Loop PWR 4 Inch Break	D-12
D-3.	L3-1 System Pressure	D-13
D-4.	Liquid Content Sensitivity Evaluation, CFT Actuation Pressure 600 psi	D-14
D-5.	CRAFT2 Noding Diagram for Small Breaks	D-15
D-6.	Pressure Vs Time, 0.15-ft^2 CLPD Break	D-16
D-7.	Pressure Vs Time, 0.1-ft^2 CLPD Break	D-17
D-8.	Pressure Vs Time, 0.085-ft^2 CLPD Break	D-18
D-9.	Pressure Vs Time, 0.07-ft^2 CLPD Break	D-19
D-10.	Core Mixture Level Vs Time, 0.15-ft^2 CLPD Break	D-20
D-11.	Core Mixture Level Vs Time, 0.1-ft^2 CLPD Break	D-21
D-12.	Core Mixture Level Vs Time, 0.085-ft^2 CLPD Break	D-22
D-13.	Core Mixture Level Vs Time, 0.07-ft^2 CLPD Break	D-23
E-1.	CRAFT2 Noding Diagram for Small Breaks Used in Previous Evaluation Model	E-13
E-2.	System Pressure Vs Time, 0.01 ft^2 Break at Pump Discharge	E-14
E-3.	Hot Leg Level, 0.01-ft^2 Break at Pump Discharge	E-15
E-4.	Base Model Noding Scheme	E-16
E-5.	Pressurizer Pressure, Base Model	E-17
E-6.	Hot Leg Mixture Level, Base Model	E-18
E-7.	Vent Valve Quality, Base Model	E-19
E-8.	Vent Valve Flow Rate, Base Model	E-20
E-9.	Leak Quality, Base Model	E-21
E-10.	Leak Flow Rate, Base Model	E-22
E-11.	Comparison of 4/1 Model to 4/2 Model, Pressurizer Pressure	E-23
E-12.	Comparison of 4/2 Model to 8/2 Model, Pressurizer Pressure	E-24
E-13.	Comparison of 8/2 Model to 6/2 Model, Pressurizer Pressure	E-25
E-14.	Comparison of 8/2 Model to 6/2 Model, Broken Loop Hot Leg Mixture Level	E-26
E-15.	Comparison of 8/2 Model to 6/2 Model, Intact Loop Hot Leg Mixture Level	E-27
E-16.	Detailed Upper Plenum Model Noding Scheme	E-28
E-17.	Detailed Upper Plenum/Upper Head Model Noding Scheme	E-29
E-18.	Pressurizer Pressure	E-30
E-19.	RV Upper Plenum Liquid Level	E-31
E-20.	Pressurizer Pressure	E-32
E-21.	Vent Valve Flow Rate	E-33
E-22.	Hot Leg Liquid Level	E-34
E-23.	Detailed Hot Leg Model	E-35
E-24.	Pressurizer Pressure	E-36
E-25.	Liquid Level in Hot Leg Riser Section (Loop A)	E-37

Figures (Cont'd)

Figure		Page
E-26.	Liquid Level in Hot Leg Riser Section (Loop B)	E-38
E-27.	Leak Flow Rate	E-39
E-28.	Vent Valve Quality	E-40
F-1.	CRAFT2 Noding Diagram, Old Base Model for Davis-Basse 1	F-12
F-2.	CRAFT2 Noding Diagram, Revised Base Model for Davis-Besse 1	F-13
F-3.	CRAFT2 Detailed Hot Leg Noding Diagram for Davis-Besse 1	F-14
F-4.	Pressure Vs Time, Hot Leg Region	F-15
F-5.	Mixture Level Vs Time, Hot Leg Region	F-16
F-6.	Liquid Volume Vs Time, Hot Leg Region	F-17
G-1.	Semiscale Mod-2A System Isometric (Cold Leg Break Configuration)	G-14
G-2.	Schematic of the System Configuration for Test S-NC-2	G-15
G-3.	CRAFT2 Noding Diagram	G-16
G-4.	System Pressure	G-17
G-5.	Hot Leg Fluid Temperature	G-18
G-6.	Mass Flow Rate	G-19
G-7.	Primary System Pressure	G-20
G-8.	Cold Leg Fluid Temperature	G-21
G-9.	Hot Leg Fluid Temperature	G-22
G-10.	Core Temperature Differential	G-23
G-11.	Steam Generator Temperature Differential	G-24
H-1.	CRAFT2 Nodal Diagram for Plant Transient Simulation	H-15
H-2.	RCS Pressure Vs Time Comparison	H-16
H-3.	Steam Generator Pressure Vs Time Comparison	H-17
H-4.	Cold Leg Temperature Vs Time Comparison	H-18
H-5.	Hot Leg Temperature Vs Time Comparison	H-19
H-6.	Pressurizer Level Vs Time Comparison	H-20

1. INTRODUCTION

This report describes the features of B&W's small-break loss-of-coolant (LOCA) emergency core cooling system (ECCS) evaluation model and is applicable to all B&W nuclear steam systems. B&W's nuclear steam plants are divided into the following three categories:

1. 177-fuel assembly plants with lowered-loop arrangement.
2. 177-fuel assembly plants with raised-loop arrangement.
3. 205-fuel assembly plants.

There are no significant system design differences between the nuclear steam systems (NSSs) and the ECCSs within each category since these design features are the basis for the grouping. The current B&W plants in each category are listed in Table 1-1.

The information presented in this document defines the B&W evaluation model. It is shown herein that this model conforms to Appendix K of Title 10, Code of Federal Regulations, Part 50 (10 CFR 50). Most of the information in this report has been submitted previously in topical reports BAW-10092, Revision 3, and BAW-10104, Rev. 3.

Specific design information for each plant category is considered input to the evaluation model and will be generated using the assumptions and technqiues described herein. A separate application report for each B&W generic plant type will be issued, if required, to show conformance to 10 CFR 50.46 (Acceptance Criteria for Emergency Core Cooling Systems for Light Water Nuclear Power Reactors) issued by the NRC in January 1974.

This report is divided into eight sections:

1. Introduction.
2. Background.
3. An overview of 10 CFR 50.46.

4. Definition of model.
5. Small-break evaluation model.
6. Maximum hydrogen generation, coolable geometry, and long-term cooling.
7. Required documentation.
8. References.

Table 1-1. Category Classifications

B&W Contract No.	Customer and site	NRC Docket No.
Category 1 - 177-Fuel Assembly Plants With Lowered-Loop Arrangement		
620-0003 NSS-3	Duke Power Company Oconee 1	50-269
620-0004 NSS-4	Duke Power Company Oconee 1	50-270
620-0005 NSS-5	Metropolitan Edison Company Three Mile Island 1	50-289
620-0006 NSS-6	Jersey Central Power & Light Three Mile Island 2	50-320
620-0007 NSS-7	Florida Power Corporation Crystal River 3	50-302
620-0008 NSS-8	Arkansas Power & Light Arkansas Nuclear One	50-312
620-0009 NSS-9	Duke Power Company Oconee 3	50-287
610-0011 NSS-11	Sacramento Municipal Utility District Rancho Seco	50-312
620-0012 NSS-12	Consumers Power Company Midland 1	50-330
620-0013 NSS-13	Consumers Power Company Midland 2	50-329

Table 1-1. (Cont'd)

B&W Contract No.	Customer and site	NRC Docket No.
Category 2 - 177-Fuel Assembly Plants With Raised-Loop Arrangement		
620-0014 NSS-14	Toledo Edison Company Davis-Besse 1 (Mark B, 15x15)	50-346
Category 3 - 205-Fuel Assembly Plants		
620-0015 NSS-15	Tennessee Valley Authority Bellefonte Unit 1	50-438
620-0016 NSS-16	Tennessee Valley Authority Bellefonte Unit 2	50-439
620-0023 NSS-23	Washington Public Power Supply System Nuclear Project No. 1	50-460
620-0032 NSS-32	Washington Public Power Supply System Nuclear Project No. 2	50-513

2. BACKGROUND

As a result of the accident at TMI-2, the Bulletins and Orders Task Force was formed within the NRC office of Nuclear Reactor Regulation. The Task Force was charged, in part, with reviewing the analytical predictions of feedwater transients and small break LOCAs to ensure the continued safe operation of all operating reactors, and determination of the acceptability of operator emergency guidelines. As a result of their reviews, the Task Force concluded that, while there were no apparent safety concerns, additional system verification of the small-break LOCA model (as required by II.4 of Appendix K to 10 CFR 50) was needed in certain areas. These improvements and concerns, as they applied to each LWR vendor's model, were documented in the various Task Force reports for each LWR vendor. The review of the B&W small-break LOCA model was documented in NUREG-0565, "Generic Evaluation of Small Break Loss-of-Coolant Accident Behavior in Babcock & Wilcox Designed 177-FA Operating Plants" (January 1980). The review of the reactor coolant pump model was documented in NUREG-0623, "Generic Assessment of Delayed Reactor Coolant Pump Trip During Small Break Loss-of-Coolant Accidents in Pressurized Water Reactors" (November 1979). On October 31, 1980, the NRC issued NURG-0737, "Clarification of TMI Action Plan Requriements." Included in NUREG-0737 is the requirement for an industry review of NUREG-0565 and -0623 and development of a program that addresses the NRC concerns therein. After a meeting with the 177-FA Owners Group and the NRC, the Small-Break LOCA Methods Program was developed to address the requirements of NUREG-0737, Section II.K.3.30, as they were identified by the staff in the meeting of December 16, 1980.

The overall goal of the Small-Break LOCA Methods Program is to address these issued identified by the staff.

3. OVERVIEW OF 10 CFR 50.46

The "Acceptance Criteria for Emergency Core Cooling Systems for Light Water Nuclear Power Reactors" (10 CFR 50.46), issued by the NRC in January 1974, include five criteria that must be met before an emergency core cooling system (ECCS) is deemed acceptable. Conformance to these criteria is established in the following manner:

1. The peak cladding temperature shall not exceed 2200F. The peak cladding temperature, calculated with the evaluation model described herein, will not exceed 2200F.

2. The percentage of local cladding oxidation shall not exceed 17%. From the analysis performed to satisfy condition 1, the total oxide thickness (combining both inside and outside oxide layers) at the location of maximum local oxidation will be less than 0.17 times the total cladding average thickness. For the ruptured location, the total cladding average thickness is taken as the thickness of the hollow cylinder, which has the same mass as the original unoxidized cladding and the same circumference as the fuel pin at the location of maximum strain.

3. The maximum hydrogen generated during the transient shall not exceed that which would be generated by oxidation of 1% of the reactor cladding. Using a conservative approach, the cladding temperature response (and thereby the degree of oxidation) is determined as a function of local power. This function is then integrated over the core power distribution to obtain the total oxidation. Division of the integrated value by the initial amount of zirconium gives the fraction of oxidized cladding; this will be limited to 1%.

4. Calculated changes in the core geometry shall be such that the core remains amenable to cooling. The changes in geometry that were calculated during the analysis for condition 1 are examined to ensure that no gross core blockage or disfiguration will occur.

5. The mode of long-term core cooling shall be established. The analysis is continued until the cladding temperatures at all locations in the core are decreasing and the fluid level in the core is rising. At this time the path to long-term cooling is established. Cooling for the long term is by pool boiling maintained by the ECCS.

It will be shown in specific analyses that all B&W plant categories conform to these five acceptance criteria. The methods used to show conformance to items 3 through 5 are described in sections 5 through 8.

Appendix K sets forth certain required and acceptable features of the evaluation model that must be used to show compliance to the five acceptance criteria of 10 CFR 50.46. The compliance of B&W's small-break evaluation models with Appendix K is demonstrated in section 5.

4. DEFINITION OF MODEL

The information presented in this document defines B&W's small break ECCS evaluation model. In particular,, this document describes the techniques and assumptions used in evaluating the consequences of a small-break loss-of-coolant accident (LOCA). These techniques and assumptions constitute the model. The required features of the ECCS evaluation model are set forth in Appendix K to 10 CFR 50. The evaluation model for small breaks is given in section 5 along with its conformance to Appendix K. The model will be changed only if the NRC issues rule changes or if improved analytical techniques become available.

Specific category-related information (such as system design, power level, etc.) is considered input to the model. These numbers are developed using the techniques and assumptions described in the model, and they will be addressed in specific category-related analyses. Within each category, new information will become available during the design life of a plant. This information will be implemented into specific analyses on a planned schedule with the NRC.

This report covers only the model. All other information needed to perform the necessary analyses is considered input and may change throughout the design life of a nuclear steam system.

5. SMALL BREAK EVALUATION MODEL

5.1. Model Applicability

At present, B&W's nuclear steam plants can be divided into three major categories:

1. 177-fuel assembly plants with lowered-loop arrangement.
2. 177-fuel assembly plants with raised-loop arrangement.
3. 205-fuel assembly plants.

There are no significant design differences between the NSSs and ECCSs in each category. Table 1-1 lists the current B&W plants in each category. The plants in these categories are described as follows:

Category 1 - The plants in this category are generally referred to as the Oconee type. They are characterized by their loop arrangement, in which the once-through steam generators are at a low elevation relative to the reactor vessel. These plants have eight internals vent valves and utilize the Mark B (15 x 15) fuel assembly.

Category 2 - The design is essentially identical to Category 1 except that the steam generators are raised in relation to the reactor vessel. The pump suction leg is shorter for these plants due to the raised configuration of the steam generators. Also, there are only four vent valves in these plants. This reduction in the number of vent valves is factored into the model as a reduced vent flow area. The HPI system comprises low-head HPI pumps.

Category 3 - These plants have the raised-loop arrangement of the Category 2 plants but are larger (more fuel assemblies) and have eight internals vent valves. The Category 3 plants employ the Mark C fuel assembly instead of the Mark B.

The small break evaluation model described in this section is applicable to all plant categories. Any item that is applicable only to certain plant categories due to differences in design, such as loop venting during reflood, or within a category due to different fuel assemblies, such as reflooding heat transfer coefficients, is specifically identified.

5.2. Code Relationships

A break is considered to be small when its cross-sectional area is 0.5 ft^2 or less. Past experience with studies of small breaks has shown that the large break concepts of bypass and reflood do not apply to breaks of this size. A brief description of the behavior of small breaks will be valuable in understanding the evaluation technique. A small break accident involves a rather slow, non-violent system depressurization. Flow conditions within the reactor coolant system change gradually and smoothly. Temperature and pressure gradients between regions tend to be small. The lack of agitation allows partial phase separation of steam and water and, in some situations, countercurrent flow. Rather than the distinct blowdown and reflood phases associated with large breaks, small breaks have a smooth transition from a period of relatively high core flow to one of relatively quiescent conditions. During the early phase, heat transfer in the core is flow-controlled and is adequate to keep the cladding cool. Later, during the quiescent period, a two-phase froth level develops in the reactor inner vessel. The portion of the core that remains covered by this mixture is cooled by pool nucleate boiling, which is adequate to maintain the cladding temperature near that of the saturated fluid. If the entire core is not covered by the mixture, the portion above the froth level is cooled by forced convection to steam. As the system depressurizes, injection flow increases, and gradually the core is recovered completely. The CRAFT2[1] code is used to predict the hydrodynamic behavior of the reactor coolant system. If CRAFT2 predicts that the core will be covered with liquid throughout the transient, no thermal analysis is required and compliance with 10 CFR 50.46 is ensured. Otherwise, FOAM[2] is used to determine the mixture height within the core, and the thermal response of the hottest fuel pin is evaluated by THETA[3]. Figure 5-1 illustrates the interrelationship of the computer codes.

5.3. Evaluation Model Features

This section addresses the features of B&W's small-break evaluation model. Its compliance with 10 CFR 50, Appendix K, is described in section 5.4. The response to the NRC concerns of NUREG-0737, Section II.K.3.30, are discussed in section 5.5.

The evaluation model described here sets forth guidelines for the use of and the interfaces among the codes used. The organization is on a subject basis and applies to all codes as appropriate. When specific details are employed in only one code, the situation is clearly identified.

5.3.1. Heat Sources

The analysis utilizes the heat sources listed below. These sources are time-dependent, and their characterization within the codes is dependent on the phase of the accident being modeled.

5.3.1.1. Initial Power

For the purpose of obtaining initial stored energy and decay heat, the reactor is assumed to be operating at 102% of the highest licensed power level for that plant category at the time of the accident.

5.3.1.2. Core Peaking Factors

If core uncovering is predicted, the core power shape chosen will be that which yields the highest peak cladding temperature.

5.3.1.3. Initial Stored Energy

The initial temperature distribution within the fuel will be that which yields the highest calculated temperature. Initial fuel temperature will be determined by the approved steady-state thermal code at the time of the analysis. Burnup and other related parameters will be chosen to produce the highest cladding temperature.

5.3.1.4. Fission Heat

The fission power of the reactor is calculated using the kinetics model in the CRAFT computer code (described in section 2.4.1 of BAW-10092, Rev. 3). Credit is taken for reactor trip and control rod insertion. The response of the reactor coolant (RC) system following a small break is characterized by a slow reduction in pressure and system flow. In the upper core and upper plenum region, this results in lower forces (ΔP and flow) opposing control rod insertion than those present during normal operation. Thus, reactor trip initiated on low RC system pressure and subsequent control rod insertion is assumed when it is calculated to occur. Provisions are made to analyze this event conservatively; that is, a minimum tripped rod worth and appropriate delay and insertion times are assumed.

5.3.1.5. Decay of Actinides

Heat from the radioactive decay of actinides is calculated from the B&W heavy isotope standard decay curve for infinite irradiation multiplied by a factor of 1.2. This represents values greater than those predicted by the ANS curve.

5.3.1.6. Fission Product Decay Heat

The ANS standard fission product decay heat curve for infinite irradiation published in October 1971 is used with a factor of 1.2 to determine fission product decay heat during the analysis.

5.3.1.7. Heat Distribution

A power distribution factor of 0.973 is used during the blowdown phase of the analysis to evaluate the power for the hot channel analysis (THETA[3]). This factor is based on the consideration that 2.7% of the fission energy is deposited directly in the coolant rather than in the fuel or cladding; thus, its heat is not transmitted through the cladding in the removal process. During the reflood phase of the accident a distribution factor of 0.96 will be used for the hot channel. This factor is based on gamma energy absorption being less in a hot pin because its neighbors are unable to provide the sources of gammas for peripheral absorption as does the hot bundle. Details on the development of these factors are presented in topical report BAW-10033.

In either phase the peak power in the core is evaluated using the following equation:

$$PLP = \frac{1.02 \times kW \times p_f \times F \times P(t)}{\text{total active pin length}}$$

where PLP = (peak linear power), linear heat rate, kW/ft,
kW = rated power,
p_f = total peaking factor,
F = appropriate power distribution factor,
P(t) = normalized transient power.

5.3.1.8. Metal-Water Reaction Rate

The rate of energy release due to metal-water reactions is calculated by the Baker-Just equation without steam limiting. Details of the model appear in sections 2.4.2 and II-6 of the CRAFT and THETA manuals.

5.3.1.9. Heat Transfer From Reactor Internals

Heat transfer from the reactor vessel walls, piping, and non-fuel internals hardware is determined by the primary heat model in CRAFT (this model is described in section 2.8 of reference 1).

5.3.1.10. Primary-to-Secondary Heat Transfer

Primary-to-secondary heat transfer in the steam generator is modeled to allow the secondary side to act as a heat source as well as a heat sink during an analysis. The steam generator model is significantly improved and modified over the previous evaluation model.[4] Details of the mechanistic steam generator model are provided in Appendix I (section 1.3) of the CRAFT2 topical report.

5.3.2. Reactor System Hydrodynamics

5.3.2.1. Noding Scheme for CRAFT

The noding description of the RC system used in the CRAFT computer model for small-break analysis requires less detail in the core and much more detail in the steam generator than for large-break analysis. The noding model was developed by performing various noding sensitivity studies. The following noding

studies were performed to achieve the optimum noding scheme that can account for all the known SBLOCA phenomena.

1. Noding sensitivity studies were performed to develop a converged steam generator model. This was done by selecting a break that relies on steam generator heat removal for plant depressurization. The spatial detail for modeling the steam generator was increased to the code capacity and the results compared. This was done to ensure that the increase in spatial detail for the steam generator model does not alter the transient response significantly.

2. To ensure that the effects of local flashing are adequately accounted for, noding sensitivity studies of the reactor vessel upper head and upper plenum were performed. Based on these studies, a converged model was developed for the upper head and upper plenum.

3. Finally, noding sensitivity studies were performed for the hot leg to ensure that the spatial detail in the hot leg is sufficient to model any interruption in the natural circulation flow due to the formation of a steam pocket in the top of the inverted U-bend in the hot legs.

Based on the noding sensitivity studies described above, a converged system model with respect to spatial noding detail was developed. The noding studies performed for 177-FA lowered-loop plants are described in detail in Appendix E. Appendix F describes the noding studies performed for the 177-FA raised-loop plants. The noding studies for 205-FA plants are described in Appendix I.

A typical small-break noding model divides the RC system into the following nodes:

	Number of nodes	
Component	177-FA plant	205-FA plant
Downcomer	2	2
Lower plenum	1	1
Hot leg (each)	1	1
Steam generator		
Primary	6 axial, 2 radial	6 axial, 1 radial
Secondary	6 axial, 1 radial	6 axial, 1 radial

The use of two radial regions for the once-through steam generator (OTSG) accounts for direct AFW cooling. The integral economizer OTSG (IEOTSG) for the 205-FA plants is modeled with six axial levels on the primary and secondary sides with one radial region because the auxiliary feedwater for 205-FA plants is near the bottom of the OTSG, and there is no need for an additional radial region. In the intact loop, the two intact cold legs are lumped together as two nodes - one each at the pump suction and pump discharge; in the broken loop each cold leg is modeled with two nodes - one each at the pump suction and discharge. The pressurizer is represented by a non-equilibrium model with two regions, and the containment is modeled by a single node.

5.3.2.2. Flow Model for CRAFT

Flow between the nodes is determined by the momentum equation. Included are terms that account for (1) temporal change of momentum, (2) momentum convection, (3) momentum change due to compressibility, (4) momentum flow due to area change, (5) pressure drop due to wall friction, (6) pressure drop due to area change, and (7) gravitational acceleration. Frictional pressure drop is determined by a fit to the Fanning curves. Two-phase friction multipliers are obtained from the Thom correlation above 250 psia and the Martinelli-Nelson correlation below 100 psia. To achieve a smooth transition from Martinelli-Nelson to Thom, a pressure-dependent interpolation is performed between 100 psi and 250 psi. Section 2.2 of the CRAFT manual[1] outlines the flow calculation procedures.

5.3.2.3. Discharge Model

The discharge of subcooled liquid through the break is determined from the orifice equation. Once the break node becomes saturated, however, the discharge of two-phase flow is based on the Moody correlation. To avoid a step change in the flow between the correlations, linear weighting is used to extrapolate between the orifice equation at 0.0 quality and the Moody correlation at 0.1% quality. A spectrum of break areas is studied as part of the whole analysis. This ensures that all breaks with areas of 0.5 ft^2 and less are adequately investigated. Section 2.2.10 of the CRAFT manual[1] explains the evaluation of leak rate.

5.3.2.4. Core Flow Model

The relatively high core flow rates early in the transient are calculated by CRAFT2. Later, however, if CRAFT2 calculates core uncovering during the quiescent stage of the accident, the steam flow rate above the froth is determined by the FOAM code. The steaming rate, determined from the average channel conditions, is applied to the thermal analysis of the hot pin. Because a significantly higher swell level and steaming rate would be associated with the hot channel, the use of average conditions implicitly allows for the effects of blockage and flow diversion to neighboring bundles.

5.3.2.5. Phase-Separation Model and Countercurrent Flow

A phase-separation model based on the Wilson bubble rise correlation is incorporated into CRAFT2 for small leak analysis. To ensure that the core mixture heights predicted in CRAFT2 closely match those produced in FOAM during the quiescent portion of the transient, the phase-separation model is adjusted in the core to reflect the proper bubble distribution. Appendix F of BAW-10104[4] shows the derivation of the factor used to adjust the phase-separation model.

Once the phase separation has developed in adjacent nodes, conflicting pressure heads of the steam and liquid could cause countercurrent flow between the nodes. To allow for this phenomenon, a physical flow channel is divided into upper and lower flow paths, each independent of the other in terms of such flow conditions as direction, velocity, and quality. Hand calculations demonstrate that relative velocities are low enough to avoid significant entrainment of liquid and to ensure that countercurrent flow is justified. Section 2.9 of the CRAFT2 manual explains the phase separation model.

To model the small-break LOCA transient with pumps on, CRAFT2 is equipped with a drift flux model for small break analysis. Appendix I (section 1.3) of the CRAFT2 topical report explains the drift flux model.

5.3.2.6. Pump Model

The reactor coolant (RC) pumps are represented by the two-phase dynamic pump model. Two-phase pump head and torque degradation are also accounted for in the pump model. The pump models are described in Appendix I (section 1.4) of the CRAFT2 topical report.

5.3.2.7. Pressurizer Model

The pressurizer for the small-break analysis is modeled using a non-equilibrium pressurizer model. The non-equilibrium pressurizer model is described in Appendix I (section 1.2) of the CRAFT2 topical report.

5.3.2.8. Mixture Height Calculation

Should CRAFT2 predict partial uncovering, the FOAM code is used to determine the mixture height in the core during the quiescent portion of the transient. Steam production due to core average power, primary metal heat, and flashing within the vessel combined with the inner vessel liquid volume is used to calculate the rate of steam loss out of the mixture and the corresponding degree of swelling due to trapped steam. The code is discussed in B&W topical report BAW-10064. The amount of swelling in the hot channel is considerably greater than for the average channel. No credit is taken for this in the hot pin thermal analysis. Also, by using average core conditions, the steaming rate above the froth level calculated by FOAM already implicitly includes the effects of blockage and crossflow.

5.3.2.9. Single Failure Condition

The single failure assumed for small breaks is that which produces the minimum ECCS injection. The single failure assumed is the loss of a diesel in conjunction with a loss of offsite power. This approach is the most conservative since the containment backpressure has little effect on small breaks. Examination of previous small leak analyses reveals that the flow through the break is important during the time the core is refilling. Therefore, any single failure chosen to minimize the containment backpressure would have no effect on the transient and would possibly increase ECC injection. Since pump injection is very important for small breaks, limiting such injection produces the worst case.

5.3.3. Heat Transfer and Thermal Analysis

5.3.3.1. Flow Controlled Portion of Transient

Heat transfer is flow controlled while core flow remains greater than 1% of the initial steady-state value. The following heat transfer correlations are

used when appropriate: Dittus-Boelter forced convection to liquid; Thom nucleate boiling; McDonough, Milich, and King transition boiling; Dougall-Rohsenow flow film boiling; and Dittus-Boelter forced convection to steam. The critical heat flux is determined by either the Macbeth correlation or a combination of the B&W-2, Barnett, and modified Barnett correlations. Once CHF is reached, the calculation will not return to nucleate boiling heat transfer at that location for the remainder of this phase of the accident.

5.3.3.2. Quiescent Portion of Transient

The system is considered to be in a quiescent condition once the core flow has decreased to less than 1% of its initial value. Heat transfer within the portion of the core covered by a steam-liquid mixture is through pool boiling, either nucleate or film. The Morgan pool film boiling correlation is used when appropriate. Above the froth level, heat transfer is determined from a Dittus-Boelter calculation of forced convection to steam. CRAFT2 will not return to pool nucleate boiling during the recovering of the core unless the cladding temperature is within 30OF of the saturated fluid temperature. Until this time, heat transfer will be by pool film boiling. The 30OF limit is based on the work of McDounough, Milich, and King. Since our analysis has shown that a pool film boiling coefficient of 50 Btu/h-ft^2-°F is sufficient to cool the core, this criterion is not a significant factor in small break analysis and is merely a convenient way of completing the transient. The FLECHT test data show that the core can be quenched rapidly from a temperature exceeding this criterion.

Should the core never become uncovered during the accident, no thermal analysis is necesary. Analyses have shown that the core can be cooled sufficiently by pool film boiling, which is the heat transfer mechanism that yields the minimum heat transfer coefficient when the core is covered. Details on the application of the various heat transfer correlations can be obtained from section II.5 of the THETA1-B code manual.

5.3.4. Cladding Rupture

5.3.4.1. Flow-Controlled Portion of Transient

The occurrence of rupture is determined during the thermal analysis of the hot pin. If rupture is indicated, flow blockage is calculated for the hot channel.

The flow is then reduced in THETA in the following manner: The flow resistance due to blockage is determined as for a large break; that is, a k-factor of 1.0 referenced to the reduced flow area is assumed for resistance. This resistance is then referenced to the channel area by multiplying it by the square of the ratio of the unblocked area to the blocked area. The resultant k-factor is added to the normal path resistance, and the flow is reduced until the blocked and average channels experience the same pressure drop. This yields the following equation for hot channel flow after rupture:

$$W_h = FW_A$$

where $F = K_n / K_n + 1.0(A_n/A_b)^2$,

W_h = hot channel flow after blockage,

F = flow correction factor,

W_A = averge channel flow,

K_n = unblocked k-factor,

A_n = unblocked channel area,

A_B = blocked channel area.

5.3.4.2. Quiescent Portion of Transient

5.3.4.2.1. Below Froth Level

Heat transfer within the mixture is by pool nucleate or pool film boiling, either of which is adequate to maintain the cladding below its rupture temperature. Because it is a pool situation, blockage would not reduce heat transfer by reducing flow. In fact, heat transfer at the ruptured location would be improved because of the increased surface area. For those reasons, it is conservative not to allow rupture below the froth level.

5.3.4.2.2. Above Froth Level

Heat transfer above the froth level is by forced convection to steam. Although the thermal analysis is for the hot pin, average core steaming rates are used for the calculation. This essentially assumes that blockage has occurred in the hot channel, and crossflow between neighboring channels is instantaneous above the froth. The location and degree of rupture are determined using the THETA1-B code; further details are available in the user's manual. Once rupture has been calculated, the metal-water reaction will be allowed on both the inside and outside surfaces of the cladding at the rupture location.

5.4. Compliance

This section demonstrates that the features of the small-break evaluation model described in section 5.3 conform to the required features for the model set forth in 10 CFR 50, Appendix K. Following the format used in Appendix K, compliance is discussed on a point-by-point basis with references made to the appropriate parts of section 5.3.

I. Required and Acceptable Features

A. Sources of Heat During LOCA

The provisions of this section are included in the evaluation model as required (sections 5.3.1.1 through 5.3.1.10).

B. Swelling and Rupture of Cladding and Fuel Rod Thermal Parameters

The B&W small-break model contains a suitable provision for calculating the effects of cladding rupture (5.3.4.1 and 5.3.4.2). However, it is B&W's position that for small breaks any change in gap conductance before rupture is slight, and the only effect would be a nominal increase in fuel temperature. The effect on cladding temperature is small. Once rupture is predicted, the cladding dimensions near the rupture will change and steam will fill the gap. Gap conductance is re-evaluated in accordance with the Final Acceptance Criteria. Specific information on this model is available in section II.2.4 of the THETA1-B code manual.

C. Blowdown Phenomena

C.1. Break Characteristics and Flow

C.1.a. Spectrum of Breaks - As required, B&W's small-leak analysis includes a spectrum of break areas up to 0.5 ft^2 (section 5.3.2.3). Breaks larger than this are evaluated with the large-break model.

C.1.b. Discharge Model - The discharge model described in section 5.3.2.3 complies with the rules of the Final Acceptance Criteria. Incorporation of a range of discharge coefficients into the analysis is already implicit for

small breaks by considering a spectrum of break areas. This results from the fact that the discharge coefficient only affects the apparent break size.

C.1.c. End of Blowdown - The bypass model described in section 2.7.3 of the CRAFT manual has been used to investigate entrainment during periods of reverse downcomer flow in small leak accidents. Based on a study of past small breaks, neither entrainment nor the associated bypass will occur. Therefore, bypass calculations are not necessary for conformance to Appendix K.

C.1.d. Noding Near Break and ECCS Injection Points - Sensitivity studies have shown that the noding model used for the small breaks is adequate (section 5.3.2.1).

C.2. Frictional Pressure Drops

The flow model used by B&W incorporates realistic two-phase multiplier and Reynolds number corrections for friction factors as required (5.3.2.2).

C.3. Momentum Equation

The flow model used by B&W is based on the momentum equation and includes terms for all seven effects listed in Appendix K (5.3.2.2).

C.4. Critical Heat Flux

The B&W small leak evaluation model includes CHF correlations mentioned as being acceptable (5.3.3). Once CHF is predicted at an axial position, the return to nucleate boiling is delayed as described in section 5.3.3.2, which is in agreement with the requirements of Appendix K.

C.5. Post-CHF Heat Transfer Correlations

Post-CHF heat transfer correlations listed as acceptable by the rule are used in the B&W evaluation model (5.2.3).

C.6. Pump Modeling

As required, the reactor coolant system circulation pumps are represented by a two-phase, dynamic pump model (section 2.5, BAW-10092, Rev. 3).

C.7. Core Flow Distribution During Blowdown

Flow through the core is smooth because of the nature of the small break accident (section 5.2). The effects of rupture and blockage during the flow-controlled portion of the accident are determined in the hot pin temperature calculation (5.3.4).

Core inlet enthalpy is determined from the adjacent upstream node conditions calculated by CRAFT. B&W's evaluation of the core flow distribution and enthalpy satisfies the requirements of Appendix K.

D. Post-Blowdown Phenomena - Heat Removal by ECCS

D.1. Single Failure Criterion

B&W assumes the worst single active failure that produces the most severe restriction on ECCS equipment available for a small break (5.3.2.8).

D.2. Containment Pressure

In most small breaks, the small discharge area and the slow depressurization result in the leak flow remaining choked until after long-term cooling has been established. In such situations, containment pressure does not influence the transient. However, some of the large small breaks may unchoke before the core has completely recovered. The containment pressure will affect depressurization somewhat in these cases, but because recovering of the core is slow with small breaks, slight variations in pressure do not appreciably influence the rate of recovering. Containment pressure is not a critical factor in these accidents as long as the value used is reasonable.

D.3. Calculation of Reflood Rate

The typical reflooding period as envisoned for large breaks does not occur for small breaks. Appendix K raises some concern over the modeling of the RC pumps during reflood. The pumps are modeled in the manner described in section 5.3.2.6.

The determination of the carryover fraction during reflooding of the core is not necessary in small breaks because of the slow recovering, the relatively low cladding temperatures reached while uncovered, and the low power level. This results in a small amount of steam being formed with a correspondingly low velocity, which is not capable of entraining liquid.

There is concern that the discharge of compressed gas from the core flooding tanks following discharge of the water may affect core recovering. Since the core flooding tanks (CFTs) discharge directly into the reactor vessel downcomer, the gas also discharges directly into the downcomer. The gas discharged after the CFTs have emptied cannot interact with the steam flowing in the pipes for cold leg breaks. This would tend to build up the pressure slightly in the downcomer, which would cause a momentary increase in the core recovery rate since the water level in the downcomer is depressed. As shown in section 4.3.6.3 of BAW-10104, this effect can be neglected.

D.4. Steam Interaction With CFT Water

The B&W CFTs empty directly into the downcomer, where the injected water is homogeneously mixed with the existing downcomer steam-liquid mixture. The phase-separation model determines the interaction of the steam and water in the mixture. Because of direct vessel injection, no constraint is placed on the steam flow in the RC system piping. Thus, the provisions of this section are satisfied by the B&W evaluation technique.

D.5. Refill and Reflood Heat Transfer

During core recovering, heat transfer above the froth is by steam cooling only. As sections of the core are recovered, they are cooled by pool film boiling until pool nucleate boiling can be appropriately established (5.3.3.2). This procedure conforms to the requriements of Appendix K.

5.5. Response to Requirements of NUREG-0737, Section II.K.3.30

This section demonstrates that the features of the small break evaluation model described in section 5.3 addresses the requirements set forth in NUREG-0737, Section II.K.3.30. The concerns and the responses are provided below.

5.5.1. Concerns in NUREG-0565

NUREG-0565, Section 4.1.1.1, identifies concerns regarding the B&W small-break evaluation model:

Concern No. 1

Following postulated small break loss-of-coolant accidents, a primary mechanism for heat removal is natural circulation. The staff is concerned about the ability of the computer programs to correctly predict the various modes of natural circulation and the interruption of natural circulation, if it occurs. Experimental data for the verification of methods for two-phase natural circulation are currently not available.

Response

In response to this concern, the CRAFT code was upgraded. Included in this modification are a non-equilibrium pressurizer model, an upgraded two-phase flow model, pump model, and a new steam generator model. These modifications to CRAFT2 and their justifications are discussed in detail in BAW-10092, Revision 3.[1]

To demonstrate the ability of the upgraded CRAFT2 code to predict the various modes of natural circulation observed during a small break, a post-test analysis of the Semiscale Mod-2A Natural Circulation Test S-NC-2 was performed. This was a natural circulation test exhibiting single- and two-phase natural circulation modes. Various modes of natural circulation were established by

draining discrete amounts of liquid out of the reactor vessel lower plenum. The results of the post-test predictions of test S-NC-2 are shown in Appendix G. It is demonstrated in the appendix that the CRAFT2 code compares reasonably well with the data. CRAFT predicted the same general trend as found in the test. The results calculated, for most data points, were within the uncertainties of the measurements. This analysis demonstrated that the upgraded CRAFT2 code is capable of predicting various modes of natural circulation observed during the small-break LOCA transient and the transition from one mode to another.

In addition, a benchmark of the small-break model against a B&W plant transient was performed. The high-pressure reactor trip incident at Arkansas Nuclear One (ANO-1) on June 24, 1980, was the selected transient. The results calculated by the upgraded CRAFT2 code were compared with the transient data to analyze the adequacy of the steam generator and the new pressurizer models.

The purpose of this analysis was to demonstrate that the upgraded CRAFT2 code is capable of predicting similar responses during a B&W plant transient which involved natural circulation and cooling by the AFW system. The report describing the analyses and the results are provided in Appendix H. It is demonstrated that the upgraded CRAFT2 code is capable of predicting the natural circulation mode observed during the B&W plant transient.

Concern No. 2

The experimental verification of small break analysis methods with systems data is currently limited. The available small-break data from Semiscale Test S-02-6, although containing a number of deficiencies, is the best information now available. The analytical methods used to predict the results of this test do not correctly predict the overall system depressurization rate, and the depressurization rate following core flood tank injection. These are significant parameters in that they affect the injection rate of the core flood tank fluid. Analyses by B&W of Semiscale Test S-07-10B and LOFT Test L3-1 have been submitted by B&W and are currently being evaluated by the staff.

Response

In addition to the pre-test predictions of Semiscale Test S-07-10B and LOFT Test L3-1, B&W has also performed the post-test evaluation of these tests as requested in the "Letter to All Babcock & Wilcox Licensees" from R. W. Reid, Chief Operating Branch No. 4, Division of Licensing, February 24, 1981.

The post-test evaluation of LOFT Test L3-1 was submitted to the NRC in June 1981.[6] It was concluded in this evaluation that CRAFT2 is capable of predicting the small-break LOCA phenomena observed in the test if the actual test conditions were utilized.

The post-test evaluation of Semiscale Test S-07-10B/10D was submitted to the NRC in June 1981.[7] It was concluded in this analysis that using initial and boundary conditions consistent with the actual test, the results calculated by CRAFT2 are in good agreement with the test data, thus confirming that CRAFT2 is capable of predicting small-break LOCA transient phenomena.

Concern No. 3

The appropriateness of the pressurizer model for analyses of small breaks at various locations is a potential concern. The equilibrium pressurizer model assumed in the B&W analyses gives somewhat different results from hand calculations assuming non-equilibrium conditions. These modeling differences may be significant for various postulated breaks. Also, the representation of flooding in the surge line could affect draining of the pressurizer. A flooding check is not made for the surge line in the computer program.

Response

In response to this concern, a non-equilibrium pressurizer model was developed and incorporated in CRAFT2. The model simulates pressurizer performance using a steam region and a liquid region. Heat and mass transfer between the two regions is controlled by steam mixture interface parameters. The model also includes the sprays, heaters, and safety valves. This model and its justification are discussed in detail in Appendix I (section 1.2) of CRAFT2 topical report, BAW-10092, Revision 3.[1]

The second part of the concern regarding the addition of flooding in the surge line was also assessed. The result of this evaluation is shown in Appendix C. It is demonstrated in the report that, based on the geometry of the pressurizer surge line, countercurrent flow within the surge line cannot exist to any significant degree. Consequently, the flow in the B&W pressurizer surge line will be in only one direction. There is no need to add flooding check to the surge line.

Concern No. 4

The calculation of core level and core heat transfer are important features of the small break model. Limited experimental data are currently available to

justify these models. Although the current comparisons have been satisfactory, the experiments are not challenging to the codes. More experimental data must be obtained for further code verification.

Response

In response to this concern, previous studies contained in BAW-10064 showing analytical and experimental agreement of the core mixture level evaluation technique are referenced. These comparisons show that the level evaluation technique employed by the B&W model is capable of predicting the core mixture level.

In order to provide the analytical and experimental agreement of the core heat transfer evaluation method, the small break core heat transfer model employed by B&W was compared for steady-state conditions to several tests performed at Oak Ridge National Laboratory (ORNL). These tests were designed to evaluate the steam cooling capability within the core in which the fluid level was allowed to fall below the top of the active core region and stabilized at an intermediate location. These comparisons demonstrated that the use of the Dittus-Boelter correlation as the sole determinant of heat transfer is acceptable for evaluating compliance with 10 CFR 50.46. Consequently, the present heat transfer model is acceptable for licensing evaluation. Appendix A contains the detailed analyses performed to support these conclusions.

Concern No. 5

The number of nodes used to represent the primary system for small break LOCA analyses should be sufficiently detailed to model the flashing of hot fluid in various locations. This modeling detail is necessary since the calculated system pressure during the decompression process is controlled by the flashing of the hottest fluid existing at any time in the model. The assumption of thermal equilibrium requires that the fluid combined in a single node be represented by the average fluid properties. If fluid from several adjacent regions is combined in one node, the calculated system process during a portion of the transient may be lower than could occur if the smaller regions of hot fluid flashed and maintained the system at the corresponding saturation pressure. Thus, the modeling detail could have a significant effect on the calculated times for various events, such as ECCS actuation.

Response

As a result of the Small-Break LOCA Methods Program developed to address the requirements of NUREG-0737, Section II.K.3.30, significant code modifications

and revisions were made to the existing small-break LOCA evaluation model. Because of these modifications and revisions of the existing evaluation model, it was necessary to perform noding sensitivity studies to develop the base noding scheme which demonstrates convergence with respect to spatial detail. To accomplish this goal, the following studies were performed:

A noding sensitivity study was performed to develop a converged steam generator model for 177- and 205-FA plants. These studies were conducted using a break that relies on the steam generator for RCS depressurization. The spatial detail for modeling the steam generator was increased to the code's capacity to assess the impact of additional spatial detail on the transient response. Based on these studies, the steam generator models that adequately accounted for all the phenomena were chosen as the appropriate models for 177- and 205-FA plants.

To ensure that the effects of local flashing were accounted for, noding sensitivity studies of the upper plenum and upper head of the reactor vessel were performed for 177- and 205-FA plants. The converged steam generator models were used for these studies. Based on these studies, a converged model was developed for the upper head and upper plenum of 177- and 205-FA plants by evaluating the results of various degrees of spatial detail in these regions.

Finally, a noding study was conducted for the hot leg to ensure that its spatial detail is sufficient to model any interruption in natural circulation flow due to the formation of a steam pocket in the top of the inverted U-bend in the hot legs.

All the noding sensitivity studies performed for 177-FA lowered-loop plants to achieve the converged base model are discussed in Appendix E. The noding studies performed for 177-FA raised-loop plants are presented in Appendix F. Appendix I includes all the noding sensitivity studies for 205-FA plants.

Concern No. 6

During the recovery period from a small-break LOCA, the thermodyanmic equilibrium assumed in fluid control volumes could result in errors in the predicted system pressure. This could, in turn, introduce errors in both the break discharge and safety injection flow. The rate at which the water is refilling the system can affect steam condensation. If the condensation efficiency is less than 100%, system pressure would be higher than predicted.

Concern No. 7

The reduction in the primary system pressure determines the rate and amount of core flood tank water injected. Core reflooding is dependent on this flow. As discussed in NUREG-0611[5], the sensitivity analyses performed demonstrate the influence of core flood tank injection. The amount of steam present at the injection location is the predominant factor that determines the core flood tank mass delivery. The results of an analysis will be influenced by the model and the modeling assumptions used to calculate the core flood tank flow. Additional studies will be required to obtain the necessary information to perform an Appendix K analysis. Additional work in this area is underway at EG&G Idaho since more recent experimental data, including LOFT Test L3-1, indicate less depressurization than Semiscale Test S-02-6.

Response (to Concerns 6 and 7)

These concerns deal with the adequacy of the ECCS injection model used in small-break LOCA evaluations. During the NRC/B&W Owners Group meeting of December 16, 1980 these concerns were clarified. The concern addressed the possibility of a large pressure disturbance after CFT actuation due to the ECCS injection location. In order to respond to this concern, previous B&W small-break transient evaluations were reviewed to determine whether they exhibit the system disturbance of concern. The review of these previous analyses showed that the downcomer liquid volume remains high throughout the transient. As a result of this high liquid content, the use of the thermodynamic equilibrium assumption does not illustrate the system disturbance of concern. The system depressurization characteristics are not significantly altered. Thus, the ECC injection modeling employed in the B&W evaluation model provided an adequate representation of the actual phenomena and the system responses. Details on the evaluation of the previous analyses are provided in Appendix D.

In NUREG-0565, Section 4.2.11, the staff expresses the following concern:

Concern

All sources of non-condensible gas generation in the RCS must be taken into consideration, including radiolytic decomposition, to determine the effect on the small-break transient. In addition, it was recommended that the licensees provide "confirmatory information to verify the predicted condensation heat transfer degradation" in responding to this concern.

Response

In response to this concern, all sources of non-condensible gas, including the radiolysis will be accounted for to assess the impact of non-condensibles on the small-break transients. The condensation heat transfer degradation model

used to assess the impact of non-condensibles on SBLOCA transients has been developed by investigating the available literature of industry data including the B&W Single-Tube Condensation Test results at ARC. The details on the degradation of condensation heat transfer model are provided in Appendix I (section 1.56) of the CRAFT topical report.

5.5.2. Concerns in NUREG-0623

The following two concerns are identified in NUREG-0623:

Concern No. 1

In NUREG-0623, Section 4.2.2, the staff expressed a concern that the two-phase flow treatment in CRAFT is not adequate to calculate the distribution of liquid in the primary system during a small break with reactor coolant pumps operating.

Response

In response to this concern, the drift-flux model was developed and incorporated in the CRAFT2 code. The details on the drift-flux model are provided in Appendix I (section 1.31) of the CRAFT2 topical report. The adequacy of the two-phase flow model was demonstrated by the successful prediction of the LOFT L3-6 test submitted to the NRC in April 1981.[5]

Concern No. 2

In NUREG-0623, Section 4.3.5, the NRC raised a concern that the two-phase pump model currently used in the evaluation of small-break transients does not adequately model the degradation of pump head and hydraulic torque during two-phase operation.

Response

In response to this concern, a new pump model was developed and incorporated into CRAFT2. The new pump model will account for the degradation of pump head and torque in a two-phase environment. The new pump model is described in Appendix I (section 1.4) of the CRAFT topical report.

5.5.3. Concern Raised at December 16, 1980, Meeting

During the NRC/B&W Owners Group meeting of December 16, 1980, a concern was raised that B&W's subcooled/saturated discharge model in the existing evaluation model may be non-conservative with respect to a "best-estimate" discharge model.

Response

The B&W small-break evaluation model utilizes an orifice-Moody discharge model with a discharge coefficient of 1.0 throughout the transient. Evaluations were performed to compare the RC system response with the "best-estimate" and existing leak discharge models. The existing leak discharge model produced results that were similar to but conservative in comparison with the "best-estimate model. Hence, no modifications are necessary to the leak discharge model used in the evaluation model. Appendix A contains the report discussing the selected "best-estimate" discharge model and the results.

5.6. Summary and Conclusions

It has been shown that the small-break evaluation model conforms to Appendix K. The techniques involved were developed specifically to model the unique behavior of a small-break accident accurately. It is also shown that the concerns identified in NUREG-0737, Section II.K.3.30, with regard to small-break LOCA methods are also fulfilled by the small-break evaluation model.

Figure 5-1. Small Break Analysis Code Interface

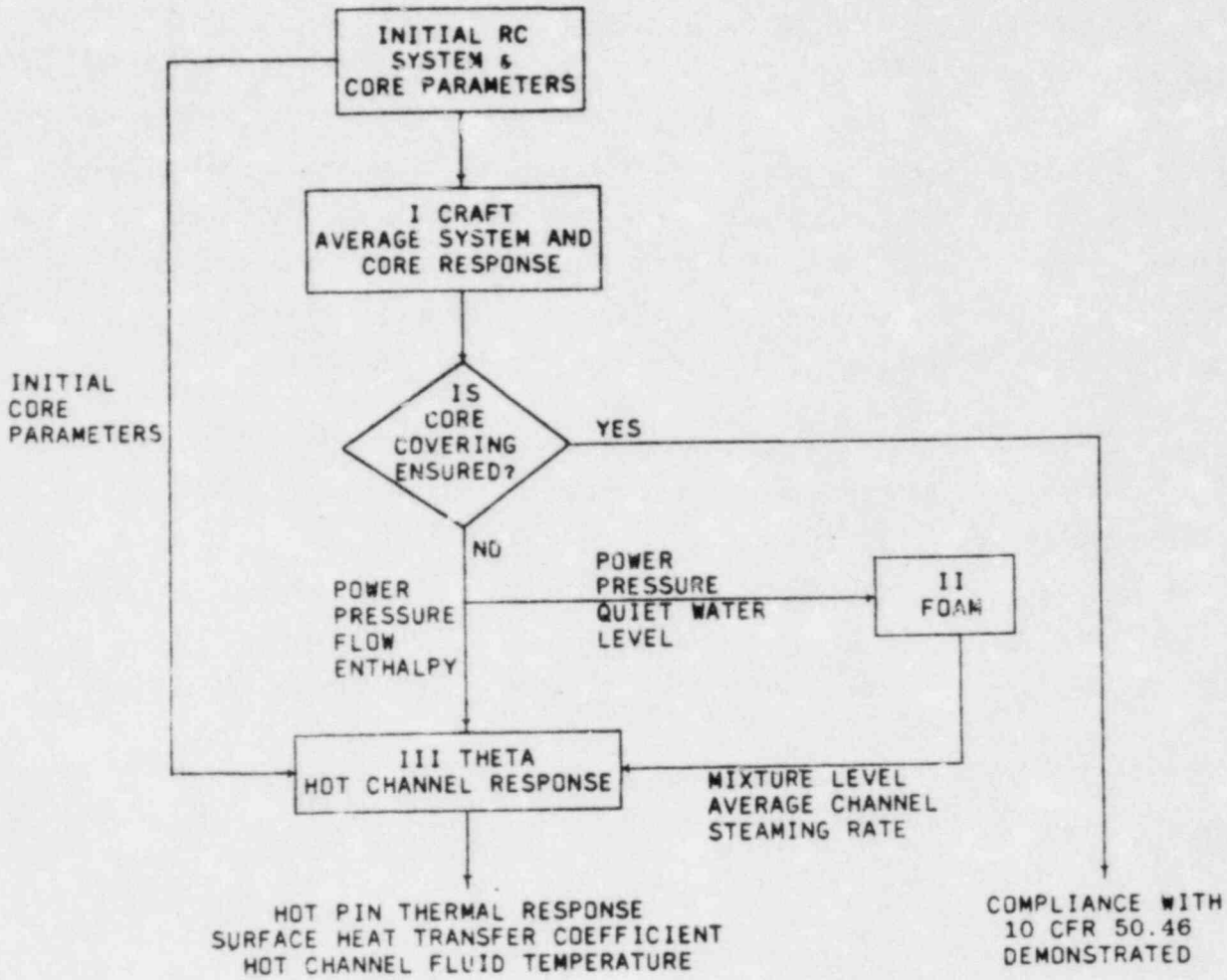

6. MAXIMUM HYDROGEN GENERATION, COOLABLE GEOMETRY, AND LONG-TERM COOLING

6.1. Maximum Hydrogen Generation

Criterion 3 of 10 CFR 50.46 states that the maximum amount of cladding oxidation during a LOCA shall be limited to 1% of the whole core cladding. Demonstrating compliance involves evaluating the metal-water reaction at all core locations. Using a conservative approach, it is demonstrated in section 6 of (approved) BAW-10104, Rev. 3, that adequate methods exist for calculating oxidation formation during a LOCA.

6.2. Coolable Geometry

Criterion 4 of 10 CFR 50.46 states "calculated changes in core geometry shall be such that the core remains amenable to cooling." It is demonstrated in section 7 of (approved) BAW-10104, Rev. 3, that adequate methodology exists for determining "coolable geometry."

6.3. Long-Term Cooling

Criterion 5 of 10 CFR 50.46 states that a low core temperature must be maintained following the calculated successful initial operation of the ECCS and that decay heat must be removed for an extended period of time. This section describes the method of compliance with this criterion.

The analysis of a LOCA is continued until the cladding temperatures at all locations in the core are decreasing and the fluid level in the core is rising. At this time the path to long-term cooling is established. Cooling for the long term is by circulation through the vessel maintained by the ECCS.

The onset of long-term cooling is defined as the time after a LOCA when the ECC systems are properly aligned and minimum performance requirements are met.

The operator actions needed to initiate long-term cooling and the required actions to be performed during its duration are addressed in specific plant analyses. For each required operator action, the instrumentation that provides the required information to the operator is described. The basis for the onset of long-term cooling is related to the performance requirements of the ECC systems and reasonable operator response time.

The duration of long-term cooling is the period between its onset and the end of the need of core cooling requirements by the ECC systems. The end of ECC cooling requirements is the time when the core is removed from the reactor vessel or when other permanent means are provided for core heat removal. The exact duration of long-term cooling will vary depending on several factors, including the size of the break and the radiation release.

6.2. Boric Acid Concentration

Since all ECC systems inject borated water, salts could build up, which could precipitate and block core channels during long-term cooling. This concern is addressed in specific analyses for each B&W plant type.

After a LOCA, there is a period during which a natural circulation loop will exist in the reactor vessel. The flow path is downcomer-core-upper head-vent valves-downcomer. This circulation will be adequate to prevent rapid increases in solute concentrations. The situation will exist for several days (and possibly for several months).

During the natural circulation period, alternate sources can be established and operated to maintain the solute concentrations below their solubility limits. The alternate source will depend on the plant type being analyzed and will be addressed in specific plant reports. The analyses will be performed in a conservative manner. All active components in the systems that will be relied on will be qualified to operate in the post-LOCA environment. System requirements will be set to meet the single-failure criterion and will provide adequate dilution to preclude precipitation within the reactor vessel.

7. REQUIRED DOCUMENTATION

This section verifies compliance with the documentation requirements (Part II) of Appendix K to 10 CFR 50.

II. Required Documentation

1.a. The computer codes that form the basis for the ECCS evaluation model are described in the following B&W topical reports:

CRAFT	BAW-10092
THETA	BAW-10094
FOAM	BAW-10064

These descriptions include the derivations of the equations used in the codes, starting with the fundamental physical laws, and all approximations.

These topical reports describe the manner in which the computer codes are used in the evaluation model. Included in each is a description of the code interfaces, the manner in which the codes are used, and the basis for selection of input parameters.

1.b. Any changes in the ECCS evaluation model that result in a deviation of more than 20F in the calculated cladding temperature transient will be documented by appropriate amendments to the evaluation model description.

1.c. The Nuclear Regulatory Commission has been provided with complete listings of each computer program.

2. Convergence of solution techniques are demonstrated by system modeling and noding sensitivity studies described in section 5.3.2 of this report.

3. Predictions and experimental data are being compared continually for the evaluation model and portions of it. Many such comparisons have been made in the past and will continue as new experimental data become available. The latest comparisons are listed below.

   a. Pre-test and post-test predictions of Semiscale Test S-07-10B/10D.
   b. Pre-test and post-test predictions of LOFT test L3-1.
   c. Post-test analysis of Semiscale Test S-NC-2.
   d. Benchmark against B&W plant transient of high-pressure reactor trip data.
   e. Post-test analysis of LOFT Test L3-6 (pumps on).

   This information has been reported to the NRC. Information on future comparisons will also be documented and supplied to the NRC.

4. The B&W topical reports that describe the ECCS evaluation model, provide the technical basis for the adequacy of the computational methods, and provide compliance with 10 CFR 50.

8. REFERENCES

1 J. J. Cudlin, M. I. Meerbaum, and J. A. Klingenfus, CRAFT2 – Fortran Program for Digital Simulation of a Multinode Reactor During Loss of Coolant, BAW-10092, Rev. 3, Babcock & Wilcox, October 1982.

2 F. Aguilar and S. I. Abdel-Khalik, FOAM2 – Computer Program to Calculate Core Swell Level and Mass Flow Rate During Small Break LOCA, BAW-10064, Rev. 1, Babcock & Wilcox, June 1975.

3 R. V. Straub and K. C. Heck, THETA1-B – Computer Codes for Nuclear Reactor Core Thermal Analysis – B&W Revisions to IN-1445 (Idaho Nuclear, C. J. Hocevar and T. W. Wineinger), BAW-10094, Rev. 1, Babcock & Wilcox, April 1975.

4 B. M. Dunn, et al., B&W's ECCS Evaluation Model, BAW-10104, Rev. 3, Babcock & Wilcox, August 1977.

5 B&W's Best-Estimate Prediction of the LOFT L3-6 Nuclear Small Break Test Using the CRAFT2 Computer Code, Document No. 12-1124993-01, Babcock & Wilcox, March 1981.

6 B&W's Post-Test Evaluation of LOFT Test L3-1, Document No. 51-1125988-00, Babcock & Wilcox, May 1981.

7 B&W's Post-Test Analysis for Semiscale Test S-07-10D, Document No. 86-1125888-00, Babcock & Wilcox, May 1981.

APPENDIX A

Comparison of SB Core Heat Transfer Model to ORNL SBLOCA Heat Transfer Tests

1. Summary

The small break core heat transfer model employed by B&W was compared for steady-state conditions to six tests performed at Oak Ridge National Laboratory (ORNL). These tests were designed to evaluate the steam cooling capability within a core in which the fluid level was allowed to fall below the top of the active core region and stabilize at an intermediate location. Core cooling under these conditions would be accomplished through pool boiling below the swell or fluid level, and by steam cooling above the swelling. The comparisons were made for that portion of the core above the swell level.

The comparison of the ORNL heat transfer test data to the B&W techniques demonstrate that utilization of the Dittus-Boelter correlation as the sole determination of heat transfer is acceptable for determining compliance to 10 CFR 50.46. For the low flow tests that are most representative of SBLOCA conditions that would be predicted for the B&W-designed NSS, the combined convective and radiant heat transfer from the ORNL tests was higher than the Dittus-Boelter prediction when clad temperatures exceed 1000F. Due to the conservatism of the Dittus-Boelter heat transfer correlation at high cladding temperatures, the present heat transfer model is acceptable for licensing evaluations.

2. Introduction

A small break loss-of-coolant accident (SBLOCA) can undergo temperature excursions within the core when a portion of the core is uncovered. Experiments conducted at General Electric[1], Hitachi[2], and Westinghouse[3], as well as the experimental work within B&W,[4] have shown that at the decay heat levels present in SBLOCAs, the portion of the core that is below the swell level remains within a few degrees of the saturation temperature. However, the mechanism for cooling the core above the swell level is forced convection to steam. For this reason, during partial core uncovering, the region of the core above the swell will undergo a temperature excursion. ORNL performed a series of SBLOCA heat transfer experiments[5] to evaluate the effectiveness of the mode of heat transfer above the swell level.

The objective of the ORNL test series and the ensuing analysis was to derive experimental heat transfer coefficients and to formulate a heat transfer model

capable of predicting heat transfer coefficients during core uncovering conditions. Six tests were performed in the ORNL electrically heated test reactor. The six tests varied pin powers and reactor coolant system (RCS) pressures under steady-state conditions at different mixture levels within the core region.

Analyses of the ORNL heat transfer tests have been performed using the Dittus-Boelter correlation as specified in the present B&W SBLOCA evaluation model.[6] These analyses, reported herein, assess the validity of the present model. The method of analysis and the results obtained are presented in sections 4 and 5, respectively.

3. Conclusion

The comparison of the ORNL heat transfer test to B&W techniques indicates that utilization of the Dittus-Boelter correlation as the sole determination of heat transfer is acceptable for determining compliance to 10 CFR 50.46. For the low flow tests, which are most representative of B&W SBLOCA conditions, the combined convective and radiant heat transfer from the ORNL tests was higher than the Dittus-Boelter prediction when cladding temperatures exceed 1000F. For all tests, the predicted heat transfer was conservative, relative to the ORNL test data, for cladding temperatures above 1400F. Due to the conservatism of the Dittus-Boelter heat transfer correlation at high cladding temperatures, the present heat transfer model is acceptable for licensing calculations.

4. Method of Analysis

In this evaluation, the FOAM code[7] was used to predict the ORNL heat transfer data. FOAM is the computer code used by B&W to calculate the core mixture level if the SBLOCA transient analysis predicts core uncovering. The capability of the code to predict core mixture levels was demonstrated in reference 7 by benchmarking the code to the mixture level data of references 1 through 3. The FOAM code also has the capability to predict steady-state heat transfer coefficients and cladding temperatures above the core mixture level. The code utilizes the Dittus-Boelter correlation to predict the convective heat transfer coefficient and assuming all core heat is removed through the cladding, the resultant steady-state cladding temperature is obtained. Since the THETA1-B code,[8] used for cladding temperature predictions within the B&W

ECCS evaluation model, also uses the Dittus-Boelter correlation, comparison of the FOAM heat transfer coefficient predictions to the ORNL data directly assesses the capabilty of the evaluation model to predit cladding temperatures above the core mixture level.

The Dittus-Boelter heat transfer model was isolated in FOAM by manipulating FOAM's input and output to be consistent with the ORNL data and results. Steady-state conditions for both FOAM and ORNL were maintained by allowing the subcooled mass flow into the core to equal the steam mass flow out of the core. The axial power profiles modeled in FOAM were flat, consistent with the ORNL experiment. The area of the assembly was the square of the fuel rod pitch multiplied by the number of rods in the assembly, since the rods adjacent to the vessel wall are one-half the pitch (Figure A-1). All other inputs into FOAM were taken directly from reference 5. These inputs included heated perimeter (Ph), flow area (A), heat flux (Q), mass flux (G), system pressure (P), and mixture level (Zm).

To prevent induced error in the heat transfer calculations, the FOAM and ORNL mixture heights were equated by iterations on inlet subcooling. The ORNL facility consisted of a 64-rod test assembly surrounded by an unheated shroud. To prevent the shroud and unheated rods from affecting the comparisons, the data taken for comparison were from a rod one row removed from any unheated structures. The rods analyzed were the fuel rod simulator (FRS) type 1, shown on Figure A-2. The other rods examined by ORNL were exposed to the relatively colder shroud or unheated rods.

5. Results

As illustrated in Figure A-3, fluid and cladding temperature measurements for the ORNL tests were taken at the 11.9- and 9.9-foot elevations in the core. Results of the analyses performed for the type 1 FRS at these elevations are summarized in Tables A-1 through A-3. Table A-1 contains the results of the FOAM analyses, which includes fluid and cladding temperatures and convective heat transfer coefficients. FOAM contains only a convective heat transfer model.

Table A-2 contains the results of the ORNL analysis from reference 5. It includes fluid and cladding temperatures, and convective, radiation to steam, and total heat transfer coefficients. The radiation and convective terms make

up the total heat transfer coefficient. As noted on the table, the radiation heat transfer accounted for 20 to 30% of the total heat transfer.

Table A-3 is a comparison of the FOAM and ORNL results based on the data tabulated in Tables A-1 and A-2. Convective HTCs are compared since they are common to both the FOAM and ORNL analyses.

Figures A-4 through A-9 graphically summarize the results shown in Tables A-1 through A-3. These figures show the comparison of the heat transfer correlations deduced by ORNL from the tests and those predicted by the B&W evaluation model for the same conditions as a function of cladding temperature. The figures show the B&W total heat transfer coefficient (i.e., from the Dittus-Boelter correlation), the total heat transfer coefficient observed in the test, and the convective heat transfer coefficent obeserved in the test. The ratio of the total test heat transfer coefficient to the B&W heat transfer coefficient is plotted at the bottom of each figure. The solid portion of the lines provide the span of the data or the calculations. The dotted portions are extrapolations.

As can be seen, the Dittus-Boelter correlation significantly overpredicted the convective heat transfer coefficient over the tested range. Based on the data, it appears that the cladding temperature must exceed 1800F before the convective heat transfer coefficient predicted by the Dittus-Boelter correlation is smaller than the measured heat transfer coefficient. However, as noted in Table A-2, radiation heat transfer from the fuel rod to the superheated steam was a significant fraction of the total heat transfer coefficient obtained in the ORNL tests. The radiation heat transfer coefficients for the experiment are illustrated in Figure A-10. The present B&W core heat transfer model does not include a radiation heat transfer model. On the basis of total heat transfer, the B&W technique is conservative for cladding temperatures above 1400F.

A further insight into the results can be obtained by arranging the tests as a function of steam flow rate. Figure A-11 shows that the Dittus-Boelter correlation becomes conservative as the flow is reduced. The significance of these results is obtained by examining the flow rates characteristic of a SBLOCA. These maximum flow rates are on the order of 0.5×10^4 lbm/h. From this figure, it is concluded that the B&W technique will predict conservative cladding temperatures for all cladding temperatures above 1000F.

Flow in the ORNL tests was atypically high for two reasons. The ORNL power shape was flat in both the radial and axial dimensions. An actual core would have a shaped power distribution in both dimensions. Power distributions for small break evaluations are typically peaked to the core outlet to provide conservative cladding temperature predictions. With a power level at the value used in the ORNL experiments, which was typical of SBLOCA conditions, smaller steam flow rates would be obtained in the small break evaluations. This is graphically shown in Figure A-12, which illustrates that the integral of the core power up to the mixture level will be significantly lower for the power distribution analyzed in small break evaluations when compared to the flat axial profile used in the ORNL experiments. The integral of the core power level up to the mixture level is a direct measure of the core steaming rate and, as noted on Figure A-12, the steaming rate expected in small break evaluations is approximately 67% of that utilized in the ORNL experiments.

In addition to the axial power profile effects on core steaming rate, there is a radial peaking effect. A typical design radial peaking factor is 1.5. The B&W evaluation model uses, as a conservatism, the average core power for steam production even when cooling the hot channel. As a result of this assumption, the power to flow ratio for the ORNL experiment will be about 1.5 times that used in a small break evaluation.

Although the tests do not provide data directly applicable to small break situations that might be incurred in a SBLOCA transient in a B&W plant, the data clearly illustrate the conservatism in the present heat transfer model at high temperatures. As can be seen by examining Figures A-4 thorugh A-9, the Dittus-Boelter correlation does not predict the data trends, observed by ORNL, for the convective heat transfer coefficient. This is further substantiated by Figure A-13, which is the ORNL comparison from reference 5, of the Dittus-Boelter correlation to the convective heat transfer coefficients obtained from all the FRS. However, since radiation heat transfer, which is a substantial portion of the overall heat transfer, is not included in the B&W model, the Dittus-Boelter correlation provides a conservative prediction of the total heat transfer for all the ORNL test data once the cladding temperatures are above 1400F.

In summary, the analyses of the ORNL data indicate that the present core heat transfer model will provide a conservative assessment of the total heat transfer coefficient for cladding temperatures above 1400F. Since this is well removed from the 2200F peak cladding temperature allowed by 10 CFR 50.46, the Dittus-Boelter correlation is acceptable for licensing evaluations.

6. References

1. Amendment 12, Wm. H. Zimmer Nuclear Power Station PSAR, Docket 50-358, Cincinnati Gas & Electric Company, Cincinnati, Ohio, April 1970.

2. H. Ogasawara, et al., Cooling Mechanism of the Low Pressure Coolant Injection System of Boiling Water Reactors and Other Studies on the Loss-of-Coolant Accident Phenomena, Hitachi Research Laboratory, Hitachi Ltd., Japan (1973).

3. J. P. Cunningham, O. J. Mendler, and R. W. Steer, Core Uncovering Test at 100 and 400 psi, DT-T&H-517, Westinghouse Electric Company, March 1973.

4. H. Windischmann, Level-Swell Emergency Core Cooling Tests for the PWR, ARC-8083, Alliance Research Center, Babcock & Wilcox, January 1974.

5. T. M. Anklam, ORNL Small Break LOCA Heat Transfer Test Series I: Rod Bundle Heat Transfer Analysis, ORNL/NUREG/TM-445.

6. B. M. Dunn, et al., B&W's ECCS Evaluation Model, BAW-10104, Rev. 3, Babcock & Wilcox, Lynchburg, Virginia, August 1977.

7. B. M. Dunn, C. D. Morgan, and L. R. Cartin, Multinode Analysis of Core Flooding Line Break for B&W's 2568-MWt Internals Vent Valve Plants, BAW-10064, Babcock & Wilcox, Lynchburg, Virginia, April 1973.

8. R. V. Straub and K. C. Heck, THETA1-B - Computer Codes for Nuclear Reactor Core Thermal Analysis - B&W Revisions to IN-1445 (Idaho Nuclear, C. J. Hocevar and T. W. Wineinger), BAW-10094, Rev. 1, Babcock & Wilcox, Lynchburg, Virginia, April 1975.

Table A-1. Results of FOAM Analysis

ORNL test[a] designation	Pressure,[a] psia	Power,[a] kW/ft	Two-phase[a] mixture level, ft	Mass flux,[a] x10^4 lbm/h-ft	Elevation,[a] ft	Fluid temp, F	Cladding temp, F	Convective[a] heat transfer coefficient, Btu/h-ft -°F
C	419	0.36	9.41	1.08	11.9	914	1413	25
					9.9	524	1024	25
D	613	0.25	8.50	0.68	11.9	1173	1630	19
					9.9	736	1244	17
E	617	0.41	8.99	1.30	11.9	975	1448	30
					9.9	613	1091	30
F	1018	0.27	8.46	0.75	11.9	1161	1608	21
					9.9	756	1225	20
G	1009	0.38	7.97	1.13	11.9	1210	1657	30
					9.9	825	1306	28
H	387	0.42	7.97	1.22	11.9	1228	1708	30
					9.9	809	1356	27

(a)From Table 1 of reference 5.

(b)B&W FOAM model does not contain a radiation model, the convective HTCs are its total heat transfer coefficient.

Table A-2. Results of ORNL Analysis

ORNL test designation[a]	Pressure, psia[a]	Power,[a] kW/ft	Two-phase mix level, ft[a]	Mass flux,[a] $\times 10^6$ lbm/h-ft^2	Elevation, ft[a]	Fluid temp, F[b]	Clad temp, F[b]	Convective HTC,[c] Btu/h-ft^2-°F	Radiation HTC,[d] Btu/h-ft^2-°F	Total HTC,[b] Btu/h-ft^2-°F	% radiation of total HTC, %[e]	Fluid superheat temp, F
C	419	0.36	9.41	1.08	11.9	881	1338	19.15	<.12	25.27	24	432
					9.9	526	1126	15.47	3.85	19.32	20	77
D	613	0.25	8.50	0.68	11.9	1006	1337	16.98	7.69	24.67	31	517
					9.9	649	1130	11.59	4.94	16.53	30	160
E	617	0.41	8.99	1.30	11.9	943	1415	20.95	7.89	28.84	27	454
					9.9	595	1273	15.64	5.42	21.06	26	106
F	1018	0.27	8.46	0.75	11.9	1050	1330	23.90	8.65	32.55	27	503
					9.9	689	1097	17.48	5.46	22.94	24	142
G	1009	0.38	8.97	1.13	11.9	1047	1437	22.89	9.38	32.37	29	501
					9.9	751	1261	18.33	6.59	24.92	26	205
H	387	0.42	7.97	1.22	11.9	1016	1443	23.35	7.10	30.45	23	470
					9.9	647	1222	18.49	4.55	23.04	20	206

[a] From Table 1 of reference 5.

[b] From data in reference 5 for rod type 1 only.

[c] From data in reference 5 for rod type 1 where convective HTC = (results of heat transfer computations) - (RAD HTC).

[d] From data in reference 5 for radiation to steam for rod type 1 where RAD to steam = (rod flux summary/ΔT).

[e] % (RAD HTC)/(Total HTC) × 100 = % radiation.

Table A-3. Comparison of FOAM to ORNL

ORNL test designation	FOAM/ORNL[a] Elevation, ft	Convective HTC	Total HTC
C	11.9/9.9	1.31/1.62	0.99/1.29
D	11.9/9.9	1.12/1.47	0.77/1.03
E	11.9/9.9	1.43/1.92	1.04/1.42
F	11.9/9.9	0.88/1.14	0.65/0.87
G	11.9/9.9	1.31/1.53	0.93/1.12
H	11.9/9.9	1.28/1.46	0.99/1.17

(a) FOAM total heat transfer model contains convective heat transfer only; ORNL heat transfer model contains convective and radiation-to-steam heat transfer model.

Figure A-1. Partial Assembly

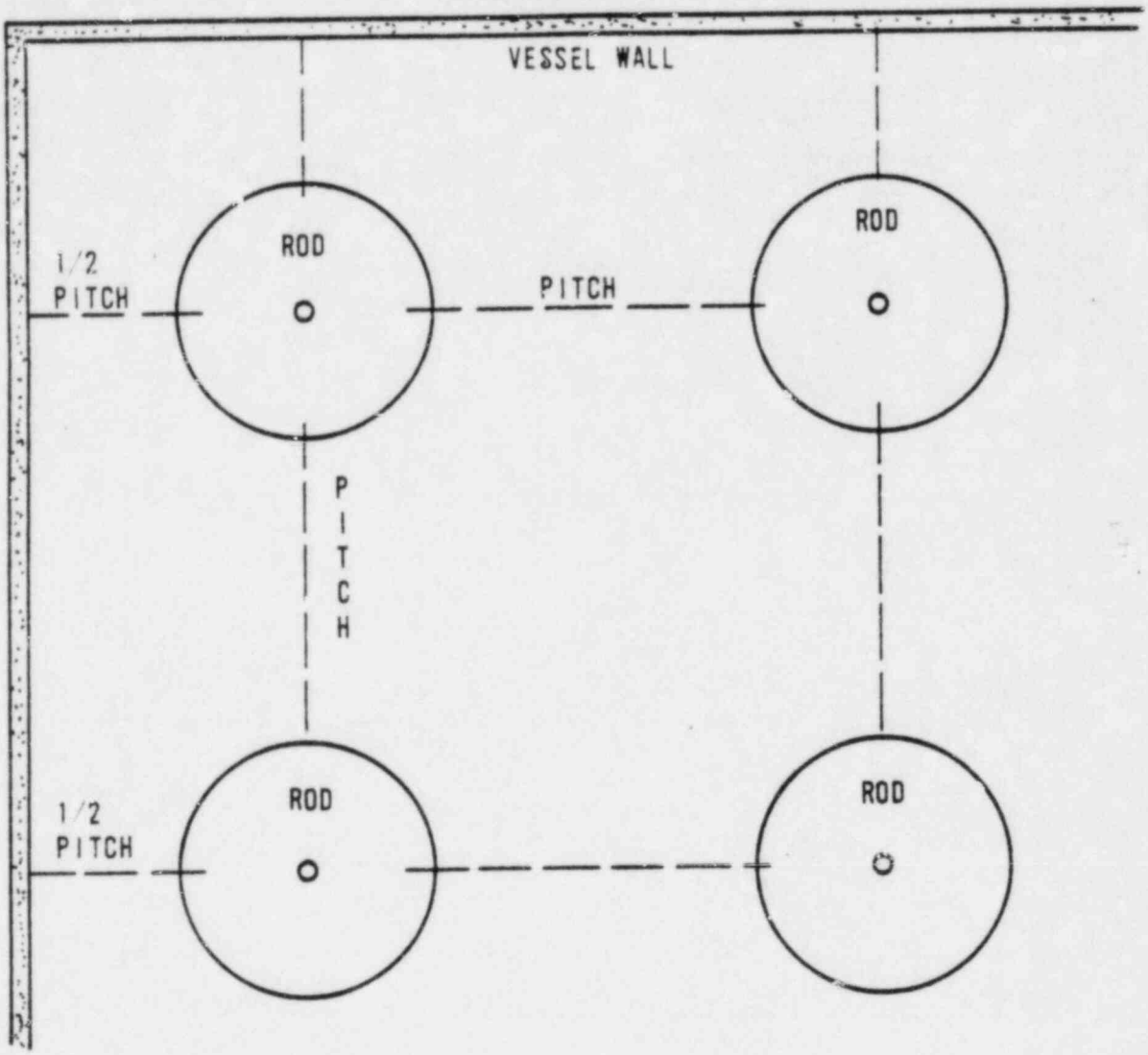

Figure A-2. Classification of THTF Bundle 3
Fuel Rod Simulators

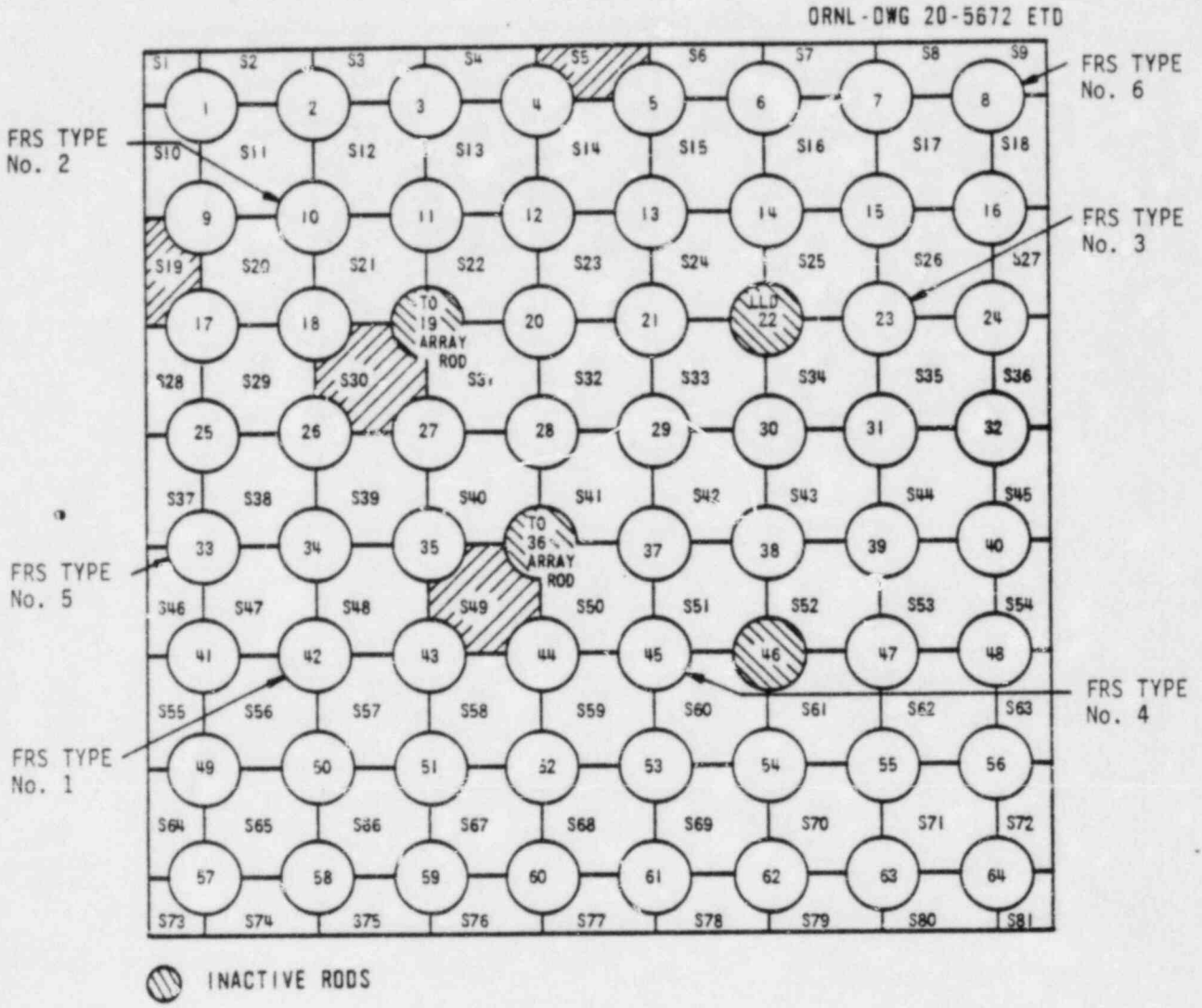

Figure A-3. Fuel Rod Elevation Diagram for ORNL Test

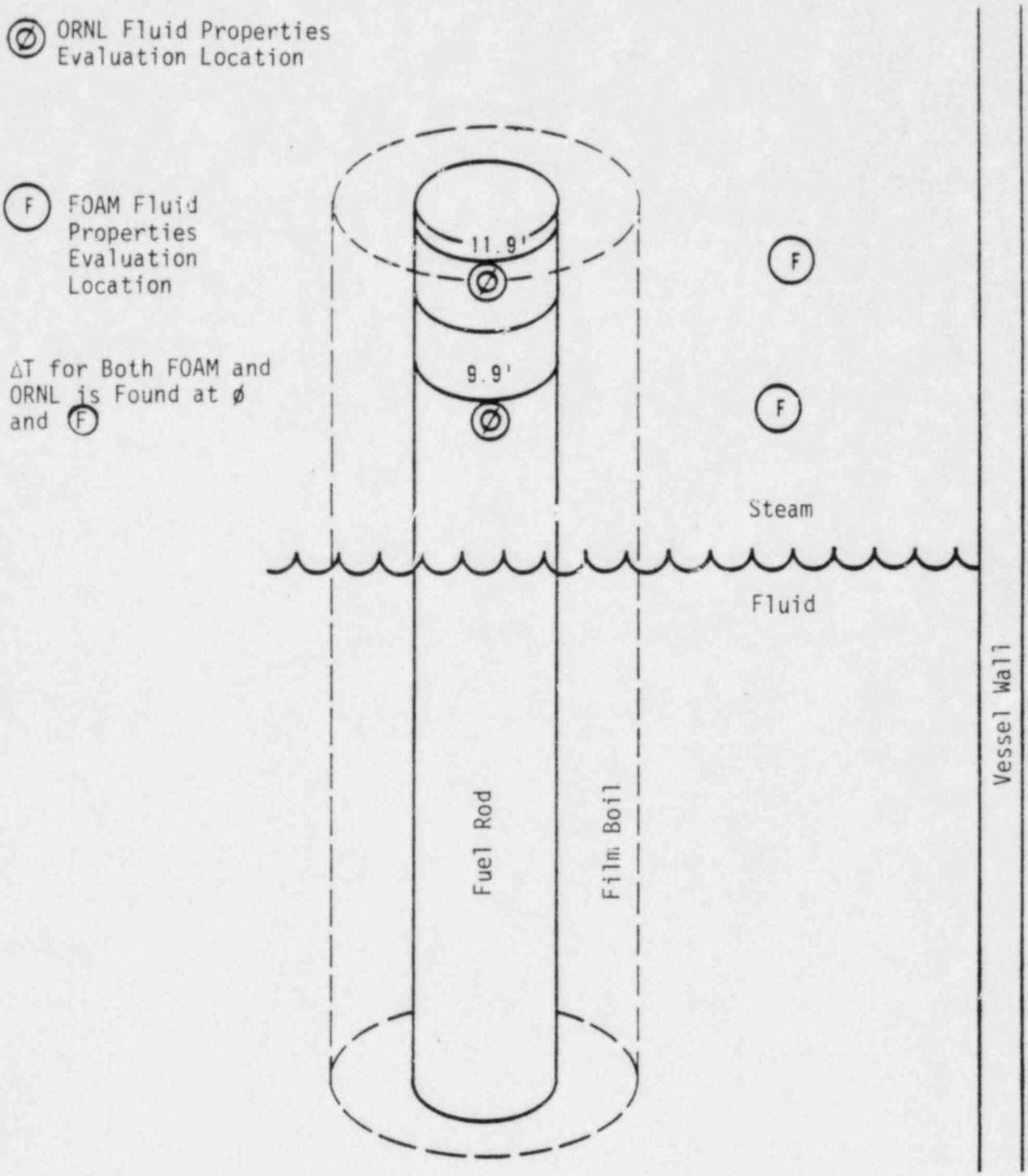

Figure A-4. Test C

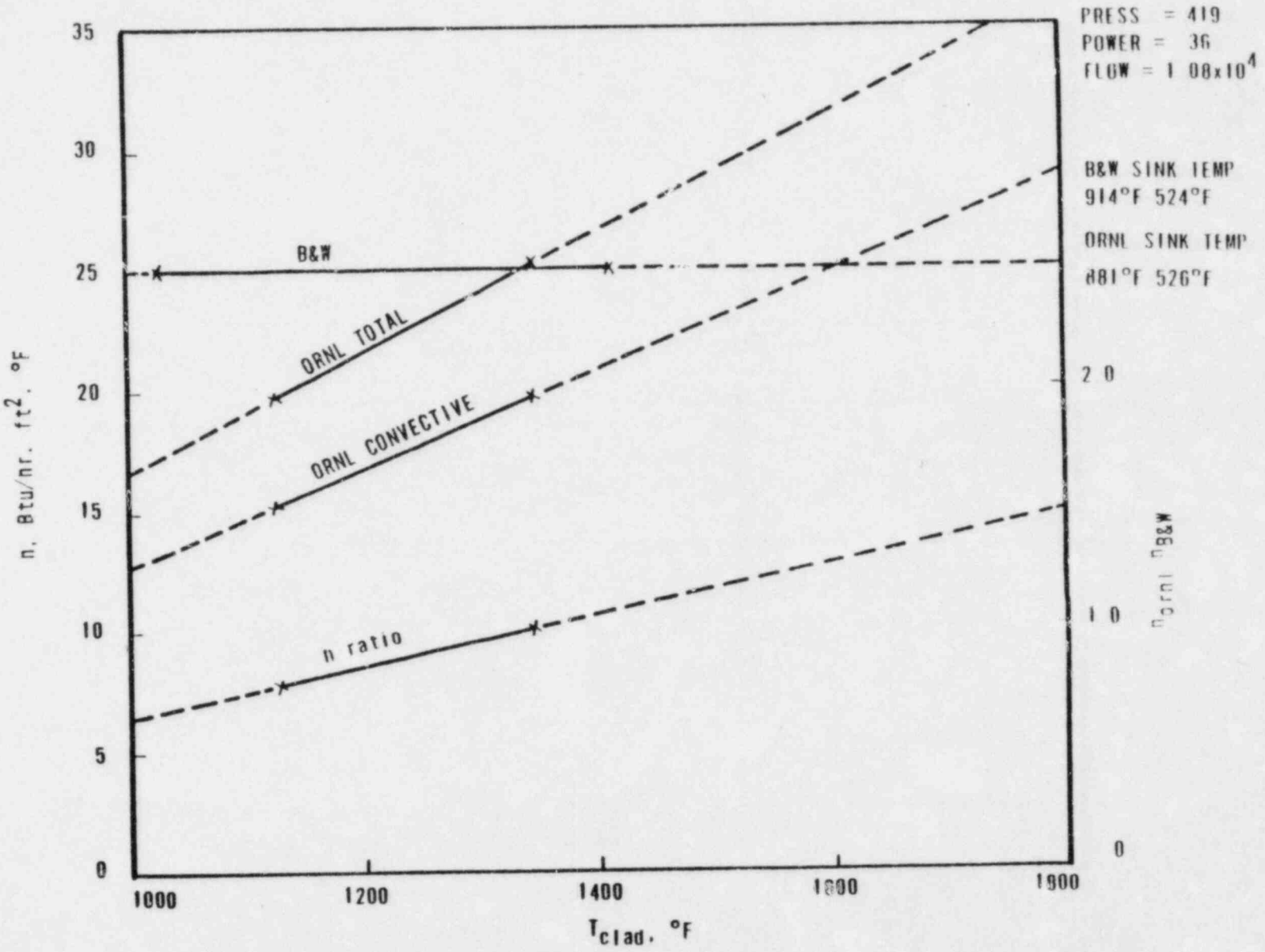

Figure A-5. Test D

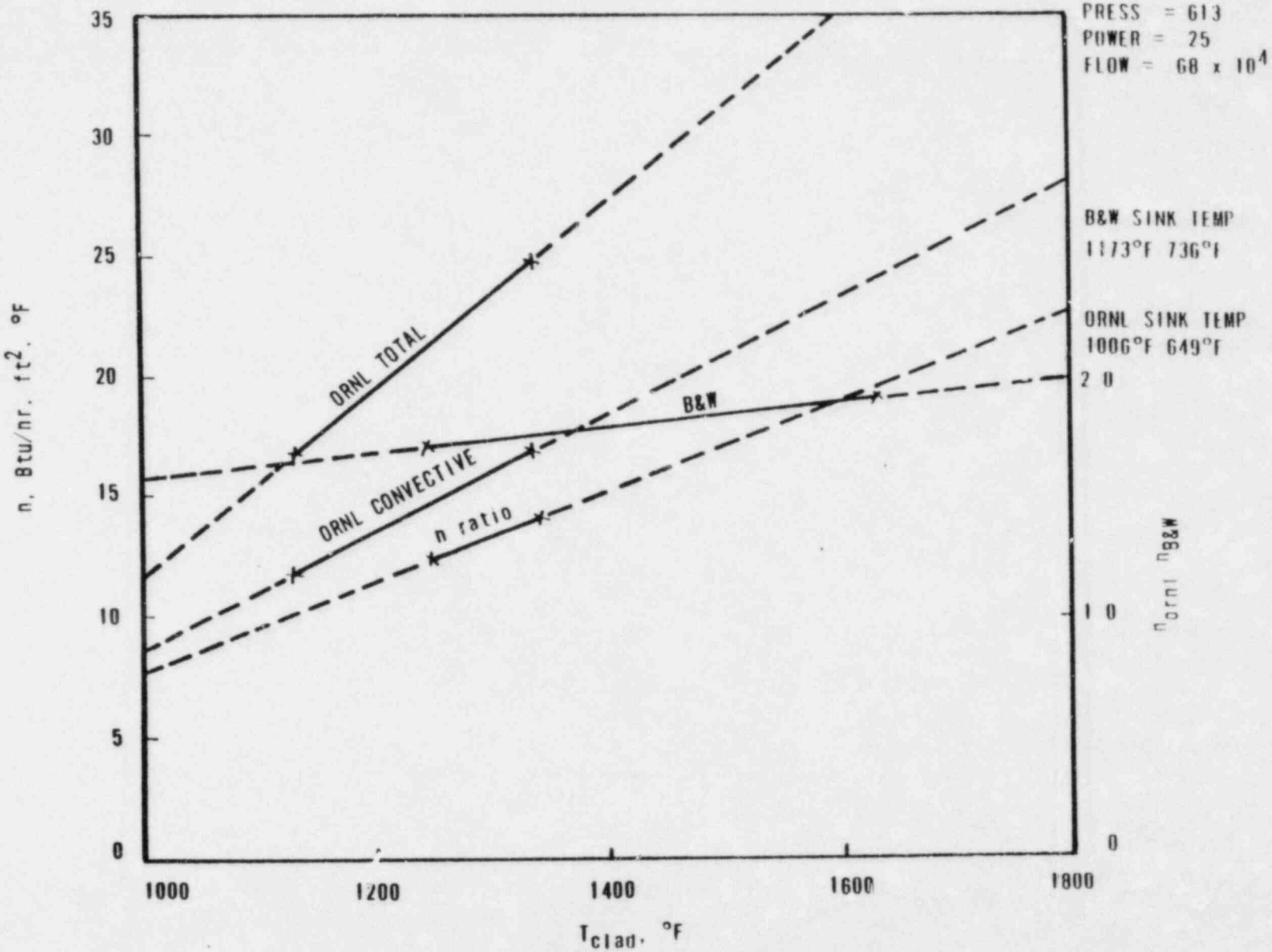

Figure A-6. Test E

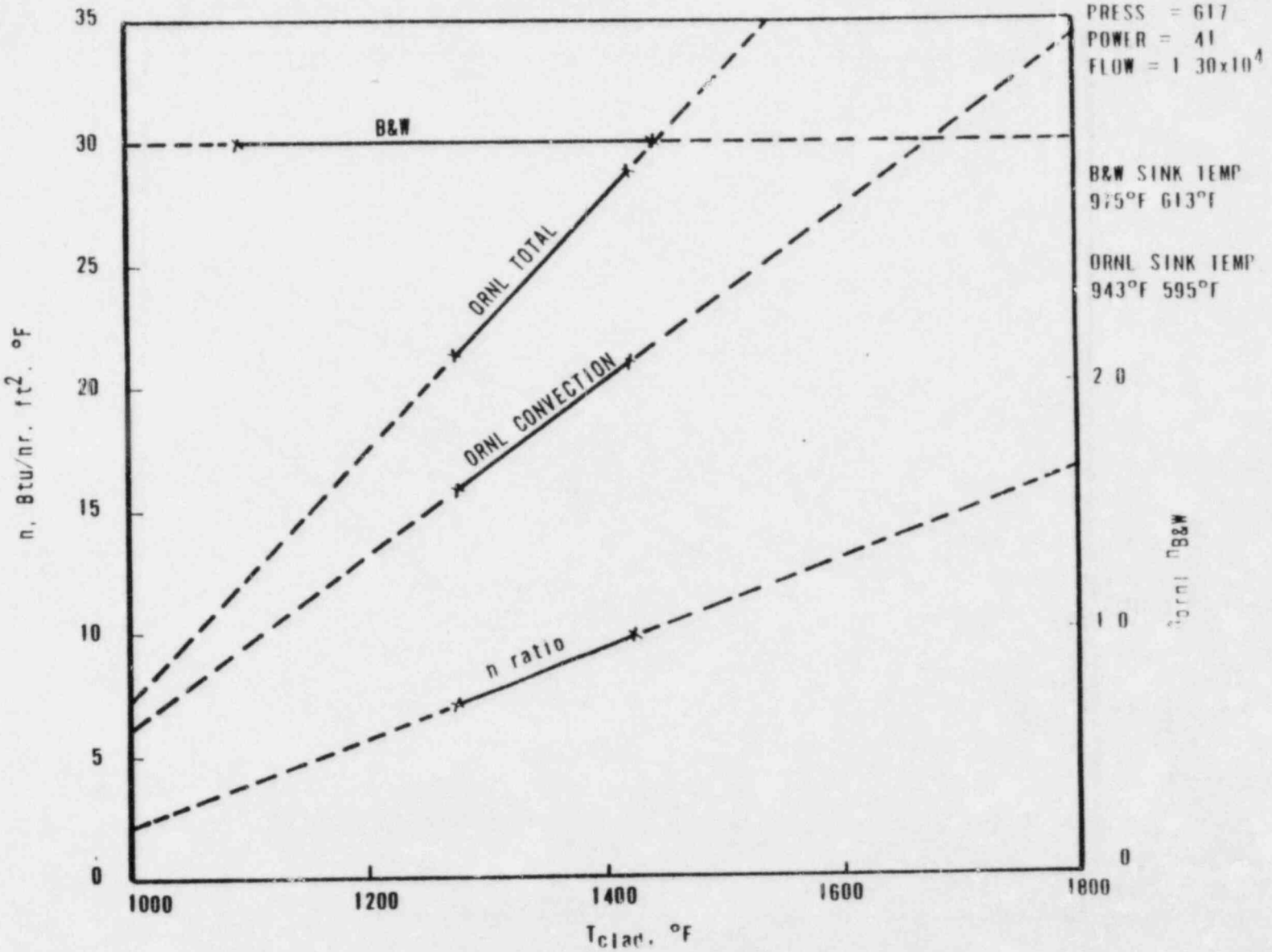

Figure A-7. Test F

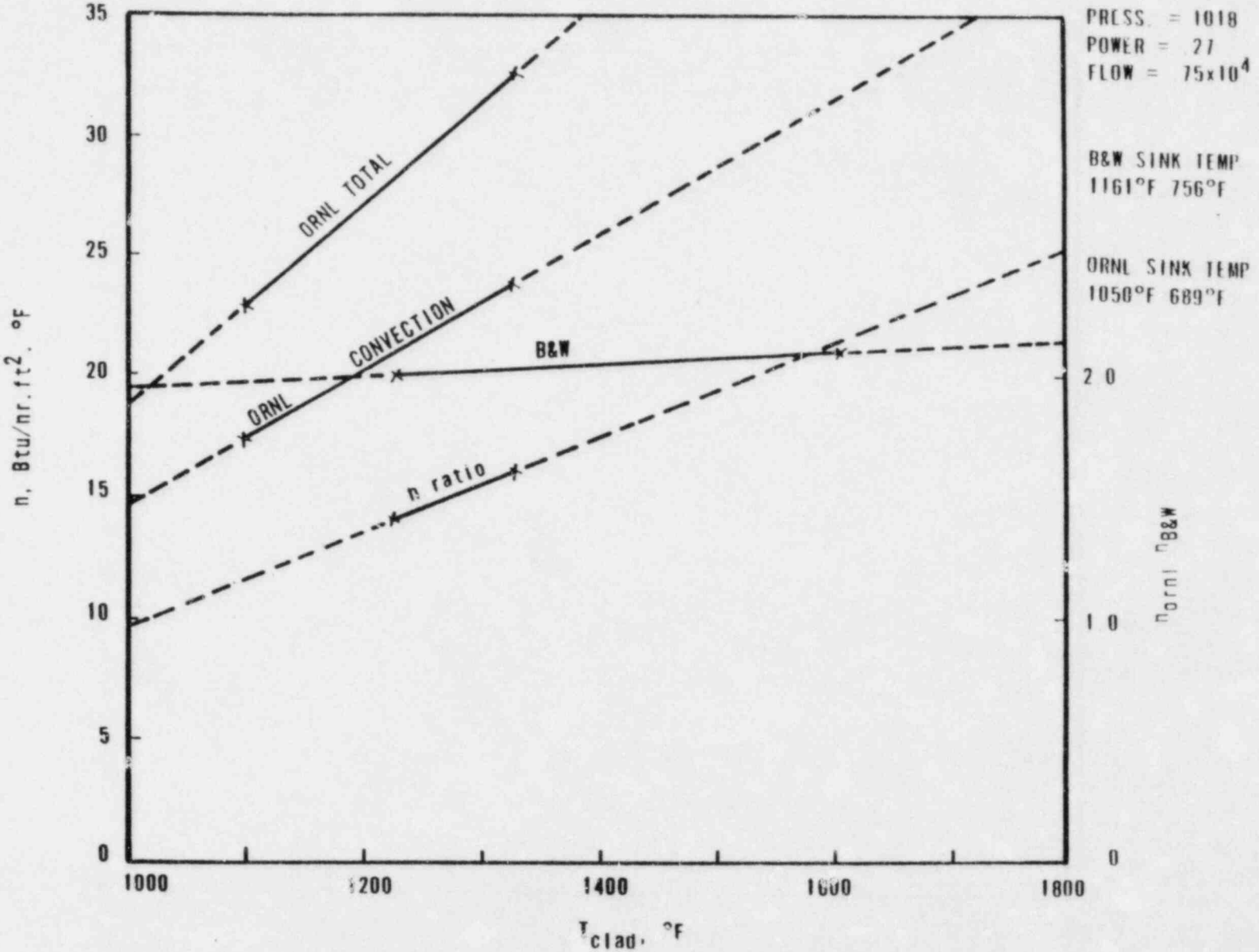

Figure A-8. Test G

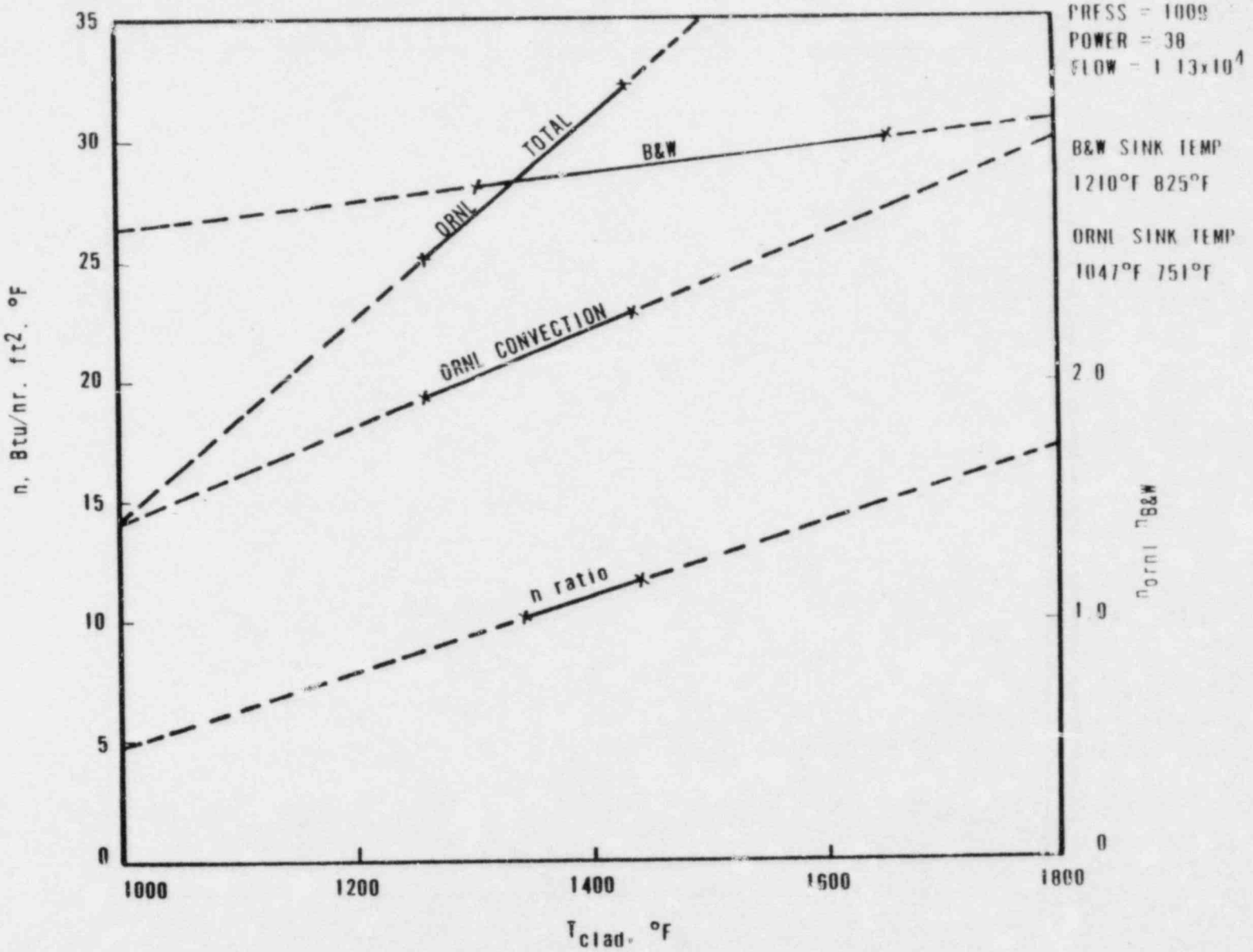

Figure A-9. Test H

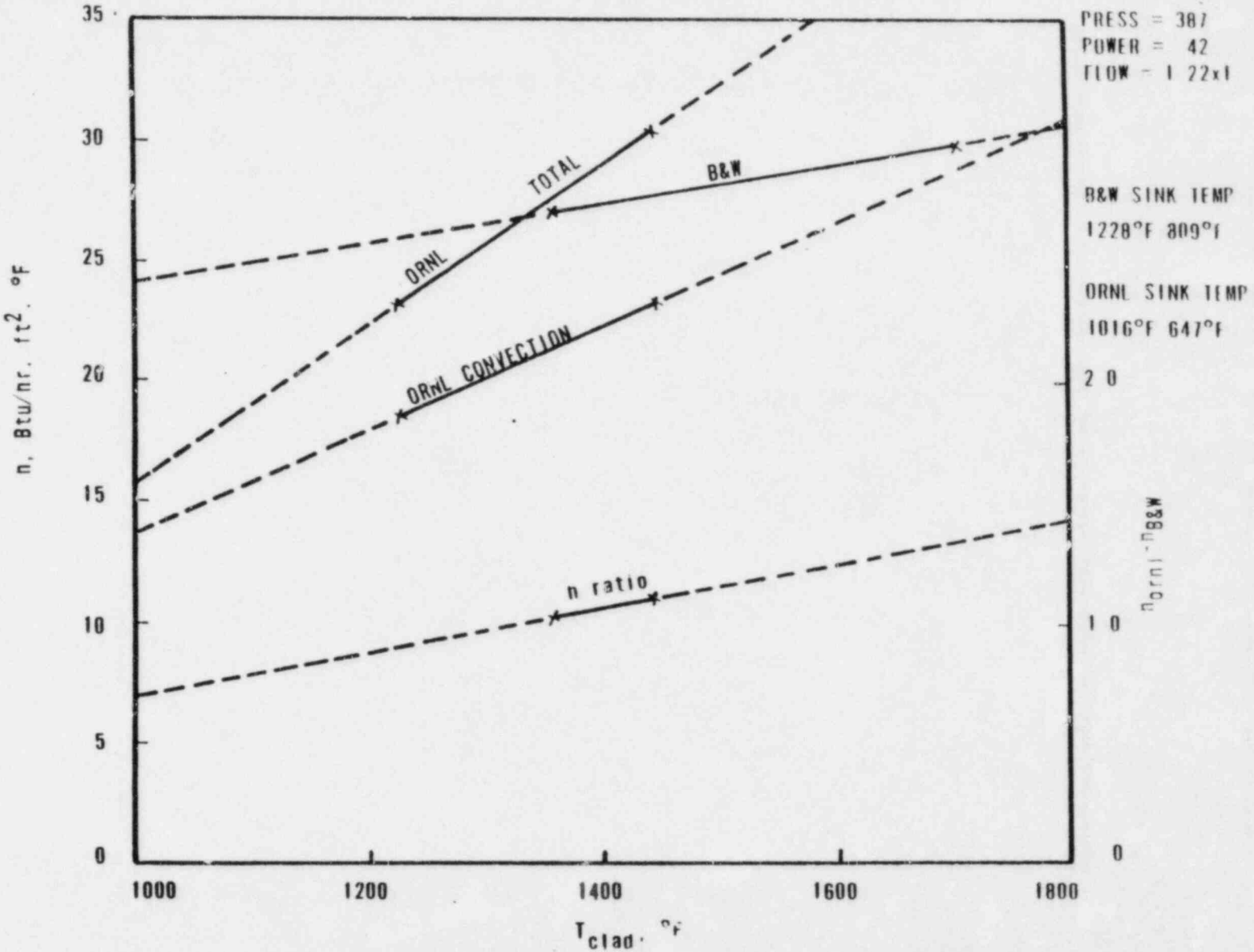

Figure A-10. Radiation HTC to Degree of Superheat

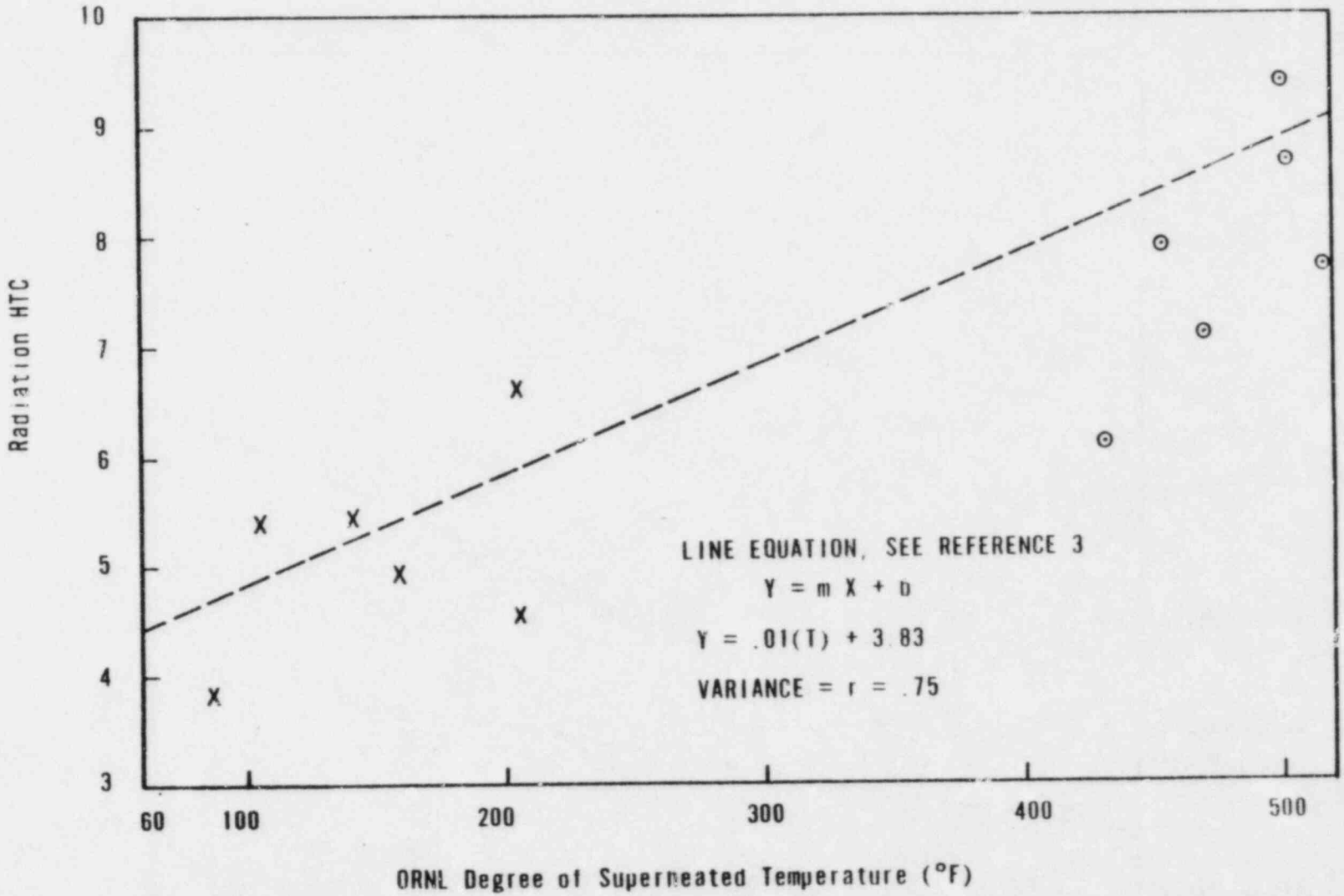

Figure A-11. Flow Rate Effect on Heat Transfer

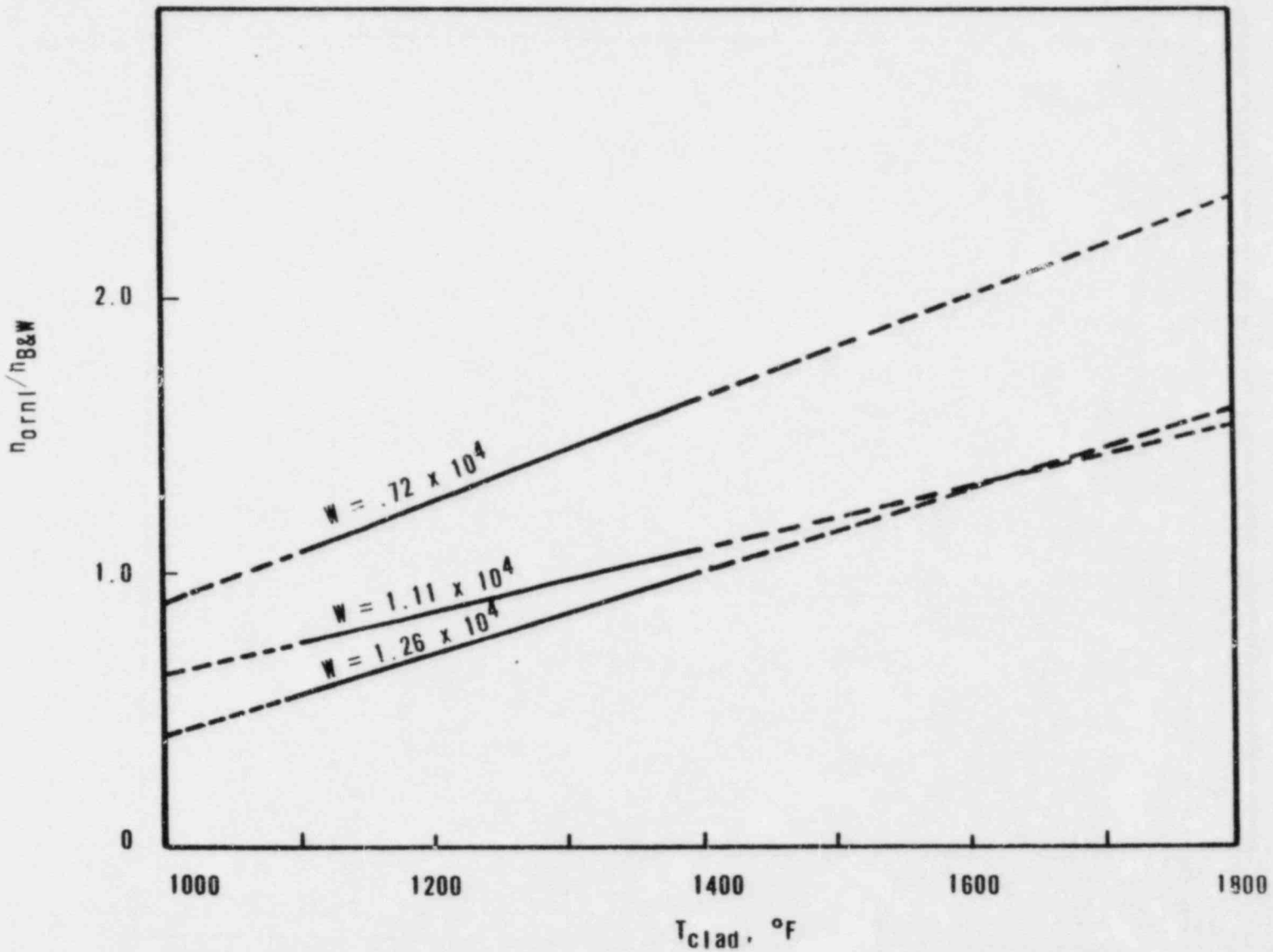

Figure A-12. Typical Core Shape Skewed Toward Core Exit

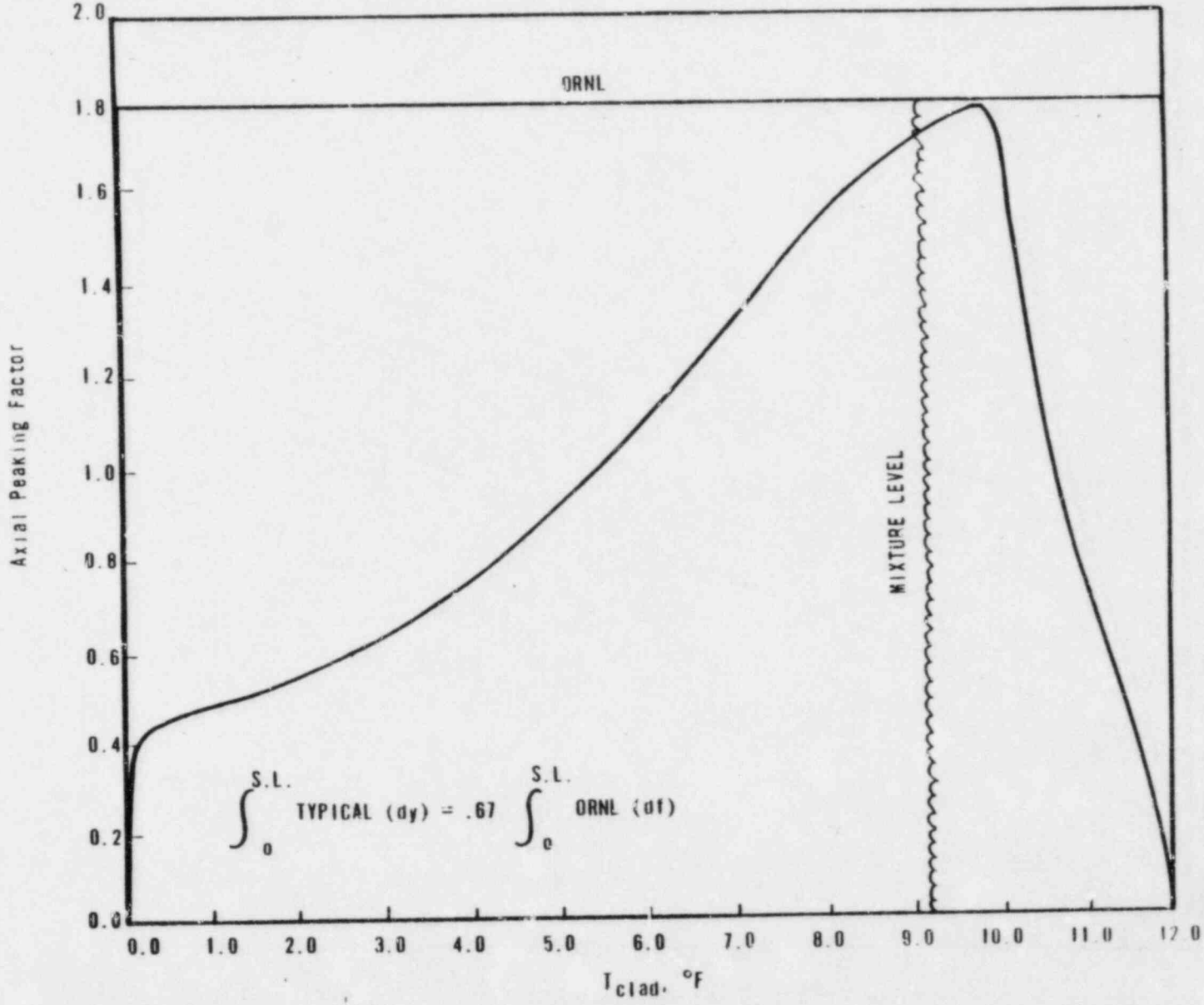

Figure A-13. Comparison of Dittus-Boelter Correlation to Data
(From Reference 5)

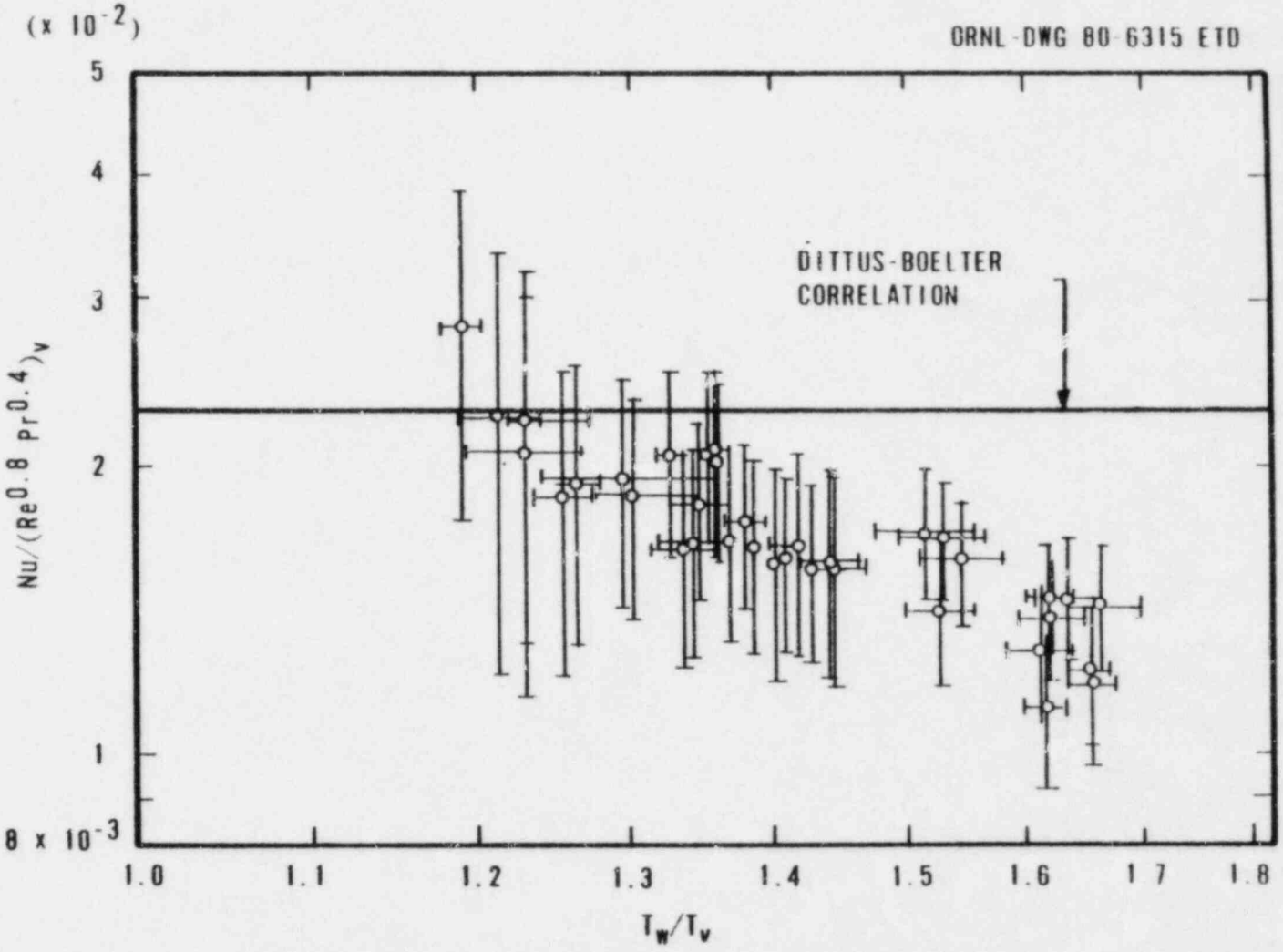

APPENDIX B
Leak Discharge Model

1. Introduction and Summary

During the December 16, 1980, meeting between the B&W Owner's Group and the NRC,[1] the NRC Staff identified a concern about the leak discharge models used in the ECCS evaluation model (EM). The staff stated that the present discharge models must be justified by demonstrating that they yield SBLOCA consequences that are in reasonable agreement with, or conservative with respect to, the consequences that would be obtained by using "best estimate" (BE) discharge models. Although this concern was not identified in NUREG-0565[2], and hence is not covered in Item II.K.3.30 of NUREG-0737[3], it has been addressed as part of the Small Break LOCA Methods Program. This report describes the results of a literature survey conducted to select and justify the best-estimate leak discharge model. It also provides the comparison of the present evalaution model with the selected best-estimate discharge model and addresses the validity of the present leak discharge model.

The B&W small break evaluation model utilizes an Orifice-Moody discharge model with a discharge coefficient of 1.0 throughout the transient. As a result of a literature survey, a best-estimate leak discharge model was selected. The selected model is the orifice equation for subcooled flow, with a discharge coefficient of 0.7, and the homogeneous equilibrium model (HEM) for saturated flow, with a discharge coefficient of 0.85. Justification of this model is provided in section 2. The calculated reactor coolant (RC) system response with the selected model is compared to that of the existing model for the worst area break in section 3. The existing leak discharge model produced results that were similar to, but conservative with respect to, those obtained with the best-estimate model; hence, no modifications to the leak discharge model used in the evaluation model are necessary.

2. Small Break Phenomena and Leak Discharge Models

A loss-of-coolant accident (LOCA) is a condition in which liquid inventory is lost from the RC system. Due to the loss of mass from the RC system, the system will begin to depressurize. The response of the primary system to a small break will differ greatly depending on the break size, its location in the system, etc. During LOCAs, extremely large pressure gradients do exist; hence, the loss of fluid through a given break is limited to a "critical" value. The value of the critical flow through the break is calculated by the leak discharge model.

In the existing ECCS evaluation model for small breaks, the Orifice - Moody leak discharge model, with a discharge coefficient of 1.0, is utilized. This section presents the results of the literature survey and the selection of the best-estimate leak discharge model. The factors affecting critical flow are discussed. The basis for selecting the best-estimate discharge model is explained, and the selected model is compared with test data. The calculated system response with the selected model is compared to that of the existing model in section 3.

2.1. Literature Survey

Numerous potential references on the subject of subcooled and two-phase critical flow were identified from a Department of Energy data base computer search, and the available articles were gathered and reviewed. Previous relevant B&W studies were also examined. Based on these studies, a best-estimate leak discharge model was selected.

Most interest was taken in studies that compared several models to data, or compared the data for different geometries and fluid conditions. Articles on the theoretical development of particular models were also of interest.

For the most part, this study relied on references that compared the models to data. D. G. Hall evaluated the accuracy of several models using measured fluid conditions from Semiscale Test S-02-4 as input to the models and compared the predictions to the measured flow rates.[4] K. H. Ardron and R. A. Furness compared model predictions and data for a range of conditions for both subcooled and two-phase fluid.[5] They compared data from experiments with different geometries and assessed when the different models were in best agreement with the data. Travis, Hirt and Rivard discussed the Hall results and used a two-dimensional computer code to analyze geometric effects.[6] Studies by Sozzi and Sozzi and Sutherland compared model predictions to data and evaluated geometric effects on flow rates.[7,8] Reocreux discussed the theoretical basis of the critical flow models and also briefly compared the theoretical and experimental results.[9]

In addition to the model comparisons to data cited above, this study relied on B&W comparisons of critical flow models to data. These include evaluations of the Sozzi and Sutherland data and post-test predictions of semiscale and LOFT experiments.[10,11]

2.2. Factors Influencing Critical Flow Rates

Several critical flow models have been developed by various authors. While all of these have been derived from the mass, momentum, and energy conservation equations, the authors use different assumptions about homogeneity, thermal equilibrium between the phases, slippage, etc. However, all the models compute the mass flux through the break based on upstream (stagnation) fluid conditions. The predicted mass flux is then multiplied by the break area to obtain the leak flow rate.

Several factors influence the critical flow rate through a given break. The two main variables are the upstream fluid state and the break geometry. Whether the upstream fluid is subcooled or saturated has a significant impact on the critical flow rate. Generally, different discharge models are used to predict the critical flow rate depending on the fluid state. Thus, each fluid state will be examined separately in selecting the best-estimate discharge model (see section 2.3).

Break geometry, which includes the length and diameter of the minimum area and the shape of the break entrance and exit, can also have a significant impact on critical flow rate. None of the critical flow models examined explicitly address different break geometries in their formulation. Rather, break geometry effects are accounted for by multiplying the predicted flow rate by an empirical discharge coefficient, which must be chosen by the analyst. Therefore, any selection of a best-estimate discharge model must be coupled with an assessment of break geometry.

2.3. Best-Estimate Discharge Model Selection and Justification

As a result of the literature survey and the review of previous relevant B&W studies, the best-estimate leak discharge model selected is the orifice equation, with a discharge coefficient of 0.7, for subcooled flow and the homogeneous equilibrium model (HEM), with a discharge coefficient of 0.85, for saturated fluid conditions. This model is expected to predict leak flows near experimental values for the expected worst-case break geometry and to predict leak flows on the conservative side for most other cases. The justification of the selected best-estimate leak discharge model is provided below.

2.3.1. Subcooled Discharge Model

2.3.1.1. Comparison to Test Data

In order to select the best-estimate subcooled discharge model, a literature review was performed to assess the capability of the various theoretical models to predict experimental data. The subsequent paragraphs summarize the results of the literature survey.

D. G. Hall compared several subcooled discharge models and the data from semi-scale test S-02-4.[4] In his comparison, Hall noted that several of the correlations - the Burnell, modified Burnell, and Henry-Fauske models - all use forms of the orifice equation:

$$G \alpha \sqrt{(P_1 - P_2/\nu}$$

where G = mass flux,
P_1 = upstream pressure,
P_2 = downstream pressure,
ν = specific volume.

The Henry-Fauske and both Burnell models predict the throat pressure (downstream pressure) for use in the orifice equation. It should be noted that in the CRAFT2 code, the containment pressure is used as the downstream pressure for the orifice equation.[12] Hall found that when the measured throat pressures for the experiment were substituted into the orifice equation, the predicted flow rates maintained a nearly constant ratio with the measured flow rates. This conclusion is illustrated in Figure B-1 (from Hall's report), which presents a ratio of the measured mass flow rate for the experiment to that predicted by various leak discharge correlations. As shown, the Bernoulli (orifice equation) mass flow ratio is essentially constant during the subcooled portion of the blowdown, approximately the first 2.9 seconds, when the measured throat pressures are utilized. While the Henry-Fauske and modified Burnell mass flow ratios shown in Figure B-1 predict the measured flow rates more closely, neither predicts the data trend. As Hall found, and as shown in Figure B-2, none of the discharge models was capable of predicting the throat pressures.

Hall's comparison of several discharge models to the test data is shown in Figure B-3. The mass flow ratio for the orifice equation, using the containment pressure as the downstream pressure, has been added to the figure. As can be seen, both the Henry-Fauske and modified Burnell models closely predict the subcooled mass flow rates. The orifice equation yields a nearly constant ratio of 0.6. Based on his comparisons, Hall concluded that the modified Burnell (Zaloudek) model, with a discharge coefficient of 1.0, should be used to predict subcooled flow.

An additional comparison of the ability of various subcooled discharge correlations to predict subcooled flow was performed by K. H. Ardon and R. A Furness.[5] Figure B-4, taken from their paper, presents the flow rates predicted by several correlations for various stagnation (upstream) pressures assuming saturated water flow. Included in the figure are measured break flow rates from various experiments. While this figure is based on saturated water flow, the authors state that data for initially subcooled fluid conditions follow similar trends. As illustrated by the figure, the break geometry can have a substantial impact on the subcooled discharge rate. Since none of the models explicitly accounts for break geometry, it is not surprising that the figure shows that the data set is not well characterized by any single model. However, as the authors note, orifice flows can be predicted by the Bernoulli (orifice) equation if a discharge coefficient of 0.65 is used. The authors also note that data for short nozzles generally fell about 50% above the values predicted by the Henry-Fauske model.

Supplementing the literature discussed above, B&W has performed an evaluation of the ability of the orifice equation and modified Burnell subcooled discharge models to predict the Sozzi and Sutherland data.[8] The results of that evaluation are shown in Figures B-5 and B-6. These figures present the discharge coefficient that would be necessary for each of the models to predict the data. As shown, the break geometry has a substantial influence on the required discharge coefficient. For high-L/D nozzles, there is also a subcooling effect that must be considered. Like the conclusions of Ardon and Furness, this comparison shows that flow rates through orifices can be simulated using the orifice equation with a single discharge coefficient.

In summary, subcooled discharge rates cannot be adequately predicted by any single model. At best, if the break geometry is known, the analyst can select

the appropriate discharge coefficient for the discharge model being utilized. Thus, in selecting the best-estimate subcooled discharge model for small break LOCA evaluations, break geometry effects must be considered.

2.3.1.2. Basis for Selecting Best-Estimate Subcooled Discharge Model

This section discusses the basis for selecting the subcooled discharge model. As is obvious from the previous section, an appropriate discharge coefficient is needed for the discharge model to predict the correct leak flow rate. This discharge coefficient depends on the geometry of the break and the fluid state. Since small break evaluations must cover any assumed break size or shape, the best-estimate model must be reasonable for worst-case break geometries and conservative for all others.

To aid in defining a conservative subcooled discharge model, previous small break evaluations were reviewed. A spectrum of small breaks at the pump discharge for B&W 177-FA lowered-loop plants was analyzed with an Orifice-Moody discharge model with a discharge coefficient of 1.0. The calculated system pressures and the core mixture levels are shown in Figures B-7 and B-8.[13] A similar analysis for a spectrum of small breaks was performed with the modified Zaloudek-Moody discharge model with a discharge coefficient of 1.0. The predicted system pressures and core mixture levels for this spectrum of small breaks are shown in Figures B-9 and B-10.[14]

Comparison of the two different leak discharge model analyses shows that the system response is similar in both cases and that the 0.07 ft^2 break size is the worst break area. The major difference in system response using the Zaloudek discharge model is that the subcooled blowdown lasts longer because it predicts less flow than the orifice equation. This results in delaying the processes that occur during the saturated discharge to a time period with lower decay heat. Consequently, the core mixture levels for each break case are higher and the core flooding tank (CFT) actuation is later than the orifice model break cases. The overall system response is very similar for both analyses, which indicates that the saturated leak flow mainly determines the long-term response and the subcooled blowdown determines the timing, which in turn determines the amount of core uncovering. The results of these studies show that the overprediction of subcooled flow is conservative with respect to core uncovering.

Review of the data comparisons reported in the previous section shows that orifices (low L/D breaks) will provide the maximum subcooled discharge rates; this is illustrated on Figure B-4. Thus, for purposes of selecting a best-estimate subcooled model, it will be assumed that the break is an orifice. As Ardon and Furness concluded[5], orifice flows can be predicted by the Bernoulli (orifice) equation with a discharge coefficient of 0.65. B&W's analysis of the Sozzi and Sutherland data also indicated that the orifice equation, with a discharge coefficient of 0.6, is suitable for predicting orifice flows.[8] Hence, the orifice equation has been chosen as the best-estimate subcooled discharge correlation. Since an overprediction of subcooled flow results in conservative analyses, and there are some uncertainties in the break geometry and test data, the selected multiplier for the best-estimate discharge model is 0.7. This is expected to predict the flow in good agreement with the test data for orifices and yet be on the conservative side (overprediction) for other break geometries.

2.3.2. Saturated Discharge Model

2.3.2.1. Comparison to Test Data

A literature review was performed to select the best-estimate saturated discharge model; that review is summarized below.

D. G. Hall compared several critical flow models and test data from semiscale test S-02-4.[4] His subcooled discharge flow comparisons are discussed in section 2.3.1.1. Figure B-11, which presents the ratio of the measured mass flow rate for the experiment to that predicted by various discharge correlations, graphically summarizes Hall's results. Hall's comparison in Figure B-11 shows that the homogeneous equilibrium model (HEM) predictions maintain a nearly constant ratio of 0.84 with the data after about 7 seconds when the quality is greater than about 0.02. None of the other models shown demonstrates a constant relationship with the predicted data. Thus, it is concluded that the other models do not predict the data trend.

Another comparison - by Ardon and Furness - of several models for two-phase discharge is shown in Figure B-12.[5] The two graphs, which are based on different stagnation (upstream) pressures, present the flow rates predicted by several correlations for various stagnation qualities. Included in the figure are measured flows from various experiments. It should be noted that no

substantial break geometry effect is shown, as was the case for subcooled fluids. As shown by the figure, the Moody model, which is the two-phase discharge correlation required by 10 CFR 50, Appendix K, for use in small-break LOCA evaluations, generally overpredicts the data. The Henry-Fauske model appears to provide the best characterization of the data. The HEM model predicts lower mass fluxes than all the other models examined. However, for fluid qualities greater than 0.2, all the models except Moody predict the data reasonably.

Supplementing the data comparisons discussed above, Travis performed a theoretical analysis of the break geometry effects on two-phase flow.[6] Figure B-13 shows the calculated discharge coefficient to be applied to the HEM, depending on the break L/D. It is shown in the figure that test data points, including the Hall analysis of S-02-4 discussed above, substantiate the validity of the Travis theoretical analysis. As shown, while there is some break geometric effect to consider, it is less substantial than that discussed for subcooled flow.

The analysis of LOFT experiment L3-6 provides further insight for development of the best-estimate saturated flow model.[11] The analysis utilized the HEM for saturated discharge. Reasonable agreement was obtained with the measured flow rates for the experiment.

In summary, several saturated discharge models could be chosen for best-estimate leak flow predictions. The Henry-Fauske model and HEM, both of which have been used for best-estimate LOFT predictions, appear as viable choices. While break geometry effects must be considered, they are less significant than that seen for subcooled discharge.

2.3.2.2. Basis for Selecting Best-Estimate Saturated Discharge Model

This section discusses the basis for selecting the best-estimate saturated discharge model. Previous small break analyses were reviewed to determine typical fluid conditions obtained during a small-break LOCA. Based on this review, a discharge correlation was selected. Finally, break geometric effects were evaluated and an appropriate discharge coefficient was chosen.

During a small break transient, the primary system generally loses inventory in three phases. Figure B-14, which presents the leak flow quality for a 0.07-ft^2 break, illustrates the three periods.[13] First there is a period of subcooled discharge, which typically lasts around 100 seconds, during which the primary system rapidly depressurizes to the saturation pressure of the hot leg. After the primary system saturates, the inventory in the primary system piping is lost more slowly through the break. During this period, which is designated the "loop draining" period, the leak qualities are between approximately 0.3 and 0.7. After the primary system piping has drained, only steam, plus any high-pressure injection into the broken pipe, is lost through the break. Break qualities range from about 0.6 to 0.8 over this period, which is designated the "boiling pot" mode since inventory from the system is only lost through boiling caused by removal of the core decay heat.

As described previously, both the HEM and Henry-Fauske models would be expected to produce reasonable predictions of two-phase critical flow. The only concern with the HEM was the fact that it underpredicted leak flows for qualities less than 0.2. However, as discussed above, the leak qualities during a small-break transient are greater than 0.2 throughout the two-phase discharge period. Thus, the HEM would provide a reasonable prediction of the two-phase discharge. In light of Hall's conclusion that the HEM would provide the best representation of the two-phase discharge for S-02-4 (Figure B-11)[4], the theoretical development of a discharge coefficient for the HEM that accounts for break geometry effects (Figure B-13)[6], and the reasonable prediction of LOFT test L3-6 using the HEM[11], the HEM has been selected as the best-estimate saturated flow model.

Figure B-13 was used to determine the appropriate discharge coefficient to be used with HEM. For the worst-case break analyzed in the small-break spectrum, the expected smallest L/D for the break would be approximately one. From Figure B-13, this yields a discharge coefficient of 0.85. Use of the smallest L/D, and hence the smallest discharge coefficient, results in the slowest depressurization for a given break size, thereby delaying CFT actuation. This will result in a conservative assessment of the small-break transient. Further discussion of the conservatism of this approach is included in section 3.

3. Best-Estimate/Evaluation Model Comparison

This section describes the analysis performed with the selected best-estimate leak discharge model. The RC system response predicted using the selected leak discharge model is compared to the response with the existing evaluation model. The results of an additional analysis, which was performed to evaluate sensitivity to the saturated discharge coefficient, are also discussed.

3.1. Break Cases Analyzed

As shown in Figure B-8, previous analysis of a spectrum of small breaks at the pump discharge for B&W 177-FA, lowered-loop plants showed that the 0.07-ft^2 break area was the worst-case break, with respect to core uncovering, using the evaluation model. For this study it was desired to analyze an equivalent case with the best-estimate model. Since both the evaluation model and the best-estimate leak discharge models use the orifice equation with different discharge coefficients, the change in the subcooled blowdown is a simple factor. However, the two-phase model was changed from Moody, with a discharge coefficient of 1.0, to the HEM, with 0.85, and the effect of the change is not as simple.

Previous studies (discussed in section 2.3.1.2) have shown that for a given two-phase discharge model and input break area, reducing the subcooled flow improves system response with respect to core uncovering.[13,14] Thus, the change with the orifice equation from a discharge coefficient of 1.0 to 0.7 would tend to improve results for a given break area, but the effect of the two-phase model change is not as clear. To assess the effect of the two-phase change, it was decided to compare the results of a break case with the same subcooled blowdown as the previous evaluation model worst-case break. This input area would be 0.1 ft^2 (0.1 x 0.7 = 0.07). Having the same subcooled flow would allow a direct assessment of the effect of the two-phase model change from Moody with a discharge coefficient of 1.0 to the HEM with a coefficient of 0.85.

It is interesting to note that an input area near 0.1 ft^2 with the best-estimate model is expected to be roughly equivalent to the evaluation model worst-case (0.07-ft^2) break for two-phase discharge based on the following reasoning. Figure B-15 shows the ratio of the HEM to Moody predictions versus pressure and quality. Since the fluid will be at pressures of approximately

1200 to 600 psi and qualities of approximately 0.3 to 0.8 for the two-phase discharge, it can be seen from the figure that the HEM prediction will be between 0.7 and 0.9 times the Moody prediction. With the discharge coefficient of 0.85 for the HEM, to have the same two-phase discharge rate, on the average, as the previous worst-case break with the best-estimate model, the input area should be between 0.12 and 0.092 ft^2 (0.12 x 0.7 x 0.85 = 0.07 and 0.092 x 0.9 x 0.85 = 0.07; the 0.1 ft^2 falls in the middle of this range. Thus, it is expected that the best-estimate analysis, using an input area of 0.1 ft^2, will be very similar to the evaluation model 0.07 ft^2 break case.

Another computer run was made to further verify that the present evaluation model is conservative with respect to a best-estimate leak discharge model and to evaluate the sensitivity of the results to a change in the saturated discharge coefficient. The same size break was analyzed (0.1-ft^2 input area) using a discharge coefficient of 0.8 with the HEM for saturated flow. The revised saturated discharge coefficient was to account for any uncertainty in the test data and in break geometry. The results of the analysis are discussed below.

3.2. Results

Figures B-16, B-17, and B-18 compare the integrated leak flow, pressure, and core node mixture level calculations for the three cases analyzed: (1) 0.7-ft^2 input area with the evaluation model 1.0 orifice/1.0 Moody, (2) 0.1-ft^2 input area with 0.7 orifice/0.85 HEM, and (3) 0.1-ft^2 input area were the same for the subcooled discharge, only the saturated portions of the transients are different.

As expected, the differences in the calculated system responses can be separated into the three distinct periods mentioned in section 2.3.2.2.

The subcooled blowdown remained the same, as prearranged. As seen in Figure B-16, during the period of lower quality, two-phase discharge (250 to 600 seconds) while the primary system loops drain, both cases with the HEM clearly had lower integrated leak flow, hence lower discharge flow rates, than the evaluation model; the 0.8 HEM had slightly lower flow rates than the 0.85 HEM. As Figure B-17 shows, the result of the lower flow rates was slower depressurization because less mass and energy were released from the system at a given time during the low quality period. During the final "boiling pot" period of

nigher quality discharge, which began at between 600 and 700 seconds, the discharge flow rates for both HEM runs exceeded that of the evaluation model case. This can be inferred from Figure B-16 by noting that the integrated leak flow over this time period increases at a faster rate for the HEM case. Because the discharge flow rates were higher during this high-quality period, the energy and mass release rate was greater, and the system began to depressurize faster for the best-estimate cases. The system pressure (shown in Figure B-17) for the 0.85 HEM case, actually "caught up" and fell below that obtained with the evaluation model, while the 0.8 HEM case, which started from a higher pressure, was approaching the evaluation model pressure but did not quite intersect it.

The effect on the time of CFT actuation and the minimum core mixture level of the different discharge flow rates with the two HEM cases is summarized in Table B-1 and illustrated in Figure B-18. With 0.85 HEM the system pressure reached the CFT actuation point about 97 seconds earlier than with the evaluation model (1.0 Moody). In addition, because of the "saving" of inventory during the low-quality discharge period and the earlier actuation of the CFT, the minimum core mixture level was 1.26 ft above that of the evaluation model results. Changing to 0.8 HEM caused the CFT actuation to occur 130 seconds later than the 0.85 HEM case, or 33 seconds later than the evaluation model case. Even though the depressurization did not quite "catch up" with the evaluation model results, because of the saving of inventory during the low-quality discharge, the minimum core mixture level was still 0.78 ft higher than with the evaluation model. Thus, even when a saturated discharge coefficient of 0.8 is used in the best-estimate discharge model to account for the low L/D possible for the largest small break, the evaluation model still gives a more conservative prediction of the core mixture level.

3.3. Effect on Break Spectrum Cases

The results of the computer analysis for the worst-case break can be generalized to determine the effect of the best-estimate discharge model on other cases in the break spectrum. As shown by the analysis the effects of the best-estimate discharge model are to decrease leak flow during the loop draining period and to increase leak flow during the boiling pot mode of the transient. The altered leak flows caused an extension of the loop draining portion of the transient and an increased depressurization rate during the

boiling pot period of the transient. The effect of these altered leak flows on other break sizes is evaluated below. The evaluation is divided into two segments: breaks smaller and larger than the worst case. As in the preceding section, the discussion below is based on the effective subcooled break area, i.e., accounting for the subcooled discharge coefficient of 0.7 in the best-estimate model.

For breaks with smaller effective areas than the worst-case break, i.e., <0.07 ft^2, the effect of the best-estimate discharge model will be to improve the minimum core mixture level that would be obtained. To help illustrate this, Figures B-19 and B-20, which present the transient system pressure and inner vessel mixture heights obtained with the evaluation model for the 0.055- and 0.04-ft^2 breaks will be used. Also shown in the figures is the expected transient for an effective break area of 0.055 ft^2 (actual area 0.0786 ft^2) with the best-estimate discharge model. The basis for this curve is described below.

As described above, the best-estimate discharge model results in a longer period of loop draining due to the decreased leak flow. This results in the higher system pressure and the delay in the start of the depressurization, which occurs during the boiling pot mode of the transient, as is shown in Figure B-19 for the 0.055-ft^2 best-estimate case. As shown in Figure B-20, the loss of the vessel mixture level, which occurs during the boiling pot mode, is delayed accordingly.

During the boiling pot period of the transient, as shown in Figure B-19, the system depressurizes faster (10% faster) with the best-estimate model. Thus, the time from the end of the loop draining period to CFT actuation is reduced. This minimizes the loss of vessel inventory during this period (as shown in Figure B-20) for the best-estimate analysis. Hence, it is clear that use of the best-estimate model for effective break sizes smaller than 0.07 ft^2 will result in improved core mixture levels relative to those obtained with the evaluation model.

The impact of the best-estimate discharge model on breaks with effective areas larger than 0.07 ft^2 has also been evaluated. Figures B-21 and B-22 show the system pressure and inner vessel mixture heights, respectively, for the 0.1- and 0.085-ft^2 breaks with the evaluation model. The expected transient

parameters for an effective break area of 0.1 ft^2 (actual area 0.143 ft^2) with the best-estimate discharge model are also included on the figures.

As previously discussed and shown in Figures B-21 and B-22, the best-estimate case, when compared to the evaluation model results for the 0.1-ft^2 break, will have a higher system pressure, a delay in the start of the boiling pot mode depressurization, and a delay in the loss of vessel inventory that occurs during the boiling pot mode. During the boiling pot mode of the transient, the best-estimate case will have a more rapid depressurization relative to the evaluation model case. However, because of the higher system pressure at the end of the loop draining period for the best-estimate case, it is not clear whether the time interval from the end of loop draining to CFT actuation will be decreased or increased by the best-estimate model. Obviously, if this time interval is decreased, the loss of vessel inventory during the period would be decreased and the best-estimate case would yield higher minimum vessel mixture heights relative to the evaluation model. However, if this time interval is increased, lower minimum vessel mixture heights would be obtained by use of the best-estimate model. Figures B-21 and B-22 show the effect of an increased time period. Obviously, the time interval from the end of the loop draining period to CFT actuation for the best-estimate case is bounded by the next smallest break size analyzed in the evaluation model spectrum. Therefore, the loss of inventory that would occur over this period with the best-estimate model is also bounded by the next smallest break in the spectrum analysis. Hence, for breaks greater than the worst-case break, while it cannot be concluded without further computer analysis that the use of the best-estimate discharge model will result in improved consequences relative to the evaluation model, it is clear that the effect of using a best-estimate discharge model is bounded within the spectrum approach used in small-break LOCA evaluations.

4. References

1. E. D. Throm (NRC) to B&W Owner's Group, Letter, "Summary of Meeting With the B&W Owners Group Concerning the Abnormal Transient Operating Guidelines (ATOG) Program and TMI Action Item II.K.3.30 Small Break Loss-of-Coolant Accident Models (December 16, 1980)," Docket Nos. 50-269, -270, -289, -302, -312, -313, and -346, January 30, 1981.

2. "Generic Evaluation of Small Break Loss-of-Coolant Accident Behavior in Babcock & Wilcox Designed 177-FA Operating Plants," NUREG-0565, U.S. Nuclear Regulatory Commission, January 1980.

3. "Clarification of TMI Action Plan Requirements," NUREG-0737, U.S. Nuclear Regulatory Commission, October 31, 1980.

4. D. G. Hall, "A Study of Critical Flow Prediction for Semiscale Model Loss of Coolant Accident Experiments," TREE-NUREG-1006, December 1976.

5. K. H. Ardron and R. A. Furness, "A Study of the Critical Flow Models Used in Reactor Blowdown Analysis," Nuclear Engineering & Design, 39 (1976), pp 257-266.

6. J. R. Travis, C. W. Hirt, and W. C. Rivard, "Multidmensional Effects in Critical Two-Phase Flow," Nuclear Science & Engineering, 68 (1978), pp 338-348.

7. G. L. Sozzi, Prediction of Critical, Two-Phase Flow, NEDO-13017, General Electric, 1969.

8. G. L. Sozzi and W. A. Sutherland, "Critical Flow of Saturated and Subcooled Water at High Pressure," Non-Equilibrium Two-Phase Flows, Annual Winter Meeting of ASME, November-December 1975.

9. M. Reocreux, Contribution to the Study of Critical Flow Rates in Two-Phase Water Vapor Flow, NUREG-TR-0002, Vol. 1, 2, 3, August 1977.

10. T. E. Geer, P. L. Thornhill, and R. C. Jones, B&W's Post Test Analysis for Semiscale Test S-07-10D, June 9, 1981.

11. J. R. Paljug, M. D. Gharakhani, and R. C. Jones, B&W's Best Estimate Prediction of the LOFT L3-6 Nuclear Small Break Test Using the CRAFT2 Computer Code, March 1981.

12. R. A. Hedrick, J. J. Cudling, and R. C. Foltz, "CRAFT2-FORTRAN Program for Digital Simulation of a Multinode Reactor Plant During Loss-of-Coolant, BAW-10092, Rev. 2, Babcock & Wilcox, April 1975.

13. J. H. Taylor (B&W) to S. A. Varga (NRC), Letter, July 18, 1978.

14. J. H. Taylor (B&W) to S. A. Varga (NRC), Letter, June 19, 1978.

Table B-1. Flow Rates Vs Time of CFT Actuation and Minimum Core Mixture Level

Case	CFT actuation time, seconds	Minimum core mixture level, ft
0.07 ft^2 1.0 orifice/1.0 Moody	1494.7	11.20
0.1 ft^2 0.7 orifice/0.85 HEM	1397.8	12.46
0.1 ft^2 0.7 orifice/0.8 HEM	1527.8	11.98

Figure B-1. Comparison of Mass Flow Ratios Calculated Using Two Critical Flow Models and the Bernoulli Mass Flux Expression (Tree-NUREG-1006)

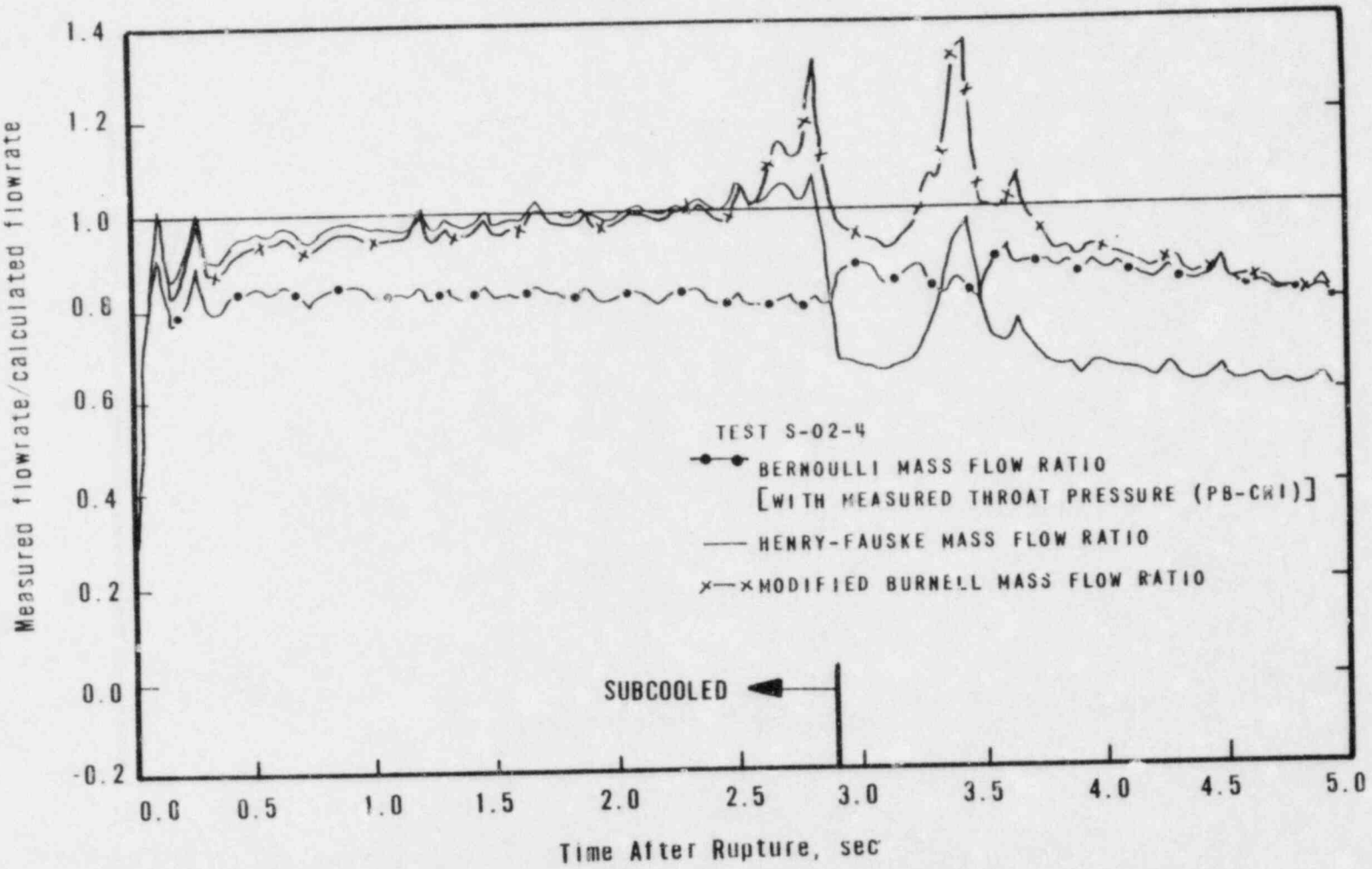

Figure B-2. Comparison of Critical Pressures Calculated Using Five Critical Models With Measured Throat Pressures (Tree-NUREG-1006)

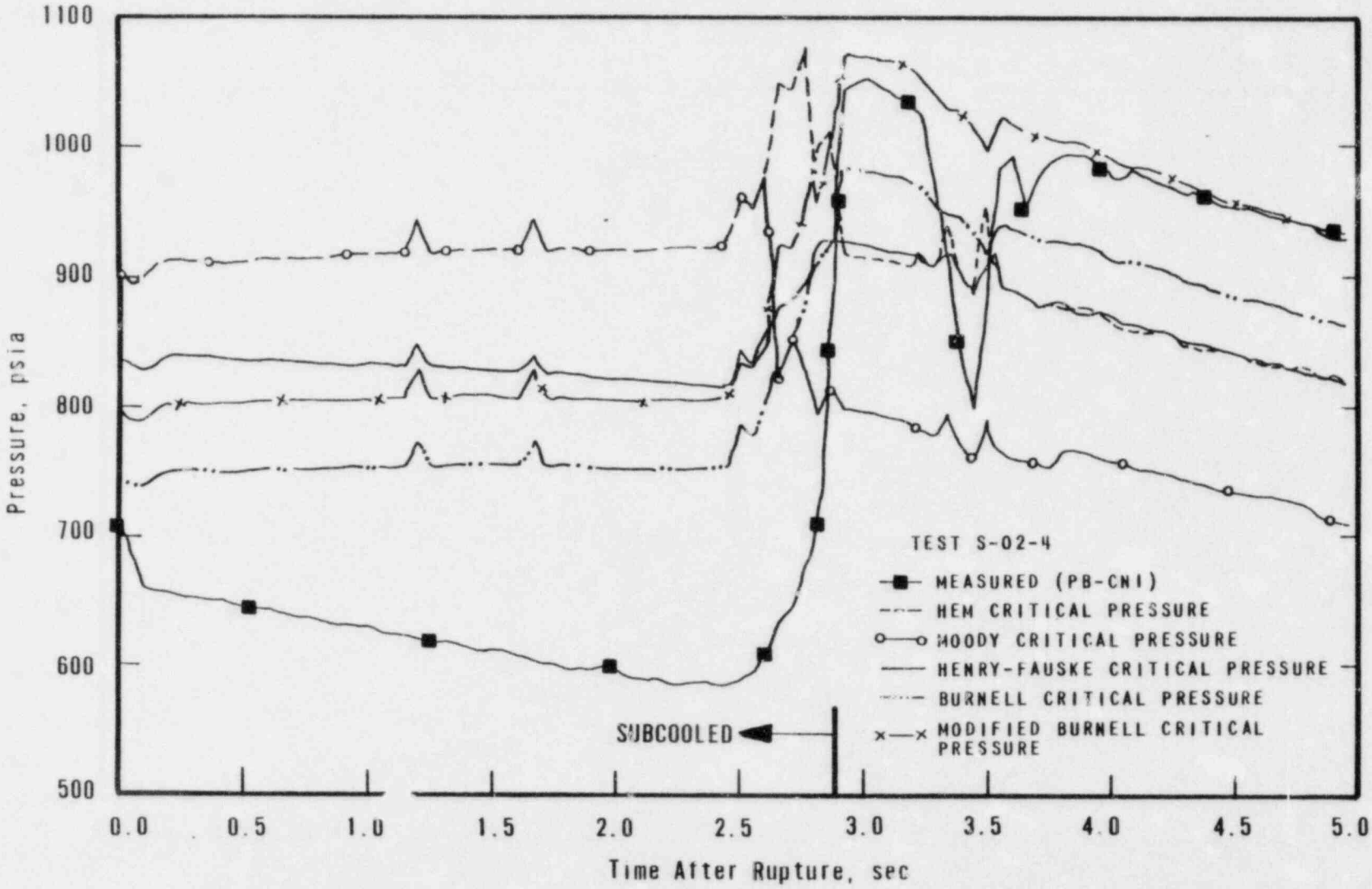

Figure B-3. Ratios of Measured Break Mass Flow Rates to Critical Mass Flow Rates Calculated Using Five Critical Flow Models (Tree-NUREG-1006)

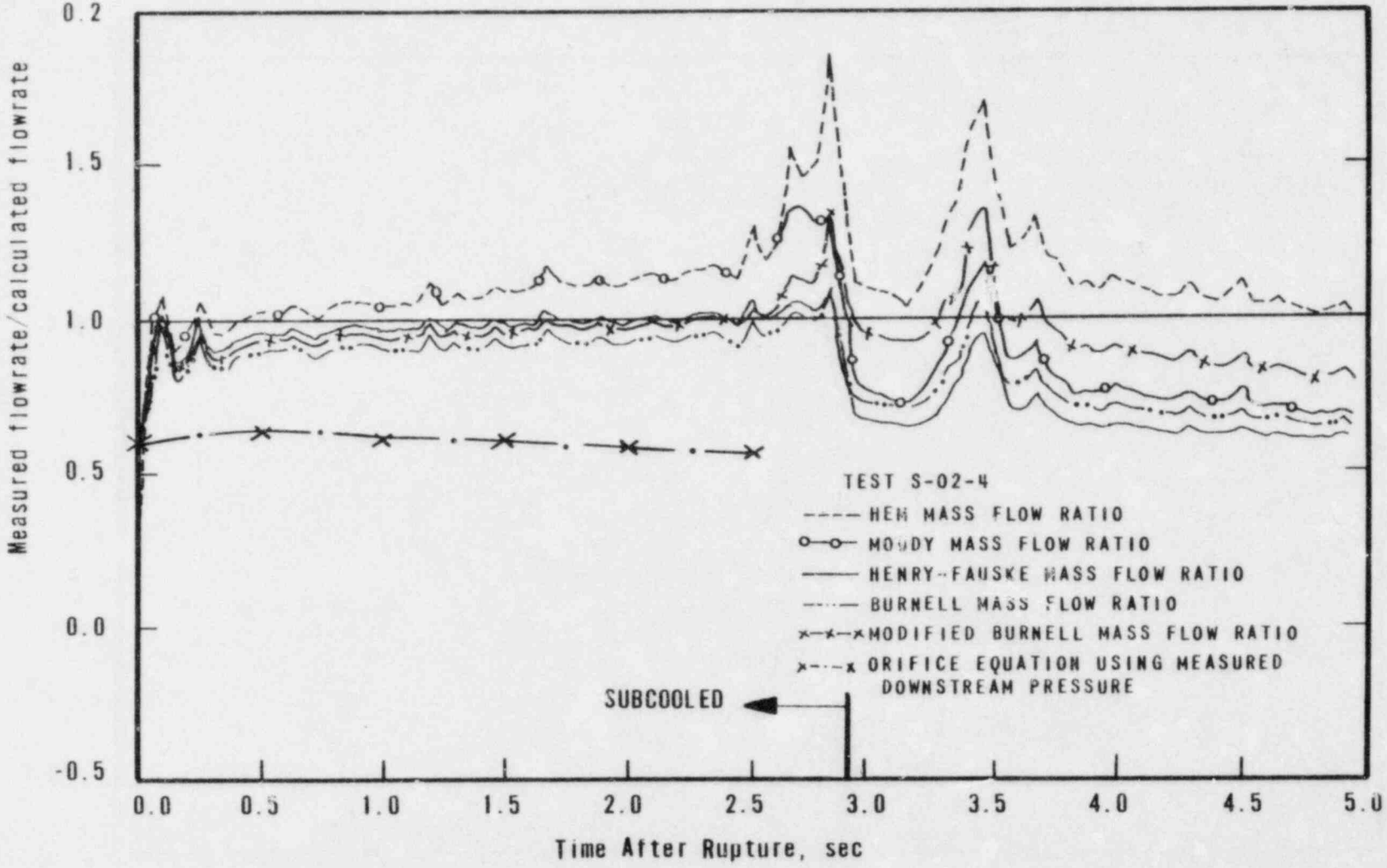

Figure B-4. Discharge of Saturated Water Through Orifices, Nozzles and Pipes (Reference 5)

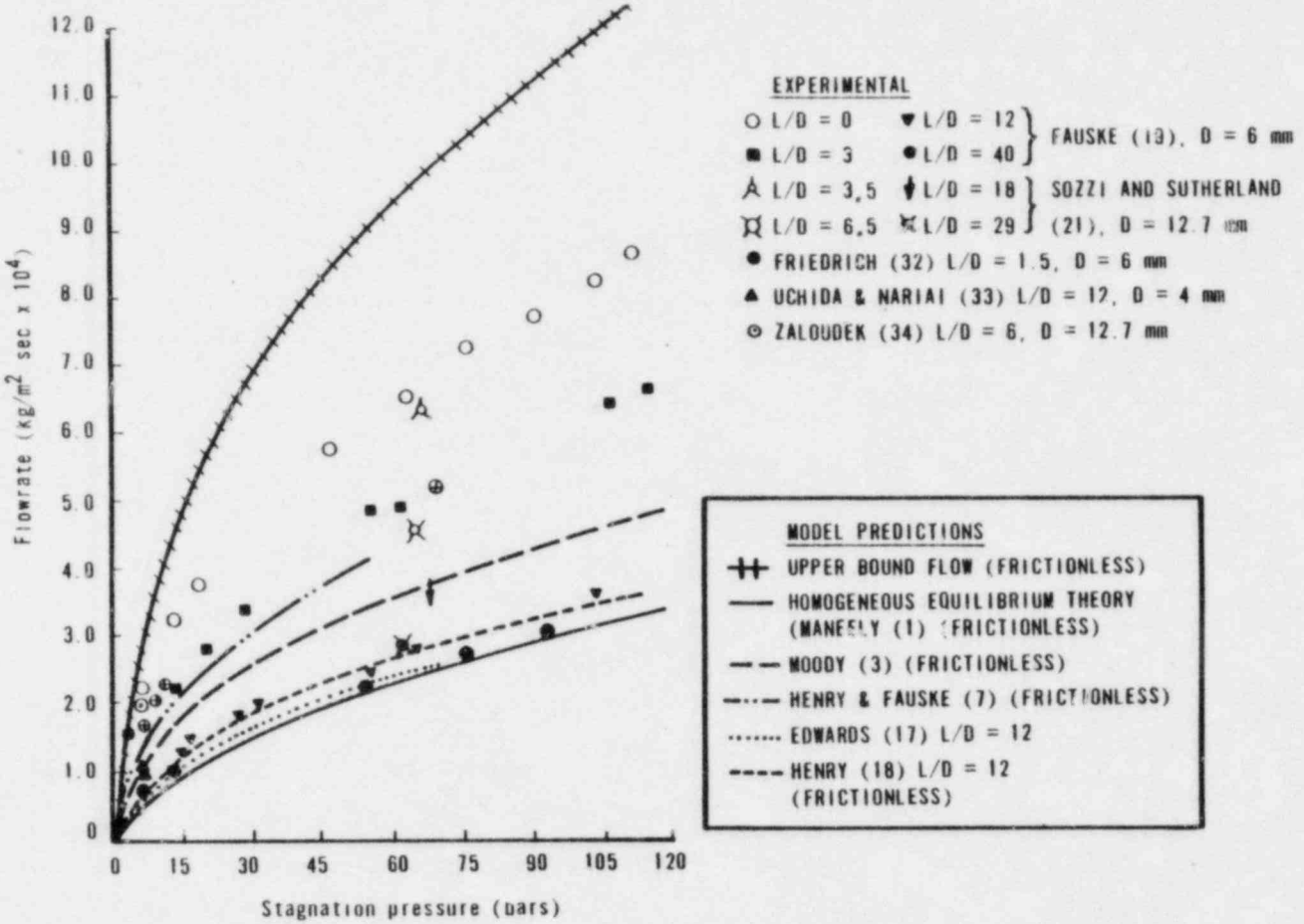

Figure B-5. Discharge Coefficient Required for Orifice Equation

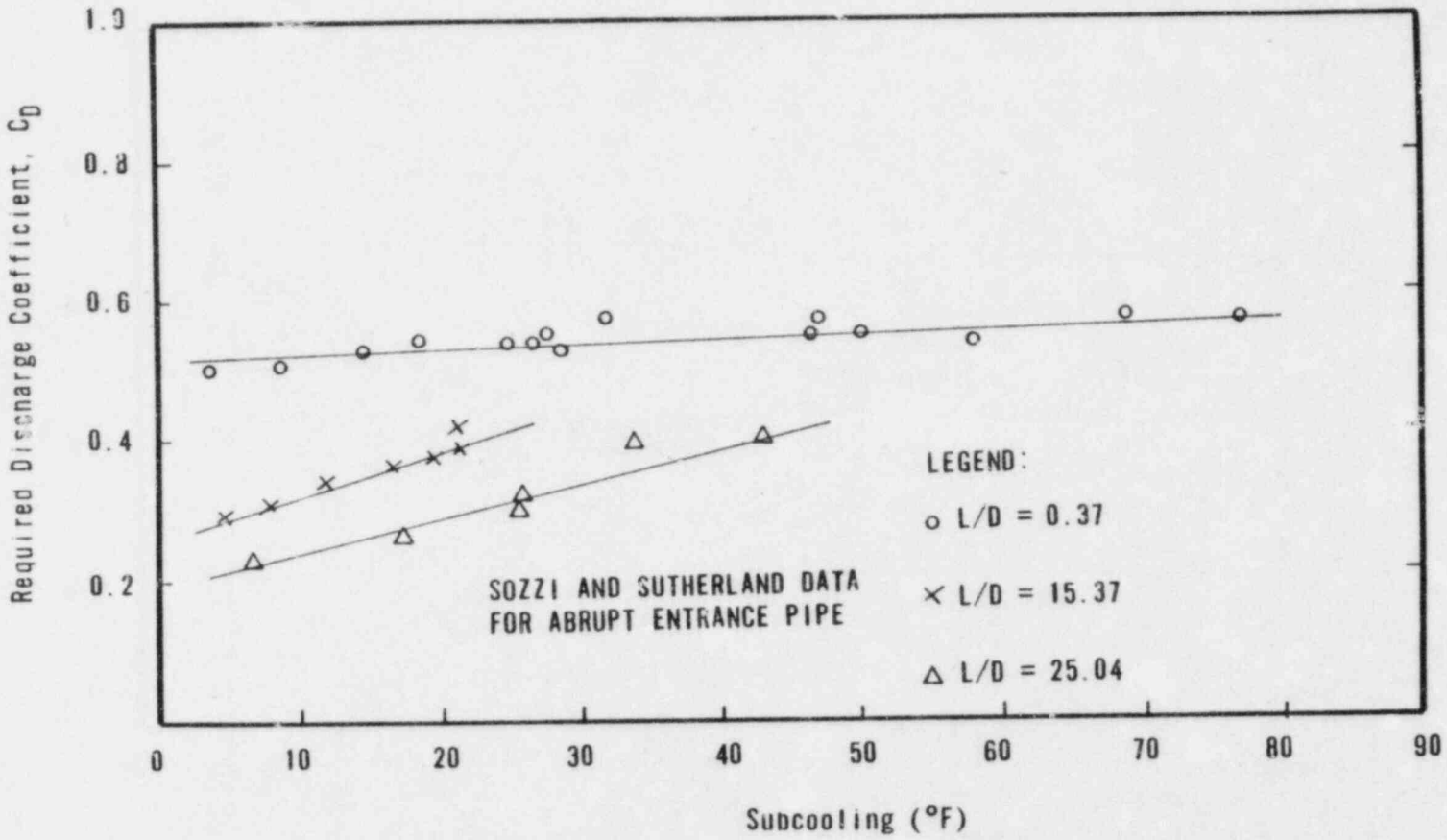

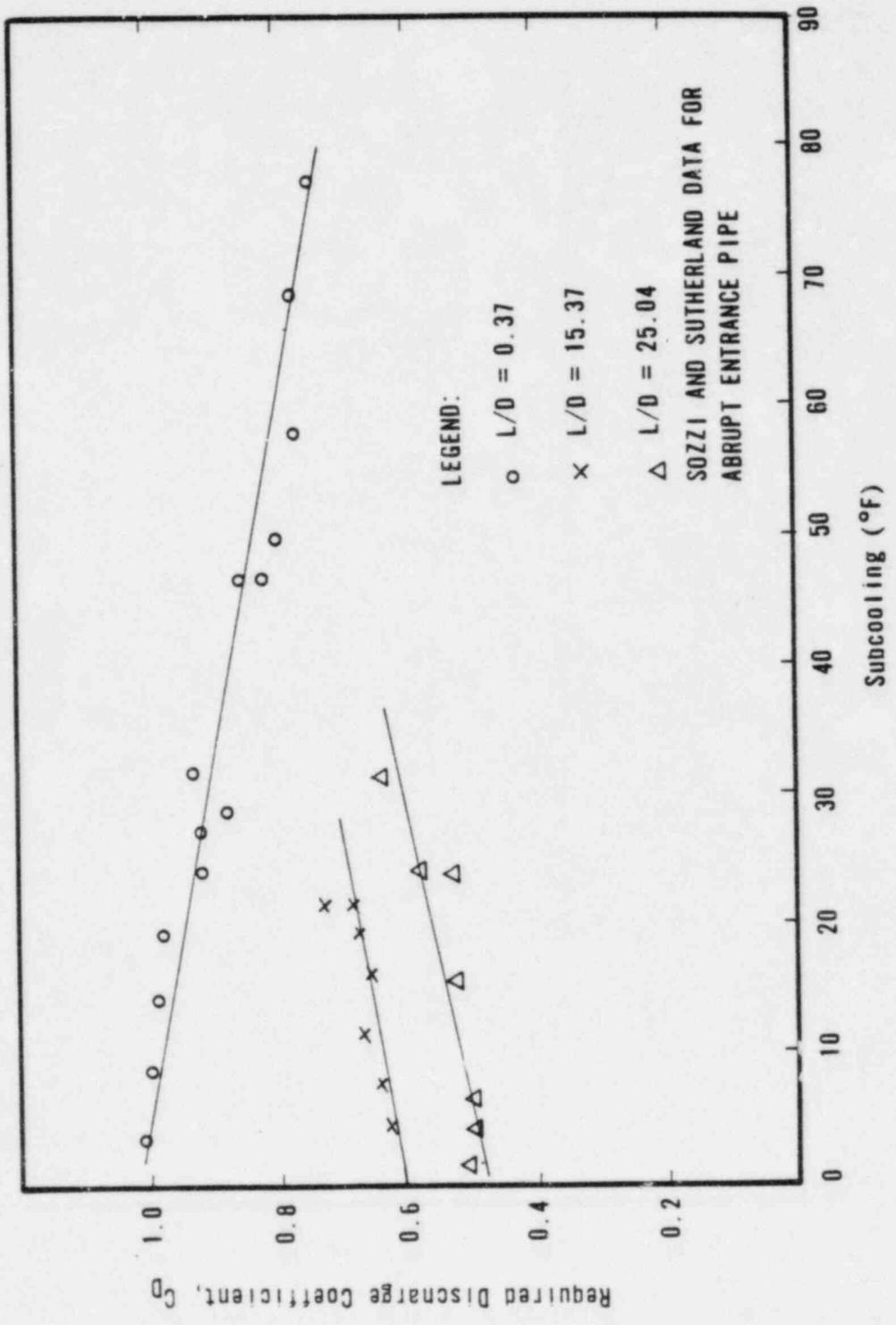

Figure B-6. Discharge Coefficient Required for Modified Zaloudek Equation.

Figure B-7. Pressure Vs Time for 177-FA Lowered-Loop Break Spectrum at RC Pump Discharge Using Orifice Equation for Subcooled Discharge

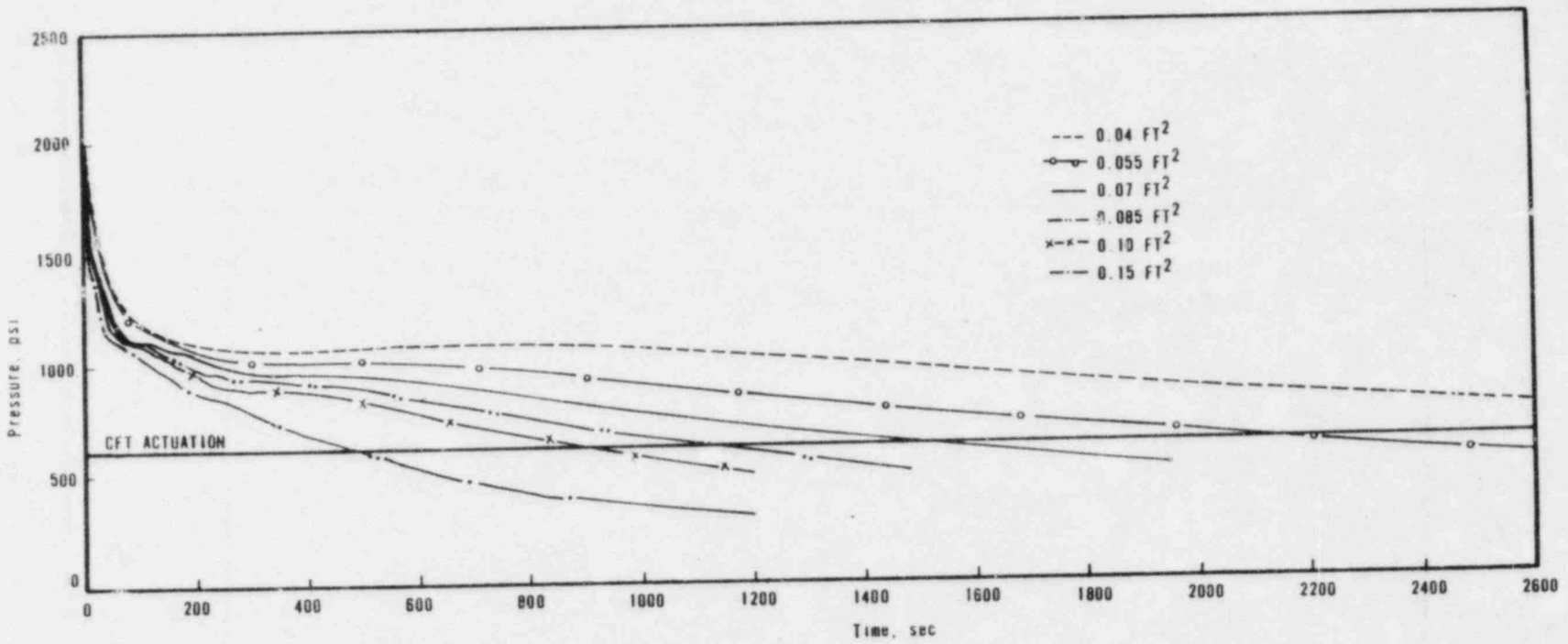

Figure B-8. Mixture Height Vs Time for 177-FA Lowered-Loop Break Spectrum at RC Pump Discharge Using Orifice Equation for Subcooled Discharge

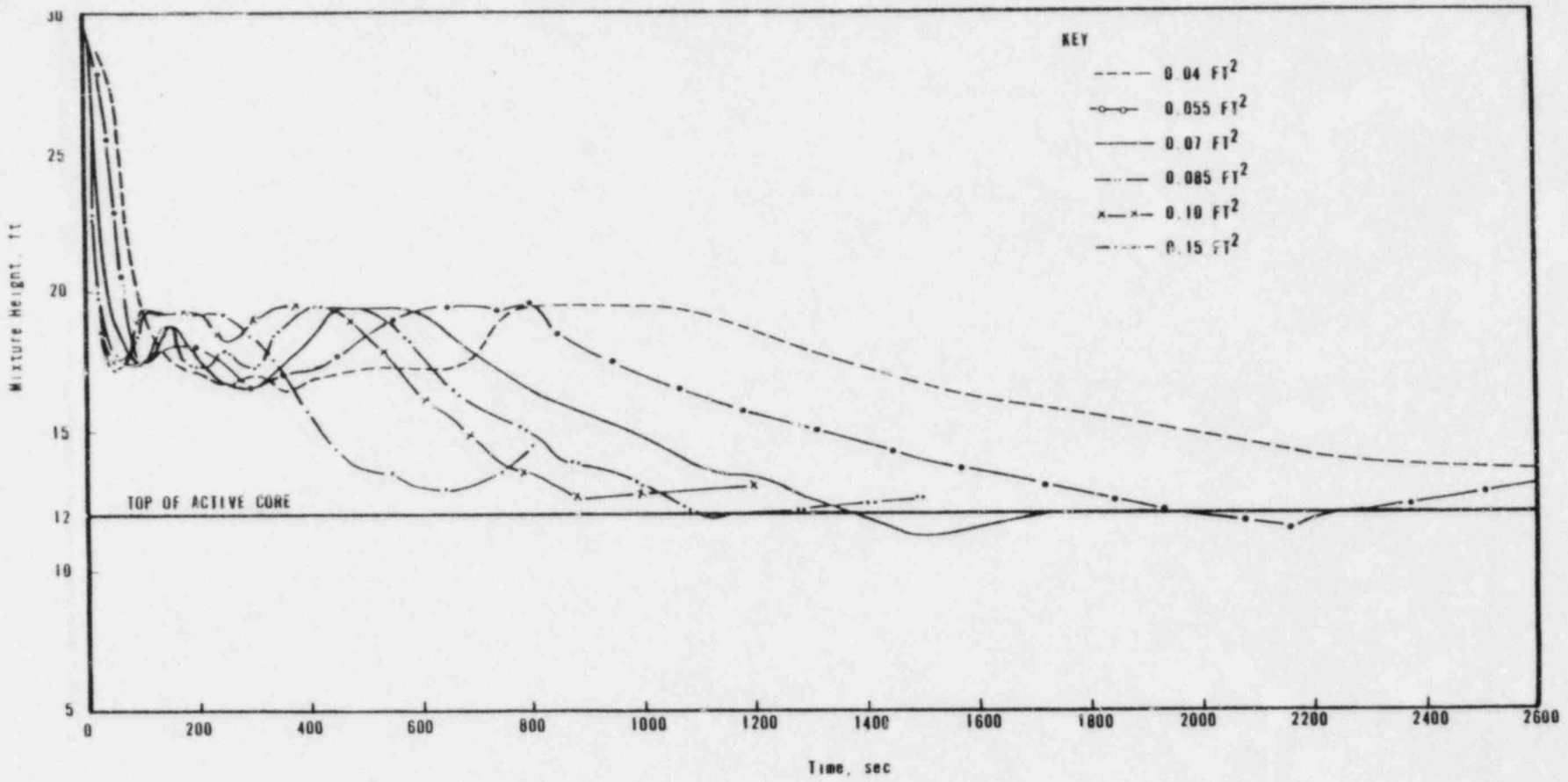

Figure B-9. Pressure Vs Time for 177-FA Lowered-Loop Break Spectrum at RC Pump Discharge Using Modified Zaloudek Subcooled Discharge Model

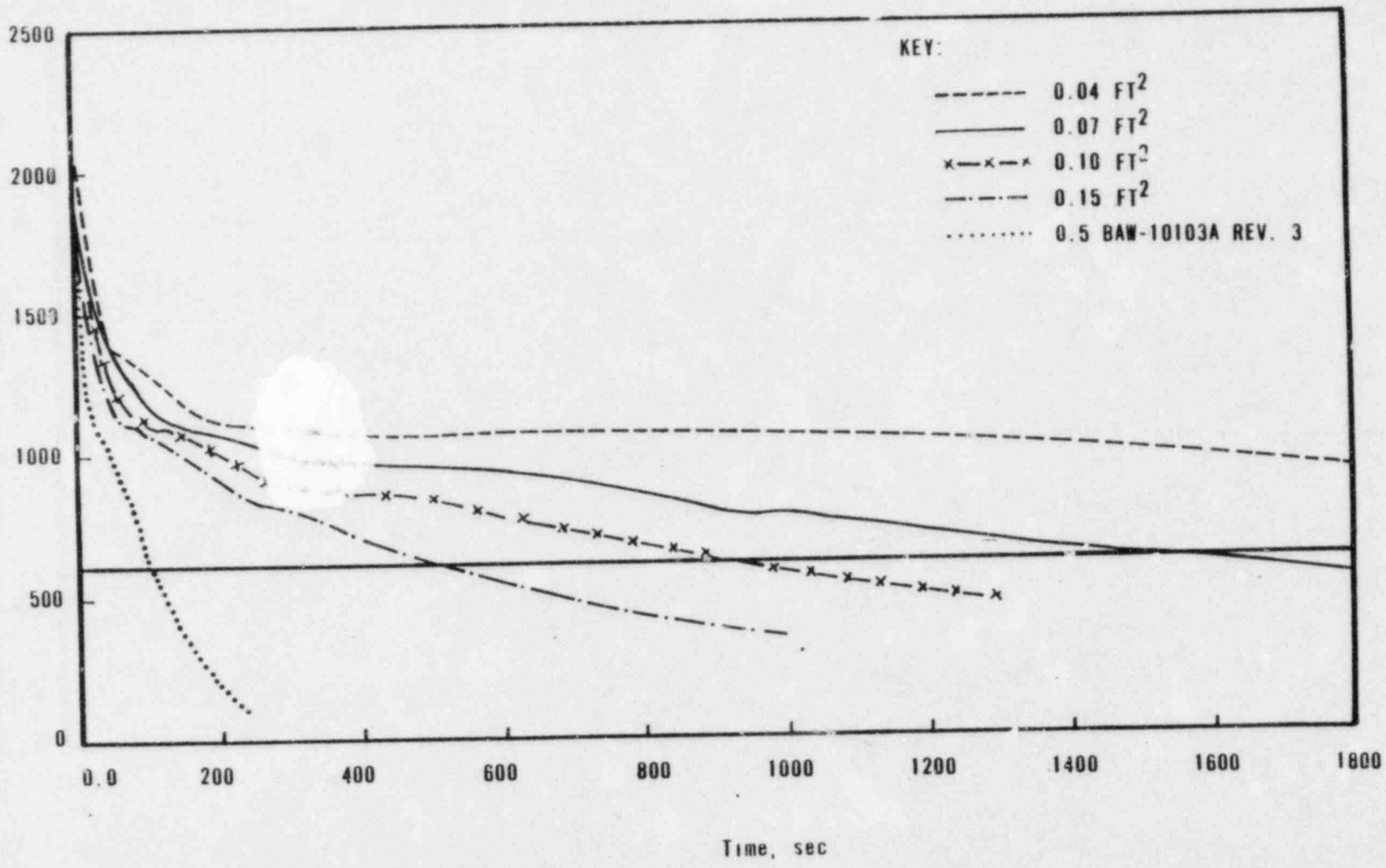

Figure B-10. Mixture Height Vs Time for 177-FA Lowered-Loop Break Spectrum at RC Pump Discharge Using Modified Zaloudek Subcooled Discharge Model

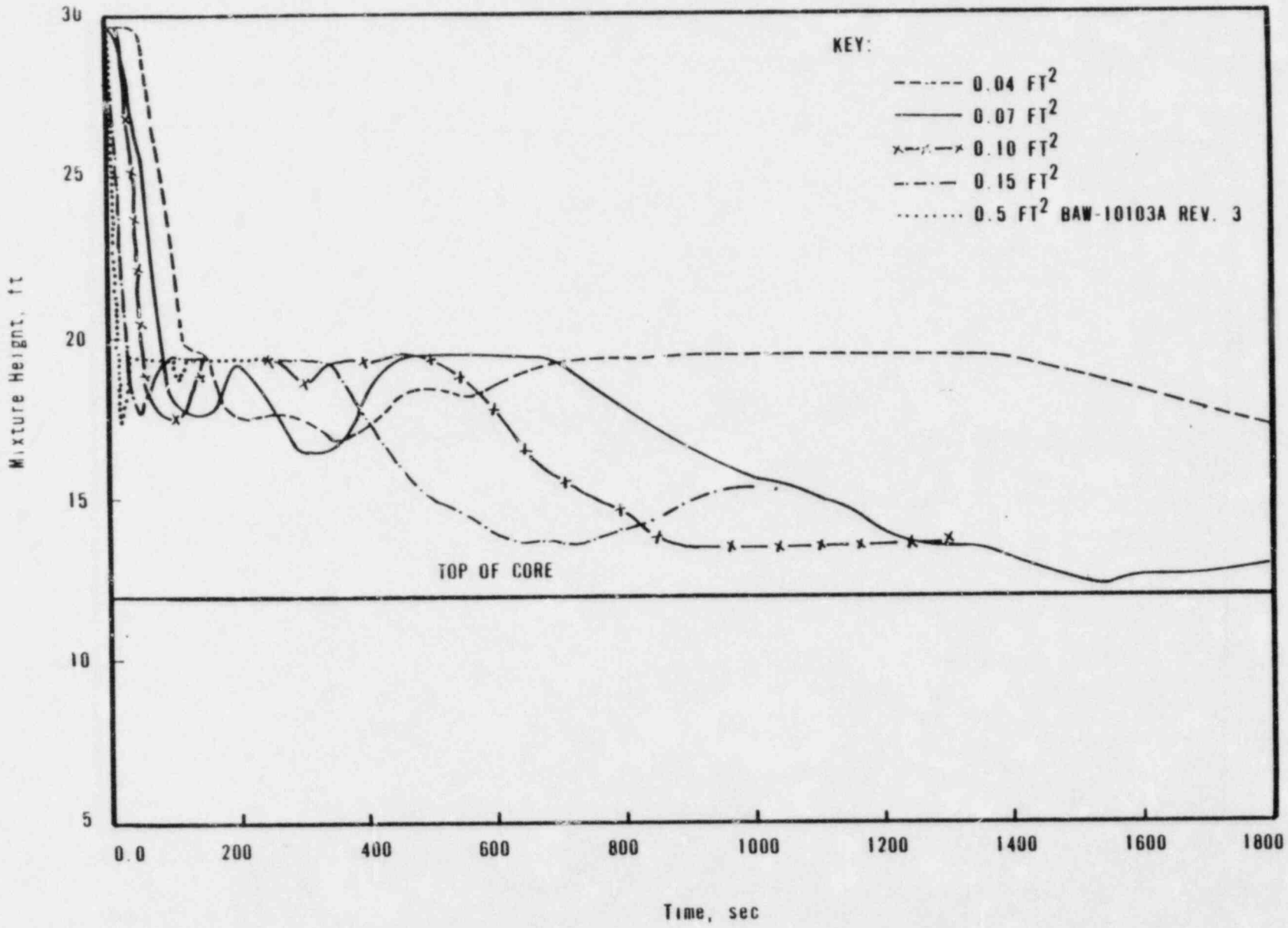

Figure B-11. Ratios of Measured Break Mass Flow Rates to Critical Mass Flow Rates Calculated Using Five Critical Flow Models (Tree-NUREG-1006)

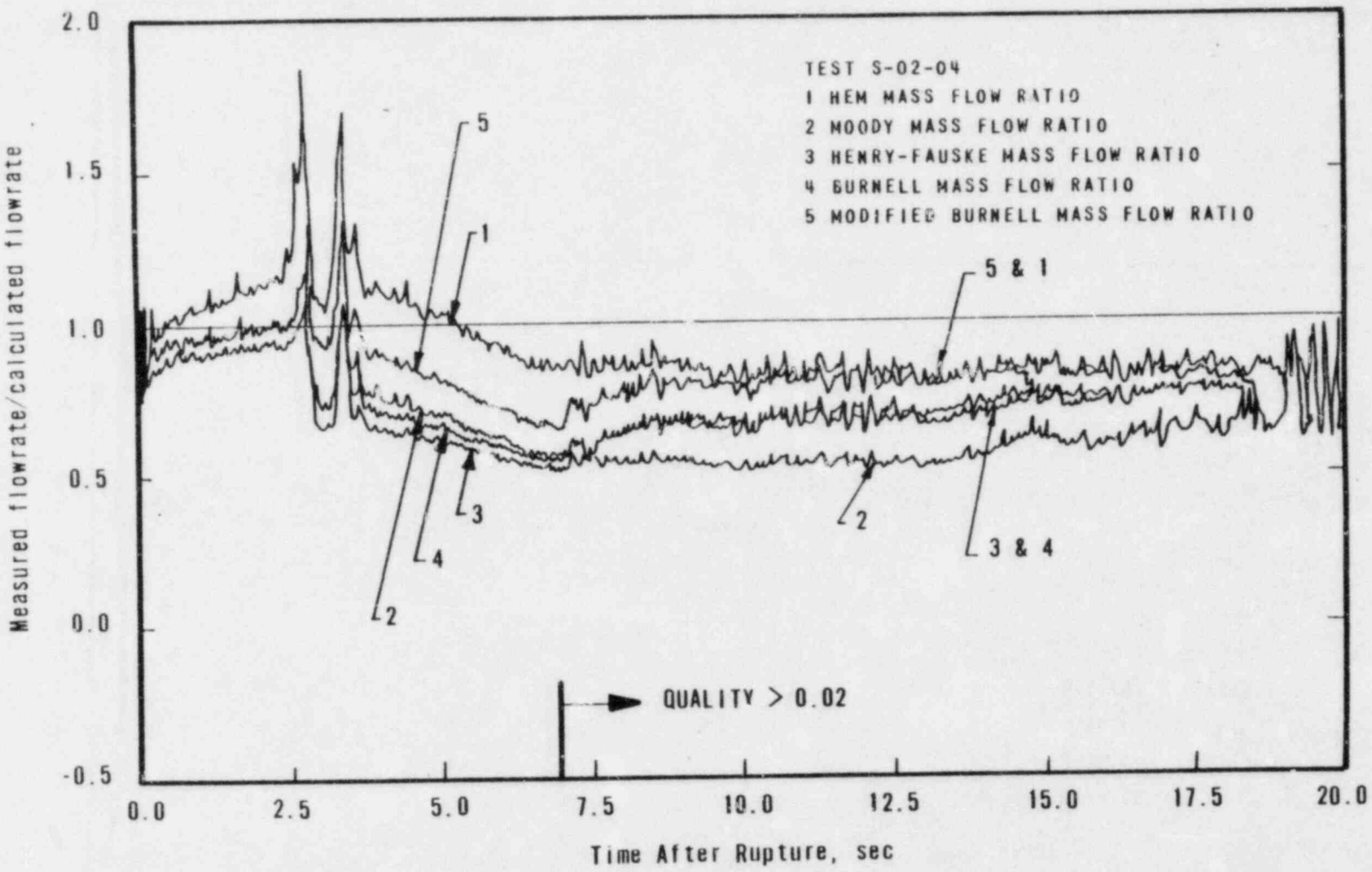

Figure B-12. Comparison of Critical Flow Models With Data[5]

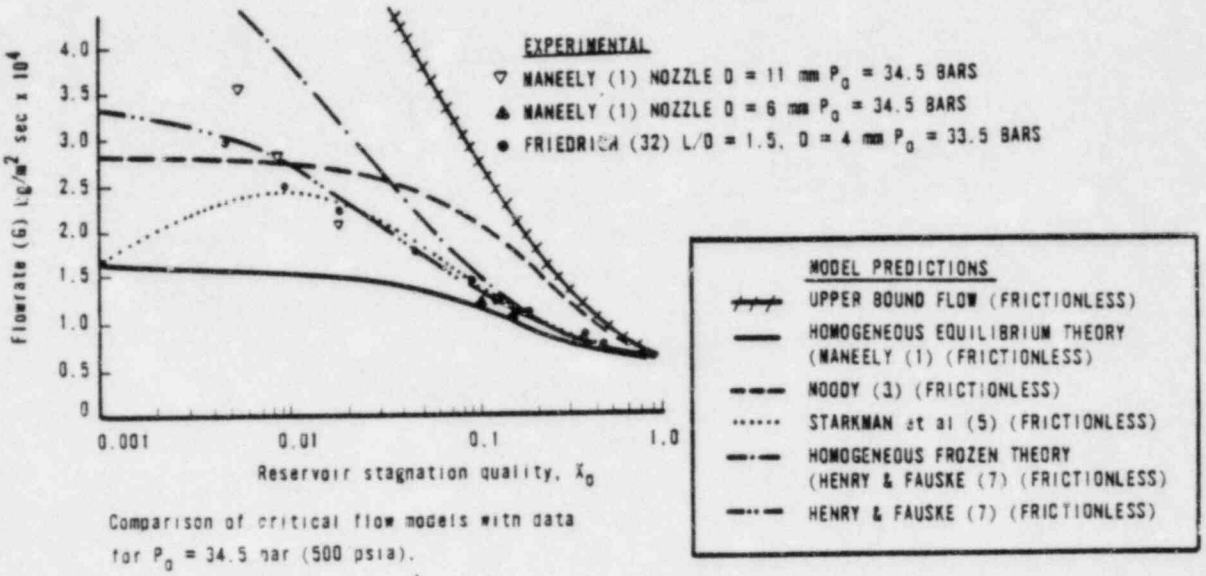

Comparison of critical flow models with data for P_0 = 34.5 bar (500 psia).

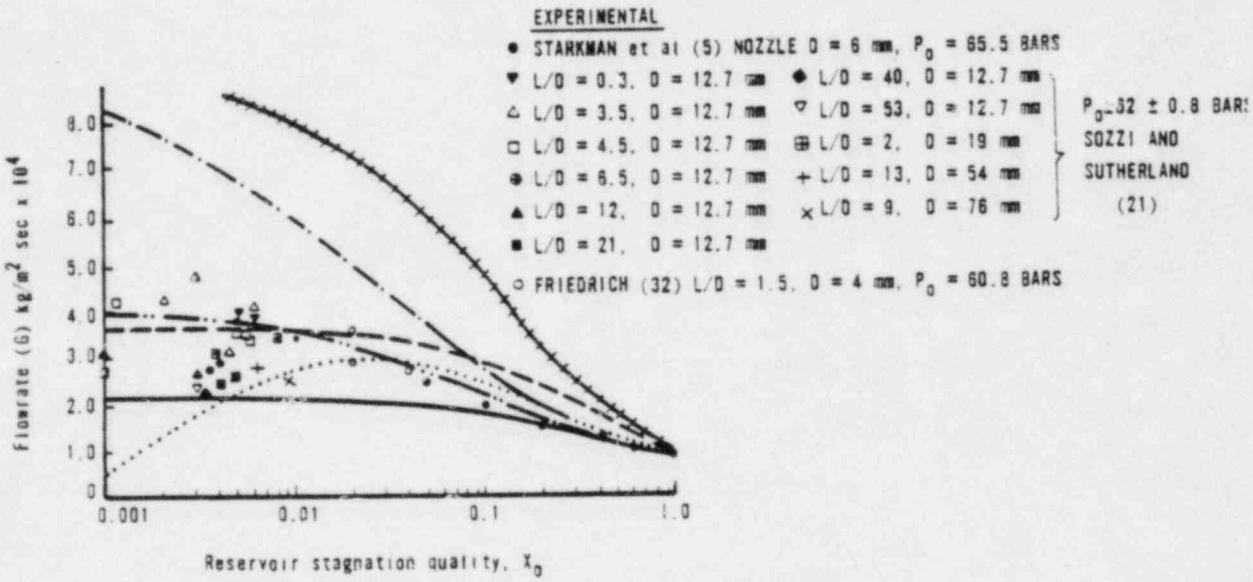

Comparison of critical flow models with data for P_0 = 62 bar (900 psia)

Figure B-13. Effect of Throat Length to Throat Diameter Ratio on Calculated Flow Multiplier for HEM[6]

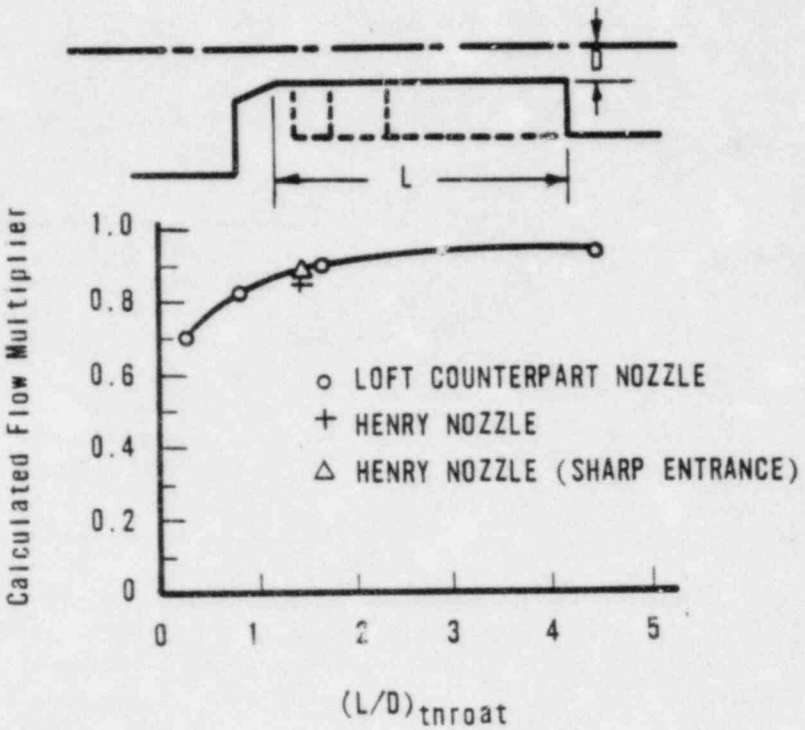

Figure B-14. Leak Quality for 0.07-ft^2 Break

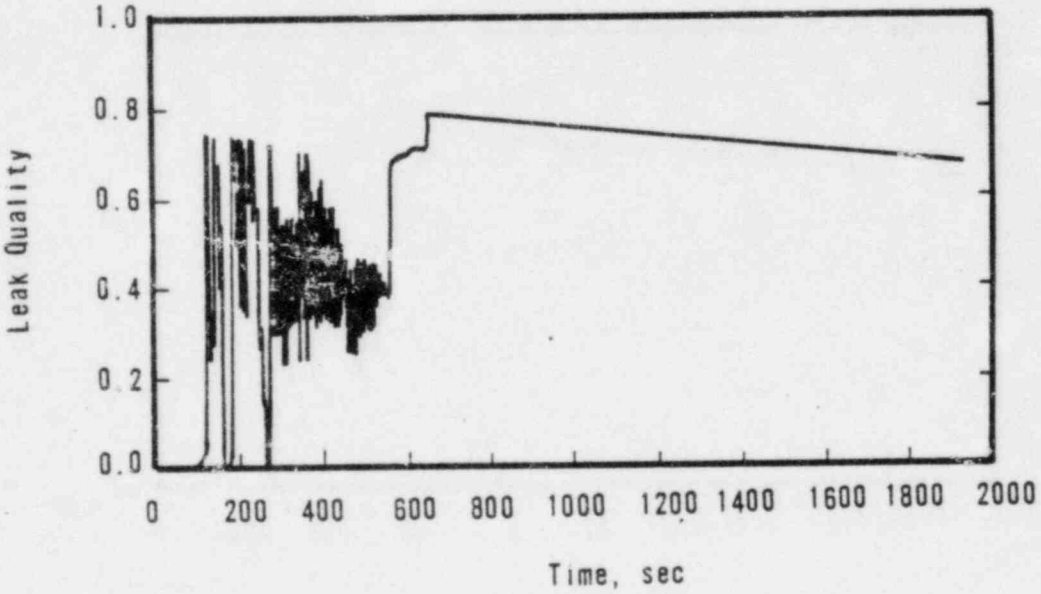

Figure B-15. Ratio of HEM to Moody Critical Flow Predictions

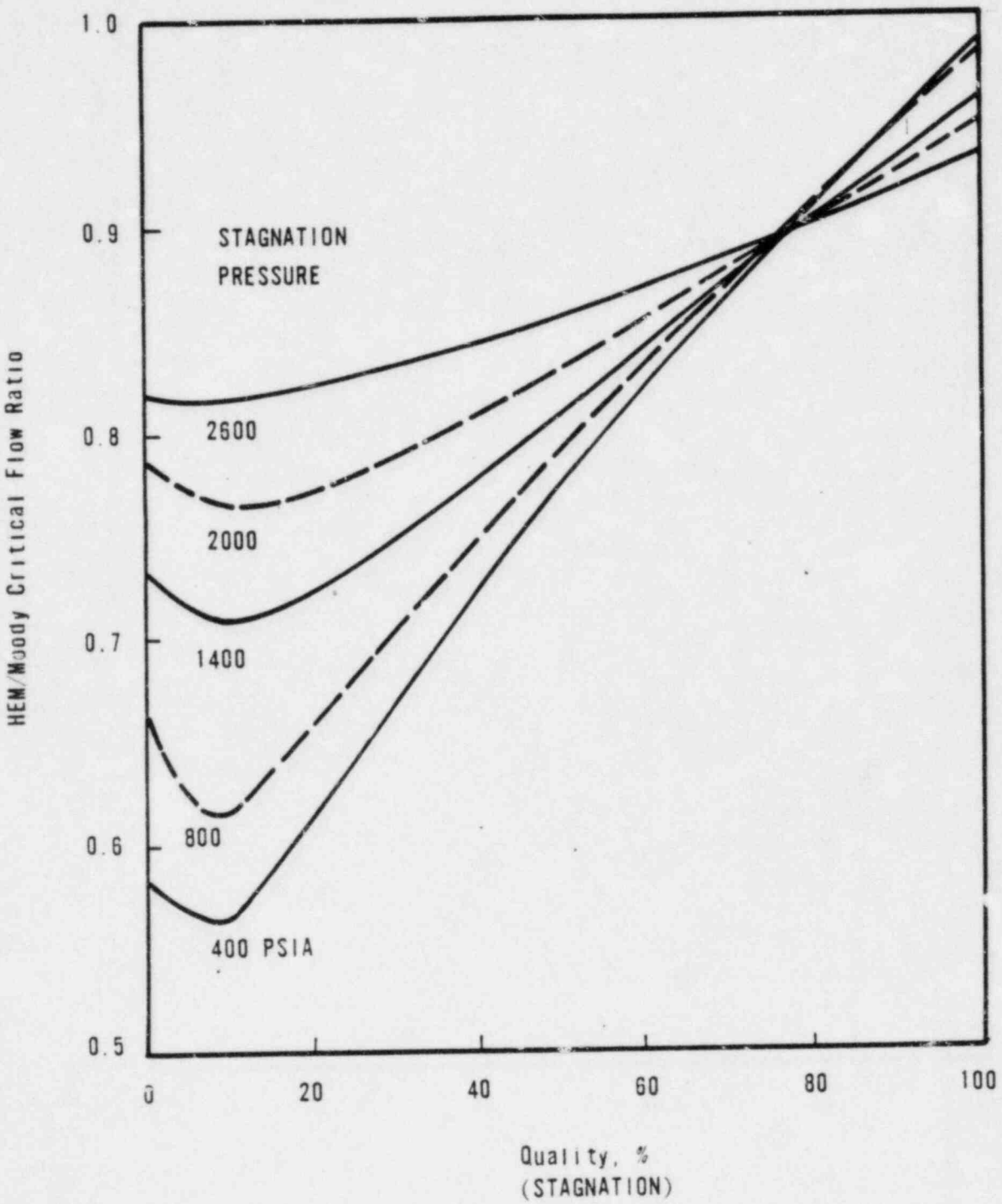

Figure B-16. Comparison of Integrated Leak Flow Vs Time for 177-FA Lowered-Loop Break at RC Pump Discharge

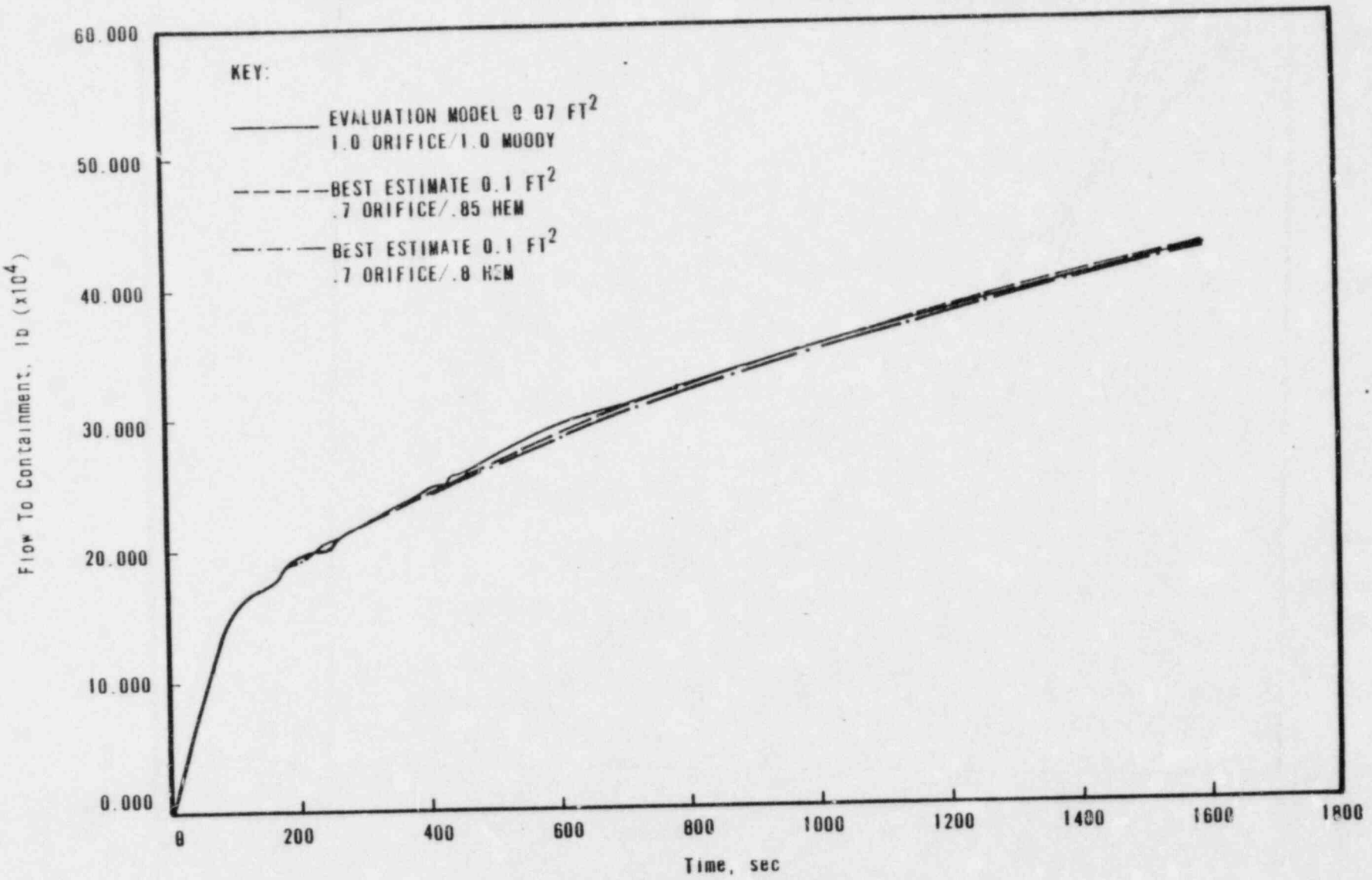

Figure B-17. Comparison of Pressure Versus Time for 177-FA Lowered-Loop Break at RC Pump Discharge

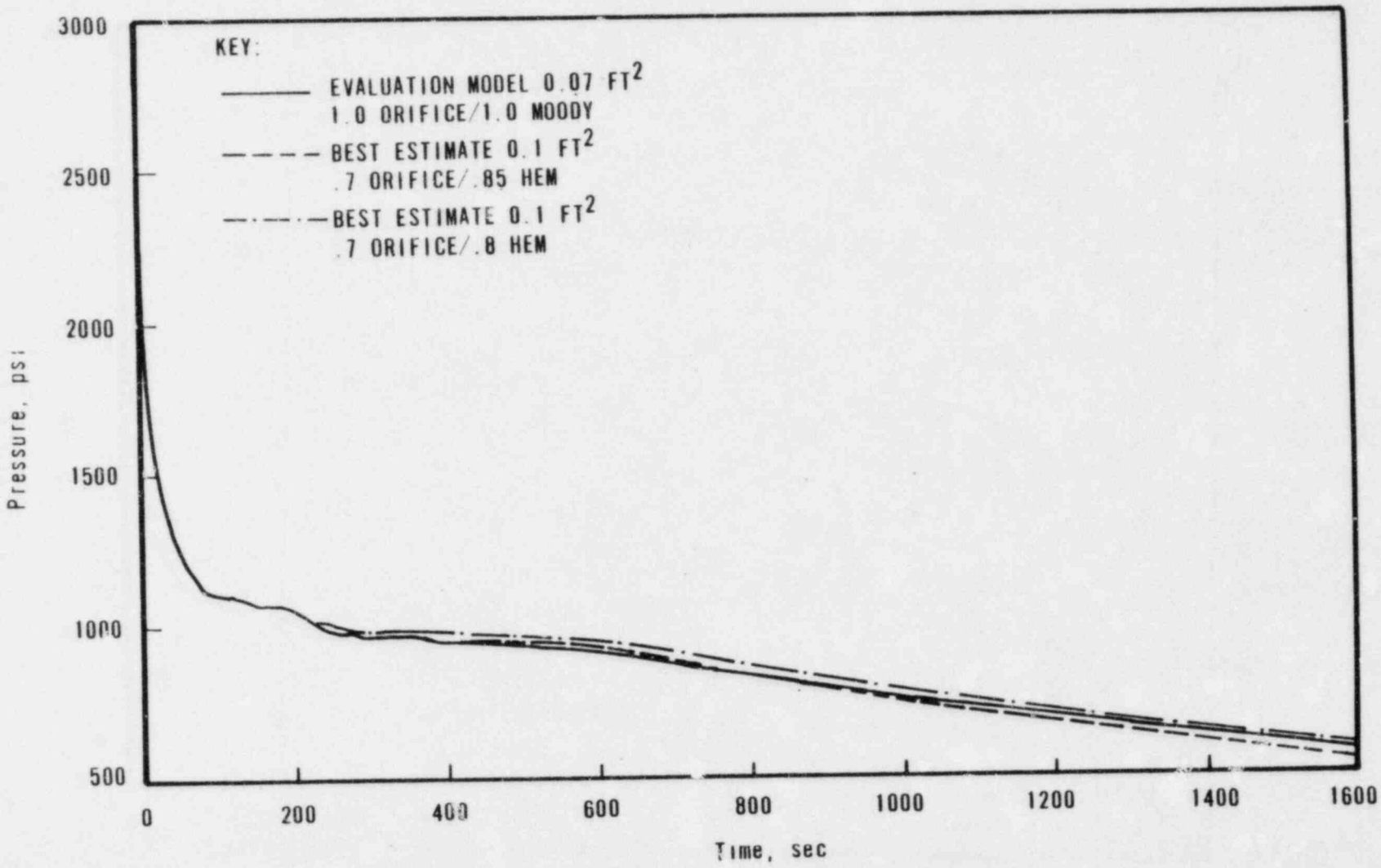

Figure B-18. Comparison of Core Mixture Level for 177-FA Lowered-Loop Break at RC Pump Discharge

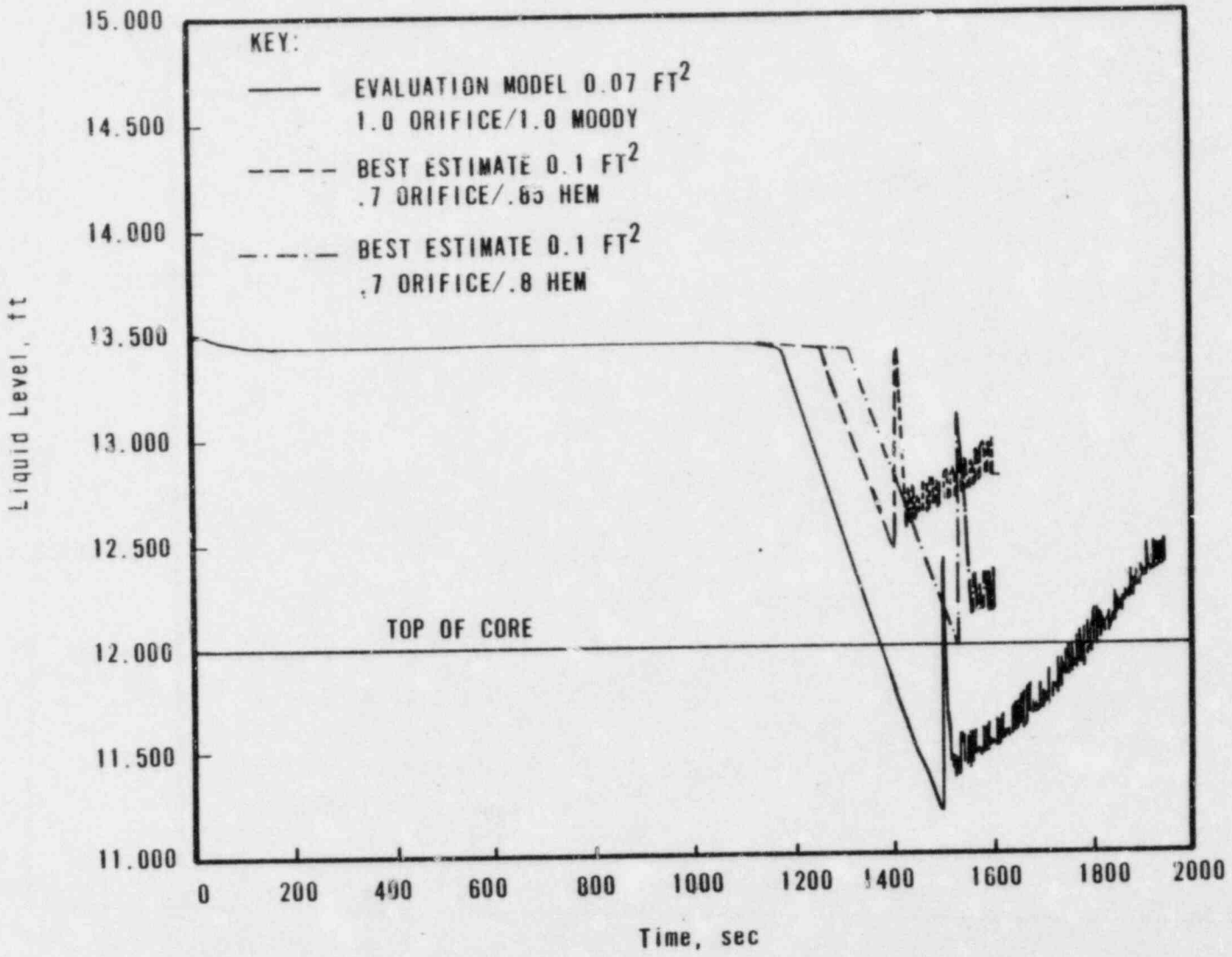

Figure B-19. Comparison of Best Estimate Pressure Prediction and Evaluation Model Results

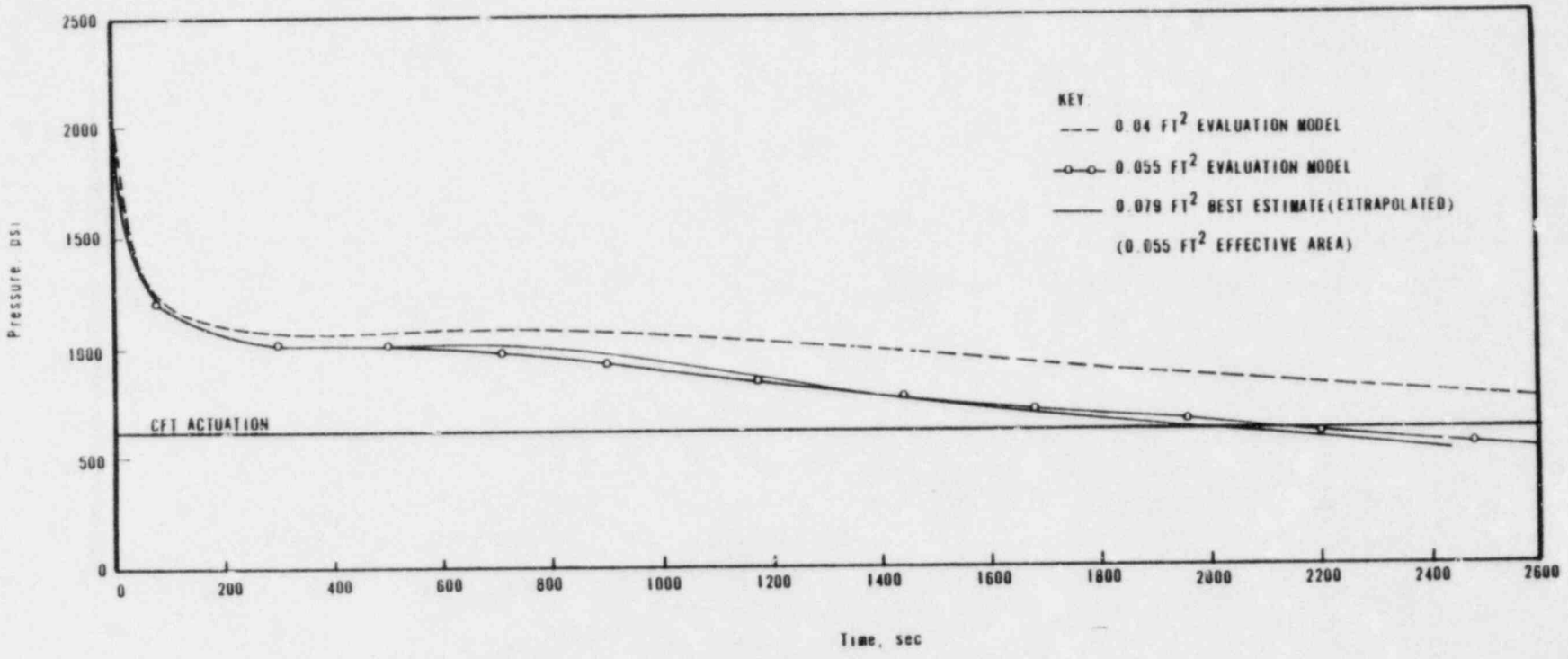

Figure B-20. Comparison of Best Estimate M ure Height Prediction and Evaluation Model Results

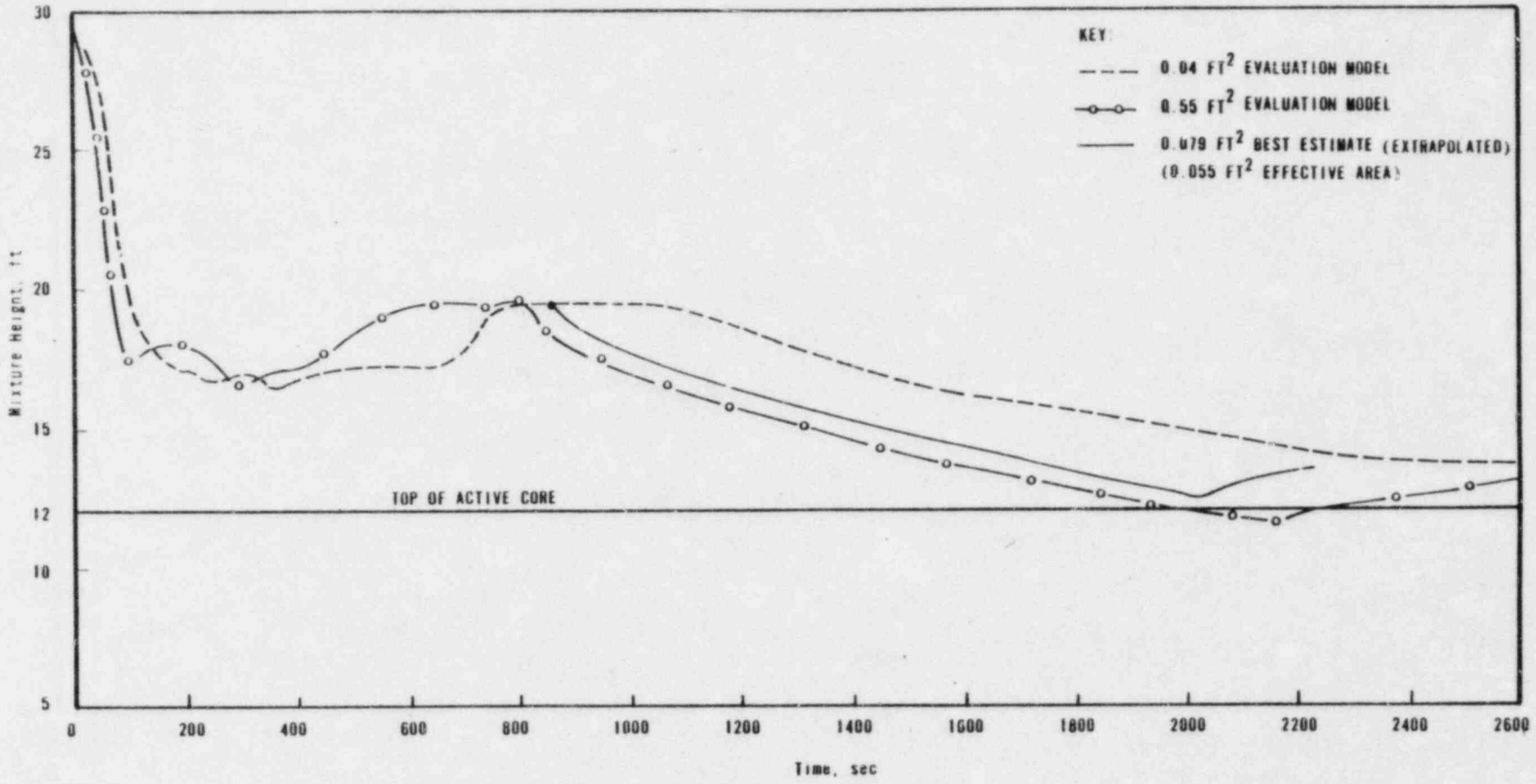

Figure B-21. Comparison of Best Estimate Pressure Prediction and Evaluation Model Results

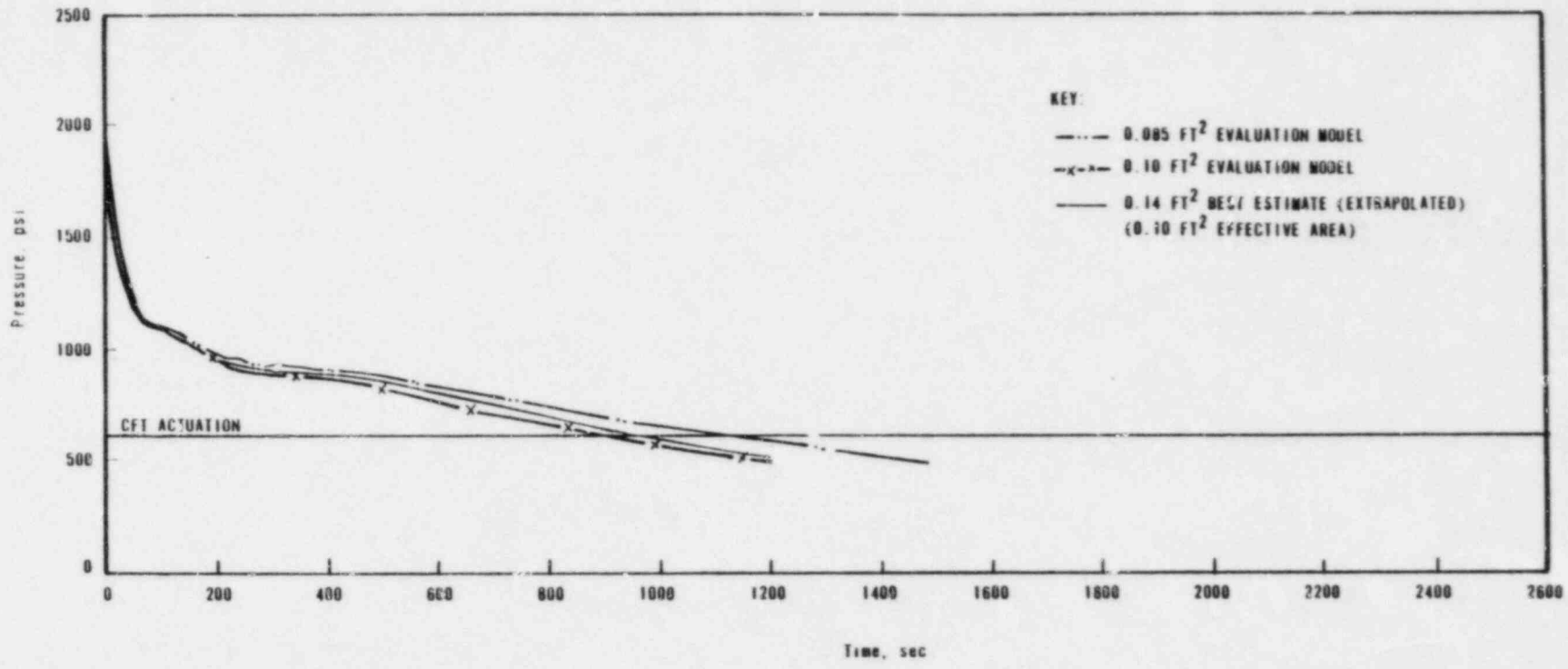

Figure B-22. Comparison of Best Estimate Mixture Height Prediction and Evaluation Model Results

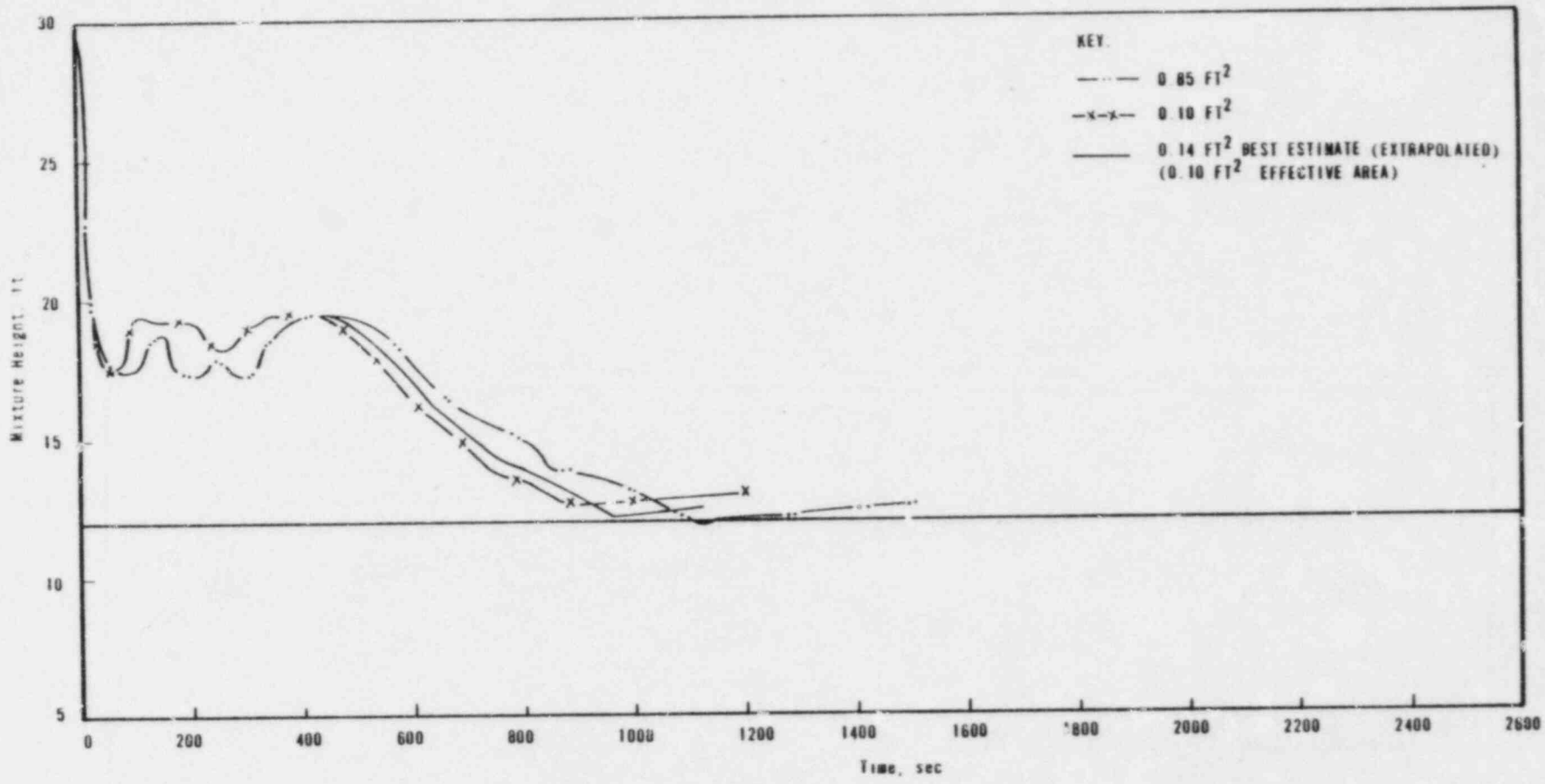

APPENDIX C

Surge Line Modeling — Task 1B of NUREG-0565 Program

1. Introduction

Pressurizer behavior played a key role in influencing operator actions in the TMI-2 accident. In particular, the insurge of fluid to the pressurizer led to incorrect operator diagnosis of system inventory. Because of this, the NRC Staff concluded that it was appropriate to re-examine the analytical modeling of the pressurizer and the surge line to determine if predicted behavior for other similar accidents would represent realistic behavior, and if it could be used by the operators for accident diagnostics. In particular, the Staff concerns focused on pressurizer and surge line modeling. This appendix addresses the concern on surge line modeling.

The B&W SBLOCA evaluation model represents the surge line connecting the hot leg to the pressurizer by a single flow path simulating a simple pipe. The flow is allowed in only one direction and is determined from the momentum equation; a critical flow check is performed. Hence, the present evaluation model does not account for countercurrent flow in the surge line should conditions predict its occurrence.

If countercurrent flow could be established in the surge line, the pressurizer liquid would drain while the hot leg steam flowed into the pressurizer. Failure to account for this countercurrent flow would not allow adequate pressurizer draining and, hence, lead to incorrectly predicted level behavior and liquid inventory distribution. As a result of this, in NUREG-0565, Section 4.1.1.1, paragraph 3, a concern is raised that the representation of the surge line could affect draining of the pressurizer and that a flooding check to the surge line should be added.

This appendix presents a discussion of the surge line response during various postulated small break scenarios and addresses whether adding a flooding check to the B&W surge line is necessary.

2. Summary

In order to assess the need for adding a flooding check to the surge line, a review of the surge line response during the following small break scenarios was made:

1. Small breaks that depressurize the reactor coolant system (RCS).
2. Small breaks that repressurize the RCS.
3. Pressurizer breaks.

The report demonstrates that, based on the geometry of the B&W pressurizer surge line, countercurrent flow within the surge line cannot exist to any significant degree. Consequently, the flow in the B&W pressurizer surge line will be in only one direction and the present modeling of the surge line by a single path is adequate. Thus, there is no need to add a flooding check in the model.

3. Small Break Phenomena and Surge Line Response for LOCA Scenarios

A loss-of-coolant accident (LOCA) is a transient in which liquid inventory is lost from the RCS. This results in system depressurization and may result in a partial or complete draining of the pressurizer. The response of the primary system to a small break will differ greatly depending on the break size, its location in the system, operation of the reactor coolant pumps, the number of ECCS trains functioning, and the availability of secondary side cooling. The extent to which the pressurizer will drain depends on surge line geometry, and fluid conditions in the pressurizer and hot leg, along with the factors described above.

The orientation of the B&W pressurizer in relation to the reactor coolant piping is shown in Figure C-1. Starting from the connection at the hot leg, the surge line is initially horizontal, and then drops vertically down, becomes horizontal again, and then rises vertically up to the pressurizer. With liquid level in the reactor coolant piping and no leak from the pressurizer, the level relationship between the pressurizer and the reactor coolant piping is $P_1 = P_2 + h$ (Figure C-1).

In order for countercurrent flow to exist within the surge line, certain conditions are necessary. The typical B&W surge line arrangement compared with the rising surge line arrangement from the hot leg to the pressurizer is shown in Figure C-2. With a surge line that is horizontal or rising from the hot leg to the pressurizer, it is possible under certain circumstances, to have countercurrent flow of steam and liquid where steam will rise toward the pressurizer and liquid will drain into the hot leg. This is not possible when either a water trap exists in the surge line or some portion of the surge line drops below the horizontal. As shown in Figure C-3, with a surge line that is continuously rising to the pressurizer, any steam that enters the surge line

will flow into the pressurizer. Otherwise, it would have to flow downward to return to the hot leg. In configurations containing a water trap and/or dropping section to the surge line, phase separation and stratification of two-phase flow tends to drive steam back into the hot leg; otherwise, the steam will have to travel downward to enter the pressurizer, which is not possible.

In order to assess the need for adding a flooding check to the B&W surge line, a review of the surge line response and the phenomena that occurs within the surge line during the following small break scenarios was made:

1. Small breaks that depressurize the RCS.
2. Small breaks that repressurize the RCS.
3. Pressurizer breaks.

3.1. Small Breaks That Depressurize RCS

A characteristic of LOCAs is system depressurization and partial or complete draining of the pressurizer. Because the RCS is initially subcooled and non-compressible, even a small loss of fluid through a break acts to depressurize the system. As the system depressurizes for this class of breaks, the pressure gradient across the surge line will quickly become quite large ($P_2 = P_1 - h$, shown in Figure C-1). This will cause the pressurizer to drain regardless of the surge line geometry The only way to stop this process is for the primary loop volume depletion to stop or for the pressurizer to empty. It is observed that the latter is always the case for the breaks analyzed previously.

In order for slip or countercurrent flow of steam and liquid to exist, the liquid will have to drain into the hot leg and the steam will have to rise to the pressurizer. A driving gradient to force slip or countercurrent flow, along with the path for steam to travel upward, is required for slip or countercurrent flow to exist within the surge line. The B&W surge line is initially horizontal from the connection at the hot leg and then drops vertically down. Therefore, in the B&W surge line the steam would have to travel downward to enter the pressurizer. Since this is not possible, countercurrent flow cannot exist in the B&W surge line during the pressurizer draining.

While the pressurizer is draining it is possible that a localized, insignificant amount of countercurrent flow can exist in the vertical section of the

surge line at the pressurizer. This is because the steam in this section of the surge line can travel upward while the liquid is draining to the hot leg. The consequences of this localized countercurrent flow within the surge line is expected to be insignificant and short lived. Once the pressurizer is empty and/or a water trap is formed on the hot leg side of the surge line, this localized countercurrent flow will stop.

Therefore, it can be concluded that for this class of breaks, there will be no appreciable countercurrent flow in the B&W surge line. The flow will be in only one direction and the present modeling of the surge line by a single flow path is adequate; thus, there is no need to add a flooding check to the B&W surge line.

3.2. Breaks That Repressurize RCS

In this category of breaks, the transient begins in a manner similar to those breaks that depressurize the RCS. That is, the RCS will depressurize and this will result in the partial draining of the pressurizer. For this class of breaks, a significant portion of the cooling, and hence, depressurization is accomplished by natural circulation. An interruption in the natural circulation can result in the repressurization of the RCS. During the repressurization the pressurizer will be refilled. Enough coolant will be forced back into the pressurizer to balance its pressure against that in the loop. Repressurization will continue until the RCS depletes sufficiently to allow the direct condensation of steam within the steam generator. This initiates the boiler-condenser mode of heat transfer which causes the system to depressurize and start emptying the pressurizer.

While the RCS is depressurizing, partial draining of the pressurizer will occur. As explained in section 3.1, during pressurizer draining countercurrent flow within the surge line cannot exist to any significant degree because of the B&W surge line geometry.

Due to the interruption in the natural circulation and temporary repressurization of the RCS, the refilling of the pressurizer will occur because the RCS will be at a higher pressure than the pressurizer. If slip or countercurrent flow occurred within the surge line, only liquid would be forced into the pressurizer and the steam would return to the hot leg. As shown in Figure C-1, for the steam to flow from the pressurizer to the hot leg during refilling of

the pressurizer it will have to travel downward. As this is not possible, the flow will be in only one direction during the refilling of the pressurizer.

Slip or countercurrent flow within the hot leg side horizontal section of the surge line may occur. This would force only liquid into the pressurizer, which may slightly alter the course of the transient. Since it would require more liquid in the pressurizer to maintain the pressure balance across the surge line, a more rapid depletion of the primary side would occur. This would result in earlier initiation of direct steam condensation in the steam generator and less system repressurization. This in turn means that more high pressure injection flow would be available and the overall leak flow would be reduced due to less time at higher pressure. As the additional liquid trapped in the pressurizer will not be lost and will return to the RCS during the subsequent depressurization phase, not allowing slip or countercurrent flow within this portion of the surge line is conservative.

Based on the above discussion, it can be concluded that the slip or countercurrent flow within the B&W surge line would only be localized and insignificant. Hence, the present technique of modeling the surge line by a single flow path with flow in only one direction is adequate. Therefore, there is no need to add a flooding check to the surge line.

3.3. Pressurizer Breaks

With regard to core cooling, a break in the hot leg or pressurizer is fundamentally less severe than the one at the lower elevation in the system. This is because the break at the lower elevation (e.g., cold leg) maximizes the potential of losing ECCS water and also maximizes the amount of RCS inventory sitting above the break location that can be lost through the break.

Although the break in the pressurizer may be less severe, it does cause some changes in the system behavior, particularly in the pressurizer itself. Therefore, it is felt that it is necessary that surge line response for this break also be analyzed. During the pressurizer break, the pressurizer loses mass and depressurizes. If this depressurization is faster than the RCS, the most likely situation, a pressure gradient will develop across the surge line that will force liquid into the pressurizer. In the case of the pressurizer initially venting steam, the level in the pressurizer will rise as the steam space is gradually replaced with the liquid from the RCS.

During the filling of the pressurizer, liquid and/or two-phase flow will enter the surge line. As explained in section 3.2, the coolant will be basically flowing in only one direction with insignificant localized countercurrent flow because of the typical B&W surge line geometry.

Once the hot legs are completely drained and/or a water trap is formed on the pressurizer side of the surge line, direct venting of steam through the surge line to the pressurizer will take place. This is because the elevation head of the liquid caught in the water trap is relatively small and a slight increase in the pressure gradient across the surge line is sufficient to force steam through the water trap (Figure C-4).

As the steam is vented through the pressurizer, localized countercurrent flow in the surge line may result in some liquid drainage from the pressurizer. However, as this liquid accumulates in the surge line, a loop seal would form in the vertical section of the surge line near the hot leg. This would stop the steam venting and the localized countercurrent flow. As a result, the RCS would repressurize slightly in order to clear the loop seal and re-establish steam venting through the pressurizer.

Thus, for this class of breaks, it is concluded that the overall flow (i.e., two-phase or steam) in the surge line will be in only one direction with insignificant localized countercurrent flow. Therefore, the current modeling technique of the surge line is adequate and there is no need to add a flooding check to the surge line.

4. Conclusions

The following conclusions can be drawn from this appendix:

1. Because of the typical B&W surge line geometry, slip or countercurrent flow within the surge line is expected to be only a localized effect.
2. A detailed review of the phenomena occurring within the surge line during the various small break scenarios was performed and demonstrates that the overall flow will be basically in only one direction within the B&W surge line.
3. Since no appreciable countercurrent flow is expected, the present technique of modeling the surge line is adequate and there is no need for code modification to add a flooding check to the surge line.

Figure C-1. Typical B&W Surge Line Arrangement

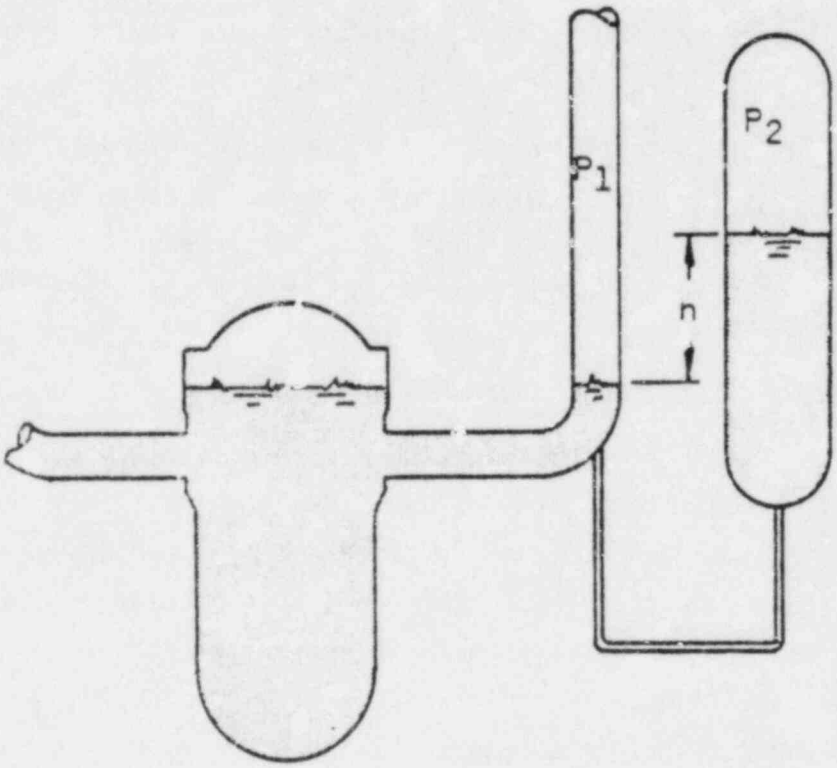

Figure C-2. Typical B&W Surge Line Arrangement Along With Rising Surge Line From Hot Leg to the Pressurizer

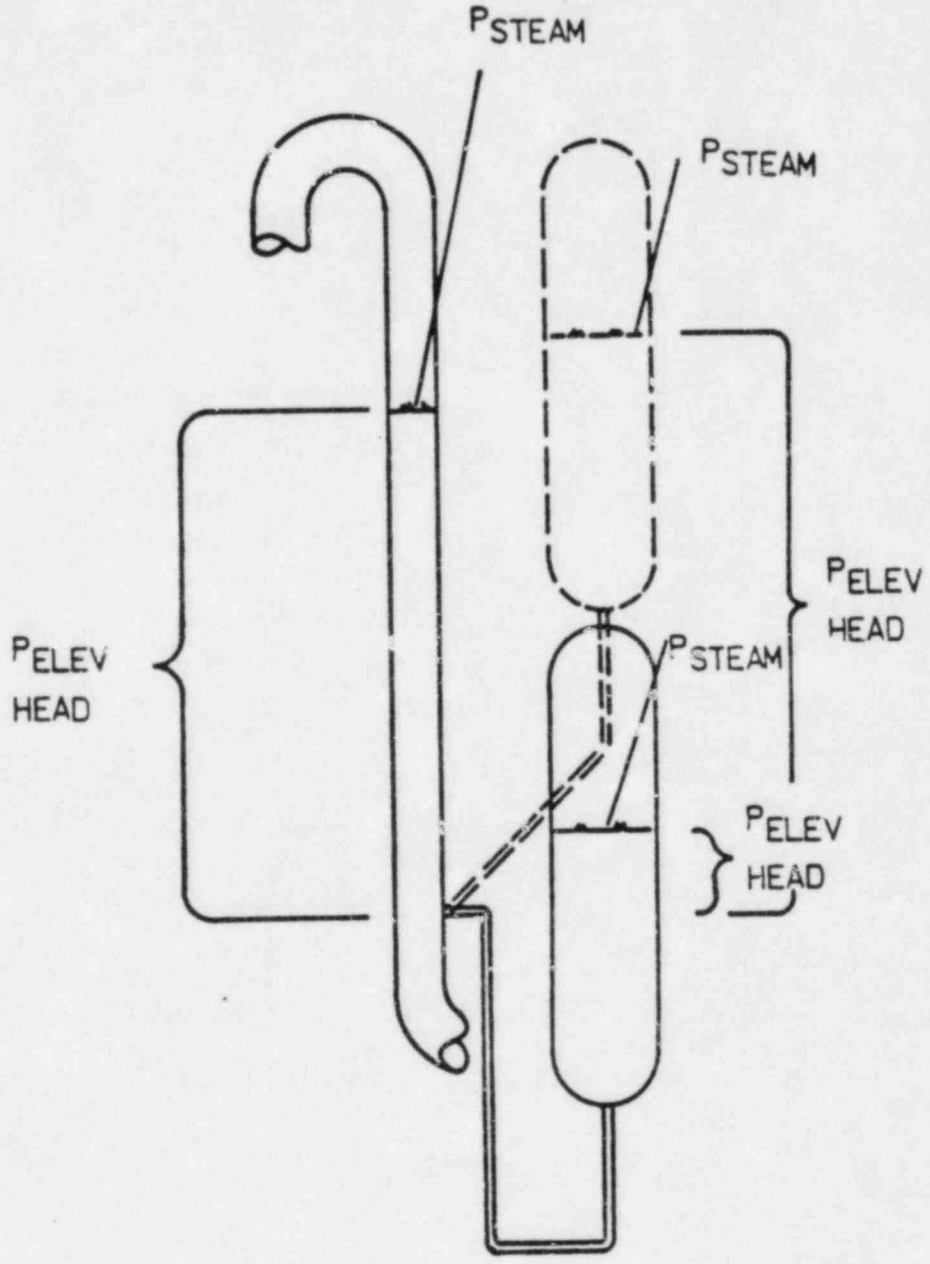

Figure C-3. Effect of Steam/Liquid Stratification and Slip in Different Surge Line Designs

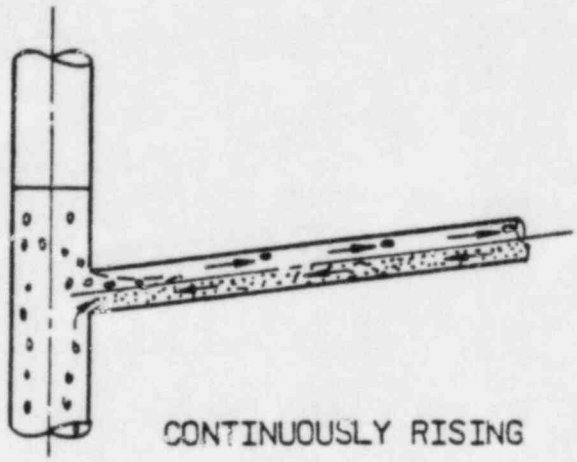

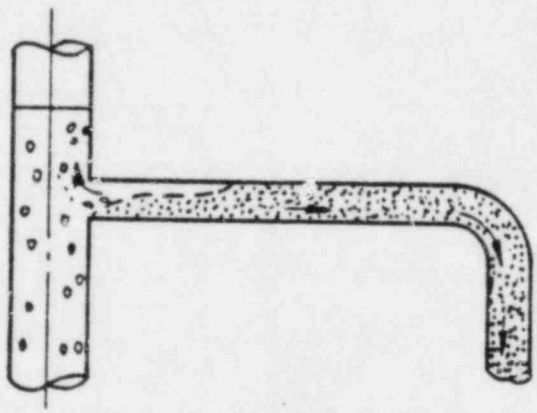

Figure C-4. B&W Surge Line With Watertrap

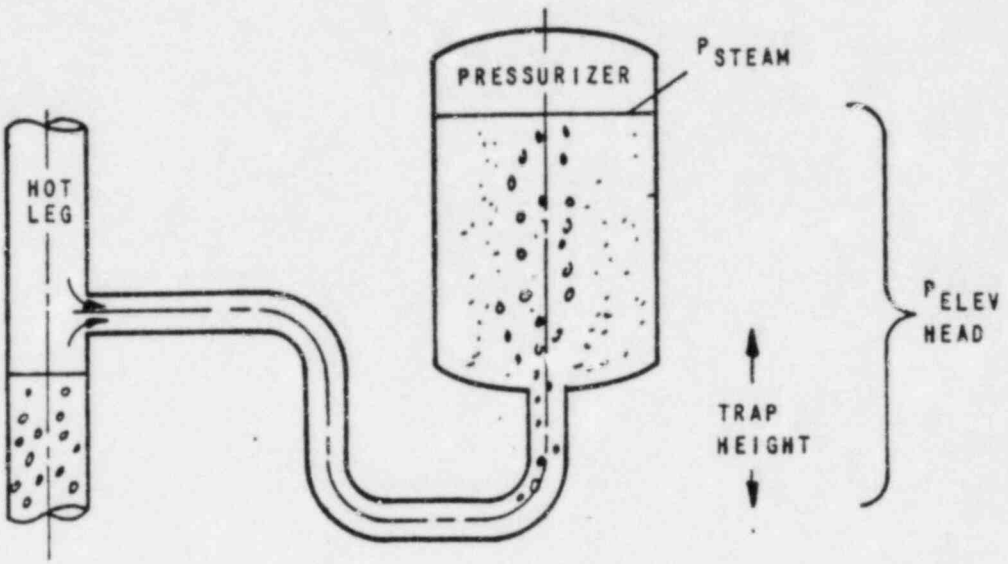

APPENDIX D

Evaluation and Justification of the B&W ECCS Injection Model

1. Introduction

In Section 4.1.1.1 of NUREG-0565[1] (item 8), the NRC questioned the adequacy of the emergency core cooling system (ECCS) injection modeling used in small-break LOCA (SBLOCA) evaluations. Specifically in question is the core flooding tank (CFT) injection model and its effect on system response. Current vendor ECCS analysis codes utilize a thermodynamic equilibrium assumption in calculating the effect of injecting subcooled CFT water into a control volume. Staff evaluations[2] indicate that, under certain conditions, using the equilibrium assumption may lead to gross distortion in the overall system response and nonconservative results.

This report provides a justification of the B&W CFT injection model. Since the CRAFT2[3] code also utilizes the thermodynamic equilibrium assumption within control volumes, previous ECCS analyses have been reviewed. It is the conclusion of this report that, because the B&W ECCS evaluation model utilizes injection into the lower downcomer region, the injection of CFT water does not result in a gross system disturbance.

A summary of the report and the conclusions drawn is included in section 2. An outline of the problem background and a further development of the NRC concern are provided in section 3. Section 4 provides a qualitative evaluation of the various parameters that affect the system response when CFT water is injected. The specific characteristics of the CFT injection model used in the B&W ECCS evaluation model are given in section 5. This section also provides the results of previous ECCS evaluations performed using the B&W model.

2. Summary and Conclusions

In NUREG-0565, the NRC questioned the adequacy of the ECCS injection modeling used in SBLOCA evaluations. Review of the basis for the NRC concern shows that the ECCS injection location used in SBLOCA evaluations can result in a gross system pressure disturbance after CFT actuation that is not seen in LOFT small-break experiments. By examining the controlling state variables, it is seen that the control volume fluid content has a significant impact on the resultant system depressurization caused by CFT actuation. Previous B&W small-break transient evaluations were reviewed to determine whether they exhibit the gross system disturbance of concern.

The review of the previous SBLOCA analyses showed that the downcomer liquid volume remains high throughout the transient. As a result of this high liquid content, the use of the thermodynamic equilibrium assumption does not illustrate the gross system disturbance of concern. The system depressurization characteristics predicted by the analyses are not significantly altered by the CFT injection. Thus, it was found that the ECCS injection modeling employed in the B&W evaluation model provides an adequate representation of the actual phenomena and system response that occurs following CFT injection.

3. Background

In NUREG-0565 the NRC questioned the adequacy of the thermodynamic equilibrium assumption, used within control volumes in the B&W CRAFT2 code, during CFT injection. As a result of the thermodynamic equilibrium assumption, if steam is present at the injection point used in the model, the temperature of the subcooled ECC water is raised by instantaneously condensing steam and thereby causing a local depressurization. The amount of local depressurization that occurs is highly dependent on the injection location, the size of the control volume, and its steam/water composition. Of concern is the effect of this local depressurization on the overall system response.

To evaluate this concern, EG&G has performed studies[2] for the NRC wherein the sensitivity of the primary system pressure response to the ECC injection location was examined. The results of these studies are shown in Figures D-1 and D-2, which have been taken directly from NUREG-0623.[2] Three injection points were studied: the cold leg, upper downcomer, and lower downcomer. Figure D-1 shows the effect of injection location on the primary system pressure transient. As can be seen from the figure, a considerable change in the system depressurization rate occurred after initiation of the CFTs, for the cold leg and upper downcomer injection points, while no alteration in the depressurization rate is seen for the lower downcomer injection case. The resultant injected mass that occurs for the various depressurizations is illustrated on Figure D-2. As is evident from the figure, the gross disturbance in the system pressure response, caused by CFT injection into the cold leg and upper downcomer locations, results in a large mass addition to the primary system. This in turn has a dominating effect on core mixture level, which directly affects the peak cladding temperature. In light of the calculated sensitivity

of system response to the injection location, experimental data must be examined to determine whether the calculated response is real or a byproduct of the thermodynamic equilibrium assumption.

Further insight to the effect of CFT injection on the primary system response can be obtained by examining small break test data obtained at the LOFT facility.[4] Figure D-3 shows the system pressure transient for LOFT test L3-1[5], which was a simulated 4-inch cold leg break. As is evident from the figure, while there was a slight increase in the depressurization rate following accumulator (CFT) injection into the cold leg, no gross alteration in the system depressurization rate occurred. This is in marked contrast to the calculated system depressurization caused by accumulator injection into the cold leg seen in Figure D-1.

Based on the computer evaluations and the LOFT test data, the NRC has questioned the adequacy of the thermodynamic equilibrium assumption used to calculate how the system response is affected by CFT injection. The computer evaluations that have been performed show that the equilibrium assumption can cause a gross alteration of the system depressurization following CFT actuation and which, in turn, can result in injection of a substantial amount of CFT liquid and a rapid core recovery. As illustrated by the LOFT test (Figure D-3), such a prediction is not realistic and would yield a non-conservative assessment of the transient consequences. Thus, the NRC has requested additional justification of the present CFT injection models.

4. ECC Injection Variables

The B&W CRAFT2 code uses a control volume representation wherein all fluid within the control volume is assumed to be in thermodynamic equilibrium. As a result of this assumption, when the subcooled ECCS water is injected into a control volume containing steam, the equilibrium model will result in an instantaneous condensation of steam as the ECC fluid is raised to saturated conditions. The subsequent response of the primary system to this instantaneous condensation is affected by several variables. As noted previously, the calculated system pressure response following CFT injection is dependent on the injection location. In order to aid in understanding the sensitivity analyses discussed in the previous section and the results obtained with the B&W ECCS evaluation model[6,7] (which are discussed in the next section), a qualitative

assessment of the important variables affecting the system response following CFT injection is provided below.

4.1. Control Volume Fluid Content

As previously described, injection of subcooled ECC liquid into a control volume that has some steam content will result in a local depressurization. The amount of depressurization that occurs depends on the control volume fluid content at the time of CFT injection. As illustrated below, CFT injection into a node containing a significant mass of liquid dampens the effect of the steam condensation, thereby ensuring a relatively stable system response.

To illustrate this effect, consider the two control volume configurations (prior to CFT injection) shown in Figure D-4. In one case (A), it is assumed that there is no liquid content in the node, i.e., steam-filled node, just prior to CFT actuation. In the second case (B), the node is assumed to be approximately three-quarters full of liquid prior to CFT acutation. Assuming a control volume size of 750 ft^3, which is the approximate size of the lower downcomer region in a B&W 177-FA plant, and a system pressure of 600 psia, which is the approximate CFT actuation pressure, the pre-CFT injection nodal conditions shown in Figure D-4 are obtained. Using one second of CFT injection at 100 lb/s, which is a typical average injection flow from the CFT for a small break transient, the post-CFT conditions shown in Figure D-4 are obtained. As can be seen, the node pressure decreased by 30 psi due to the effect of the cold CFT injection into the steam-filled node, while in the case of the three-quarter-filled node, the local depressurization was dampened to only 6 psi. Thus, it is seen that the liquid content at the injection point has a significant impact on the local depressurization that occurs after CFT actuation.

4.2. Control Volume Size

The control volume size can also affect the amount of local depressurization that can occur following CFT actuation. Obviously, if the control volume is small, the impact of any cold ECC injection would be more pronounced since the resultant change in the nodal mass and energy content of the control volume would be larger. Thus, it is expected that to minimize any gross distortion in the overall system response, the ECC injection volume should be as large as practicable for the transient evaluation.

To examine the influence of control volume size on local depressurization, several simplified calculations were performed using the same assumptions discussed in section 4.2 except that node size and liquid/vapor content were varied. Table D-1 is a summary of the cases analyzed and the resultant system pressure following CFT actuation.

As can be seen from the table, while the depressurization which occurs is somewhat sensitive to node size, the control volume fluid content is the more sensitive parameter. For the initially steam-filled control volumes (cases 1 through 3), varying the control volume size from 375 to 1500 ft^3 results in final system pressures of 540 to 585 psia, respectively. For the cases where a liquid content was assumed (cases 4 through 7), variation of the control volume size from 375 to 1500 ft^3 resulted in a final pressure state that varies only from 587 to 597 psia.

Based on the evaluations described above, it is concluded that the control volume size should be as large as practicable in order to minimize the potential for gross distortion of the system response due to CFT actuation. However, if the control volume is assured of having a significant liquid content, control volume size is a second-order effect. Thus, other modeling considerations, such as ensuring adequate nodal detail for the model, can be used to define the control volume size.

4.3. Injection Location

Depending on the selection of control volume size and the fluid content, the ECC injection location can impact prediction of the system response following CFT actuation. The sensitivity studies discussed in section 3 illustrate the potential effect of this parameter. The subsequent paragraph relates the results of the sensitivity analyses (discussed in section 3) to the qualitative analyses provided above concerning control volume fluid content and size effects on the resultant system pressure.

In the sensitivity studies, three ECC injection points were studied: the cold leg, upper downcomer, and lower downcomer. As seen in Figure D-1, the cold leg and upper downcomer injection cases exhibited a large system depressurization following CFT actuation, while the system pressure response for the lower downcomer injection case was not altered by CFT injection. These differing responses are primarily a result of the different control volume fluid contents

and sizes at each injection location. At the time of CFT actuation, the majority of the primary system inventory would have been lost through the break with the remaining liquid inventory residing primarily in the lower regions of the reactor vessel. Thus, at the time of CFT actuation, the cold leg and upper downcomer regions of the system are expected to contain only steam. As a result of the CFT actuation, portions of the steam within the control volume are condensed, causing a system depressurization. This phenomenon was shown in the studies performed in section 4.1. For the lower downcomer injection case, a significant amount of liquid resides within the control volume. As a result of the large liquid fraction, and as shown in the studies in sections 4.1 and 4.2, CFT actuation had little effect on system pressure response.

As described above, the ECC injection location used in the model can influence the overall system response following CFT actuation. In order to ensure that CFT injection does not cause gross distortion of the system response, the injection location must be chosen to ensure that a significant liquid content will exist in the volume at the time of CFT actuation. In the B&W evaluation model the lower downcomer volume is used as the CFT injection point. The adequacy of this choice is discussed in section 5.

5. B&W System Features and Evaluation Model Results

Sections 1-4 provided background to the NRC concern on ECC injection modeling and the important variables affecting system response after CFT injection. This section describes the B&W system design features related to the concern, along with the techniques used in the B&W evaluation model. Also presented are small-break LOCA results obtained with the evaluation model. As will be seen, the evaluation model results exhibit stable system pressure response to CFT actuation. Thus, the evaluation model does not produce the system response of concern, and the modeling techniques utilized are adequate.

5.1. B&W System Features

The B&W-designed NSS employs direct CFT injection into the reactor vessel downcomer, as opposed to the cold leg injection employed in other PWR designs. In addition, the B&W system has RV internals vent valves, which provide a direct communication path between the upper plenum and downcomer regions of the vessel. The communication path provided by the vent valves ensures essentially

equal downcomer and upper plenum pressures during a small break transient. As a result of this pressure equivalence, the water levels in the downcomer and the core are maintained at similar values. Since the core is generally calculated to remain covered throughout a small-break transient in a B&W plant, a significant liquid inventory is maintained in the downcomer. Thus, CFT actuation is not expected to cause significant depressurization.

5.2. Evaluation Model Results

Figure D-5 is a typical noding diagram used in previous small-break evaluations. As can be seen, the downcomer region is modeled in two axial nodes separated at the inlet nozzles. To preclude potential problems of CFT injection into a steam-filled region, the CFT is modeled as injecting into the lower downcomer region (node 1). This region generally maintains a significant liquid inventory throughout a small-break transient, minimizing the potential for gross system distortion due to CFT injection.

Previous small break transient evaluations have been reviewed to determine the adequacy of the ECC injection modeling.[8-10] Figures D-6 through D-9 present the system pressure responses for a spectrum of small breaks for the 177-FA lowered-loop plants.[8] Similar results were obtained in other plant evaluations.[9,10] As can be seen from these figures, system pressure response to CFT actuation was stable; i.e., it did not exhibit the gross disturbance of concern. Examining the influence of CFT actuation on the core mixture level response (Figures D-10 through D-13), it is seen that while some oscillatory mixture level behavior occurs after CFT actuation, these oscillations are small (generally less than 0.2 ft) and exhibit a slow, steady recovery of the core mixture level.

As a result of the review of previous evaluations, it is clear that the B&W evaluation model does not exhibit the gross system disturbance of concern. Because the modeling approach employs direct CFT injection into the reactor vessel downcomer, the large liquid volume in this region "dampens" the depressurization effect of CFT injection, thereby ensuring a stable system pressure transient. Thus, it is concluded that the ECC injection modeling used in the B&W evaluation model provides an adequate representation of the actual phenomena and system response that occur following CFT injection.

6. References

1. "Generic Evaluation of Small Break Loss-of-Coolant Accident Behavior in Babcock & Wilcox-Designed 177-FA Operating Plants," NUREG-0565, U.S. Nuclear Regulatory Commission, January 1980.

2. "Generic Assessment of Delayed Reactor Coolant Pump Trip During Small Break Loss-of-Coolant Accidents in Pressurized Water Reactors," NUREG-0623, U.S. Nuclear Regulatory Commission, November 1979.

3. R. A. Hedrick, J. J. Cudlin, and R. C. Foltz, CRAFT2 - FORTRAN Program for Digital Simulation of a Multinode Reactor Plant During Loss of Coolant, BAW-10092, Rev. 3, Babcock & Wilcox, November 1982.

4. D. L. Reeder, LOFT System and Test Description, NUREG/CR-0247, TREE-1208, July 1979.

5. P. D. Bayless, J. B. Marlow, and R. H. Averill, Experiment Data Report for LOFT Nuclear Small Break Experiment L3-1, NUREG/CR-1145, EGG-2007, January 1980.

6. B. M. Dunn, et al., B&W's ECCS Evaluation Model, BAW-10104, Rev. 2, Babcock & Wilcox, May 1976.

7. J. H. Taylor (B&W) to S. A. Varga (NRC), Letter, May 26, 1978.

8. J. H. Taylor (B&W) to S. A. Varga (NRC), Letter, July 18, 1978.

9. R. C. Jones, B. M. Dunn, and C. E. Parks, Multinode Analysis of Small Breaks for B&W's 205-Fuel Assembly Nuclear Plants With Internals Vent Valves, BAW-10074A, Rev. 1, Babcock & Wilcox, March 1976.

10. L. R. Cartin, J. M. Hill, and C. E. Parks, Multinode Analysis of Small Breaks for B&W's 177-Fuel assembly Nuclear Plants With Raised-Loop Arrangement and Internals Vent Valves, BAW-10075A, Rev. 1, Babcock & Wilcox, March 1976.

11. B&W Calculation File No. 86-1134304-00, Babcock & Wilcox, May 1982.

Table D-1. Control Volume Size Study

Case No.	Volume, ft^3	Liquid/ steam, vol %	Initial mass, lb liquid/ steam	Resultant pressure, psia
1	375	0/100	0/487	540
2	750	0/100	0/974	570
3	1500	0/100	0/1948	585
4	750	75/25	27,943/244	594
5	1500	75/25	55,887/487	597
6	1500	37.5/62.5	27,943/1218	595
7	375	75/25	13,972/122	587

Figure D-1. Safety Injection Location Studies — Westinghouse Four-Loop PWR 4-Inch Break

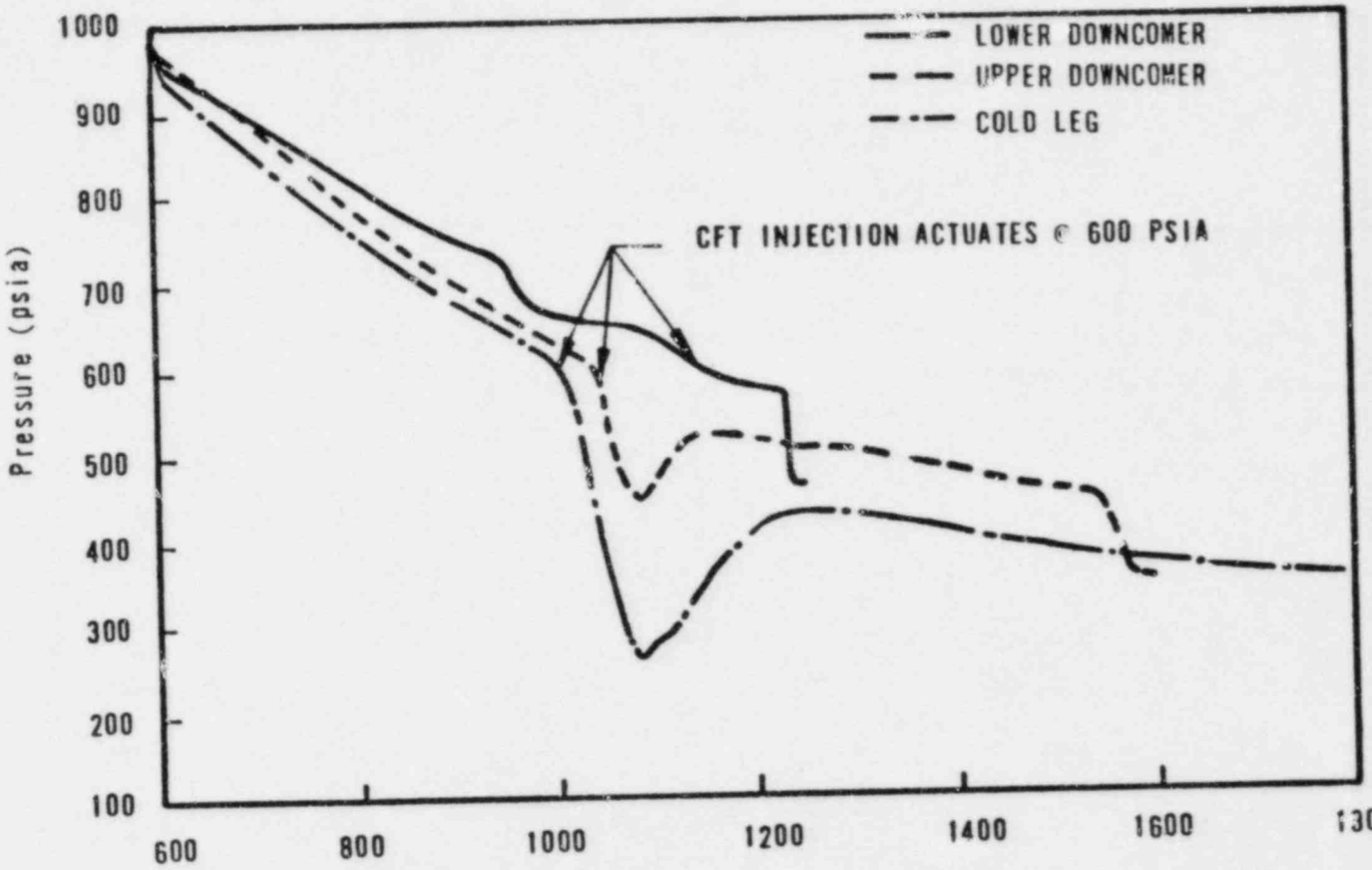

RELAP4/MOD7 SENSITIVITY ANALYSES

FROM NUREG-0623

Figure D-2. Safety Injection Location Studies — Westinghouse Four-Loop PWR 4-Inch Break

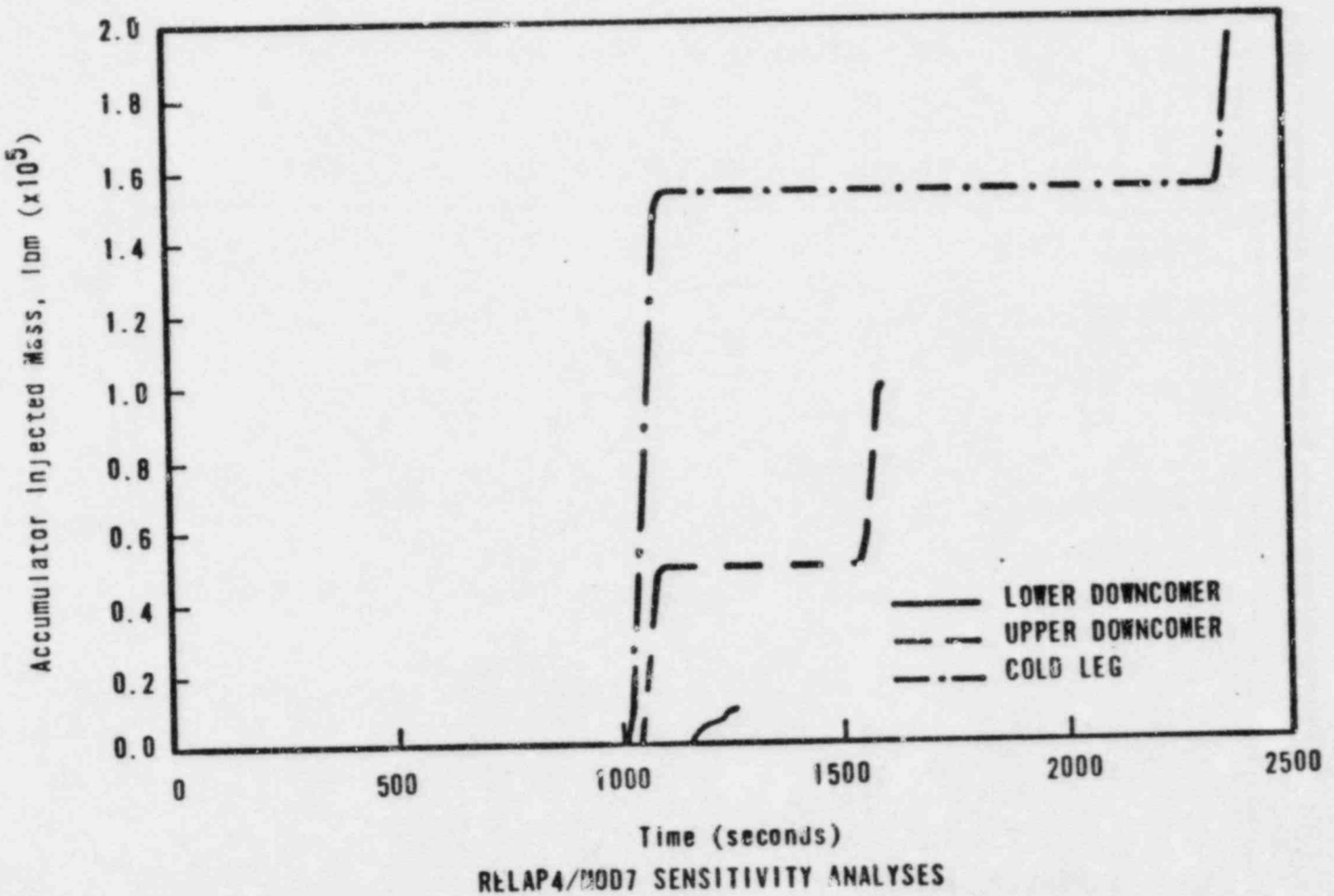

RELAP4/MOD7 SENSITIVITY ANALYSES

FROM NURGE-0623

Figure D-3. L3-1 System Pressure

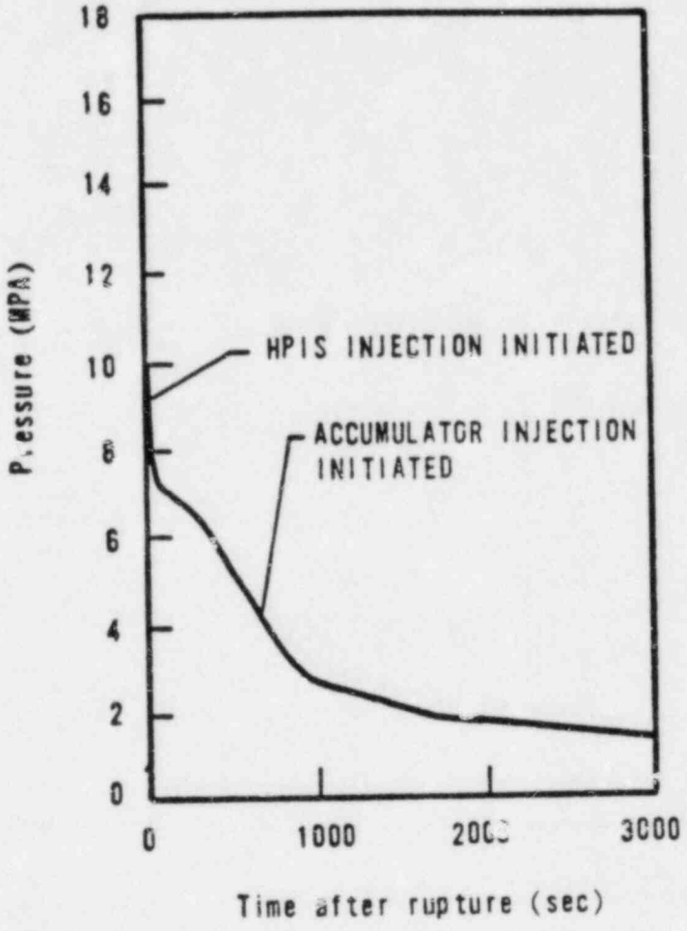

Figure D-4. Liquid Content Sensitivity Evaluation, CFT Actuation Pressure 600 psi

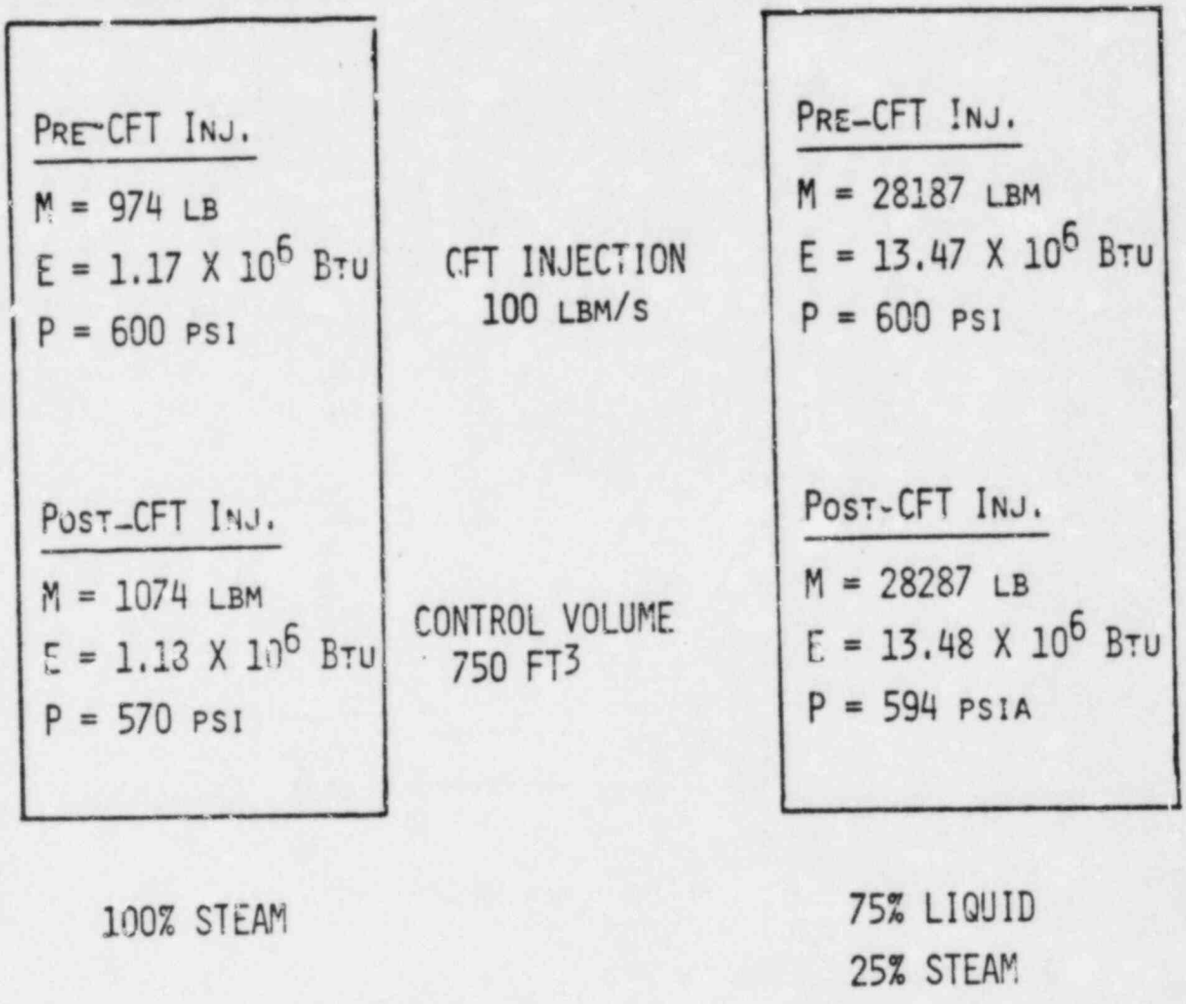

Figure D-5. CRAFT2 Noding Diagram for Small Breaks

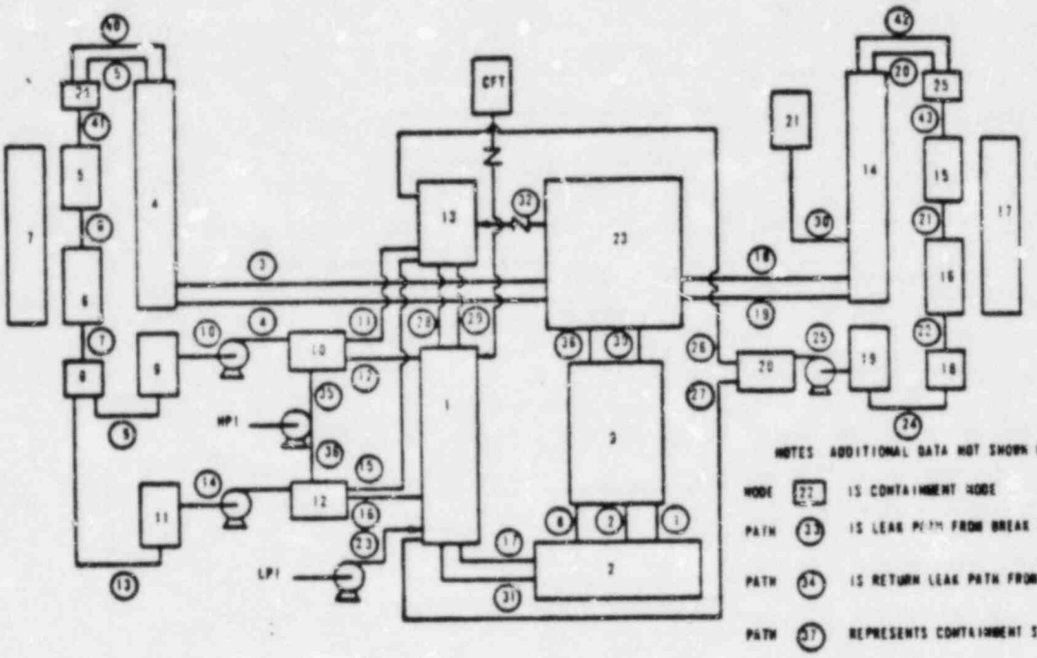

NODE NO	IDENTIFICATION
1	DOWNCOMER
2	LOWER PLENUM
3	CORE
4,14	HOT LEG PIPING
5,15	SG & UPPER HEAD
6,16	STEAM GENERATOR TUBES
7,17	SECONDARY SG
8,19	SG LOWER HEAD
9,11,18	COLD LEG PIPING
10,12,20	COLD LEG PIPING
13	UPPER DOWNCOMER
21	PRESSURIZER
22	CONTAINMENT
23	UPPER PLENUM
24,25	SG UPPER HEAD

PATH NO	IDENTIFICATION
1,2	CORE
3,4,18,19	HOT LEG PIPING
5,20,40,42	HOT LEG, UPPER
6,21	SG TUBES
7,22	SG LOWER HEAD
8	CORE BYPASS
9,13,24	COLD LEG PIPING
10,14,25	PUMPS
11,12,15,18,26,27	COLD LEG PIPING
17,31	DOWNCOMER
23	LPI
28,29	UPPER DOWNCOMER
30	PRESSURIZER
32	VENT VALVE
33,34	LEAK & RETURN PATH
35,36	HPI
37	CONTAINMENT SPRAYS
41,43	SG UPPER HEAD

Figure D-6. Pressure Vs Time, 0.15-ft^2 CLPD Break

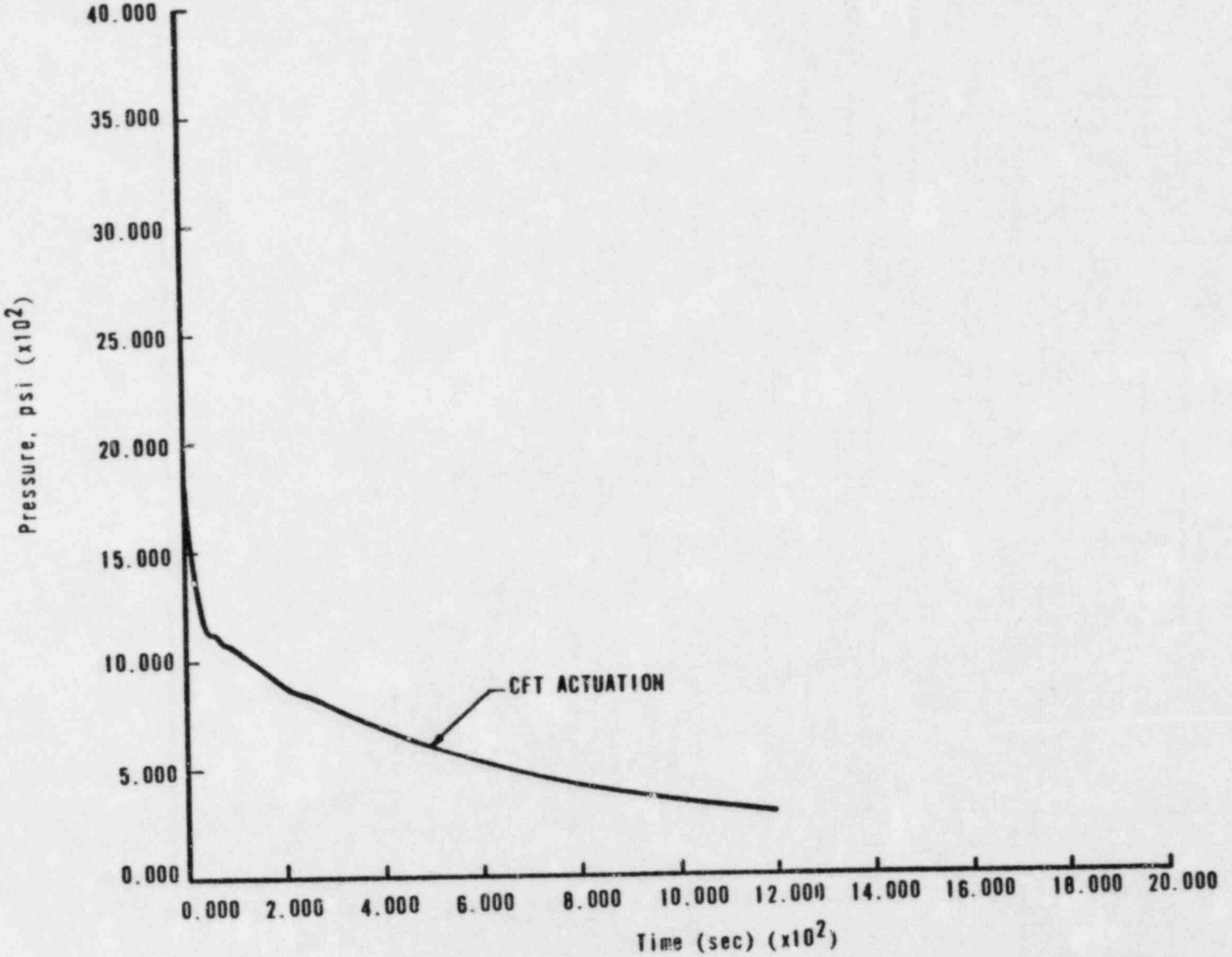

Figure D-7. Pressure Vs Time, 0.1-ft^2 CLPD Break

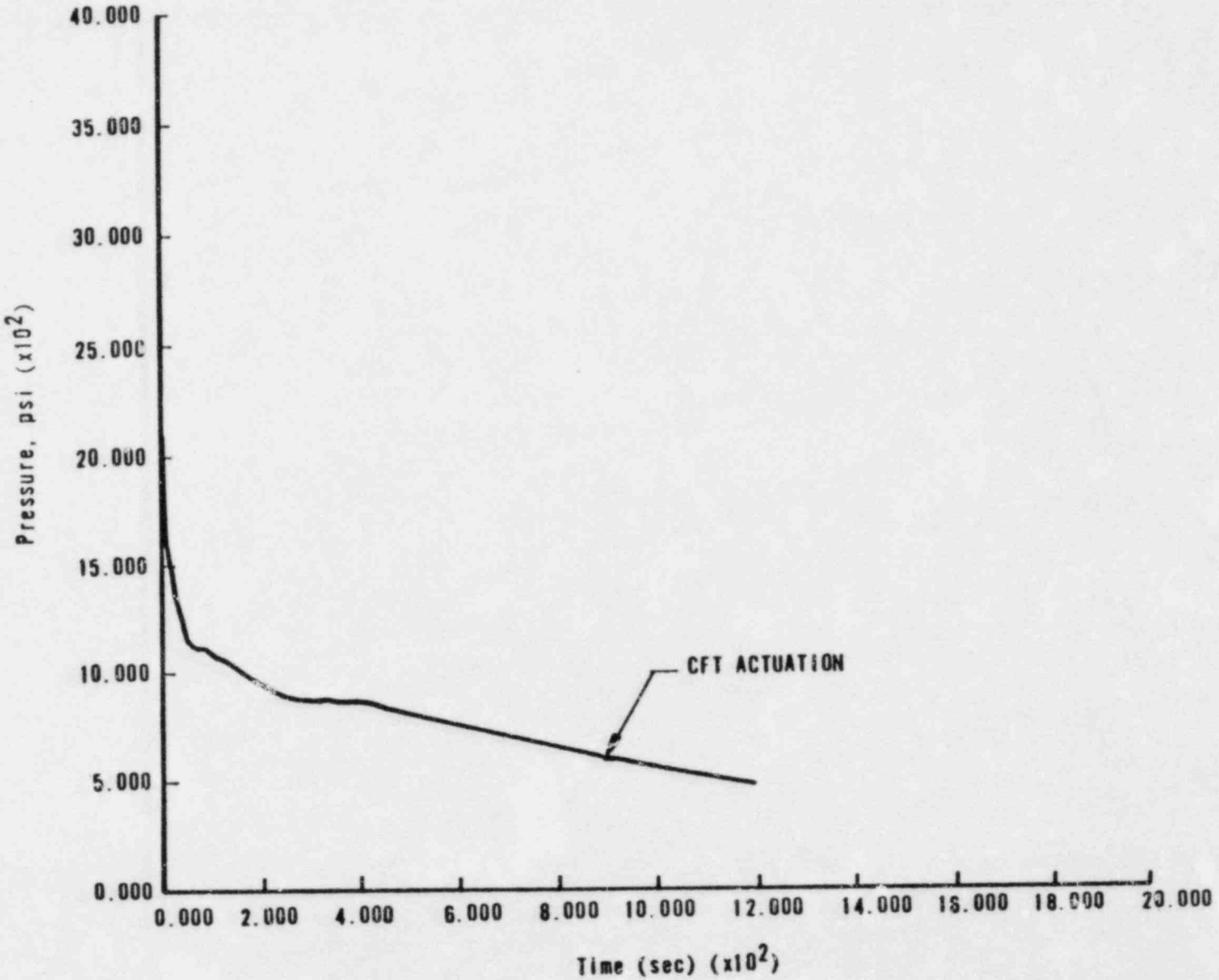

Figure D-8. Pressure Vs Time, 0.085-ft^2 CLPD Break

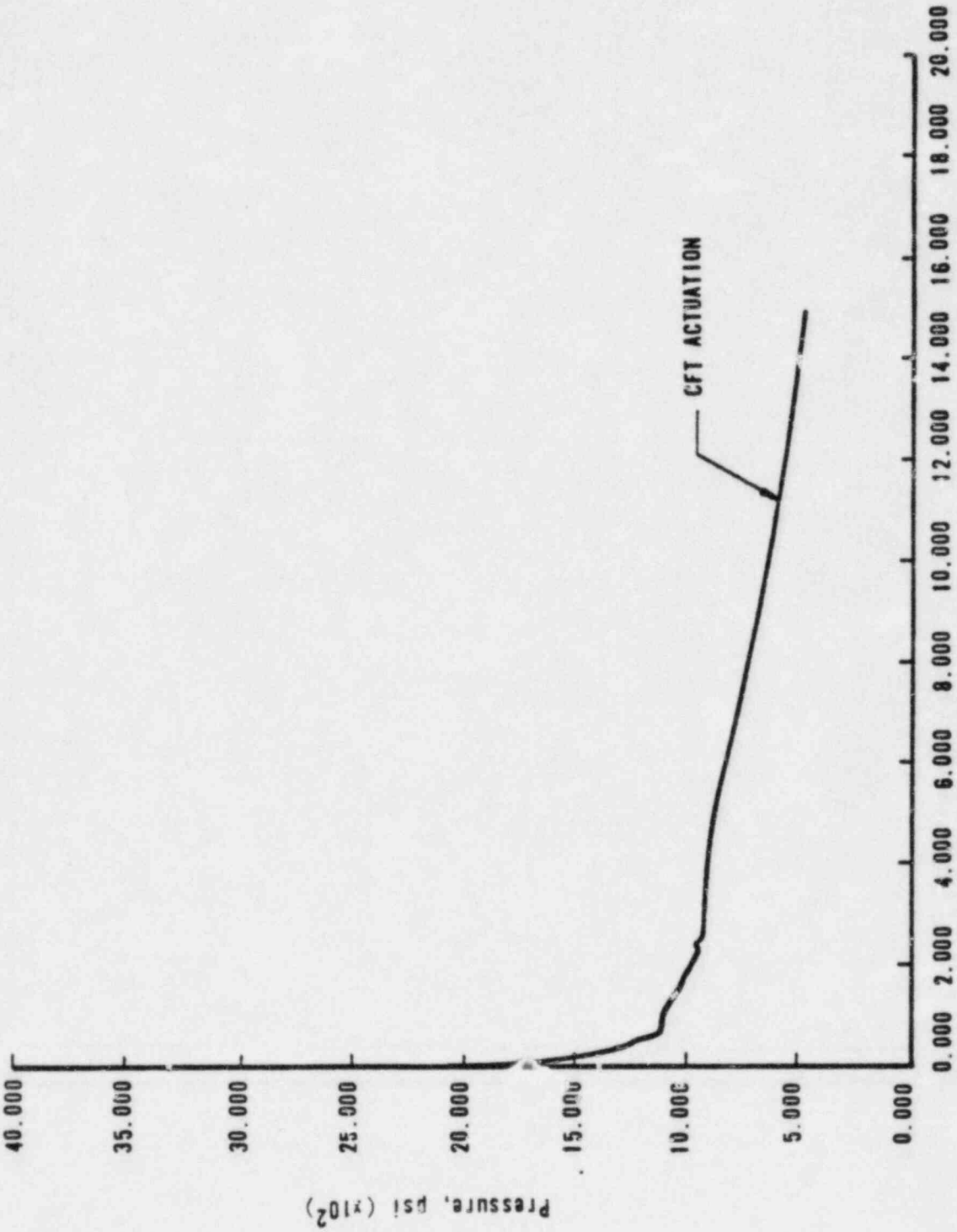

Figure D-9. Pressure Vs Time, 0.07-ft^2 CLPD Break

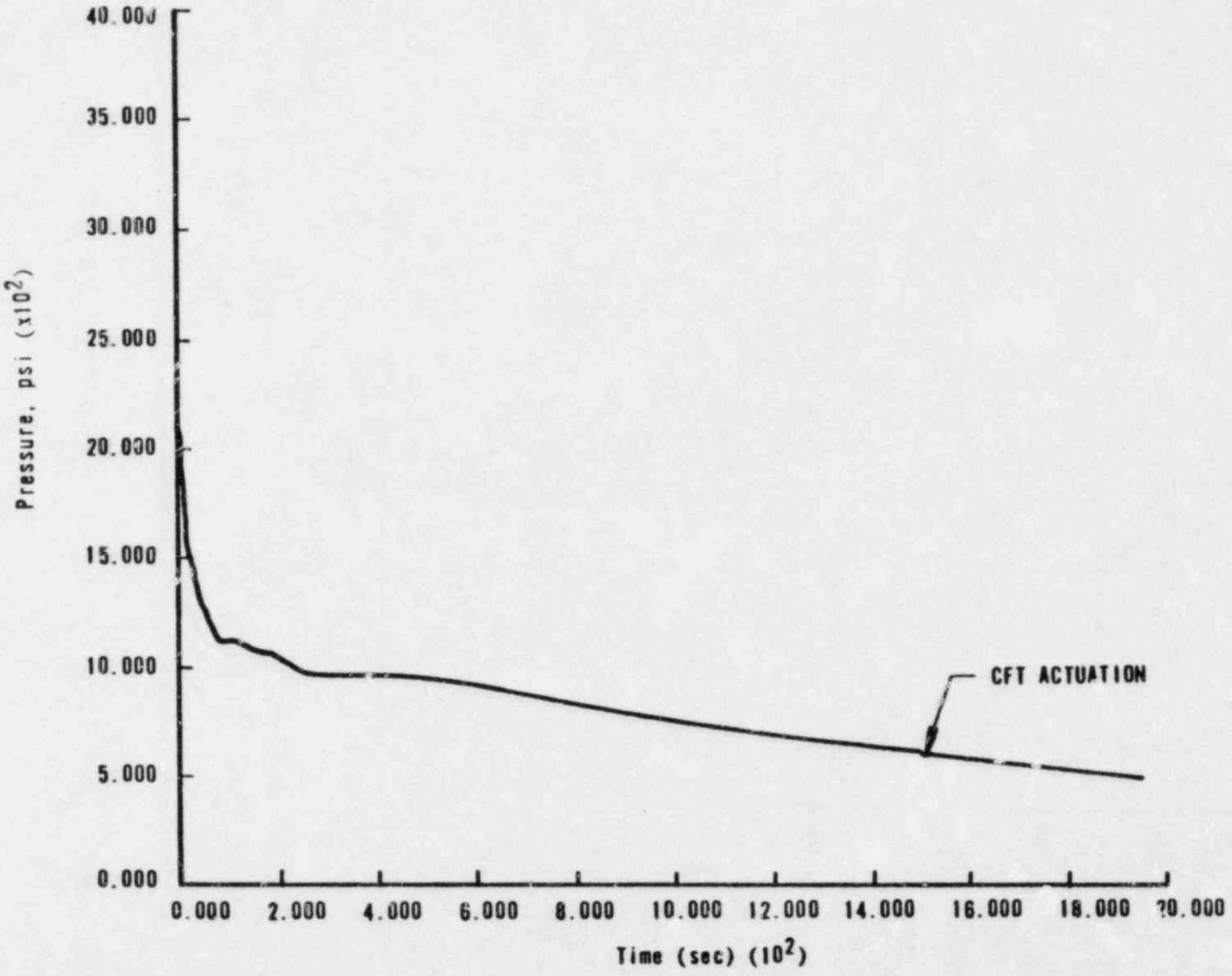

Figure D-10. Core Mixture Level Vs Time, 0.15-ft^2 CLPD Break

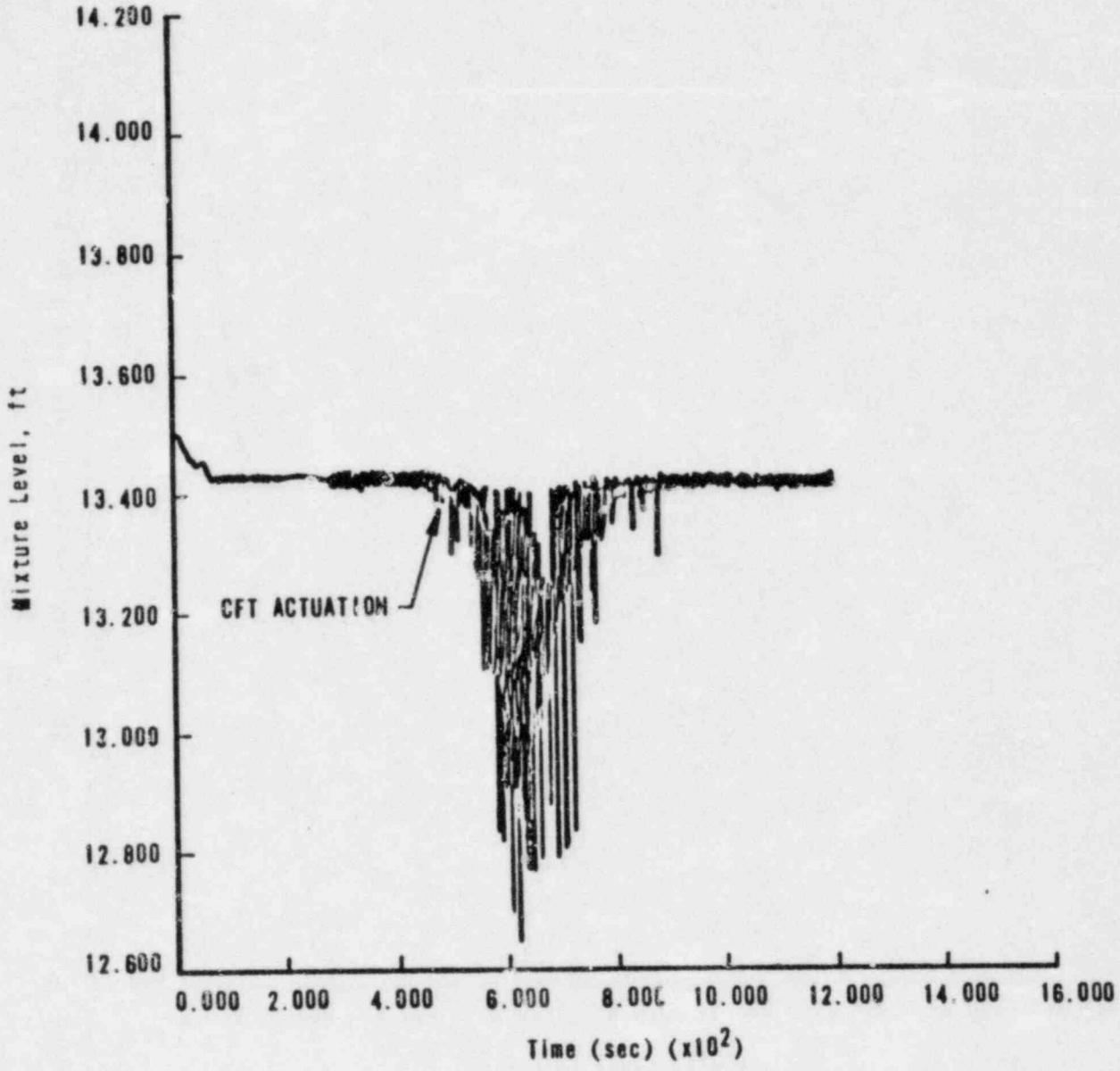

Figure D-11. Core Mixture Level Vs Time, 0.1-ft^2 CLPD Break

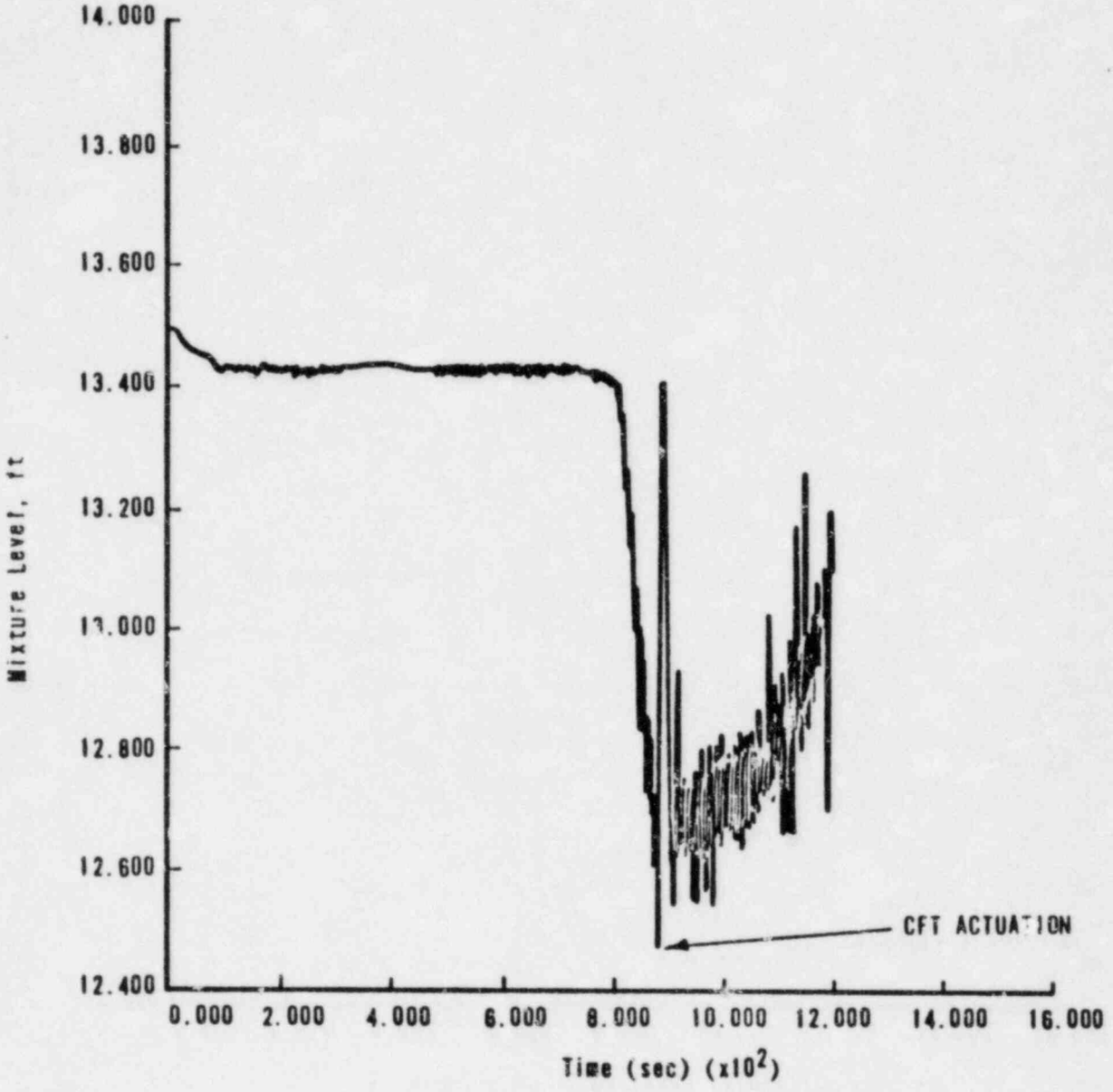

Figure D-12. Core Mixture Level Vs Time, C.085-ft^2 CLPD Break

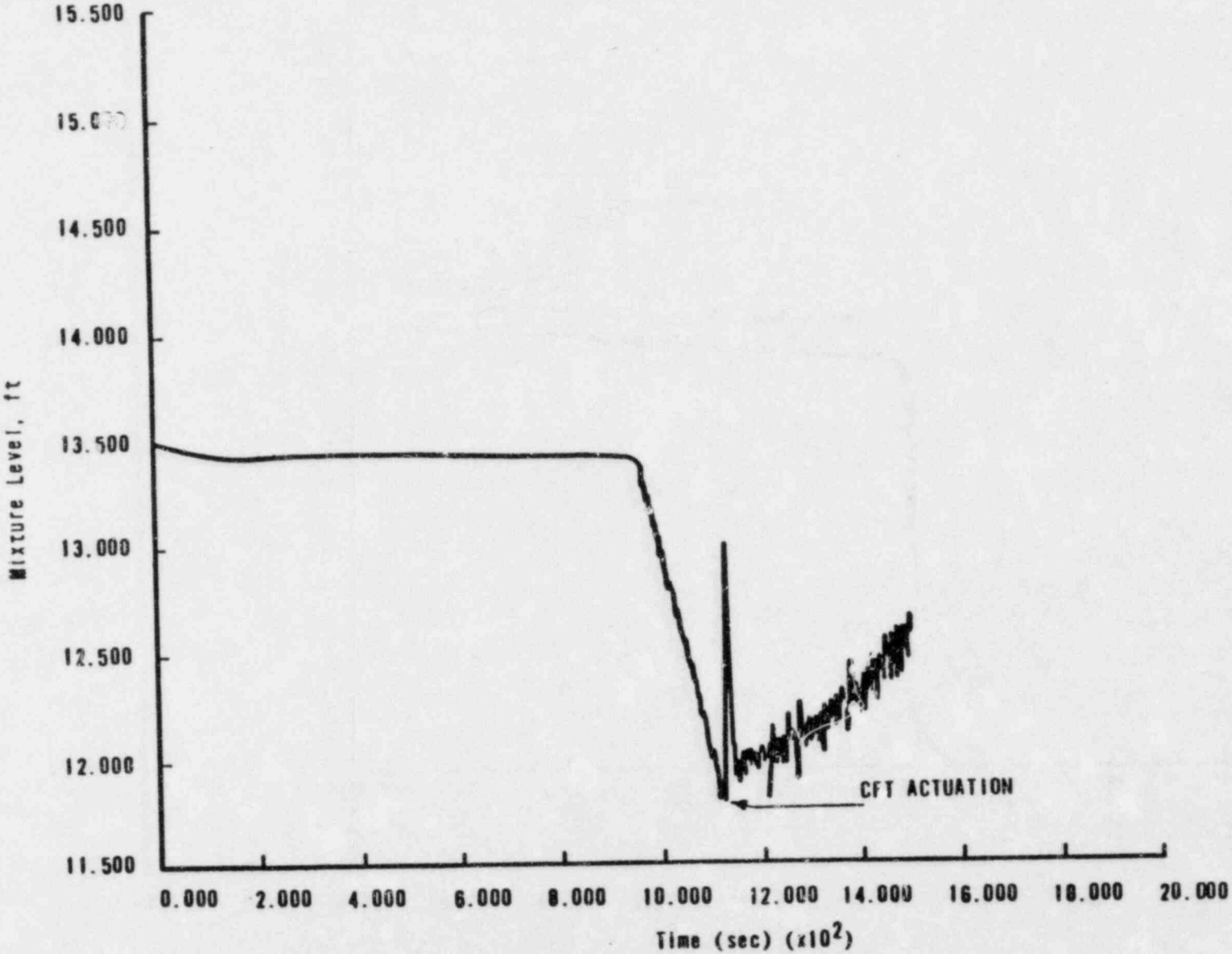

Figure D-13. Core Mixture Level Vs Time, 0.07-ft^2 CLPD Break

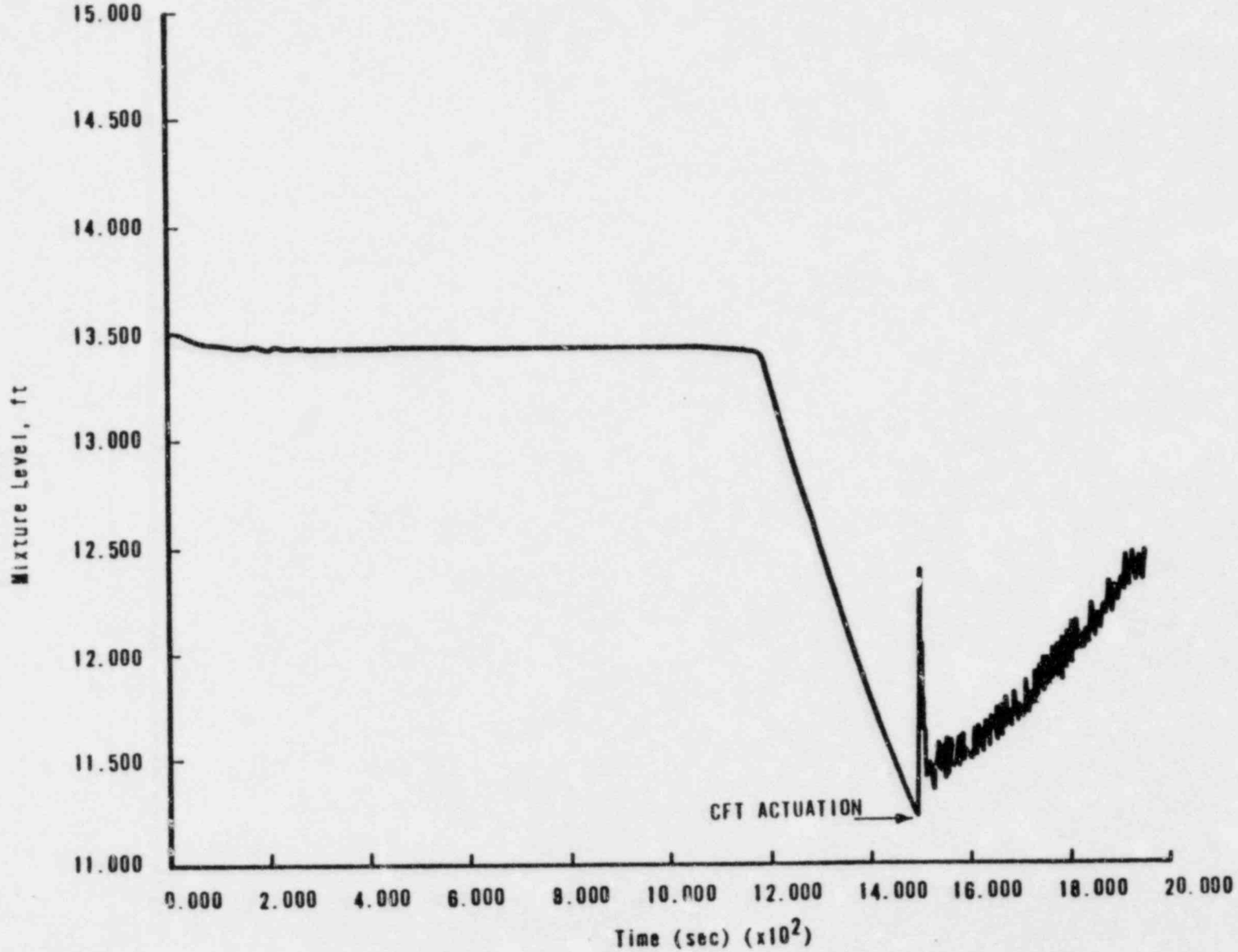

APPENDIX E

Noding Sensitivity Studies for 177-FA Lowered-Loop Plants

1. Introduction

On October 31, 1980, the Nuclear Regulatory Commission (NRC) issued NUREG-0737, "Clarification of TMI Action Plan Requirements." Included in the regulation is the requirement for an industry review of NUREG-0565 and NUREG-0623 and the development of a program addressing the NRC concerns therein. Three of the concerns are steam generator performance, the effects of local flashing in the reactor vessel (RV) upper head, and loss of natural circulation due to void formation in the hot legs. For a more detailed discussion of the concerns refer to section 5.5. This appendix addresses these three concerns through a re-analysis of the 0.01-ft^2 cold leg pump discharge (CLPD) break.[1] This re-analysis includes noding sensitivity studies performed using the revised SBLOCA steam generator model (section 5), the RV upper head (section 6), and the hot leg (section 7). The results of all these studies exhibited adequate convergence, and the conclusions are stated in section 8.

2. Summary

In response to the NRC concerns raised in NUREG-0737, the B&W SBLOCA evaluation model was reviewed, and various models were modified and upgraded. Among the upgrades was the development of the new SBLOCA steam generator (SG) model. The new model includes more detailed and mechanistic heat transfer correlations along with provisions for more realistic auxiliary feedwater (AFW) modeling. This model is discussed in detail in the CRAFT2 topical report.[2]

Noding sensitivity studies were performed with the SG model to determine a converged SG noding scheme. These studies produced an SG noding arrangement consisting of six axial and two radial regions. This configuration allows all significant phenomena to be exhibited.

Sensitivity studies were also conducted in the regions of the hot leg and RV upper head. These evaluations addressed the concerns regarding the effects of loss of natural circulation in the hot legs and local flashing in the RV upper head. To resolve the issues, the noding for the hot legs and RV upper head was subdivided into a more detailed arrangement. The results of the detailed RV upper head noding study showed convergence with the base case model. The detailed hot leg noding study results exhibited the basic phenomena, but the magnitude of the response was altered.

Based on these noding studies, it was concluded that the revised SBLOCA evaluation model should comprise an SG model of six axial and two radial regions, a two-node hot leg model, and a one-node representation of the RV upper head and upper plenum combination.

3. Previous 0.01-ft^2 CLPD SBLOCA Analysis

The evaluations described herein are a re-analysis of the previous 0.01-ft^2 CLPD SBLOCA analysis.[1] Thus, it is considered necessary to discuss this transient briefly as analyzed with the previous SBLOCA evaluation model. The 0.01-ft^2 break was selected as a representative size in that the high-pressure injection (HPI) and break flow cooling combination is insufficient to balance decay heat energy production. Therefore, SG performance is important in this transient for energy removal. As natural circulation is lost, SG heat transfer is lost, and system repressurization should occur until a condensation surface is established on the primary side of the SG tubes. This condensation surface will re-establish heat transfer, and depressurization will occur, allowing for long-term cooling. Figure E-1 is the noding diagram for this analysis. Table E-1 lists the pertinent sequence of events for this previous analysis.

The reactor coolant system (RCS) depressurizes rapidly over the first 100 seconds to a saturation pressure of about 1400 psia (Figure E-2). At this point, steam formation in the hot leg and upper plenum slows the rate of depressurization.

As a result of excessive SG heat transfer, RCS depressurization continues until about 650 seconds, when natural circulation ceases as the hot leg level continues to decrease. The loss of SG heat removal causes the primary system pressure to begin increasing. At 1500 seconds, the maximum system pressure is reached (1750 psia) and begins to decrease slowly because steam condensation by the SG is established. This additional energy removal results in a decreasing RCS pressure transient. The hot leg mixture heights are shown in Figure E-3. As can be seen in the figure, natural circulation is lost at approximately 340 seconds in the intact loop and at approximately 650 seconds in the broken loop.

4. 0.01-ft^2 CLPD SBLOCA Analysis Using the New SBLOCA Evaluation Model

The SG model in the former SBLOCA evaluation model used a simplistic heat transfer correlation relying solely on the primary-to-secondary liquid temperature difference. The previous SG model calculated a heat transfer coefficient based on initial conditions. The new model alters the heat transfer coefficient during the transient based on fluid conditions, ΔT, and boiling lengths. Thus, the prediction of the magnitude of the initial depressurization through subcooled blowdown has been altered. The new SG model with reduced overall heat transfer depressurizes to 1500 psia, corresponding to a higher saturation temperature than in the previous analysis, which depressurized to 1400 psia. Furthermore, the previous SG model had sufficient heat transfer to allow the system to continue depressurizing due to a larger cold driving head. This allowed for greater and longer circulation flows. With its more mechanistic heat transfer correlation, the new SG model exhibited less heat transfer, which essentially stopped depressurization after the initial blowdown. A representation of the noding arrangement is provided in Figure E-4 with the transient response comparisons shown in Figure E-5 through E-10. A listing of the sequence of events is given in Table E-2.

As the system reached saturation, the energy produced was balanced by the energy removed, and the pressure response remained essentially steady at 1520 psia through 350 seconds. As the transient continues, more inventory is lost through the break, which causes a reduction in the hot leg level and reduced two-phase flow into the SG. Consequently, RV steam relief is maintained through the internals vent valves, which saturates the upper downcomer, thereby supplying saturated fluid to the break node with condensation in the cold legs ensuing. This sequence of events allows for system depressurization to occur at 375 seconds. However, as SG heat transfer decreases, this depressurization is short-lived due to an overall imbalance in energy removal versus energy production. This imbalance quickly changes the pressure response to an upward trend, which continues to 440 seconds.

At 420 seconds, steam in the upper downcomer mixture region separates and cold leg condensation terminates. Now, RV steam relief is increased to the hot legs, which causes an increase in the two-phase circulation through the SG. SG heat transfer is thus increased as steam in the two-phase flow condenses in

the SG. Energy removal has now been increased above the amount of energy produced, and a depressurization results at 440 seconds. By 530 seconds, the energy terms have again balanced, causing a steady system pressure at 1500 psia.

In the time frame from 500 to 550 seconds, enough system inventory has been lost to disrupt natural circulation and saturate the break node. These events produce a decrease in energy removal, thus increasing system pressure. By 630 seconds, the decrease in break flow due to saturated conditions in the break node has caused a hot leg level swell, which returns two-phase circulation to the SG. With the return of SG heat transfer, a depressurization occurs until 670 seconds. By this time, however, the system liquid inventory is not sufficient to maintain the necessary hot leg level, and the circulation pattern is again lost and the depressurization is stopped. System pressure remains steady at 1470 psia as the energy terms are once again balanced. The main contributors to the energy removal term are steam relief out the break and ECCS flow, with a minor contribution by SG heat transfer. (During the next 3 transient minutes, intermittent two-phase circulation exists, allowing for enough SG heat transfer to aid in the system energy balances.)

At 940 seconds, the intermittent two-phase circulation is lost, and at 950 seconds the secondary side level setpoint (50% on the operating range) is reached, and AFW is turned off. The SGs are now completely lost as a means of heat removal, and the energy balance is upset, causing a continuous increase in the system pressure response. This is similar to the previous analysis where the loss of natural circulation caused a repressurization at 650 seconds. This repressurization was allowed to continue until the level in the SG primary side dropped to expose a condensation surface at approximately 1500 seconds. At this time, AFW was injected, and the expected result of primary side steam condensation was established, which brought about an abrupt end to the repressurization, enabling the system to be put into a long-term cooling mode.

As discussed, the basic difference between the former and current 0.01-ft^2 CLPD SBLOCA transient analyses involves SG behavior. However, the overall concern of system repressurization due to loss of natural circulation is indeed exhibited by both SG models. The repressurization phenomenon has thus been shown with the new SBLOCA SG model.

5. Steam Generator Noding Studies

Included in NUREG-0737 is an NRC concern questioning the adequacy of the previous SG model used in the B&W SBLOCA evaluation model. Of specific concern were the heat transfer correlation and the effects of AFW on the transient response. In response to this concern, B&W has developed a more mechanistic SG model with multiple heat transfer correlations and more realistic AFW interaction based on more physical characteristics. Sensitivity studies were performed to determine the noding arrangement required to exhibit the various transient phenomena of interest. Included among these are forced convection heat transfer during circulation, loss of heat transfer during loss of natural circulation, condensation heat transfer at the time the condensation surface is established, and the effects of AFW heat transfer throughout the transient.

To study the effects of AFW on SG response, two models were developed, both comprising four axial regions but differing in that the models had one and two radial regions, respectively. A 0.01-ft^2 CLPD SBLOCA transient was run to 600 seconds and the results evaluated. Figure E-11 is a pressure comparison of the two models. As illustrated, the two models exhibited similar characteristics and events. Therefore, the choice of one versus two radial regions was based on the effects expected much later in the transient, particularly the effects AFW should have on system pressure as a condensation surface is established in the primary side SG tubes. It was deemed more realistic to model two radial regions to better predict the effects of AFW during this particular transient phenomenon.

The next step was to determine the number of axial nodes necessary to model adequate SG heat transfer performance. An SG model was constructed consisting of eight axial and two radial regions. This model allowed for the maximum SG detail considering the total number of RCS control volumes and flow paths permitted by the CRAFT2 code.

This detailed SG model was then used to analyze the 0.01-ft^2 break and was compared to the SG model containing four axial and two radial regions. Figure E-12 compares RCS pressure responses for the two models. Of particular importance is the rapid initial depressurization shown in the 4/2 SG model. It was determined that the four-axial-region model was inadequate in conservatively predicting SG heat transfer performance compared to the model with eight axial

regions. Consequently, the increased SG heat transfer (four axial regions) caused faster depressurization, which allowed for larger surge line flows. This eventually resulted in a pressurizer steam outsurge into a still subcooled hot leg, causing further divergence of depressurization. For this reason, the four-axial/two-radial region SG model was determined to be non-conservative and was eliminated from consideration as an appropriate model.

Based on the previous information, an SG model with six axial and two radial regions was developed. The noding diagram for this model is shown in Figure E-4. This model was believed to have sufficient detail to show convergence with the more detailed eight-axial-region model. The same 0.01-ft^2 break transient was run with the six-axial-node model and compared with the eight-node model. Figures E-13, 14, and E-15 illustrate the comparisons. The two models show adequate convergence through 900 seconds where the dominant SG performance is convective heat transfer. The remaining phenomena include loss of circulation and condensation heat transfer. The SG model with six axial and two radial regions was used to evaluate these additional phenomena. The analysis was continued to 1550 seconds and the results accounted for the expected phenomena. Therefore, it is concluded that the 6/2 SG model exhibits the phenomena of concern, and it is recommended for use in the SBLOCA evaluation model.

6. RV Upper Plenum-Upper Head Noding Studies

The upper plenum and upper head regions of the reactor vessel were modeled in various ways to show that the effects of any local flashing are adequately simulated. Since flashing of the hottest liquid in the system at any time controls system pressure during depressurization, this flashing and its effects on the system must be adequately modeled. Each control volume is assumed to be in thermal equilibrium, and thus its fluid properties are represented by average fluid properties. As an example, if the entire RV was modeled as one control volume, it would be represented by average properties even though the liquid in the lower plenum might be subcooled and that in the upper plenum might be saturated. The model must be detailed enough to account for any "hot spots," which could cause flashing.

In the base model, the upper plenum and upper head regions of the vessel were modeled as one control volume as shown in Figure E-4. In the detailed upper plenum model, Figure E-16, the upper plenum and upper head regions were modeled using four control volumes: one to represent the upper plenum region inside the plenum cylinder, one to represent the upper head region of the vessel, and two to represent the outer annulus region between the core support shield and the plenum cylinder. The third model of the upper plenum/upper head region used five nodes to represent the region. This model is identical to the detailed upper plenum model except for the detailed upper head region (Figure E-17). The upper head region is modeled with two control volumes to provide the detail necessary to allow possible additional flashing.

A small break loss-of-coolant accident (SBLOCA) was simulated using both of the detailed upper plenum/upper head models. The break size for the simulation was 0.01 ft^2. The transient was simulated for 350 seconds, and predictions from each model were compared. It can be seen from Figure E-18 that the predicted system pressure response is basically the same for both models. The predicted liquid levels for the upper plenum (Figure E-19) are also the same for both models.

After reviewing the predictions by each of the detailed upper plenum/upper head models, it became obvious that there were no significant differences between the four- and five-node upper plenum/upper head models. At 350 seconds into the transient, the top node of the detailed upper plenum/upper head (five-node) model has drained completely, and thus, this model was essentially the same as the four-node detailed upper plenum/upper head model.

The SBLOCA transient was simulated to 525 seconds using the four-node detailed upper plenum model. Predictions from the detailed four-node upper plenum model were then compared to predictions made by the single-node upper plenum base model. From Figure E-20 it can be seen that the predicted system pressure from the detailed upper plenum model is approximately 10 psi higher than that predicted by the base model. The models predicted essentially the same vent valve flow (Figure E-21). The predicted level responses of the hot leg are very similar for both models, as shown in Figure E-22.

The detailed upper plenum model showed only slight changes in the magnitude of the predicted system response when compared to the single-node upper plenum model. These models predicted identical events with slight changes in event

timing. Therefore, it was concluded that the base model was adequate to model the upper regions of the RV.

7. Hot Leg Noding Studies

Energy is normally removed from the reactor core of a PWR by maintaining flow through the primary system. Natural circulation is the predominate mode of flow in the primary system during a SBLOCA. The inverted U-bends in the hot legs, the high points in the RCS, are most susceptible to steam void formation. As fluid is lost out the break, the liquid level in the hot legs decreases. If the level decreases sufficiently, the riser section of the inverted U-bend may void sufficiently to interrupt natural circulation. To ensure that the SBLOCA model (as presented in section 4) adequately predicts the loss and re-establishment of circulation, a more detailed hot leg model was developed.

In the SBLOCA base model, the hot legs are modeled with one control volume as shown in Figure E-4. The detailed hot leg model uses four control volumes as shown in Figure E-23. The added detail is intended to provide a more precise prediction of the loss of natural circulation in the system during a SBLOCA.

Using the detailed hot leg model, the 0.01-ft^2 CLPD SBLOCA transient was reanalyzed through the first 800 seconds of the transient. A description of events for the SBLOCA base model is provided in section 4. A comparison of event timing as predicted by each model is provided in Table E-3 and Figure E-24 is an illustration of the pressure comparison for each model. Other comparisons are provided in Figures E-25 through E-28. The major differences are discussed below.

The initial blowdown period of the transient remains unaltered as expected. Through 200 seconds there is insufficient steam formation to cause any differences in flow patterns or energy removal. By 200 seconds steam voiding in the detailed hot legs begins to decrease flow to the SG as compared to the base case. This decrease in flow causes a decrease in SG heat transfer, which results in a rise in the system pressure.

By 335 seconds the liquid level in the RV has decreased to the internals vent valves elevation, thereby introducing higher quality fluid into the upper downcomer region. As the upper downcomer saturates, quality fluid is passed to

the break node. This series of events allows for steam condensation in the cold leg that increases the energy removal term and levels the system pressure. However, the steam relief through the vent valves causes a decrease in two-phase flow in the hot legs that results in less SG heat transfer and a pressure increase at 300 seconds. This series of events is the same scenario that takes place in the base case from 375 to 420 seconds. Due to the effect of more detailed noding, the sequence timing has been altered somewhat.

In a short period of time, steam bubbles formed in the saturated upper downcomer begin to separate out of the mixture region causing an end to steam condensation in the cold leg. This, in turn, forces an increase in two-phase flow through the hot legs, which causes an increase in hot leg level and SG heat transfer. The resultant response is a decrease in pressure as shown at 390 seconds. By 450 seconds the energy production and removal terms have balanced the system pressure at 1550 psia. This balance was achieved in the base model at 530 seconds and 1500 psia.

Due to the detailed modeling of the hot legs, the recovery of natural circulation lasts for a much smaller period of time than in the base case. At approximately 470 seconds, natural circulation is lost in both loops of the detailed model. The magnitude of the repressurization caused by this loss of circulation is also increased due to the detailed modeling. However, the same sequence of events occurs in both models and the hot leg level swell causes a return of two-phase circulation to the SG resulting in increased SG heat transfer, loop flow, and a depressurization. This swelling of the hot leg level results from the same phenomena in both cases. The continuous small break flow routes core-produced steam into the hot legs causing a constant rate of level increase. Depressurization occurs when the level reaches the elevation of recirculating two-phase flow into the SG.

Based on the transient comparison, it has been judged that both models exhibit the same sequence of events. As expected, the detailed model showed a difference in event timing and magnitude. However, the base model, in demonstrating the ability to predict the events of loss and re-establishment of natural circulation, is judged to be an adequate representation for the hot leg in this SBLOCA evaluation model.

8. Conclusions

The detailed noding studies described herein have shown adequate convergence for the transients analyzed. The results of these studies have demonstrated that increasing spatial detail results in consistent transient response predictions, even though there are some differences regarding event timing and magnitude. The models with less detail have generally shown adequate convergence and are recommended. Therefore, B&W's SBLOCA evaluation model will consist of an SG containing six axial and two radial regions, a one-node hot leg, and an RV upper plenum/upper head combination represented by one control volume. This configuration is illustrated in Figure E-4.

9. References

1. Evaluation of Transient Behavior and Small Reactor Coolant System Breaks in the 177 Fuel Assembly Plant, Volume II, Babcock & Wilcox, May 7, 1979.
2. J. J. Cudlin, et al., CRAFT2 - Fortran Program for Digital Simulation of a Multinode Reactor Plant During Loss of Coolant, BAW-10092, Rev. 3, Babcock & Wilcox, October 1982.
3. Small Break 177-FA Lower Loop Noding Sensitivity Studies, Babcock & Wilcox, October 1982.

Table E-1. Sequence of Events for Previous SBLOCA Analysis

Event sequence	Time, seconds
Break occurs (0.01 ft^2 at pump discharge)	0
Reactor trip, turbine trip, RC pump coastdown	50
Main feedwater coastdown ends	65
AFW flow to both SGs begins	90
Hot leg voiding begins	100
HPI begins	190
Loss of natural circulation in intact loop	340
Loss of natural circulation in broken loop	650
Maximum repressurization (1750 psia) reached	1500

Table E-2. Sequence of Events for Upgraded SBLOCA Analysis

Event sequence	Time, seconds
Break occurs (opens)	0
Reactor trips	43
RC pumps trip	48
AFW turned on	85
Core saturates	115
Upper RV head saturates	125
Hot leg saturates	130
HPI initiation	150
Vent valves uncovered	355
Upper region of downcomer saturates	370
Loss of natural circulation	505
Break node saturates	530
Natural circulation re-established	560
Intermittent two-phase circulation	675-940
Two-phase circulation lost	940
AFW setpoint reached (AFW off)	950

Table E-3. SBLOCA Event Sequence and Timing Predicted by Revised Base Case and Detailed Hot Leg Models

Major event sequence	Time, seconds	
	Revised base case	Detailed hot leg
Break opens	0	0
Reactor trips	43	43
RC pumps trip	48	48
AFW turned on	85	85
Core saturates	115	115
RV upper head saturates	125	120
Hot leg saturates	130	125
HPI initiation	150	150
Vent valves uncovered	355	335
Upper region of downcomer saturates	370	375
Loss of natural circulation	505	425
Break node saturates	530	470
Natural circulation re-established	560	680

Figure E-1. CRAFT2 Noding Diagram for Small Breaks Used in Previous SBLOCA Evaluation Model

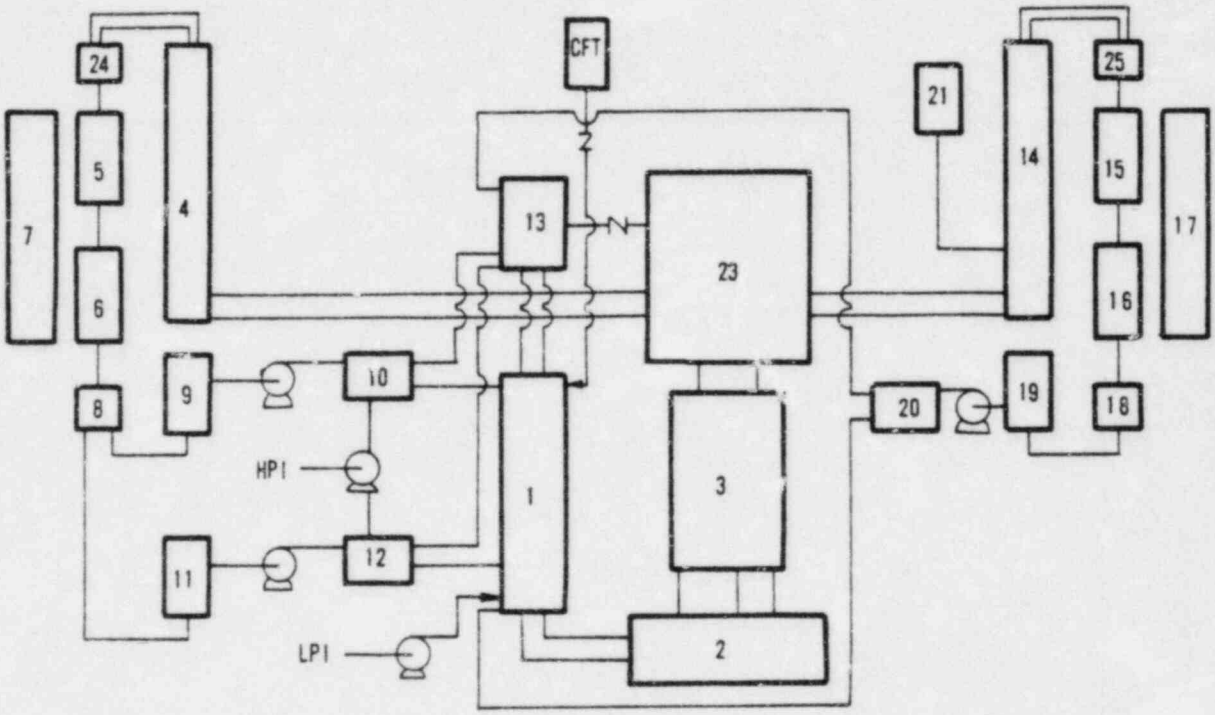

NODE NO.	IDENTIFICATION
1, 13	DOWNCOMER
2	LOWER PLENUM
3	CORE
4, 14	HOT LEG PIPING
5, 6, 15, 16	STEAM GENERATOR
7, 17	SECONDARY, SG
8, 18	SG LOWER HEAD
9, 11, 19	COLD LEG PIPING
10, 12, 20	COLD LEG PIPING
21	PRESSURIZER
22	CONTAINMENT
23	UPPER PLENUM
24, 25	SG UPPER HEAD/TOP OF HL

Figure E-2. System Pressure Vs Time, 0.01-ft^2 Break at Pump Discharge (Results Based on Former SBLOCA Evaluation Model)

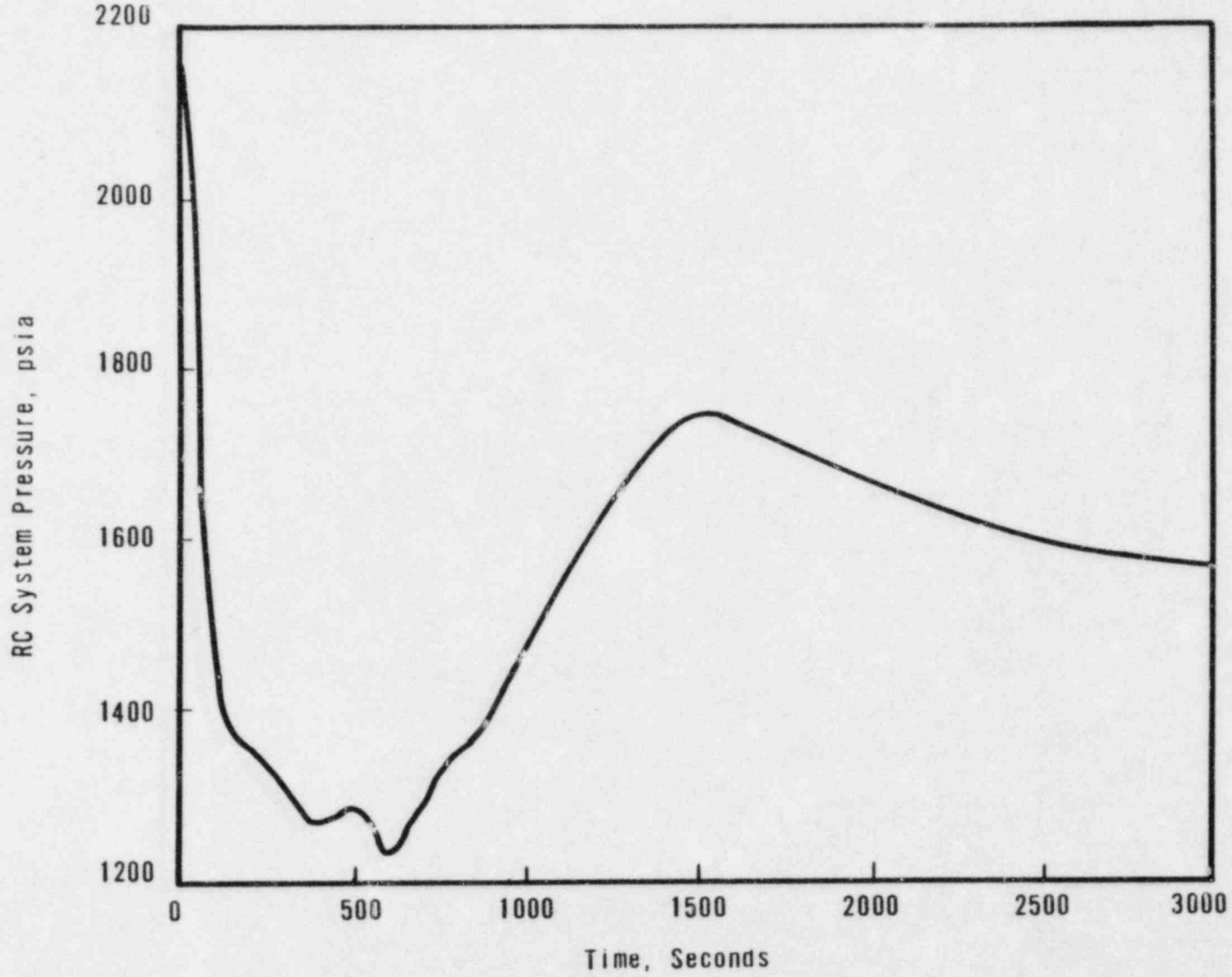

Figure E-3. Hot Leg Level, 0.01-ft^2 Break at Pump Discharge

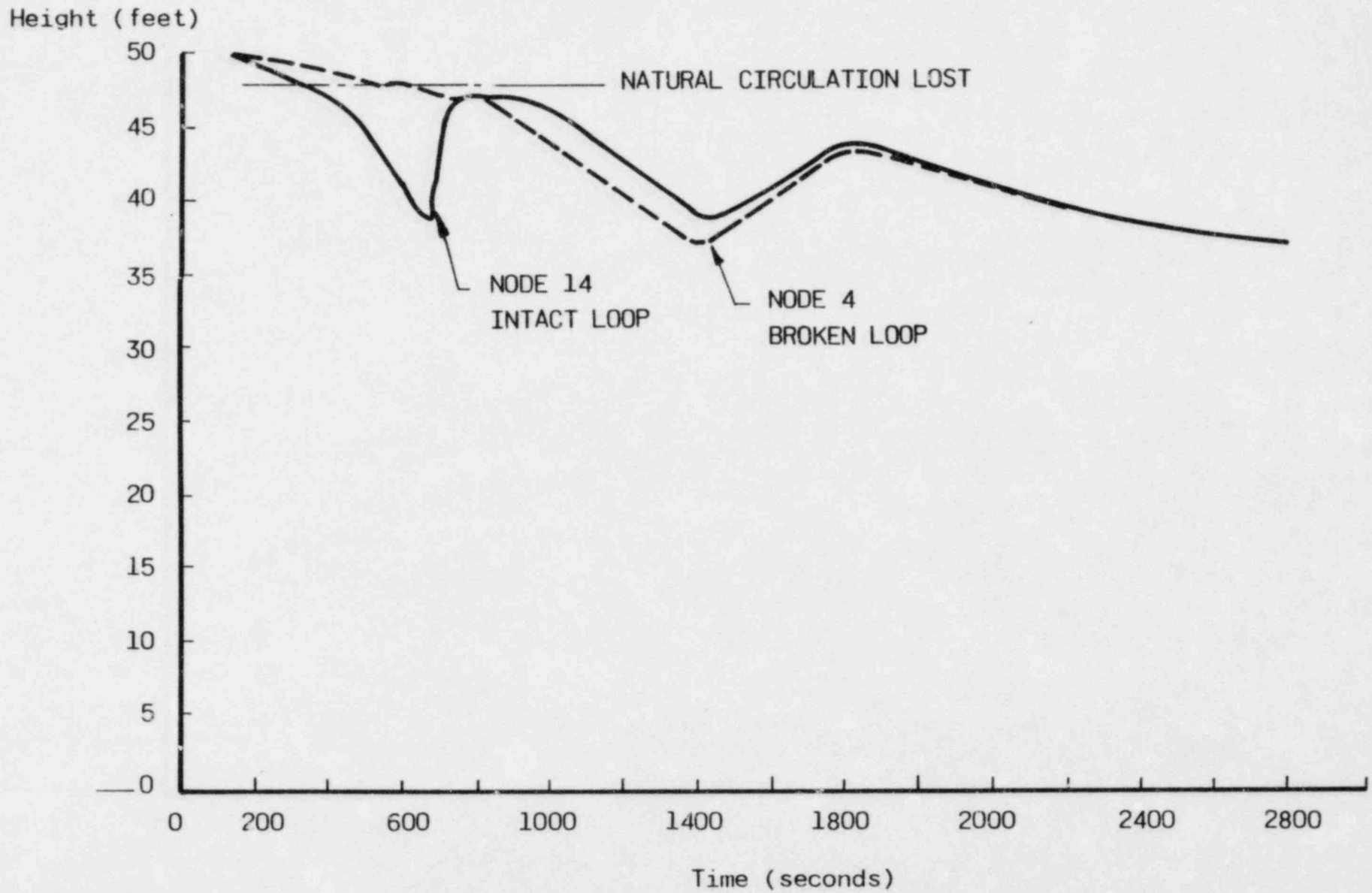

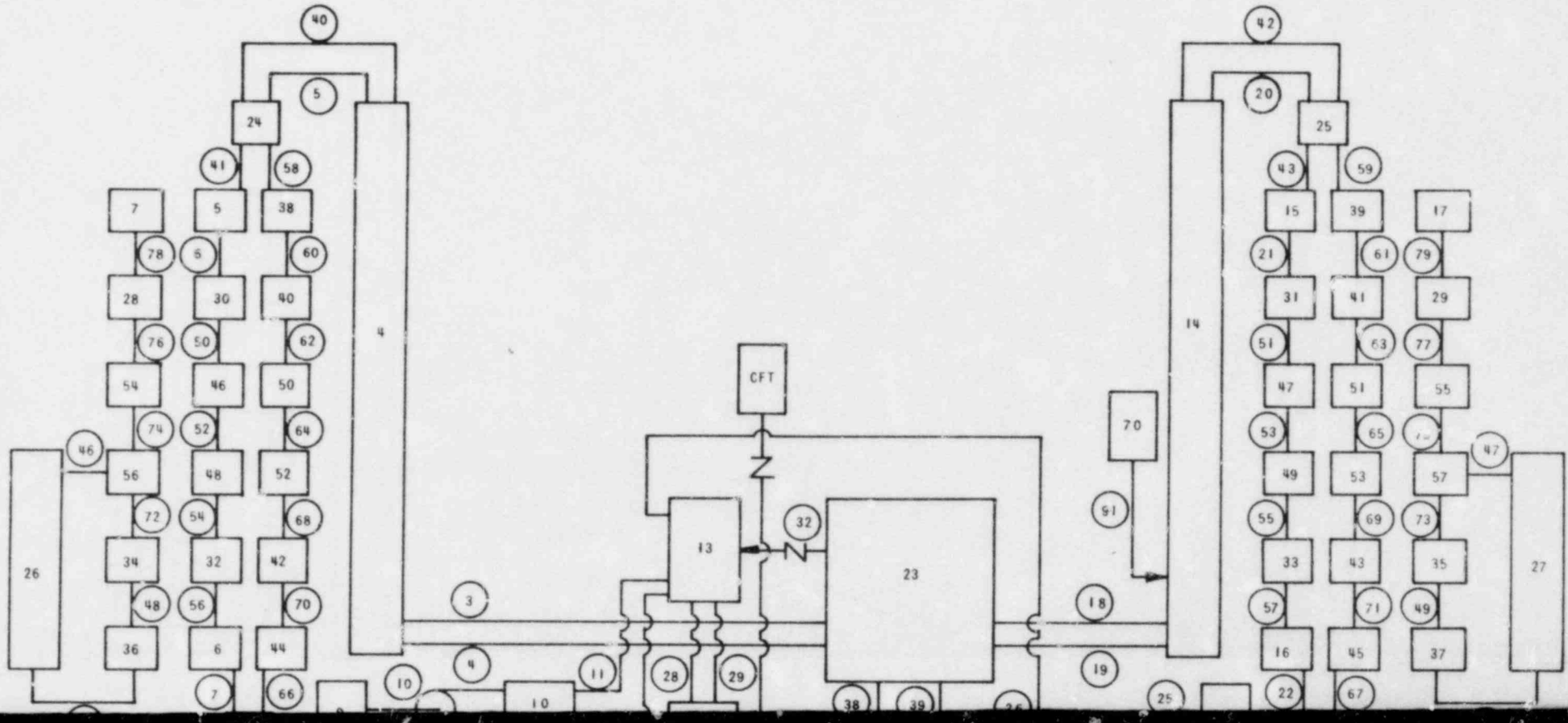
40
5
24
41
58
7
5
38
78
6
60
28
30
40
76
50
62
54
46
50
74
52
64
46
56
48
52
72
54
68
34
32
42
48
56
70
36
6
44
7
66
4
26
3
4
10
10
11
28
29
38
39
CFT
13
32
23
70
91
18
19
25
14
42
20
25
43
59
15
39
17
21
61
79
31
41
29
51
63
77
47
51
55
53
65
49
53
57
47
55
69
73
33
43
35
27
57
71
49
16
45
37
22
67

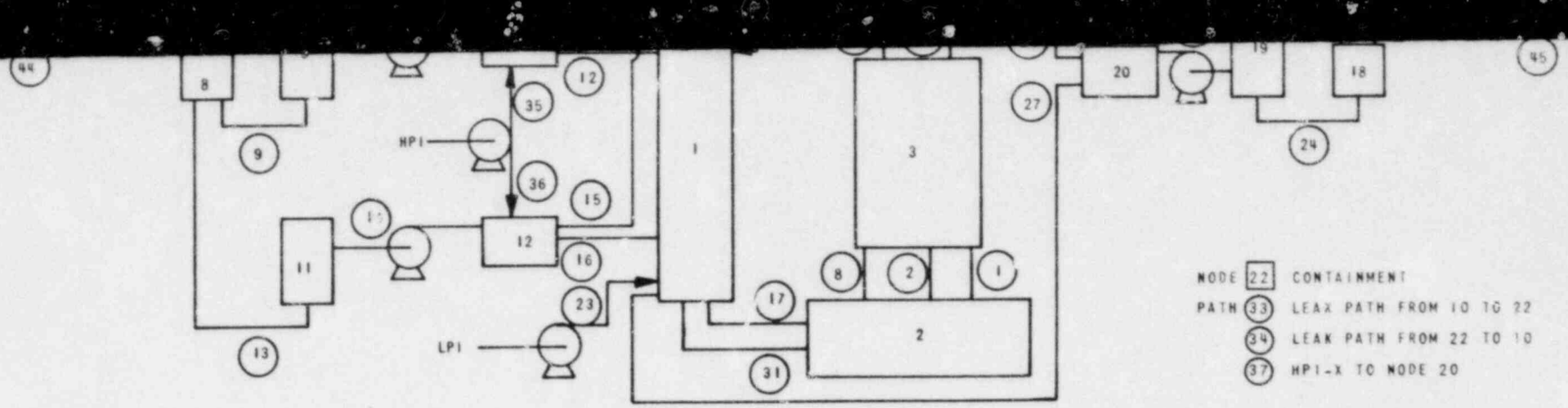

NODE NO.	IDENTIFICATION
1	DOWNCOMER
2	LOWER PLENUM
3	CORE
4, 14	HOT LEG PIPING
5, 6, 30, 32 38, 40, 42, 44 46, 48, 50, 52	SG TUBES
26, 28, 34, 36, 54, 56	SG-SECONDARY SIDE
8, 18	SG LOWER HEAD
9, 11, 19	COLD LEG PIPING
10, 12, 20	COLD LEG PIPING
13	UPPER DOWNCOMER
15, 16, 31, 33 39, 41, 43, 45 47, 49, 51, 53	SG TUBES
17, 29, 35, 37 55, 57	SG-SECONDARY SIDE
22	CONTAINMENT
23	UPPER PLENUM
24, 25	SG UPPER HEAD
26, 27	SG-DOWNCOMER
70	PRESSURIZER

PATH NO.	IDENTIFICATION
1, 2	CORE
3, 4, 18, 19	HOT LEG PIPING
5, 20, 40, 42	HOT LEG, UPPER
6, 41, 50, 52 54, 56, 58, 60 62, 64, 68, 70	SG TUBES
7, 66	SG LOWER HEAD
8	CORE BYPASS
9, 13, 24	COLD LEG PIPING
10, 14, 25	PUMPS
11, 12, 15, 16 26, 27	COLD LEG PIPING
17, 31	DOWNCOMER
21, 43, 51, 53 55, 57, 59, 61 63, 65, 69, 71	SG TUBES
22, 67	SG LOWER HEAD
23	LPI
28, 29	UPPER DOWNCOMER
32	VENT VALVE
33, 34	LEAK AND RETURN PATH
35, 36	HPI
37	CONTAINMENT SPRAYS
38, 39	UPPER PLENUM
44, 46, 48 72, 74, 76, 78	SG-SECONDARY
45, 47, 49, 73, 75, 77, 79	SG-SECONDARY

Figure E-4. Base Model Noding Scheme

Figure E-5. Pressurizer Pressure, Base Model

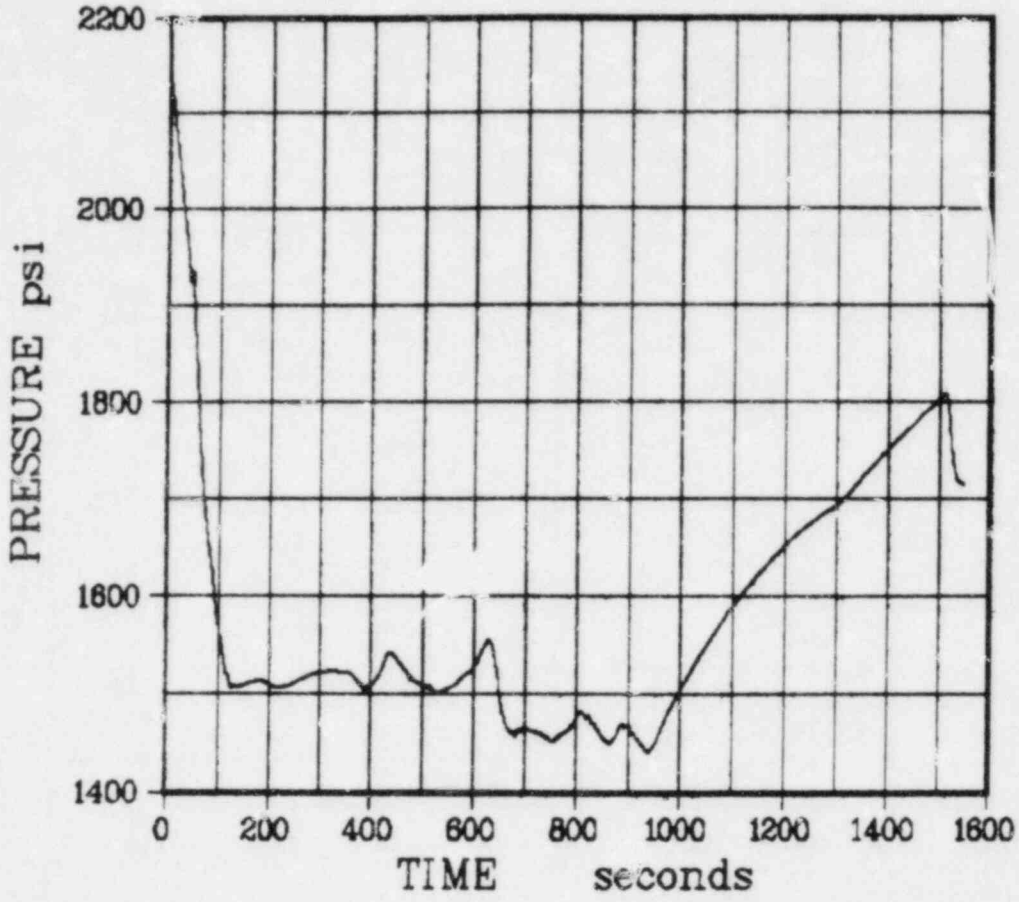

Figure E-6. Hot Leg Mixture Level, Base Model

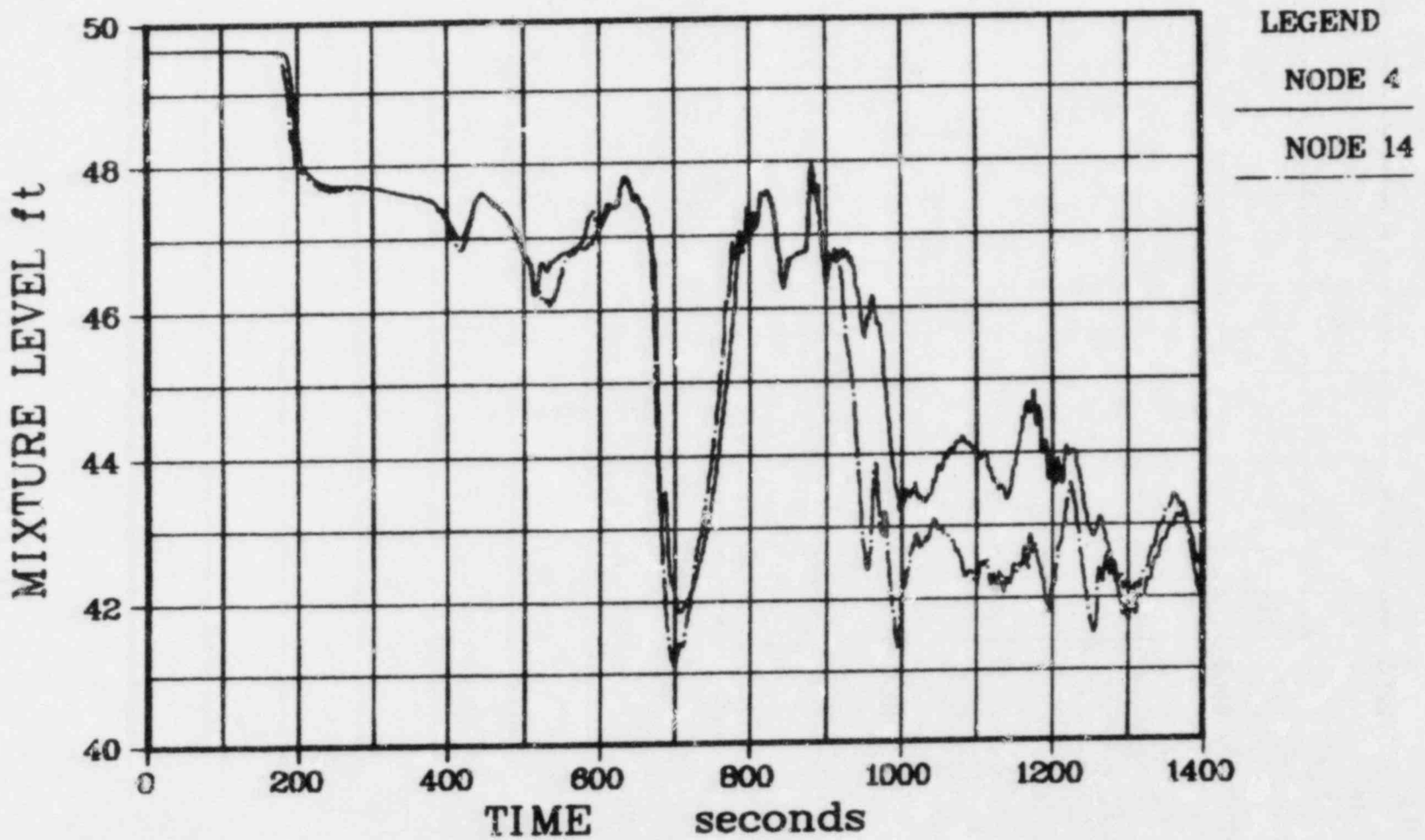

Figure E-7. Vent Valve Quality, Base Model

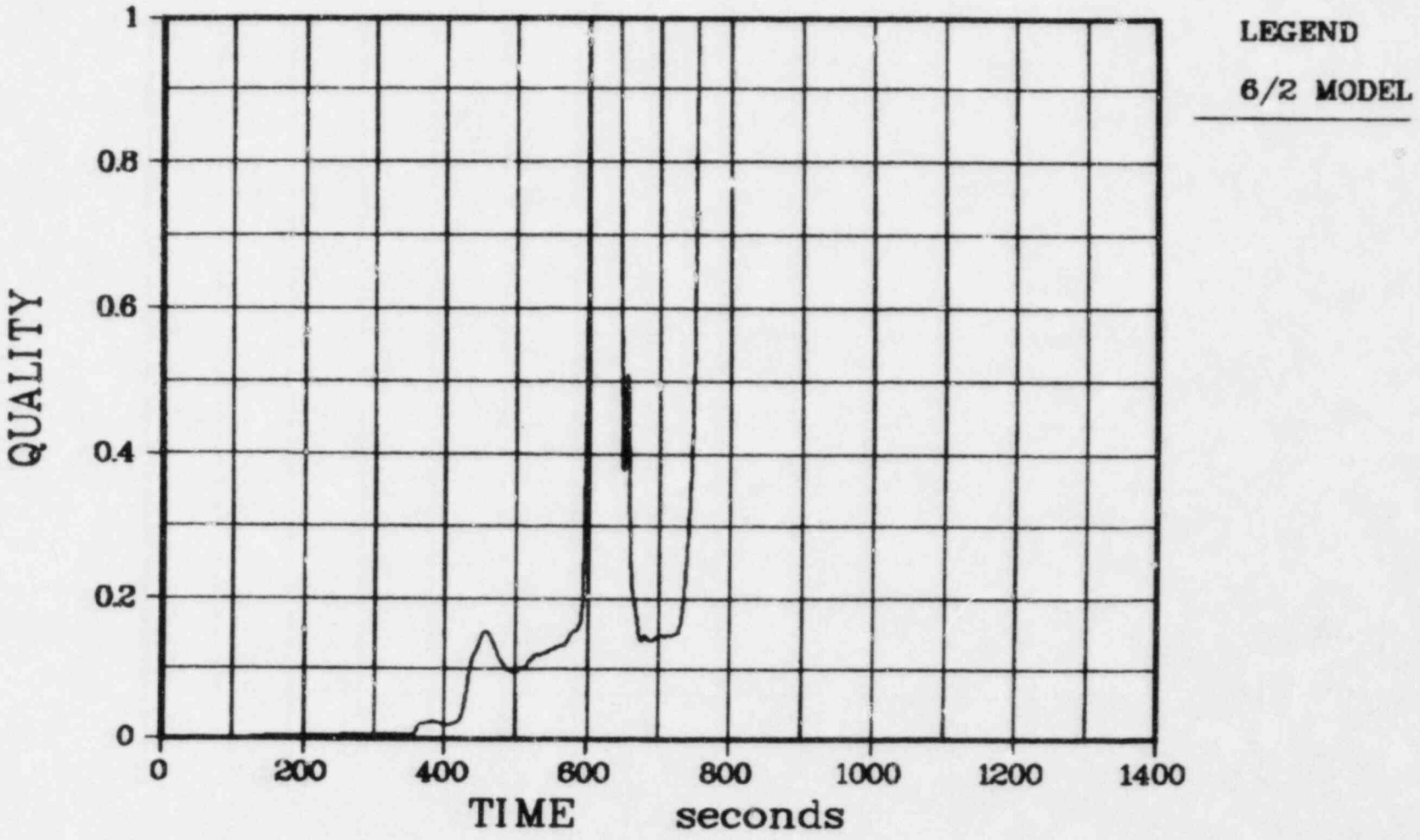

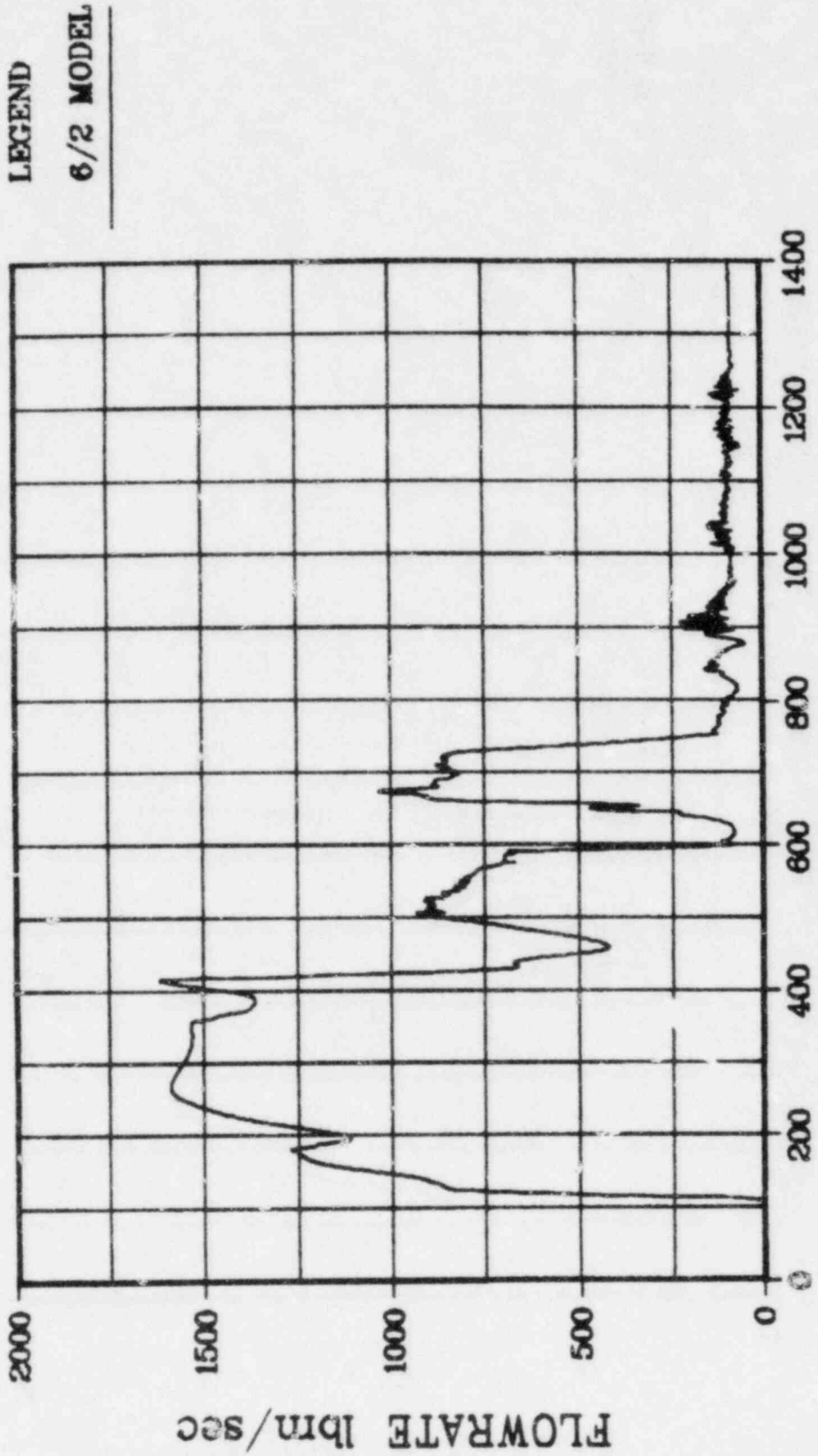

Figure E-8. Vent Valve Flowrate, Base Model

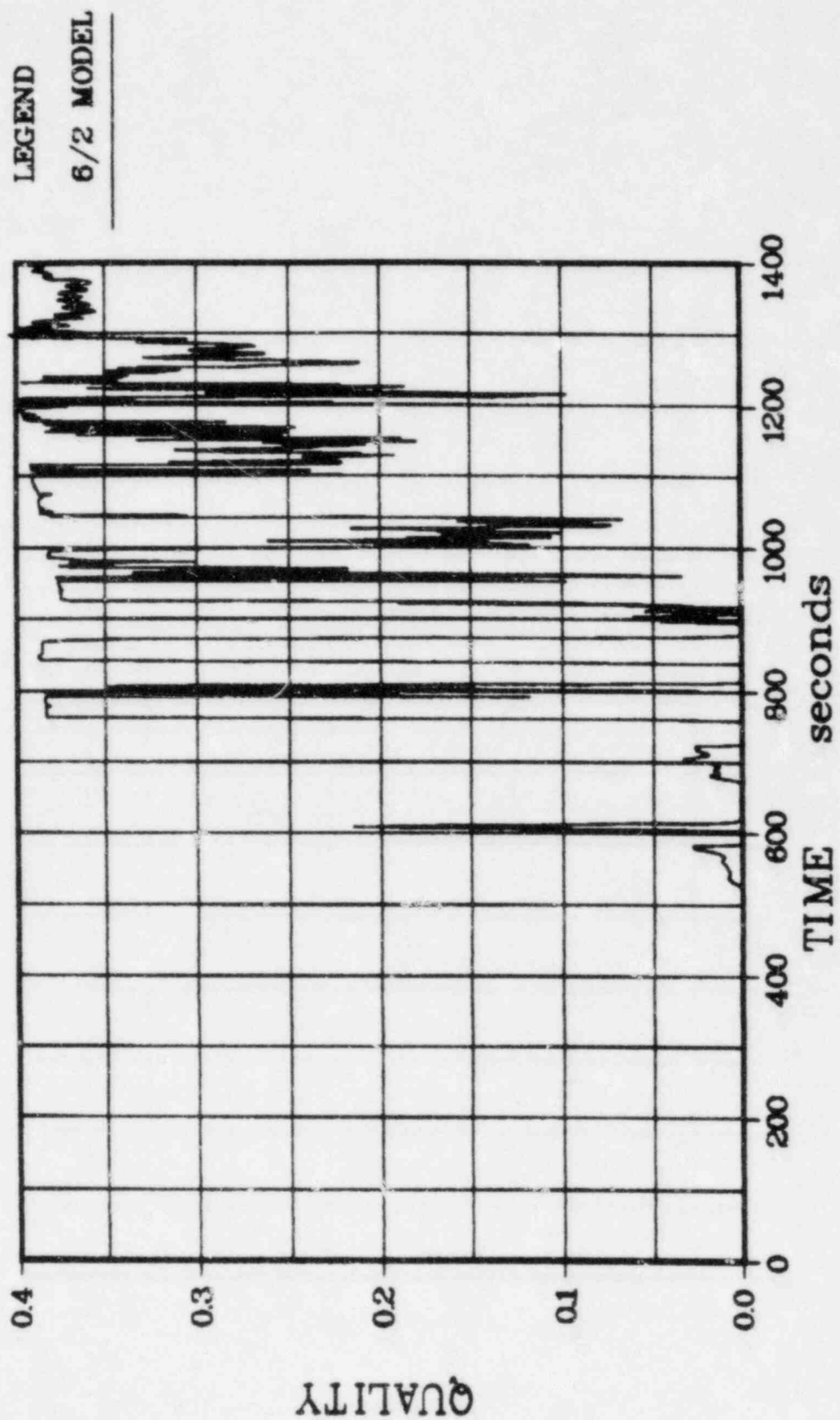

Figure E-9. Leak Quality, Base Model

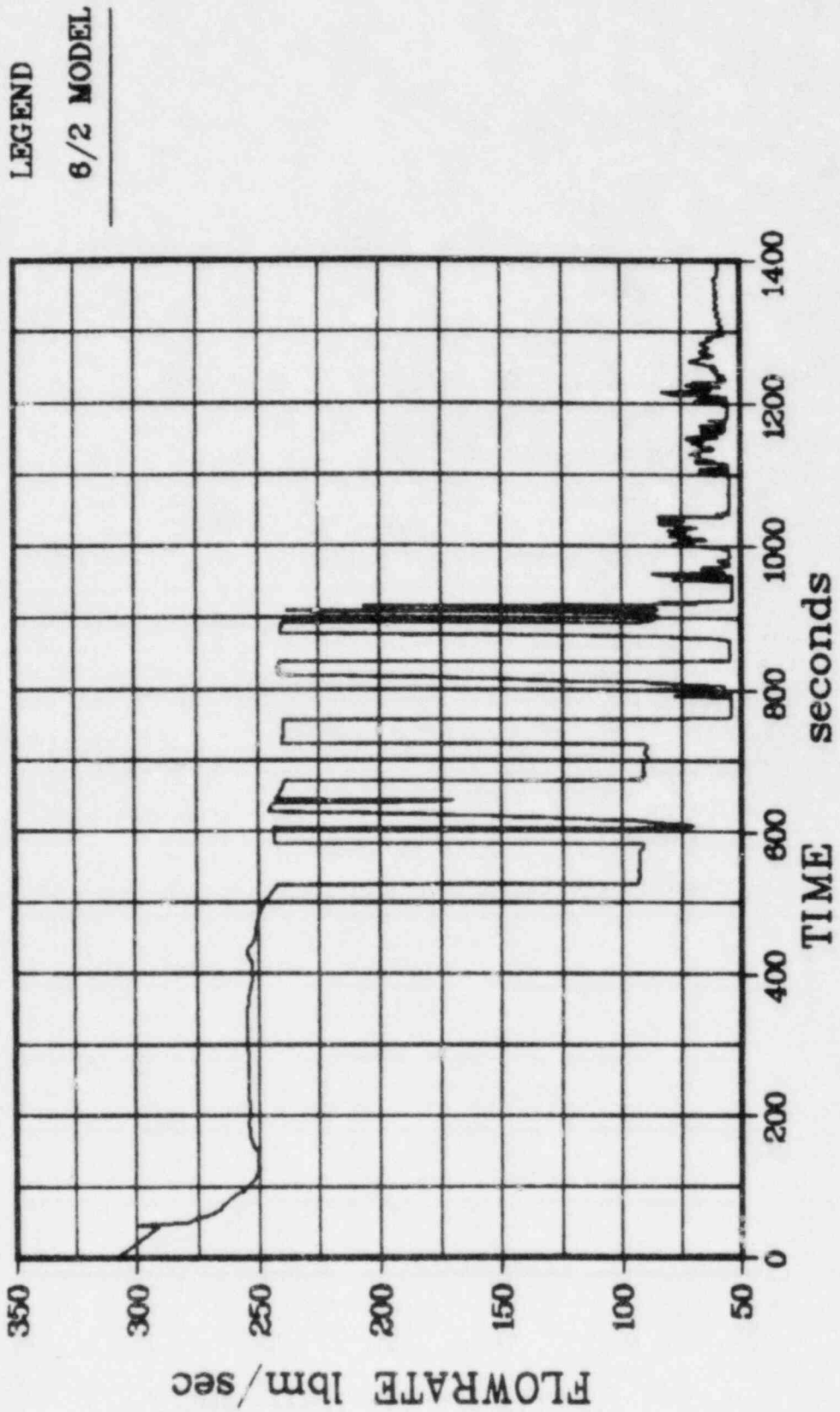

Figure E-10. Leak Flow Rate, Base Model

Figure E-11. Comparison of 4/1 Model to 4/2 Model, Pressurizer Pressure

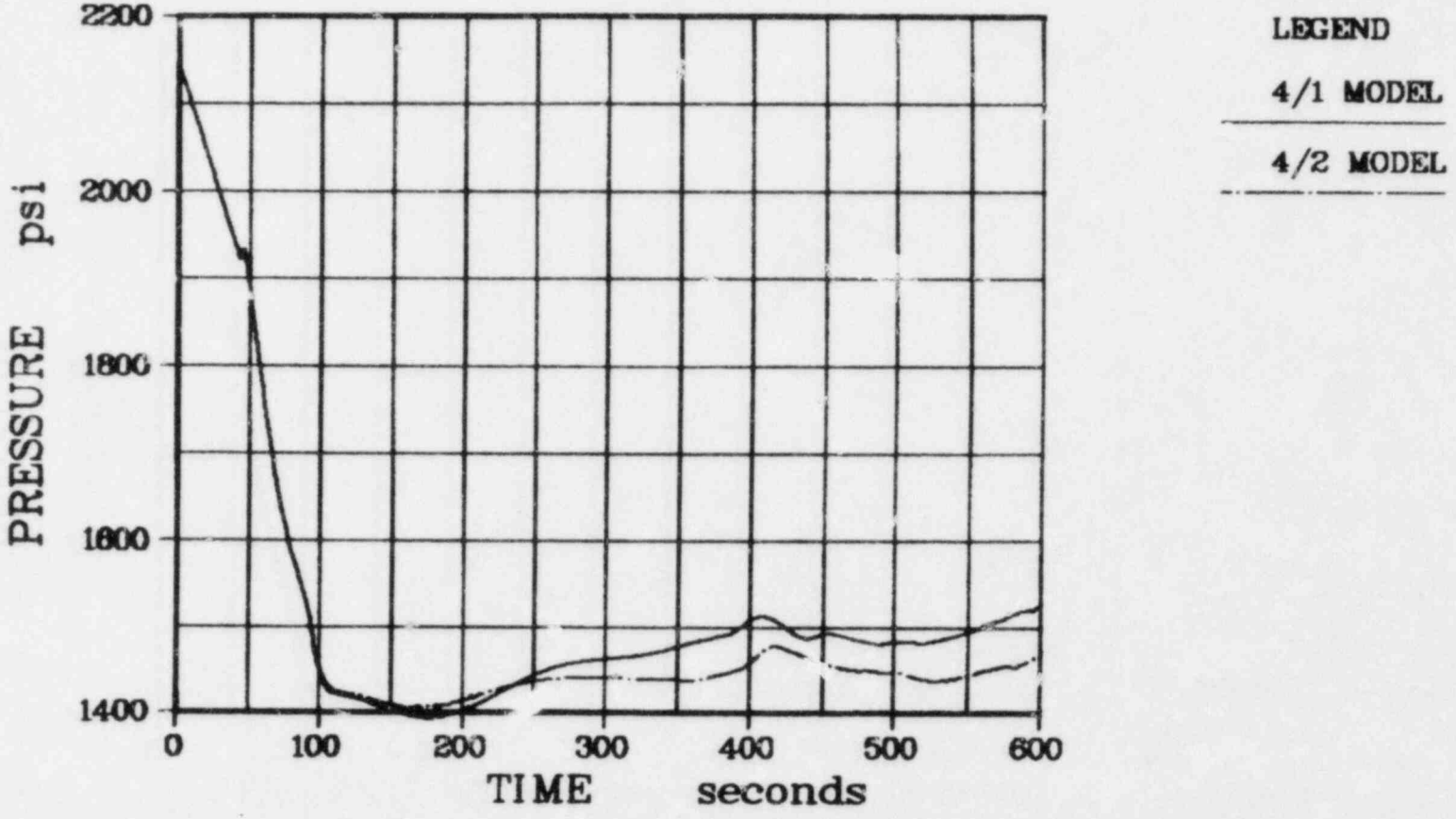

Figure E-12. Comparison of 4/2 Model to 8/2 Model, Pressurizer Pressure

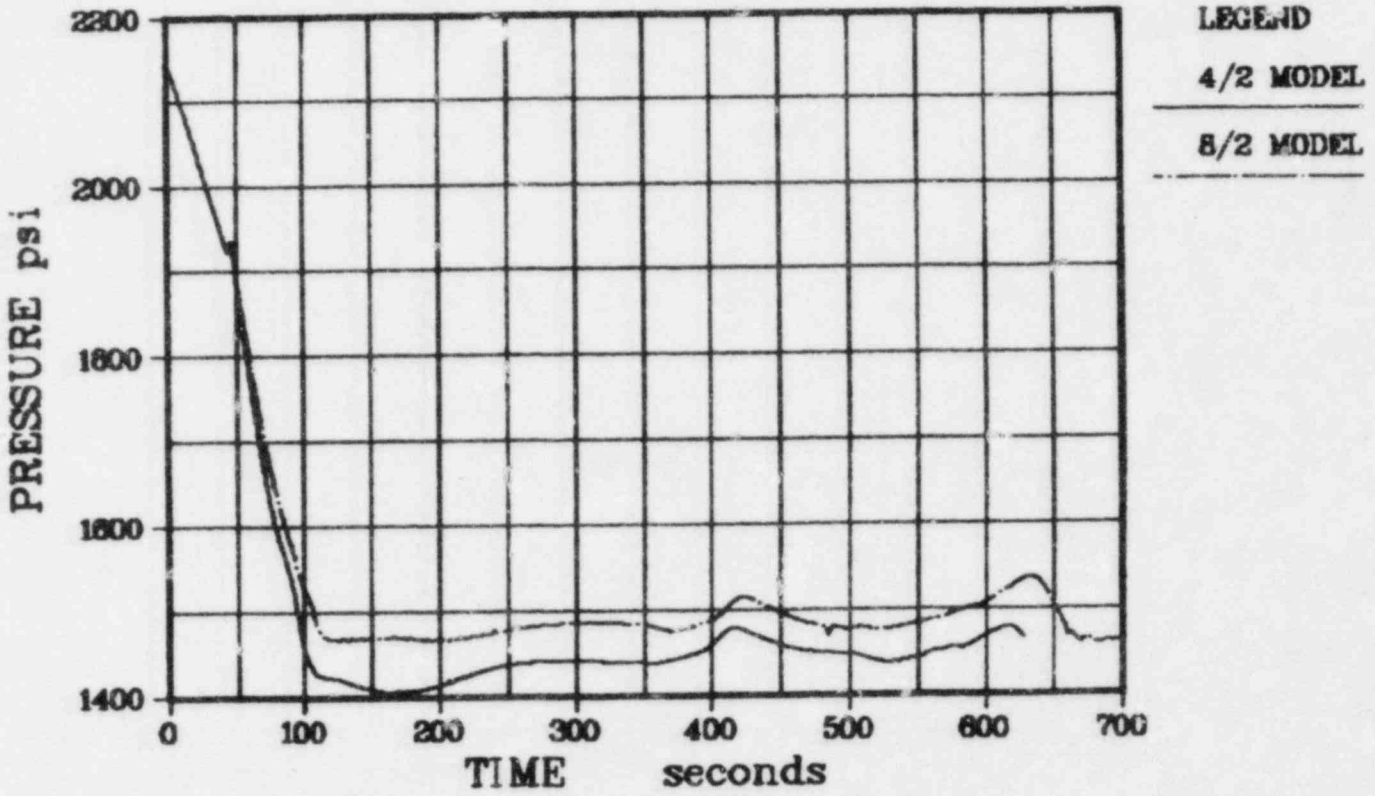

Figure E-13. Comparison of 8/2 Model to 6/2 Model, Pressurizer Pressure

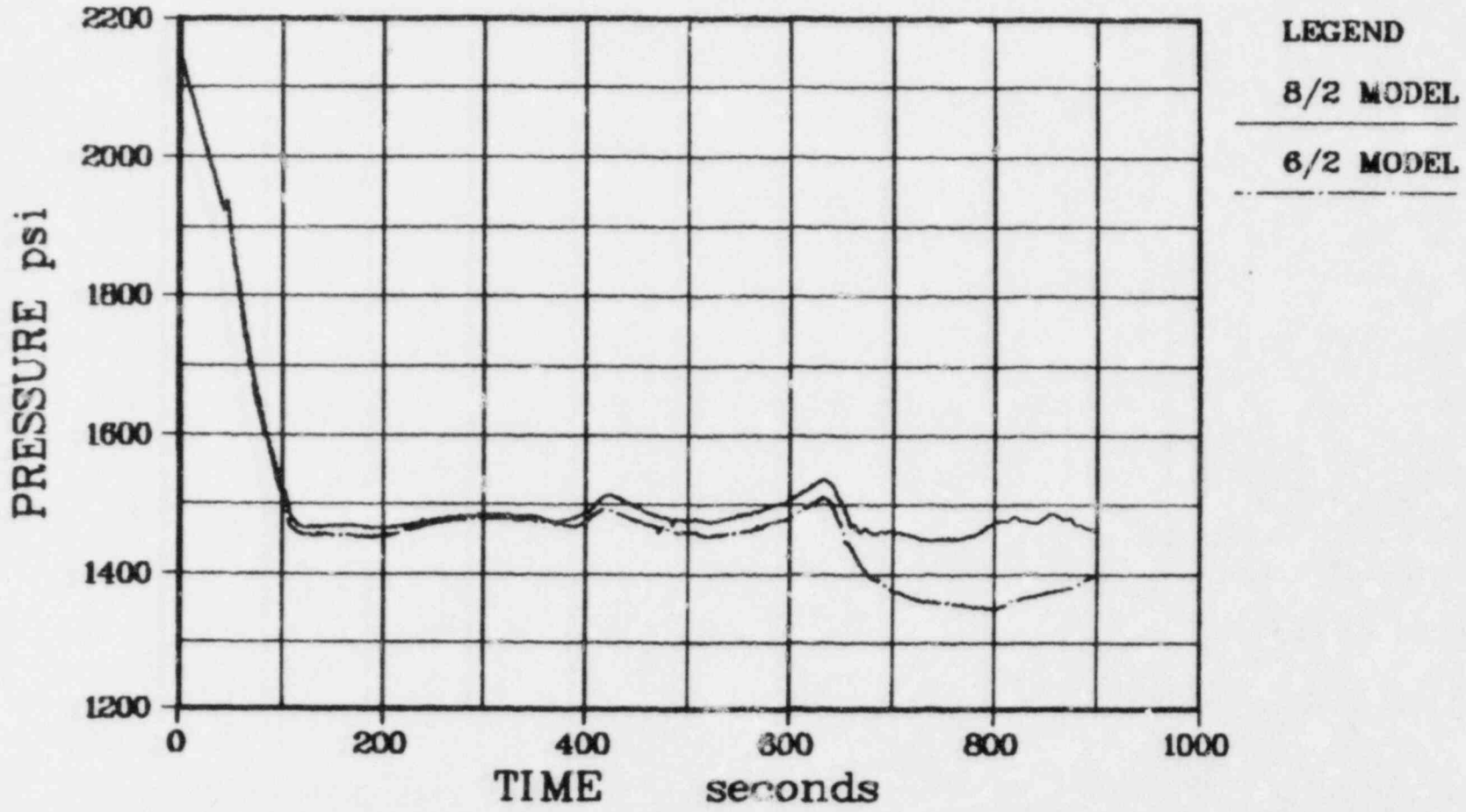

Figure E-14. Comparison of 8/2 Model to 6/2 Model, Broken Loop Hot Leg Mixture Level (Node 4)

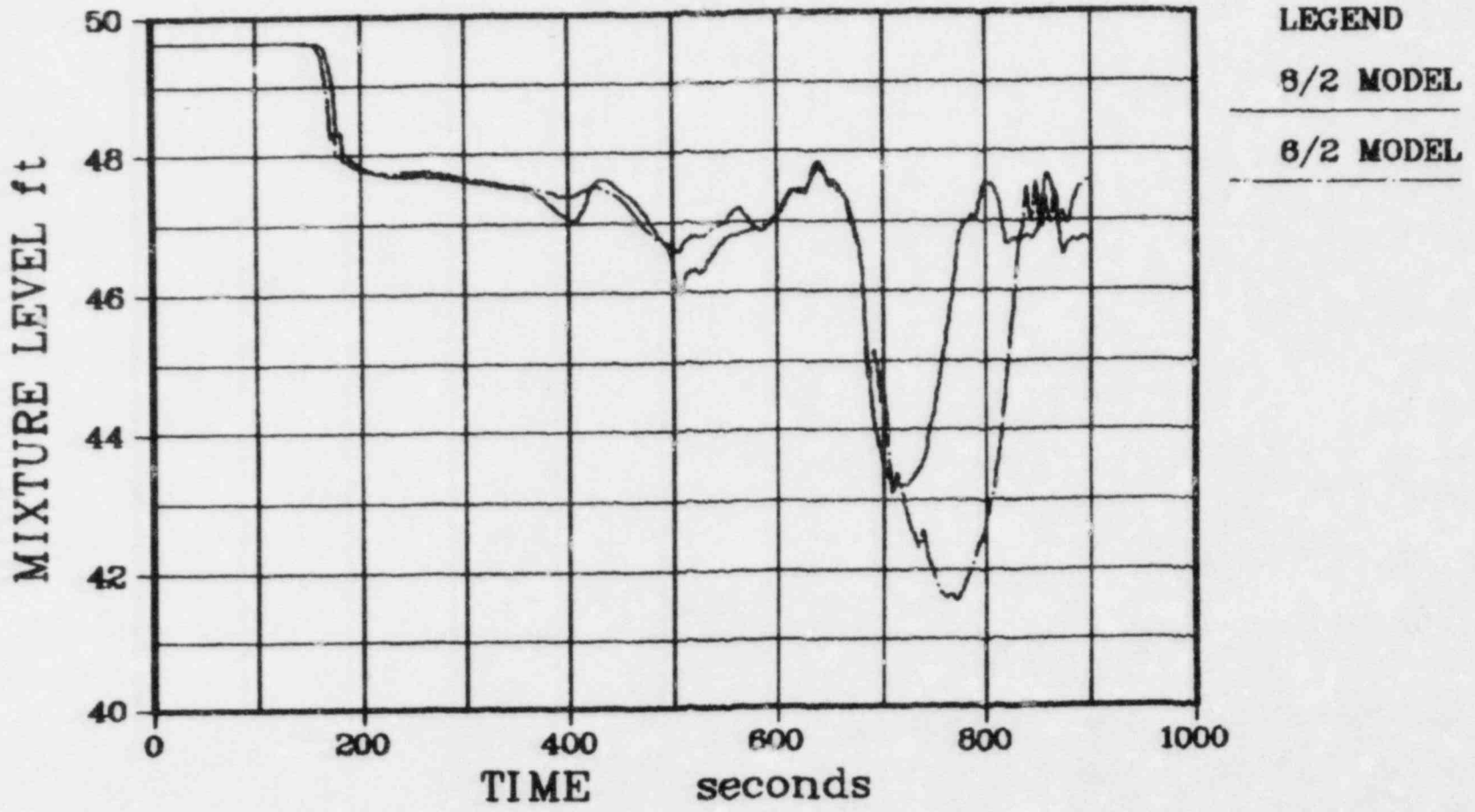

Figure E-15. Comparison of 8/2 Model to 6/2 Model, Intact Loop Hot Leg Mixture Level (Node 14)

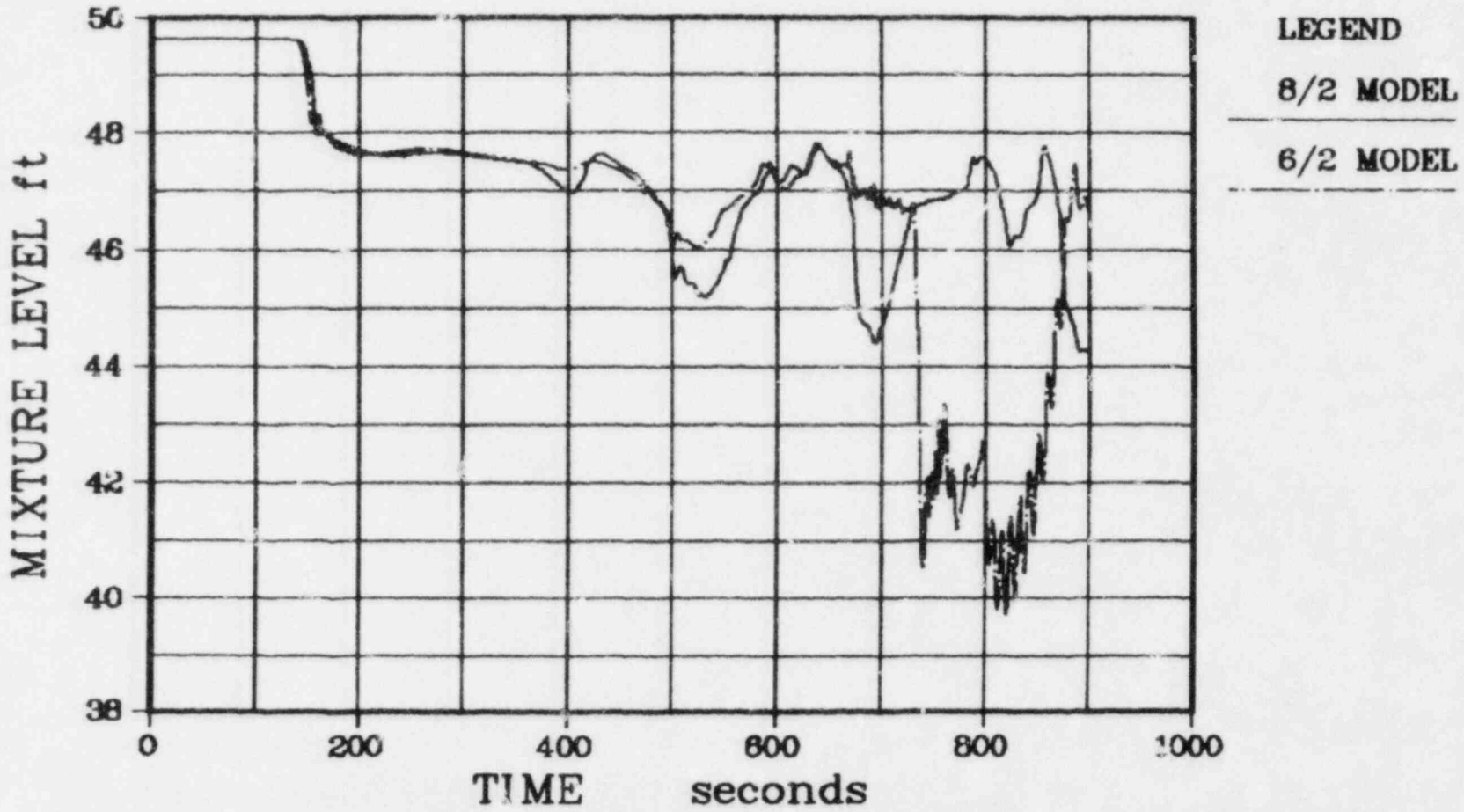

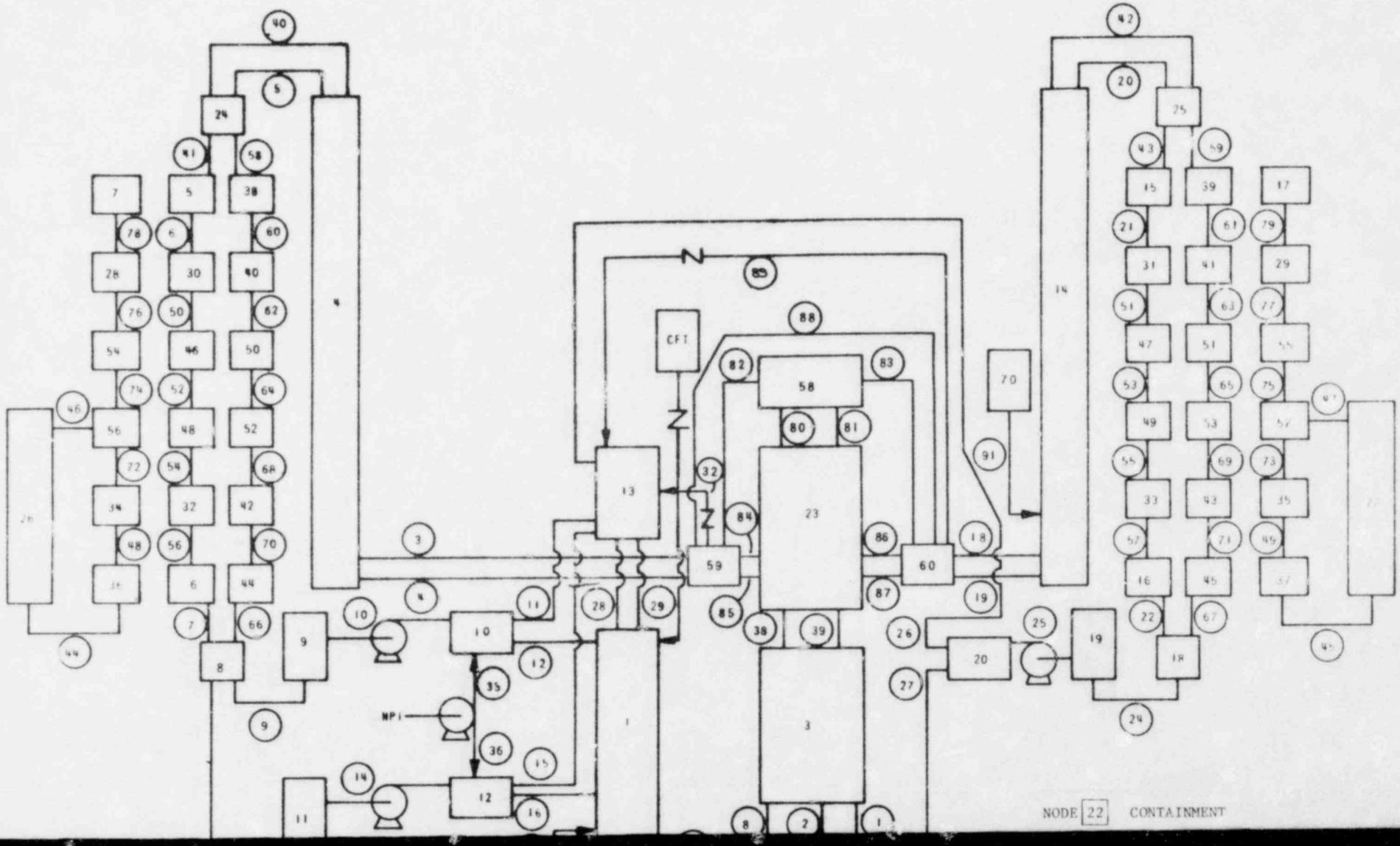
CFT
NPI
NODE 22 CONTAINMENT

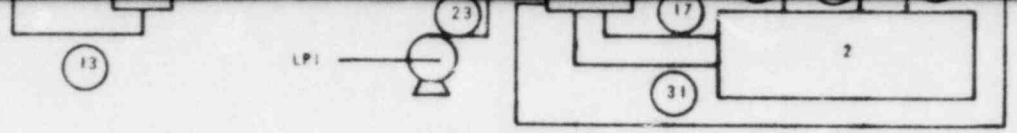

PATH (33) LEAK PATH FROM 10 TO 22

(34) LEAK PATH FROM 22 TO 10

( ) HPI-X TO NODE 20

NODE NO.	IDENTIFICATION
1	DOWNCOMER
2	LOWER PLENUM
3	CORE
4, 14	HOT LEG PIPING
5, 6, 30, 32 38, 40, 42, 44 46, 48, 50, 52	SG TUBES
7, 28, 34, 36 54, 56	SG-SECONDARY SIDE
8, 18	SG LOWER HEAD
9, 11, 19	COLD LEG PIPING
10, 12, 20	COLD LEG PIPING
13	UPPER DOWNCOMER
15, 16, 31, 33 39, 41, 43, 45 47, 49, 51, 53	SG TUBES
17, 29, 35, 37 55, 57	SG-SECONDARY SIDE
22	CONTAINMENT
23	UPPER PLENUM
24, 25	SG UPPER HEAD
26, 27	SG-DOWNCOMER
70	PRESSURIZER
58	UPPER HEAD
59	OUTER PLENUM
60	OUTER PLENUM

PATH NO.	IDENTIFICATION
1, 2	CORE
3, 4, 18, 19	HOT LEG PIPING
5, 20, 40, 42	HOT LEG, UPPER
6, 41, 50, 52 54, 56, 58, 60 62, 64, 68, 70	SG TUBES
7, 66	SG LOWER HEAD
8	CORE BYPASS
9, 13, 24	COLD LEG PIPING
10, 14, 25	PUMPS
11, 12, 15, 16 26, 27	COLD LEG PIPING
17, 31	DOWNCOMER
21, 43, 51, 53 55, 57, 59, 61 63, 65, 69, 71	SG TUBES
22, 67	SG LOWER HEAD
23	LPI
28, 29	UPPER DOWNCOMER
32, 89	VENT VALVE
33, 34	LEAK AND RETURN PATH
35, 36	HPI
37	CONTAINMENT SPRAYS
38, 39, 80, 81	UPPER PLENUM
44, 46, 48 72, 74, 76, 78	SG-SECONDARY
45, 47, 49, 73, 75, 77, 79	SG-SECONDARY
82, 83, 84, 85, 86, 87, 88	OUTER PLENUM

Figure E-16. Detailed Upper Plenum Model Noding Scheme (Four-Node Model)

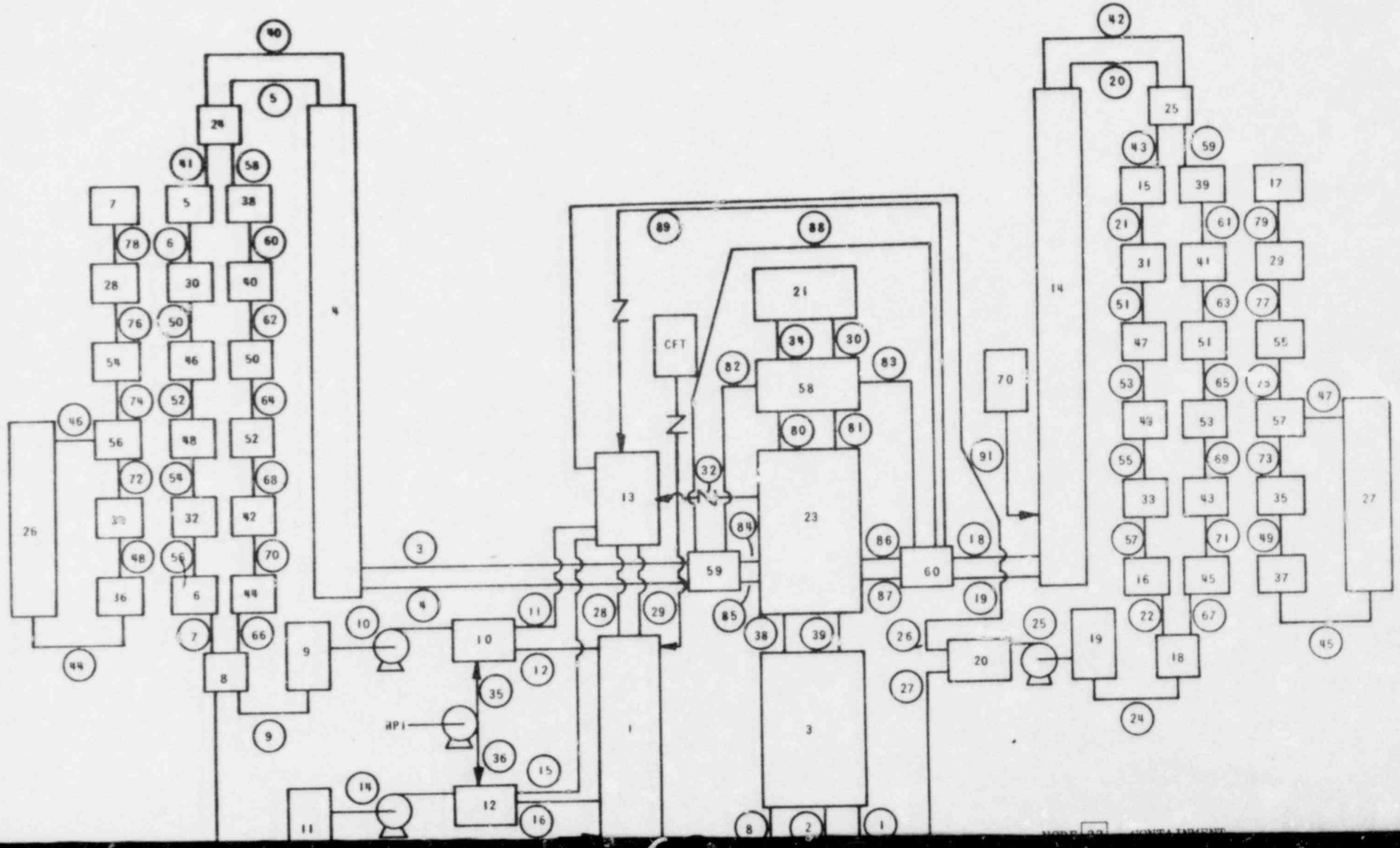
CFT
API

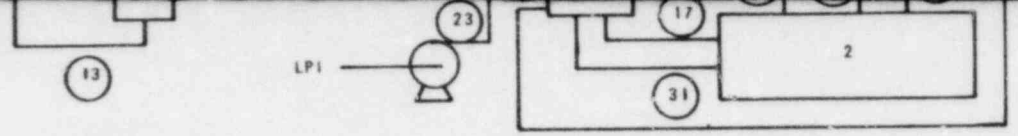

PATH (33) LEAK PATH FROM 10 TO 22

(37) HPI-X TO NODE 20

NODE NO	IDENTIFICATION
1	DOWNCOMER
2	LOWER PLENUM
3	CORE
4, 14	HOT LEG PIPING
5, 6, 30, 32 38, 40, 42, 44 46, 48, 50, 52	SG TUBES
7, 28, 34, 36, 54, 56	SG-SECONDARY SIDE
8, 18	SG LOWER HEAD
9, 11, 19	COLD LEG PIPING
10, 12, 20	COLD LEG PIPING
13	UPPER DOWNCOMER
15, 16, 31, 33 39, 41, 43, 45 47, 49, 51, 53	SG TUBES
17, 29, 35, 37	SG-SECONDARY SIDE
55, 57	
22	CONTAINMENT
23	UPPER PLENUM
24, 25	SG UPPER HEAD
26, 27	SG-DOWNCOMER
70	PRESSURIZER
21, 58	UPPER HEAD
59, 60	OUTER PLENUM

PATH NO.	IDENTIFICATION
1, 2	CORE
3, 4, 18, 19	HOT LEG PIPING
5, 20, 40, 42	HOT LEG UPPER
6, 41, 50, 52 54, 56, 58, 60 62, 64, 68, 70	SG TUBES
7, 66	SG LOWER HEAD
8	CORE BYPASS
9, 13, 24	COLD LEG PIPING
10, 14, 25	PUMPS
11, 12, 15, 16 26, 27	COLD LEG PIPING
17, 31	DOWNCOMER
21, 43, 51, 53 55, 57, 59, 61 63, 65, 69, 71	SG TUBES
22, 67	SG LOWER HEAD
23	LPI
28, 29	UPPER DOWNCOMER
32	VENT VALVE
33	LEAK PATH
35, 36	HPI
37	CONTAINMENT SPRAYS
38, 39, 80, 81 44, 46, 48 72, 74, 76, 78	UPPER PLENUM SG-SECONDARY
45, 47, 49, 73, 75, 77, 79	SG-SECONDARY
30, 34 82, 83, 84, 85 86, 87, 88	UPPER HEAD OUTER PLENUM

Figure E-17. Detailed Upper Plenum/ Upper Head Model Nodding Scheme (Five-Node Model)

Figure E-18. Pressurizer Pressure

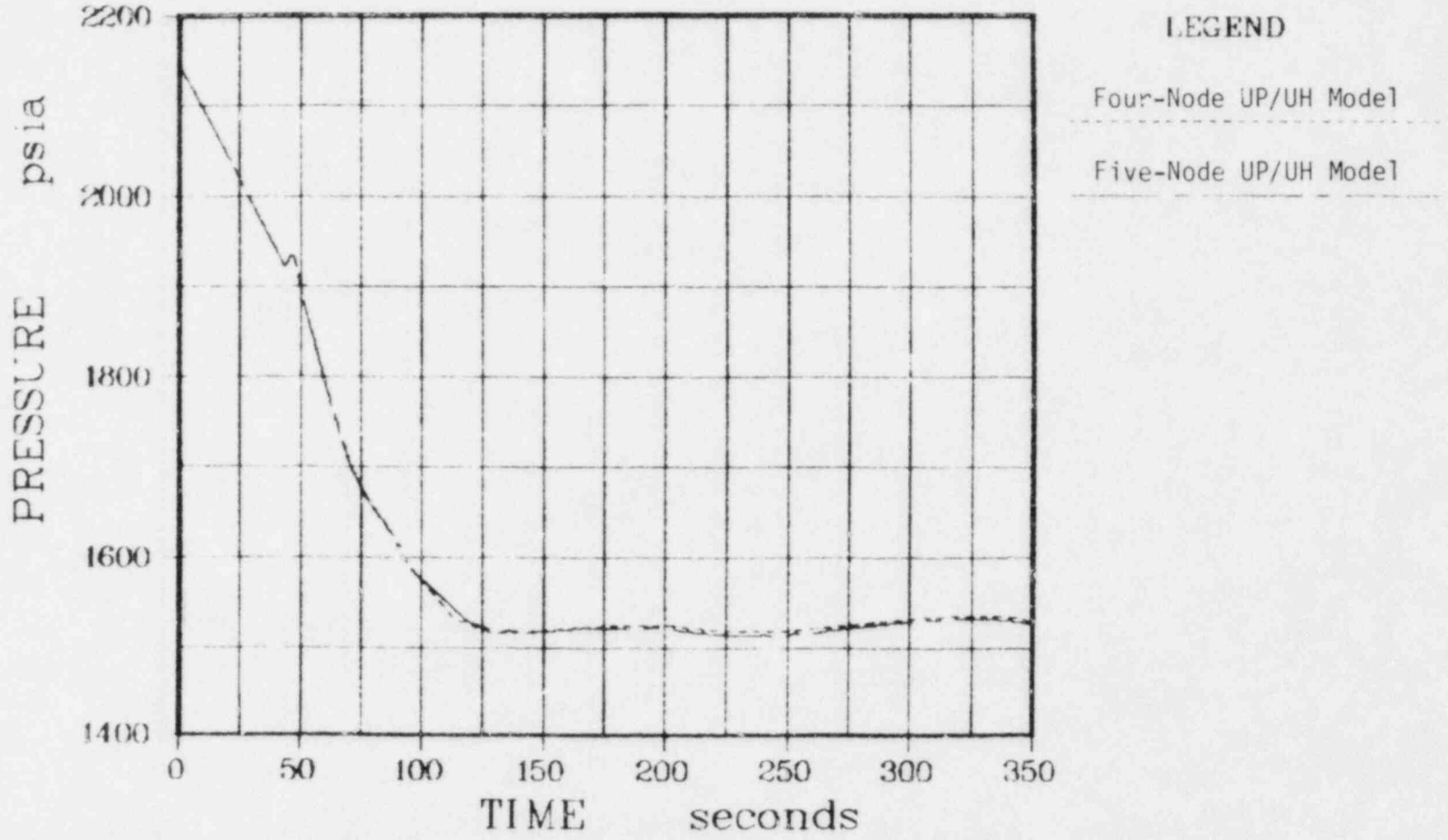

Figure E-19. RV Upper Plenum Liquid Level

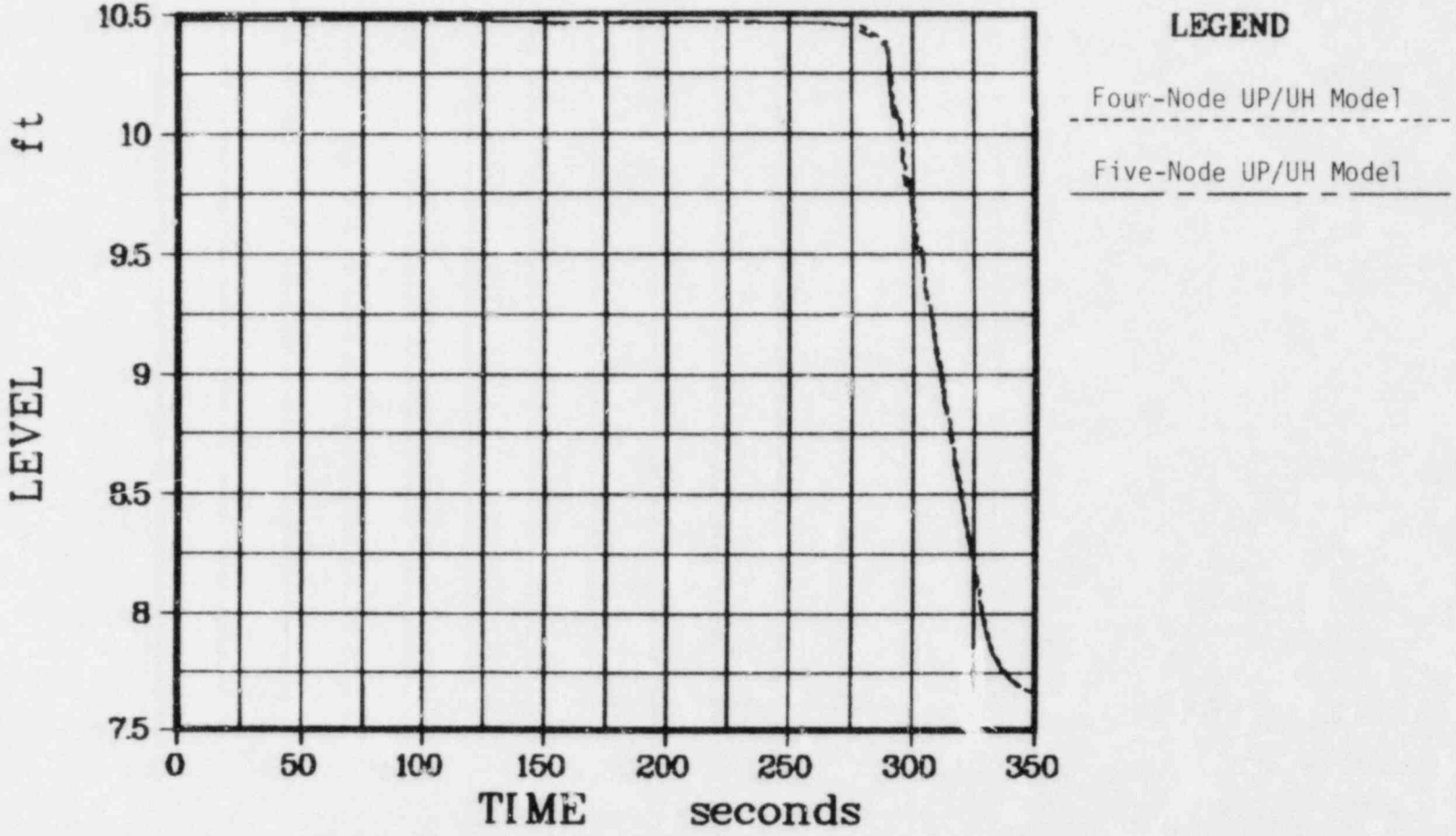

Figure E-20. Pressurizer Pressure

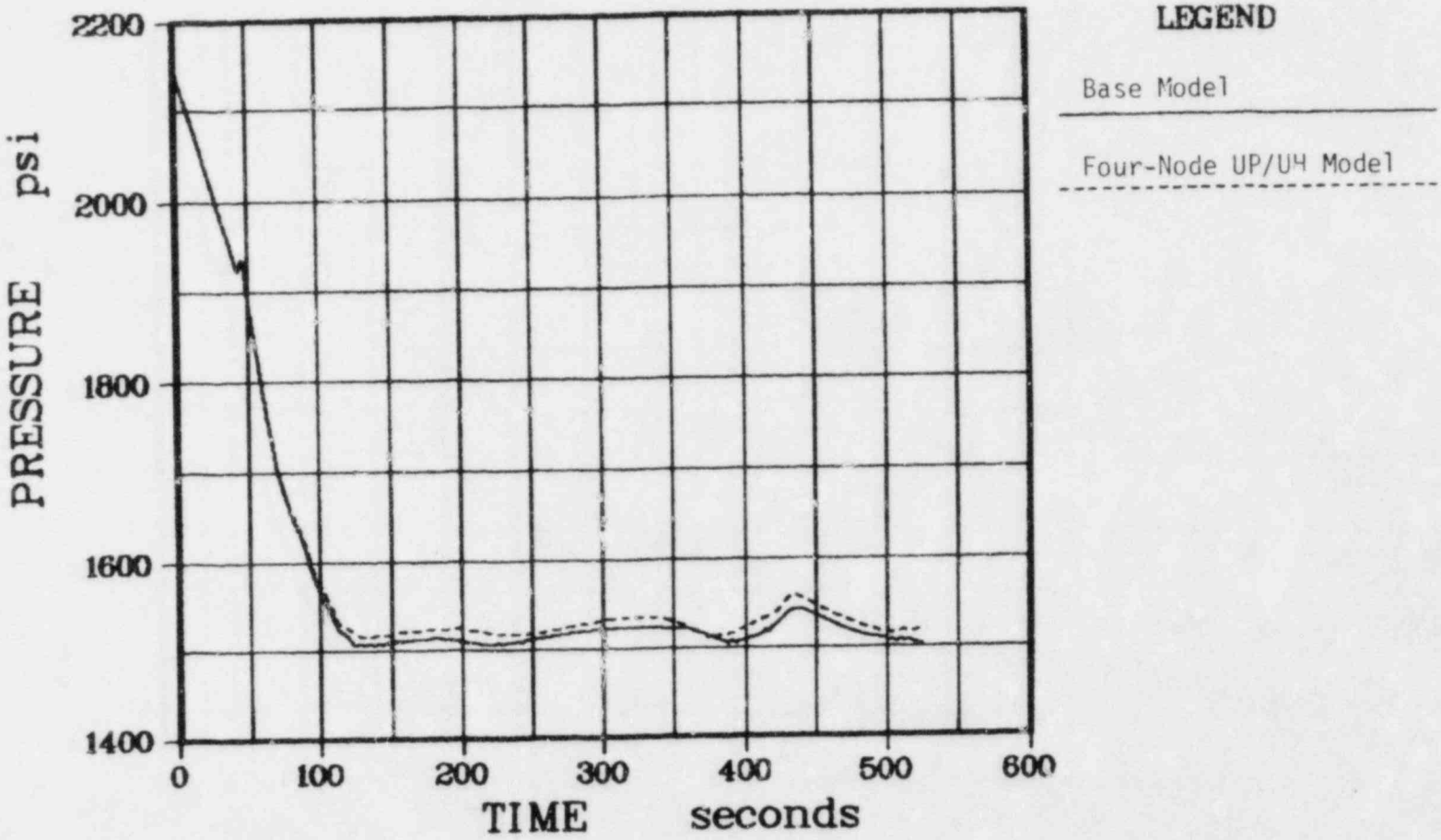

Figure E-21. Vent Valve Flow Rate

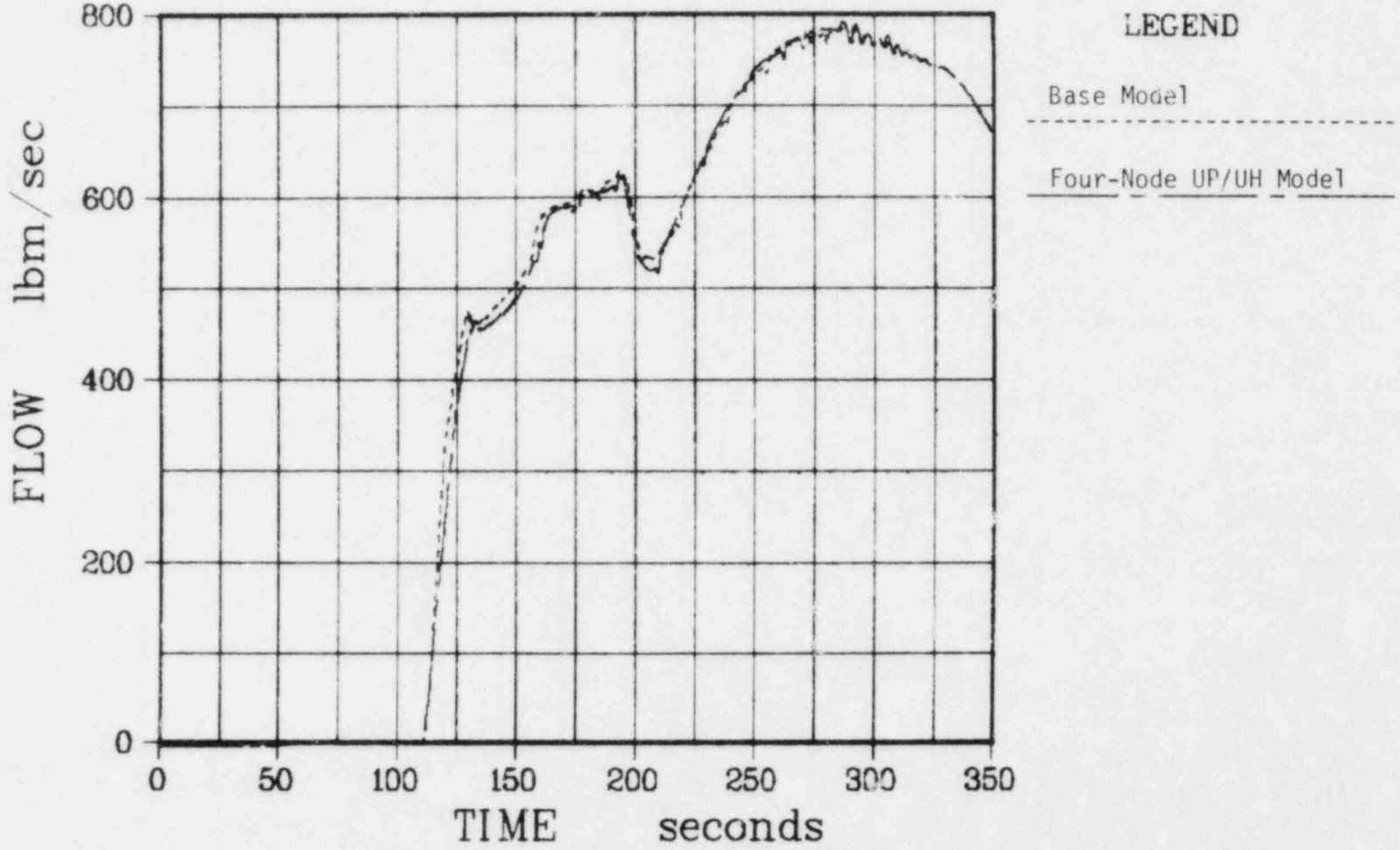

Figure E-22. Hot Leg Liquid Level (Loop B)

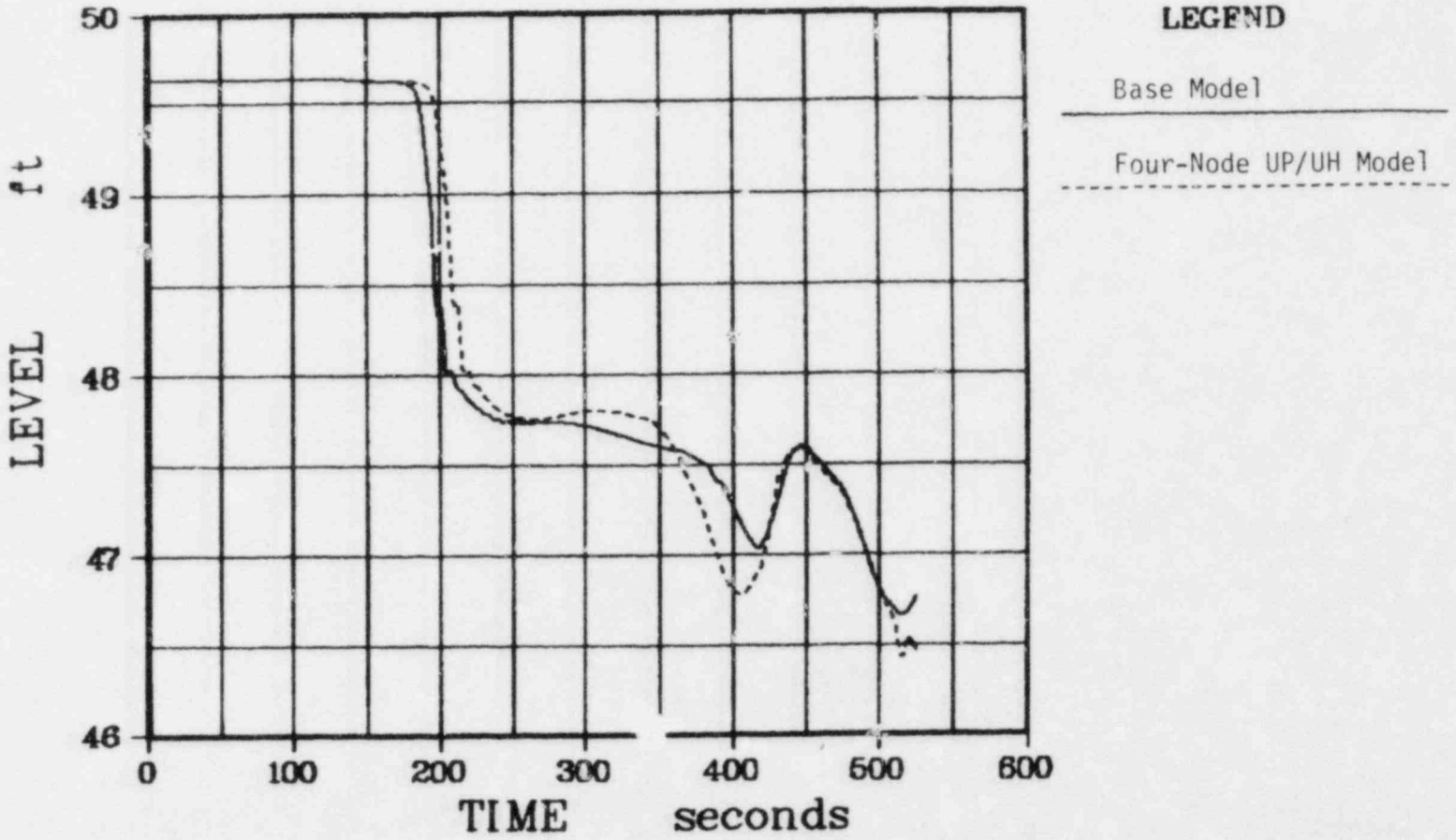

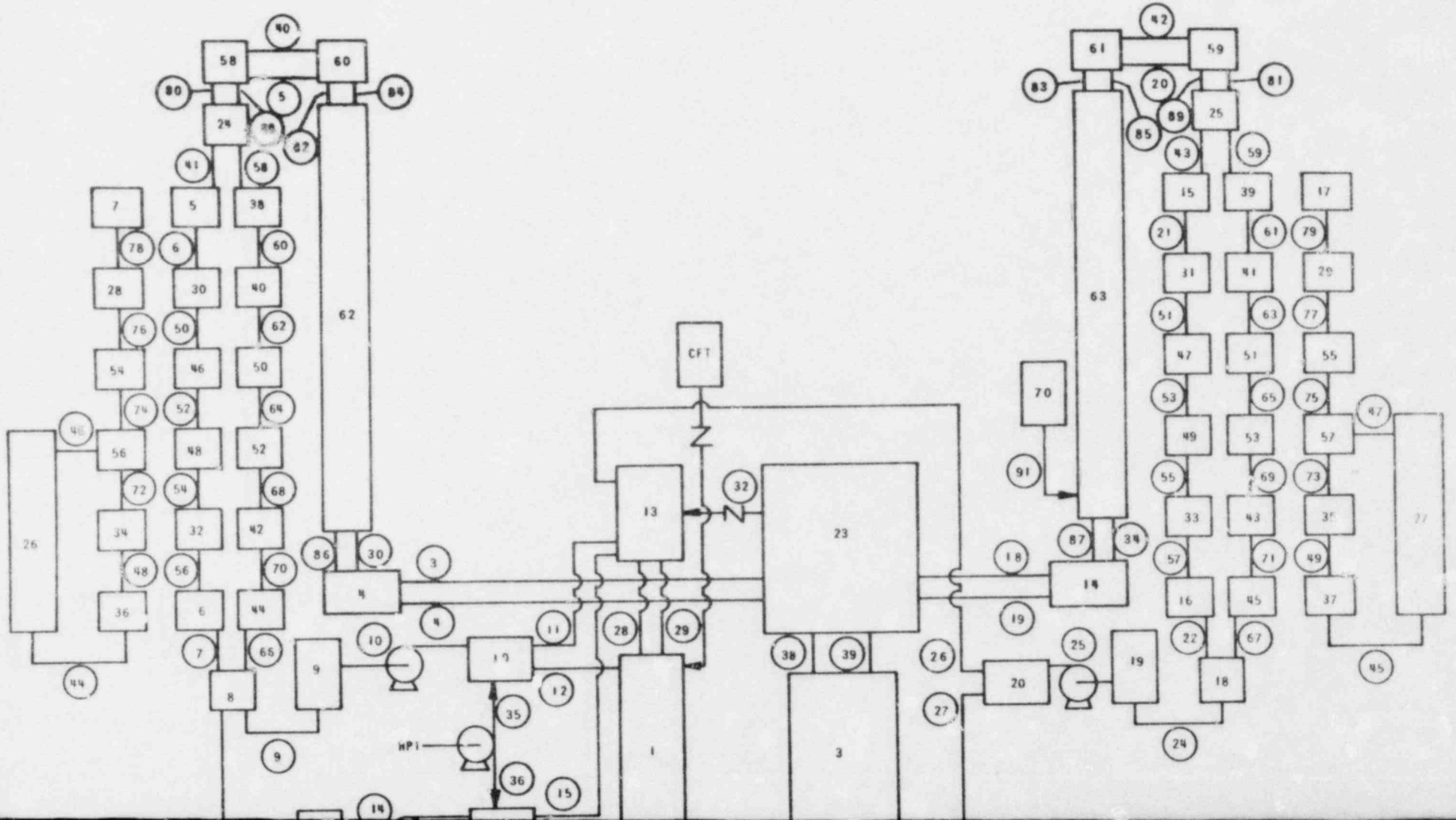
CFT
HPI
1
3
13
23
62
63

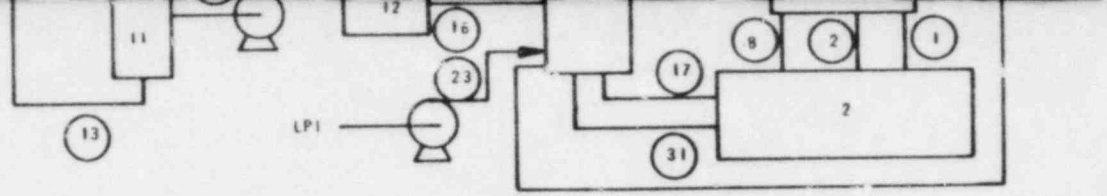

NODE 22 CONTAINMENT

PATH 33 LEAK PATH FROM 10 TO 22

37 HPI-X TO NODE 20

NODE NO.	IDENTIFICATION
1	DOWNCOMER
2	LOWER PLENUM
3	CORE
4, 14, 60, 61, 62, 63	HOT LEG PIPING
5, 6, 30, 32, 38, 40, 42, 44, 46, 48, 50, 52	SG TUBES
7, 28, 34, 36, 54, 56	SG-SECONDARY SIDE
8, 18	SG LOWER HEAD
9, 11, 19	COLD LEG PIPING
10, 12, 20	COLD LEG PIPING
13	UPPER DOWNCOMER
15, 16, 31, 33, 39, 41, 43, 45, 47, 49, 51, 53	SG TUBES
17, 29, 35, 37, 55, 57	SG-SECONDARY SIDE
22	CONTAINMENT
23	UPPER PLENUM
24, 25, 58, 59	SG UPPER HEAD
26, 27	SG-DOWNCOMER
70	PRESSURIZER

PATH NO.	IDENTIFICATION
1, 2	CORE
3, 4, 18, 19, 30, 34, 82, 83, 84, 85, 86, 87	HOT LEG PIPING
5, 20, 40, 42, 80, 81, 88, 89	HOT LEG UPPER
6, 41, 50, 52, 54, 56, 58, 60, 62, 64, 68, 70	SG TUBES
7, 66	SG LOWER HEAD
8	CORE BYPASS
9, 13, 24	COLD LEG PIPING
10, 14, 25	PUMPS
11, 12, 15, 16, 26, 27	COLD LEG PIPING
17, 31	DOWNCOMER
43, 51, 53, 55, 57, 59, 61, 63, 65, 69, 71	SG TUBES
22, 67	SG LOWER HEAD
23	LPI
28, 29	UPPER DOWNCOMER
32	VENT VALVE
33	LEAK PATH
36, 36	HPI
37	CONTAINMENT SPRAYS
38, 39	UPPER PLENUM
44, 46, 48, 72, 74, 76, 78	SG-SECONDARY SG-SECONDARY
45, 47, 49, 73, 75, 77, 79	SG-SECONDARY

Figure E-23. Detailed Hot Leg Model Noding Scheme

Figure E-24. Pressurizer Pressure

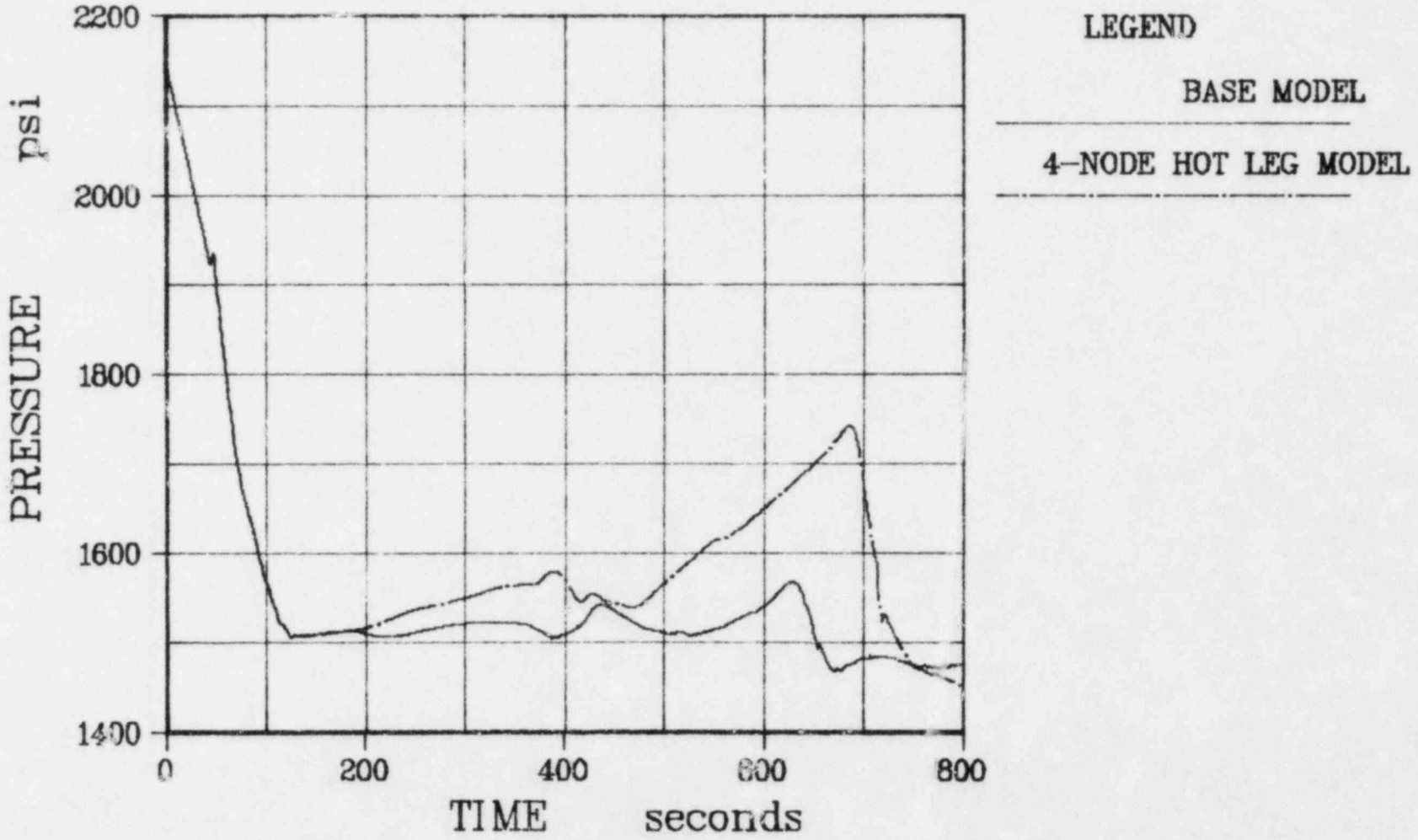

Figure E-25. Liquid Level in Hot Leg Riser Section (Loop A)

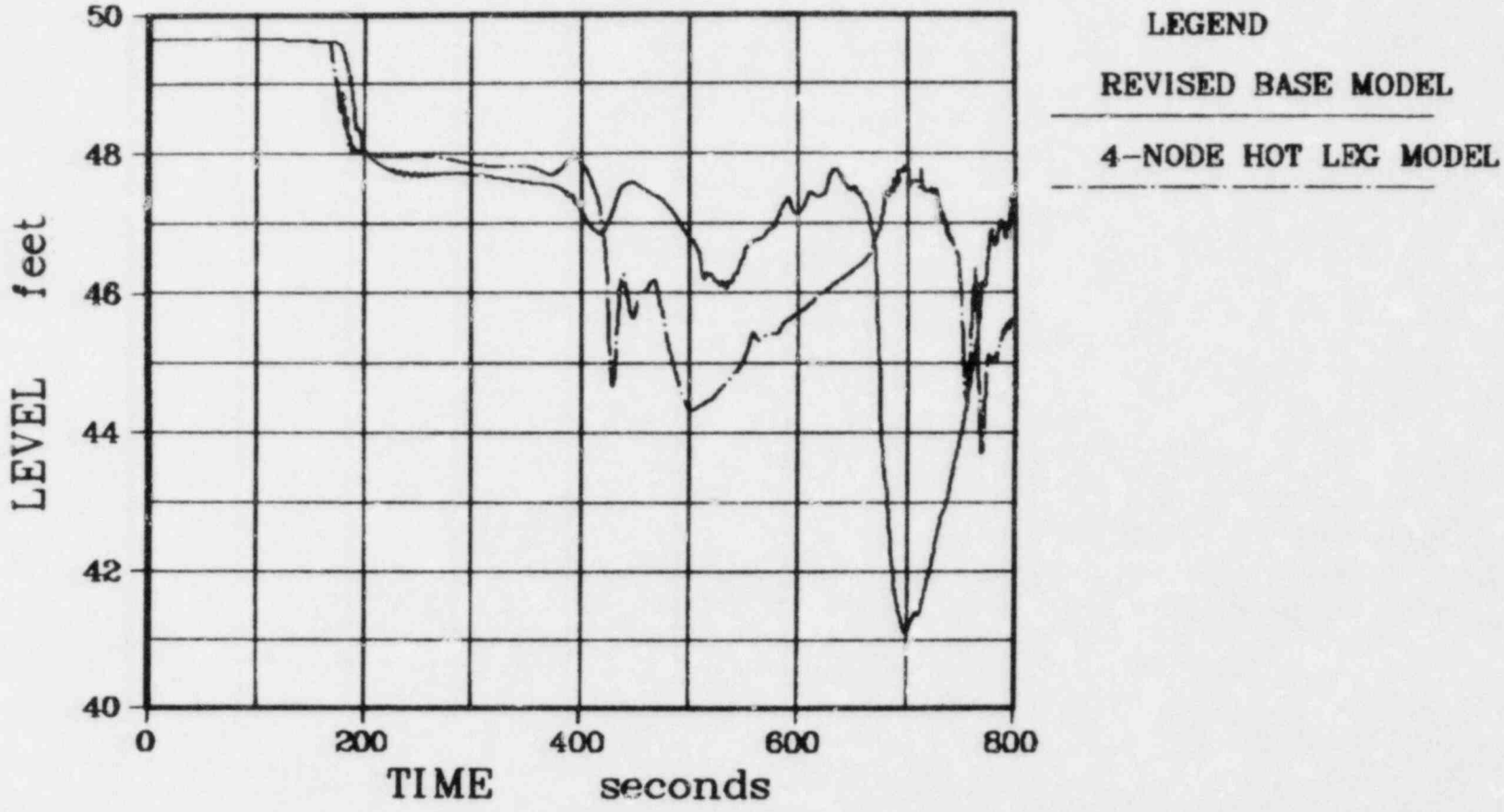

Figure E-26. Liquid Level in Hot Leg Riser Section (Loop B)

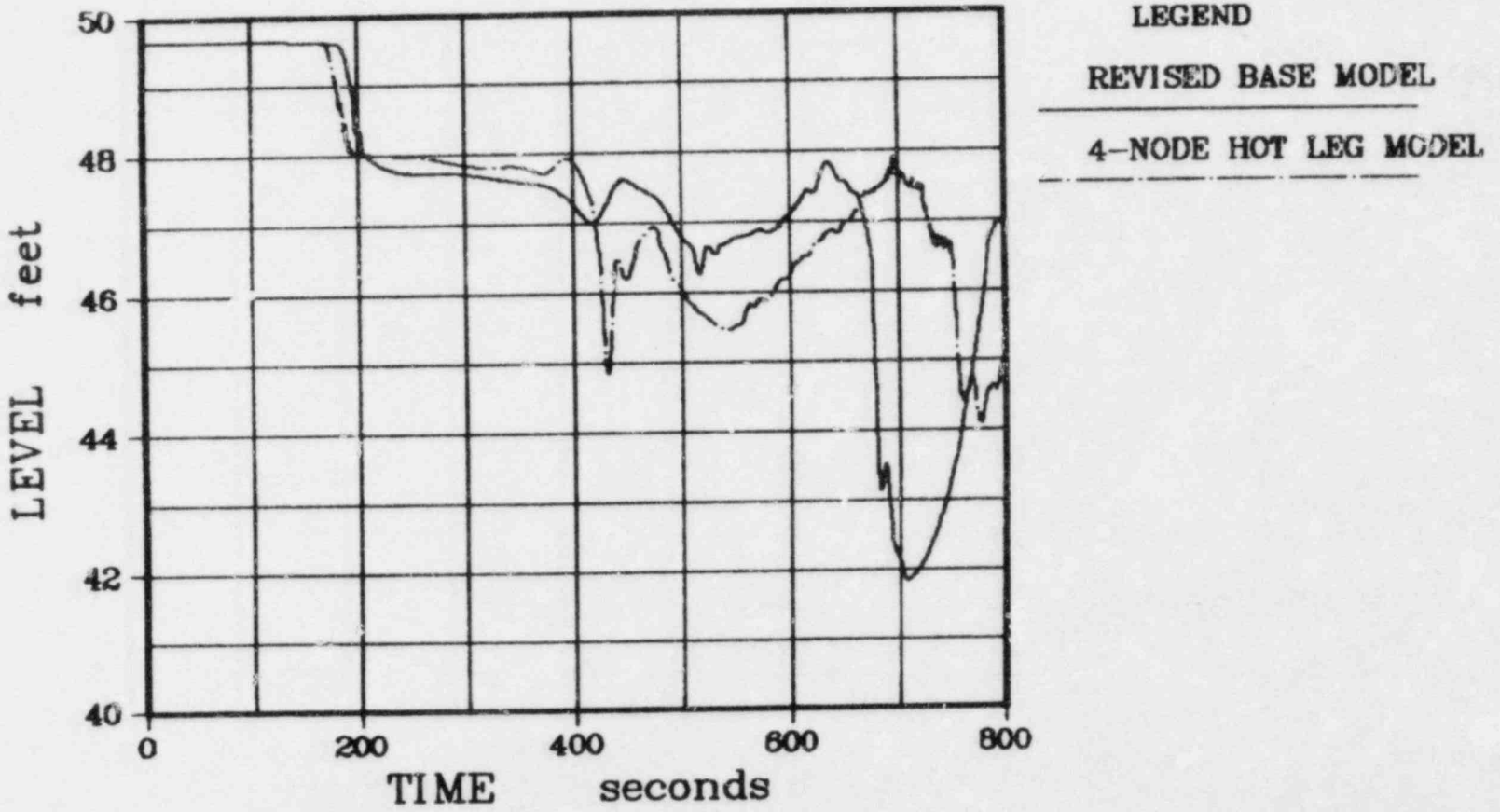

Figure E-27. Leak Flow Rate

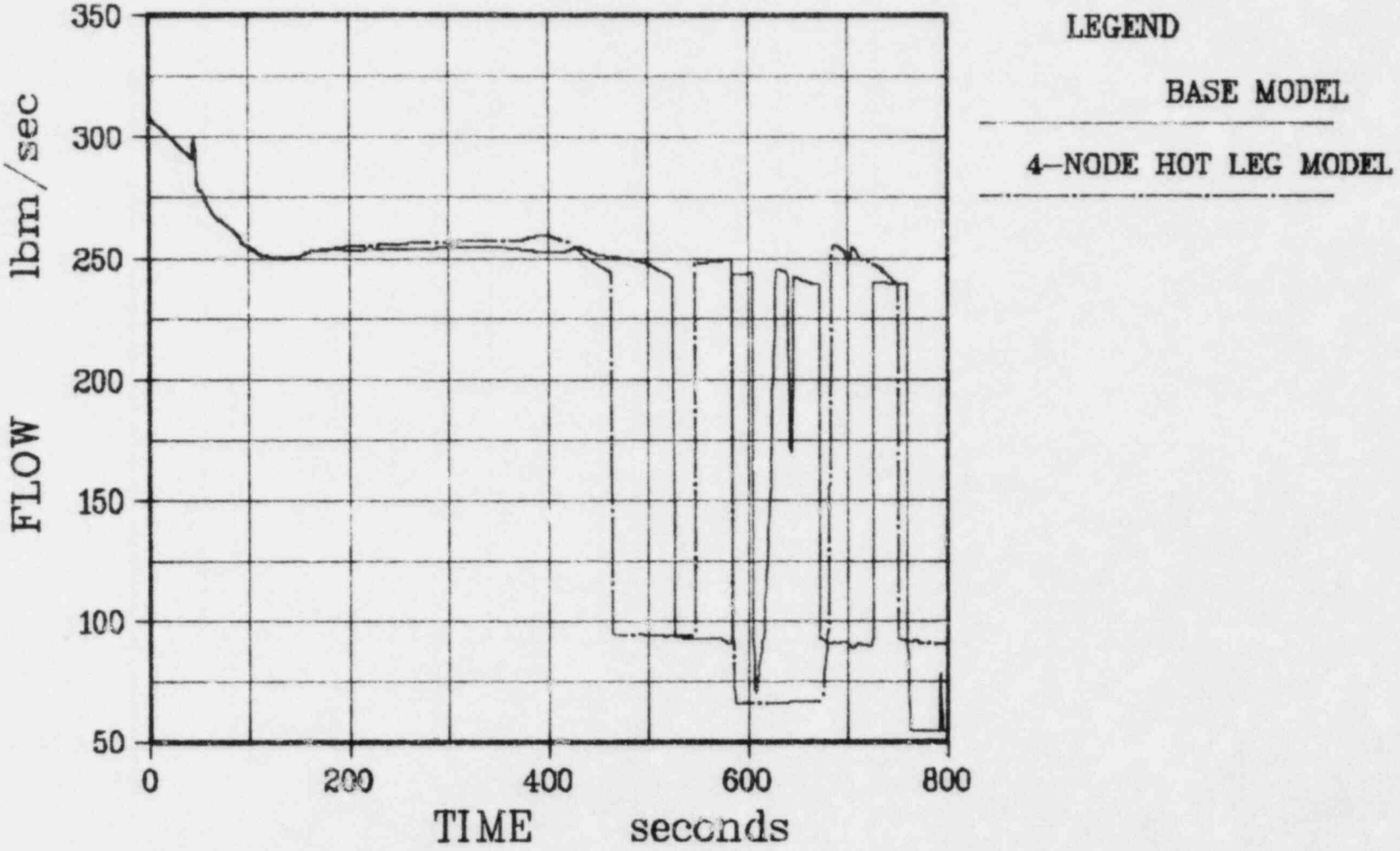

Figure E-28. Vent Valve Quality

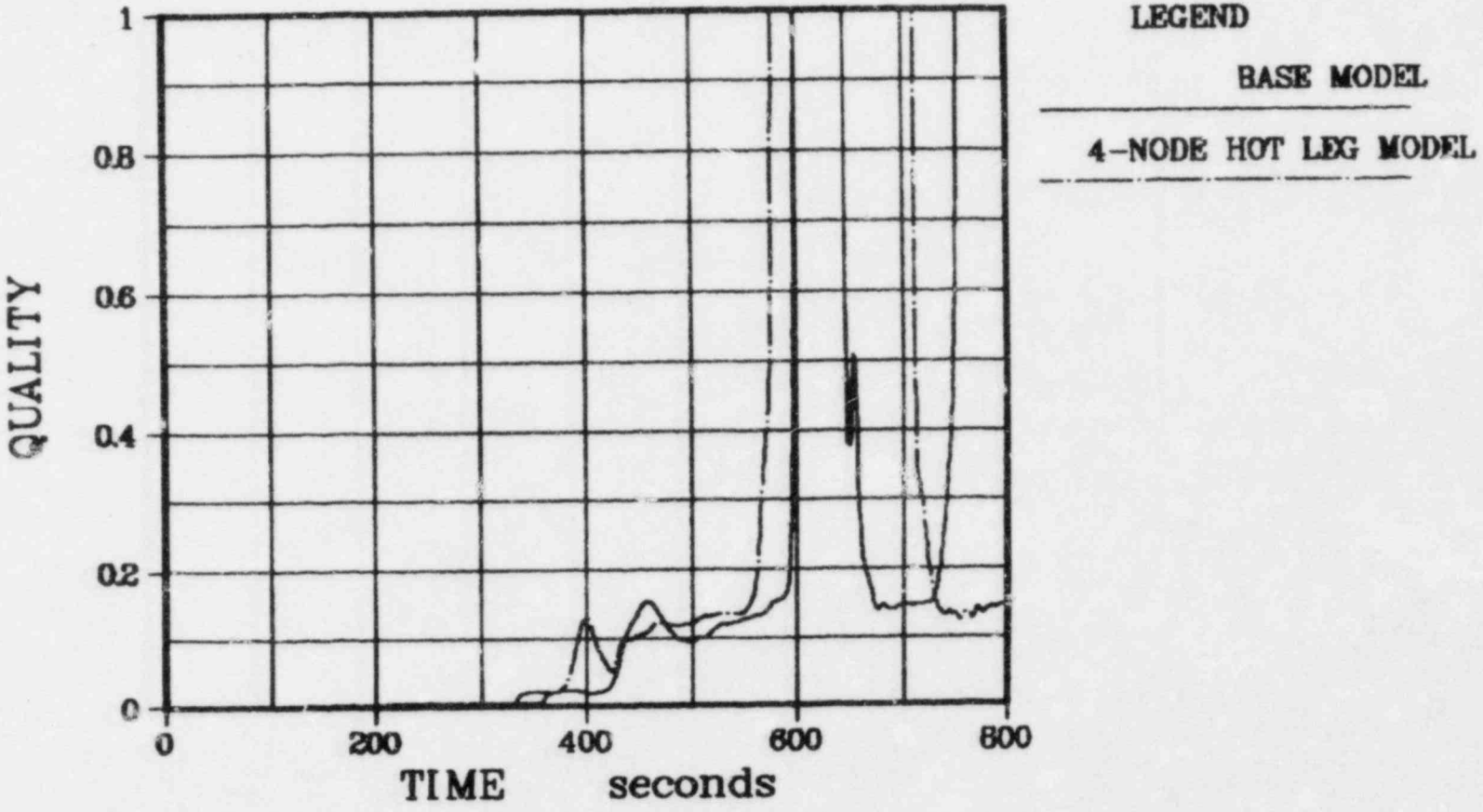

APPENDIX F

Noding Sensitivity Studies for 177-FA Raised-Loop Plants

1. Introduction

As a result of the Small-Break LOCA Methods Program developed to address the requirements of NUREG-0737, Section II.K.3.30, significant code modifications and revisions were made to the existing SBLOCA evaluation model. Included in these modifications were a nonequilibrium pressurizer, a two-phase pump, and new upgraded mechanistic steam generator models. Because of these significant modifications and revisions of the existing evaluation model, it was necessary to perform several noding sensitivity studies to develop the base noding scheme that demonstrated convergence with respect to spatial detail.

A generic noding sensitivity study was performed for the 177-FA lowered- and raised-loop plants to develop a converged steam generator model.[1] For this study, a break (0.01 ft^2 at pump discharge) that relied on the steam generator for RCS depressurization was analyzed. The spatial detail for modeling the steam generator was increased to the Code capacity to assess the impact of additional spatial detail on the transient response. Based on this study, the steam generator model that adequately accounted for all the phenomena was chosen as the appropriate model.

In order to ensure that the effects of local flashing were accounted for, a noding sensitivity study of the reactor vessel upper plenum and upper head was performed. This study was also performed on a generic basis for 177-FA lowered- and raised-loop plants, using the converged SG model. A converged model was developed for the upper head and upper plenum by evaluating the results of various degrees of spatial detail in these regions.

Finally, a noding study was conducted for the hot leg to ensure that its spatial detail is sufficient to model any interruption in natural circulation flow caused by formation of a steam pocket in the top of the inverted U-bend in the hot legs. Because of the significant differences in geometry and elevation of the hot leg in the raised-loop versus the lowered-loop plants, separate hot leg noding studies were performed for the two types of loop arrangements.

This appendix describes the noding sensitivity studies performed for the 177-FA raised-loop plant (Davis-Besse 1), to achieve the converged base model. The model description for this analysis is provided in section 3. The actual studies performed are discussed in section 4.

2. Summary

This appendix describes the noding sensitivity studies performed for the 177-FA raised-loop plants to develop the revised base model. It is demonstrated here that the revised base model adequately accounts for the phenomena during small-break transients. It is also concluded that the results predicted by this revised model for a 0.01-ft^2 break at the pump discharge are essentially the same as those calculated by the former evaluation model.

3. Model Description

The upgraded CRAFT2 code[2] was used to calculate the reactor coolant (RC) system hydrodynamics during a small-break transient. Comparisons are provided for this analysis with results obtained using the evaluation model described in the 1979 report on the 177-FA raised-loop plant small-break analysis.[3] The general philosophy used to generate the revised base model is the same as that utilized in the generic 177-FA lowered-loop plant small-break analysis reported in a letter from J. H. Taylor to S. A. Varga.[4] The actual geometry of the model reflects the raised-loop arrangement. The noding diagram of the former evaluation model for Davis-Besse 1 is shown in Figure F-1. The revisions and modifications made to the base model to obtain the revised base noding scheme for the 177-FA raised-loop plant (shown in Figure F-2) are described below. The bases for these revisions are provided in section 4.

1. The existing single-node pressurizer model was replaced by the new non-equilibrium model[2] developed during the Small-Break LOCA Methods Program.

2. The new two-phase pump model[2] was used instead of the existing model to adequately account for the degradation of pump head and hydrualic torque during two-phase operation.

3. The former simplistic steam generator model was replaced by a new mechanistic model.[2] The new steam generator model was developed in response to the NRC's concern regarding the ability of the existing computer code to "correctly predict the various modes of natural circulation and the interruption of natural circulation, if it occurs."[5]

The revised steam generator noding scheme comprises six axial levels and two radial regions for the primary side with six axial levels for the secondary side. The two radial regions represent 10 and 90% of the total number of tubes in the steam generator. This scheme models the auxiliary feedwater (AFW) spray more realistically.

The revised converged noding scheme of the CRAFT2 computer model uses 56 nodes to simulate the RC system, 14 nodes for the secondary system, and one node for the reactor building. These control volumes are connected by 78 flow paths. The revised base noding scheme shown in Figure F-2 was used for the hot leg noding study for the 177-FA raised-loop plants.

4. Noding Sensitivity Studies

As mentioned earlier, significant code modifications and revisions of the former evaluation model were made during the Small-Break LOCA Methods Program to address the requirements of NUREG-0737, Section II.K.3.30. Therefore, it was necessary to perform noding sensitivity studies to develop a base noding scheme that can adequately account for all the phenomena during small-break LOCA transients. Since the raised- and lowered-loop plants have essentially the same full-power levels and basically similar size and geometry of components, it is possible to perform the noding sensitivity studies on a generic basis, except for the hot leg. Consequently, the steam generator and upper head and upper plenum noding sensitivity studies were performed using the lowered-loop model. These studies are summarized briefly below.

Steam generator noding studies were performed by selecting a break (0.01 ft^2 at the pump discharge) that relies on steam generator heat removal for RC system depressurization. Four models with varying details in axial and radial regions of the steam generator model were used to evaluate the impact of additional spatial detail on the transient response. Based on this study, the steam generator model that adequately accounted for all the phenomena was chosen as the base model for the steam generator. This model consists of six axial and two radial regions for the primary side and six axial levels for the secondary side of the steam generator. The radial regions represent 10 and 90% of the total number of tubes in the steam generator. The 10% region is used to account for direct cooling affects of the AFW spray.

To ensure that the effects of local flashing were accounted for, noding sensitivity studies of the reactor vessel upper head and upper plenum were performed. These studies were performed only on lowered-loop plants since the reactor vessels are essentially identical for lowered- and raised-loop plants. These studies were conducted using the detailed steam generator model described above. Three models with varying spatial detail in the upper head and upper plenum regions were analyzed. By evaluating these results, it was demonstrated that the existing model is capable of predicting the small break transient response with no additional spatial detail. The detailed analyses and the actual computer runs of these studies are discussed in detail in reference 1.

4.1. 0.01-ft^2 Break at Pump Discharge With Former and Revised Models

Based on the studies above, the base noding scheme for the raised-loop plants was developed. This model is described in section 3, and the noding diagram is shown on Figure F-2. To permit comparison of the former and the revised models, the 0.01-ft^2 break at the pump discharge was used. The 0.01-ft^2 break case was run with the revised base model for 177-FA raised-loop plants. Key events during the transient with the former and revised models are compared in Table F-1.

The hot leg pressure transient for the former and the revised models are shown in Figure F-1. In both cases, the RC system depressurized rapidly to approximately 1400 psia. At this time, flashing in the hot legs and the upper plenum of the reactor vessel caused the system to repressurize due to a loss of natural circulation (see Figure F-5). Between 200 and 700 seconds into the transient, the RC system repressurized in both cases with some intermittent depressurization due to momentary re-establishment of natural circulation. Around 700 seconds, the system depressurized as natural circulation was re-established for a significant period of time. The depressurization in both cases stopped at approximately 800 seconds.

The basic transient rsponse predicted by the revised model is essentially the same as that predicted by the former model. In the early part of the transient, the revised model predicts slightly higher pressure. This is due to the shorter main feedwater coastdown in the revised model by approximately 20

seconds (see Table F-1) and to a new mechanistic steam generator model. The significant difference between the two models is after 700 seconds of the transient. In the former model, the system depressurizes to approximately 1100 psia. This is due to re-establishment of natural circulation in both loops for approximately 150 seconds with the intact loop sustaining circulation for approximately 600 seconds. On the other hand, the system only depressurizes to approximately 1400 psia with the revised model because this re-establishment of natural circulation lasts for only about 50 seconds. This difference between the two cases is primarily due to the pressurizer and steam generator models. In the former model, a single-node equilibrium pressurizer and a simplistic steam generator model are utilized. During the transient, the surge line goes through oscillations of insurges and outsurges. Because of these oscillations in the surge line with the exit elevation 3 feet above the bottom of the pressurizer, the net effect on the system is that the lower quality fluid enters into the pressurizer and the higher quality fluid comes back to the hot leg. As a result, the intact hot leg has a significantly larger quantity of bubbles. Consequently, the mixture level in the hot leg is above the natural circulation point, as shown in Figure F-5. Hence, natural circulation is sustained for the longer period of time. Continuous circulation brings more bubbles to the hot legs from the core, which in turn sustains the mixture height above the natural circulation points. This results in depressurizing the system to a much lower value.

In the revised model, a nonequilibrium pressurizer is used, along with a mechanistic steam generator model. The nonequilibrium pressurizer model produces considerably fewer oscillations of insurges and outsurges. In addition to this, the exit elevation of the pressurizer is 1 foot above the bottom of the pressurizer. As a result, there is no significant increase in the bubbles in the intact hot leg loop with the revised model. Hence, the mixture level stays below the natural circulation point (see Figure F-5) and consequently, the system does not depressurize to the value calculated by the former model (see Figure F-4).

Based on the discussion above, it can be concluded that the results calculated by the revised model are essentially the same up to the loss of natural circulation in both loops. The differences in the latter part of the transients are due to the upgraded CRAFT2 computer models, which are more realistic approximations than the ones used in the former model. The next step is to

perform the hot leg noding sensitivity study to ensure that the hot leg includes sufficient spatial detail to model the interruption in natural circulation.

4.2. Hot Leg Noding Studies

Because of the significant differences in the geometry and the elevations of the hot legs in the raised- versus lowered-loop plants, a separate hot leg noding study was performed specifically for the raised-loop plants. For this study, the revised base model described in section 4.1 was used. The break case analyzed was again the 0.01-ft^2 break at the pump discharge. The basic objective of this study was to demonstrate that the additional detail in the hot leg would not significantly alter the transient or the timing of the interruption and re-establishment of natural circulation. To achieve this goal, a detailed four-node hot leg model was developed. The control volumes in the hot legs were connected by dual flow paths to allow for the countercurrent flows. The Wilson bubble rise model was used for these additional nodes in the hot legs. The detailed hot leg model used in this study is shown in Figure F-3.

The 0.01-ft^2 break at pump discharge was rerun with the detailed hot leg model. Key events during the transient for the single-node and four-node hot legs are compared in Table F-2.

The hot leg pressure transient for the single-node and four-node hot leg models is shown in Figure F-4. In both cases, the RCS depressurized rapidly to approximately 1450 psia. From there on, the RCS essentially repressurizes in both cases. The repressurization is basically due to the interruption in natural circulation (see Figure F-5). The basic transient calculated by the four-node hot leg model is essentially the same as calculated by the single-node hot leg model. The slight differences between the two transients are explained below.

In the single-node hot leg model, the bubbles travel through the entire hot legs at the Wilson bubble rise model velocity. The bubbles escape near the top of the level. On the other hand, in the four-node hot leg model the bubbles are being carried by the flow paths in addition to the Wilson bubble rise velocity. This can be visualized by the sketch on the following page.

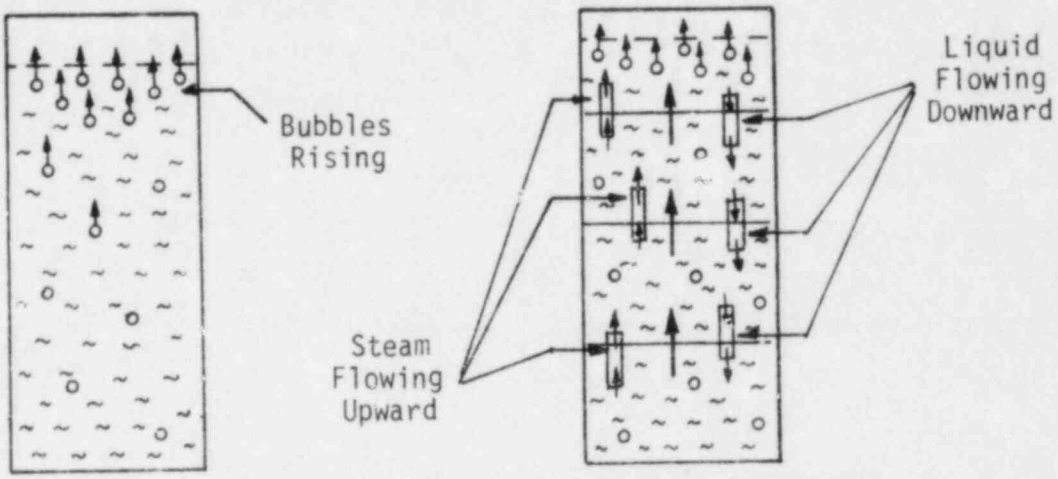

Single-Node Hot Leg Model

Four-Node Hot Leg Model With Dual Flow Paths

It should also be realized that the single-node hot leg model has a considerably larger volume than the top node in the four-node hot leg model. Hence, the mixture level in the four-node model will be more sensitive to the bubble mass than that of the single-node model.

During the initial RCS depressurization, the entire hot leg will be saturated at the same time in the single-node hot leg model, while only the top node will be saturated first in the detailed hot leg model. As a result, the mixture level in the four-node hot leg model will start dropping earlier and faster as the bubbles escape with none being transported to the top node. This process will continue until the lower nodes are saturated and the bubbles are carried to the top node. The use of dual flow paths in the four-node hot leg model will allow the bubbles to be transported to the top of the candy cane. Consequently, the mixture level in the detailed hot leg model is expected to drop slowly thereafter. Hence, the first interruption in natural circulation with the four-node model will occur later than in the single-node model. Once the interruption in natural circulation has occurred, the mixture level in the detailed hot leg model is expected to drop faster because the level is more sensitive in the detailed hot leg than in the single-node model. This is because the single-node hot leg model has a considerably larger volume than the top node in the four-node model. Hence, the mixture level in the detailed hot leg model will be more sensitive to the bubble mass than that in the single-node hot leg model.

The discussion above explains the difference between the two transients. The results calculated by the four-node model are not expected to make a significant impact in terms of the overall transient. The four-node hot leg model case was analyzed up to 600 seconds since, after this time the RCS is basically stagnant and the steam and liquid have been distributed accordingly. Since the basic transients are essentially similar up to this point and they are not expected to diverge during the latter part of the transient, the detailed hot leg model was not run further.

Based on this study, it was concluded that the single-node hot leg model adequately accounts for the interruption in natural circulation. Hence, there is no need to add more spatial detail in the hot legs. In addition to this, the results obtained bythe single-node hot leg model are expected to be slightly conservative. This is because the overall system response calculated by the single-node model is higher in pressure than the detailed hot leg model predictions. Consequently, the system with the single-node hot leg model will discharge more inventory through the break and there will be less HPI flow than for the detailed model. Therefore, the revised base model for 177-FA raised-loop plants will use a single-node hot leg model.

5. Conclusions

The noding sensitivity studies for the 177-FA raised-loop plants has been completed, and the results discussed in this report demonstrate that the revised noding scheme shown in Figure F-2 adequately accounts for all the phenomena during small break transients. It can also be concluded that the revised noding scheme essentially calculates the same results that were calculated by the former evaluation model for a 0.01-ft^2 break at the pump discharge. The slight difference between the two results is due to the upgraded models, which are more realistic approximations than those used in previous analyses.

6. References

1. Noding Sensitivity Studies for 177-FA Lowered-Loop Plants, Document No. 86-1137820-00, Babcock & Wilcox, October 1982.

2. J. J. Cudlin, et al., CRAFT2 - Fortran Program for Digital Simulation of a Multinode Reactor Plant During Loss of Coolant, BAW-10092, Rev. 3, Babcock & Wilcox, October 1982.

3. Evaluation of Transient Behavior and Small Reactor Coolant System Breaks in the 177-Fuel Assembly Plant, Babcock & Wilcox, May 7, 1979.

4. J. H. Taylor (B&W) to S. A. Varga (NRC), Letter, July 18, 1978.

5. "Generic Evaluation of Small Break Loss-of-Coolant Accident Behavior in Babcock & Wilcox-Designed 177-FA Operating Plants," NUREG-0565, January 1980.

Table F-1. Comparison of Key Events in Former and New Models

Sequence of events	Time, seconds	
	Former model	Revised model
Rupture (0.01 ft^2 at RC pump discharge)	0.0	0.0
Reactor trip, turbine trip	50	46.4
Pump coastdown occurs	52	51
Main feedwater coastdown ends	80	60
Auxiliary feedwater starts	200	86.4
HPI begins	150	225
Natural circulation lost	500	490
Maximum repressurization reached	700	680

Table F-2. Comparison of Key Events in Single-Node and Four-node Hot Leg Models

Sequence of events	Time, seconds	
	Single-node hot legs	Four-node hot legs
Rupture (0.01 ft^2 at RC pump discharge)	0.0	0.0
Reactor trip, turbine trip	46.4	46.3
Pump coastdown occurs	51	51.3
Main feedwater coastdown ends	60	60
Auxiliary feedwater starts	86.4	86.3
HPI begins	225	230
Natural circulation lost	490	510
Maximum repressurization reached	680	(a)

(a) The four-node hot leg model case was run only up to 600 seconds. Based on these results, this event is expected to be delayed by 50-100 seconds with the four-node hot leg model.

Figure F-1. CRAFT2 Noding Diagram, Old Base Model for Davis-Besse 1

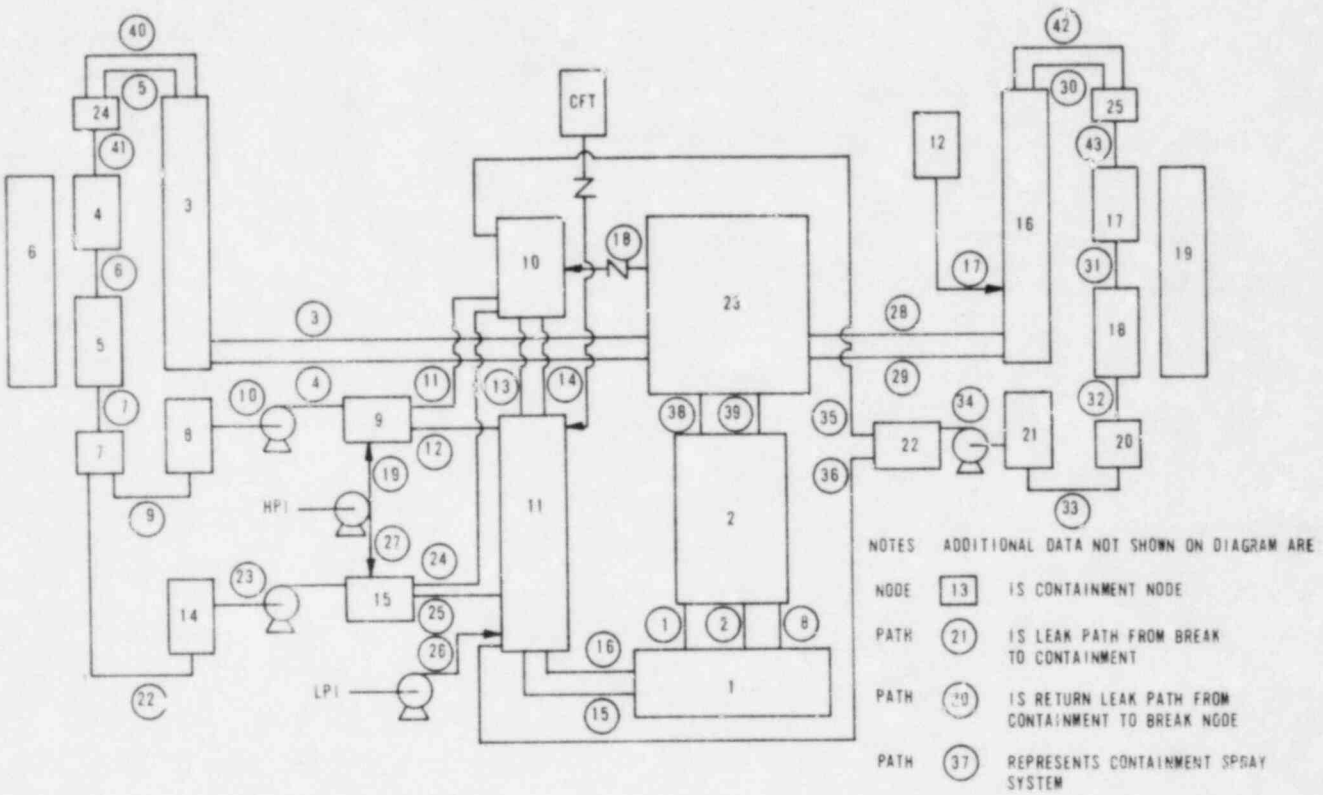

NODE NO	IDENTIFICATION
11	DOWNCOMER
1	LOWER PLENUM
2	CORE & UPPER PLENUM
3,16	HOT LEG PIPING
4,17	SG & UPPER HEAD
5,18	STEAM GENERATOR TUBES
6,19	SECONDARY SG
7,20	SG LOWER HEAD
8,14,21	COLD LEG PIPING
9,15,22	COLD LEG PIPING
10	UPPER DOWNCOMER
12	PRESSURIZER
13	CONTAINMENT
23	UPPER PLENUM
24,25	SG UPPER HEAD

PATH NO	IDENTIFICATION
1,2	CORE
3,4,28,29	HOT LEG PIPING
5,30,41,43	HOT LEG, UPPER
6,31	SG TUBES
7,32	SG LOWER HEAD
8	CORE BYPASS
9,22,33	COLD LEG PIPING
10,23,34	PUMPS
11,12,24,25,35,36	COLD LEG PIPING
15,16	DOWNCOMER
26	LPI
13,14	UPPER DOWNCOMER
17	PRESSURIZER
18	VENT VALVE
19,27	HPI
37	CONTAINMENT SPRAYS
38,39	CORE TO UPPER PLENUM
40,42	SG UPPER HEAD
20,21	LEAK & RETURN PATH

Figure F-2. CRAFT2 Noding Diagram, Revised Base Model for Davis-Besse 1

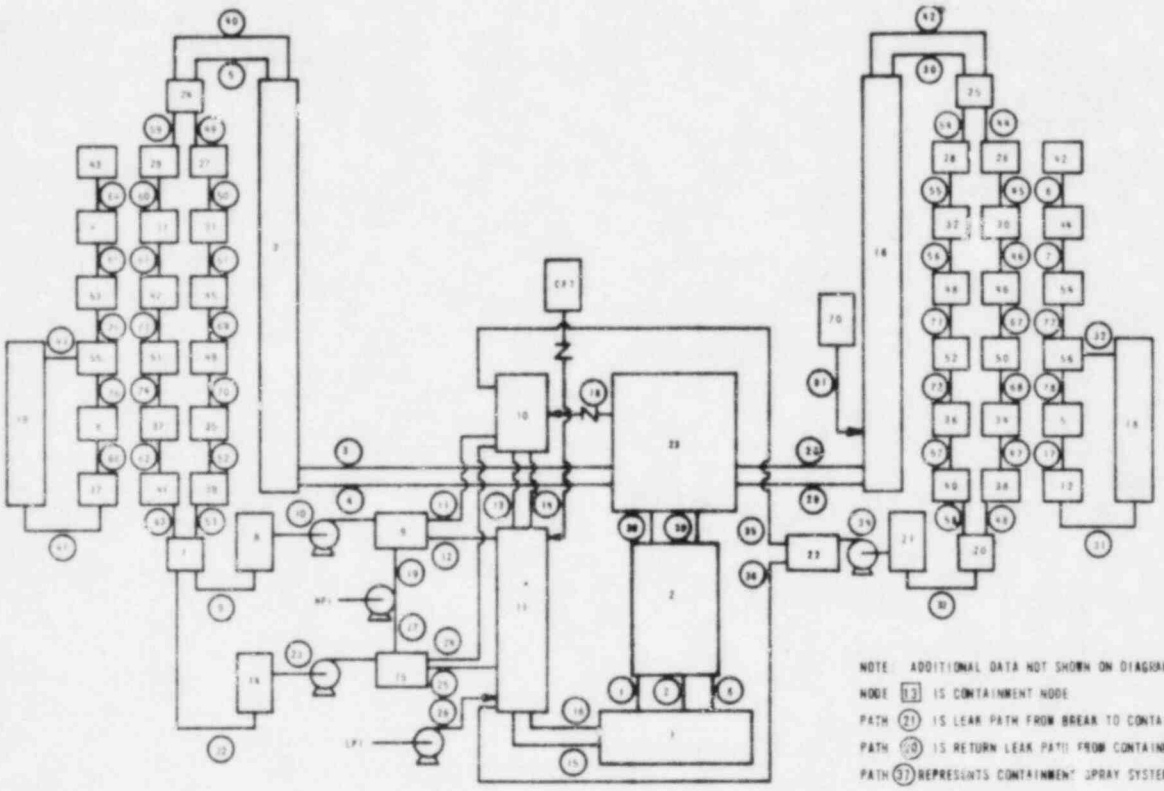

NOTE: ADDITIONAL DATA NOT SHOWN ON DIAGRAM ARE
NODE (13) IS CONTAINMENT NODE
PATH (21) IS LEAK PATH FROM BREAK TO CONTAINMENT
PATH (28) IS RETURN LEAK PATH FROM CONTAINMENT TO BREAK NODE
PATH (37) REPRESENTS CONTAINMENT SPRAY SYSTEM

NODE NO.	IDENTIFICATION
11	DOWNCOMER
1	LOWER PLENUM
2	CORE & UPPER PLENUM
3, 16	HOT LEG PIPING
7, 20	SG LOWER HEAD
8, 14, 21	COLD LEG PIPING
9, 15, 22	COLD LEG PIPING
10	UPPER DOWNCOMER
70	PRESSURIZER
12	CONTAINMENT
23	UPPER PLENUM
24, 25	SG UPPER HEAD
26 THRU 41	SG TUBES
45 THRU 62	SG TUBES
42, 43, 59, 58, 5, 12	SG-SECONDARY SIDE
63, 4, 57, 55, 6, 17	SG-SECONDARY SIDE
18, 19	SG-DOWNCOMER

PATH NO.	IDENTIFICATION
1, 3	CORE
2, 4, 30, 29	HOT LEG PIPING
5, 30, 40, 42	HOT LEG, UPPER
6	CORE BYPASS
9, 33, 35	COLD LEG PIPING
10, 28, 34	PUMPS
11, 13, 24, 25, 36, 38	COLD LEG PIPING
15, 16	DOWNCOMER
26	LPI
18, 19	UPPER DOWNCOMER
81	PRESSURIZER, SURGE LINE
18	VENT VALVE
15, 27	HPI
37	CONTAINMENT SPRAYS
39, 39	CORE TO UPPER PLENUM
44 THRU 63	SG TUBES
67 THRU 79	SG TUBES
8, 7, 77, 78, 17, 31	SG-SECONDARY SIDE
65, 66, 75, 76, 64, 61	SG-SECONDARY SIDE
80, 82	ASPIRATOR

Figure F-3. CRAFT2 Detailed Hot Leg Noding Diagram for Davis-Besse 1

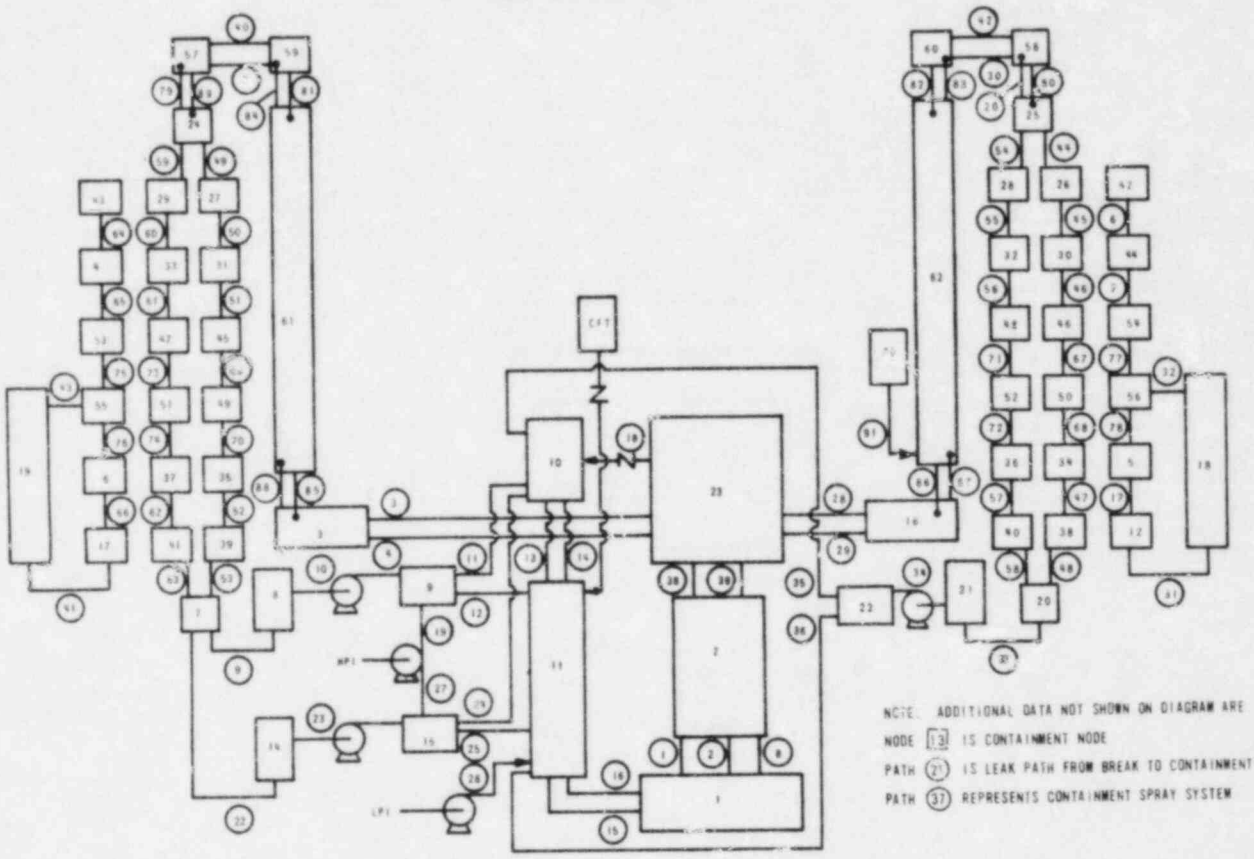

NODE NO.	IDENTIFICATION
11	DOWNCOMER
1	LOWER PLENUM
2	CORE & UPPER PLENUM
3, 16, 57 THRU 62	HOT LEG PIPING
7, 20	SG LOWER HEAD
8, 14, 21	COLD LEG PIPING
9, 15, 22	COLD LEG PIPING
10	UPPER DOWNCOMER
70	PRESSURIZER
13	CONTAINMENT
23	UPPER PLENUM
24, 25	SG UPPER HEAD
26 THRU 41	SG TUBES
45 THRU 52	SG TUBES
42, 44, 54, 56, 5, 12	SG-SECONDARY SIDE
43, 4, 53, 55, 6, 17	SG-SECONDARY SIDE
18, 19	SG-DOWNCOMER

PATH NO.	IDENTIFICATION
1, 2	CORE
3, 4, 20, 28, 29, 78 THRU 85	HOT LEG PIPING
5, 30, 40, 42	HOT LEG, UPPER
8	CORE BYPASS
9, 22, 33	COLD LEG PIPING
11, 12, 24, 25, 35, 36	COLD LEG PIPING
15, 16	DOWNCOMER
26	LPI
13, 14	UPPER DOWNCOMER
91	PRESSURIZER, SURGE LINE
18	VENT VALVE
19, 27	HPI
37	CONTAINMENT SPRAYS
38, 39	CORE TO UPPER PLENUM
21	LEAK PATH
44 THRU 63	SG TUBES
67 THRU 74	SG TUBES
[illegible]	SG-SECONDARY SIDE
[illegible]	SG-SECONDARY SIDE
[illegible]	ASPIRATOR

Figure F-4. Pressure Vs Time, Hot Leg Region

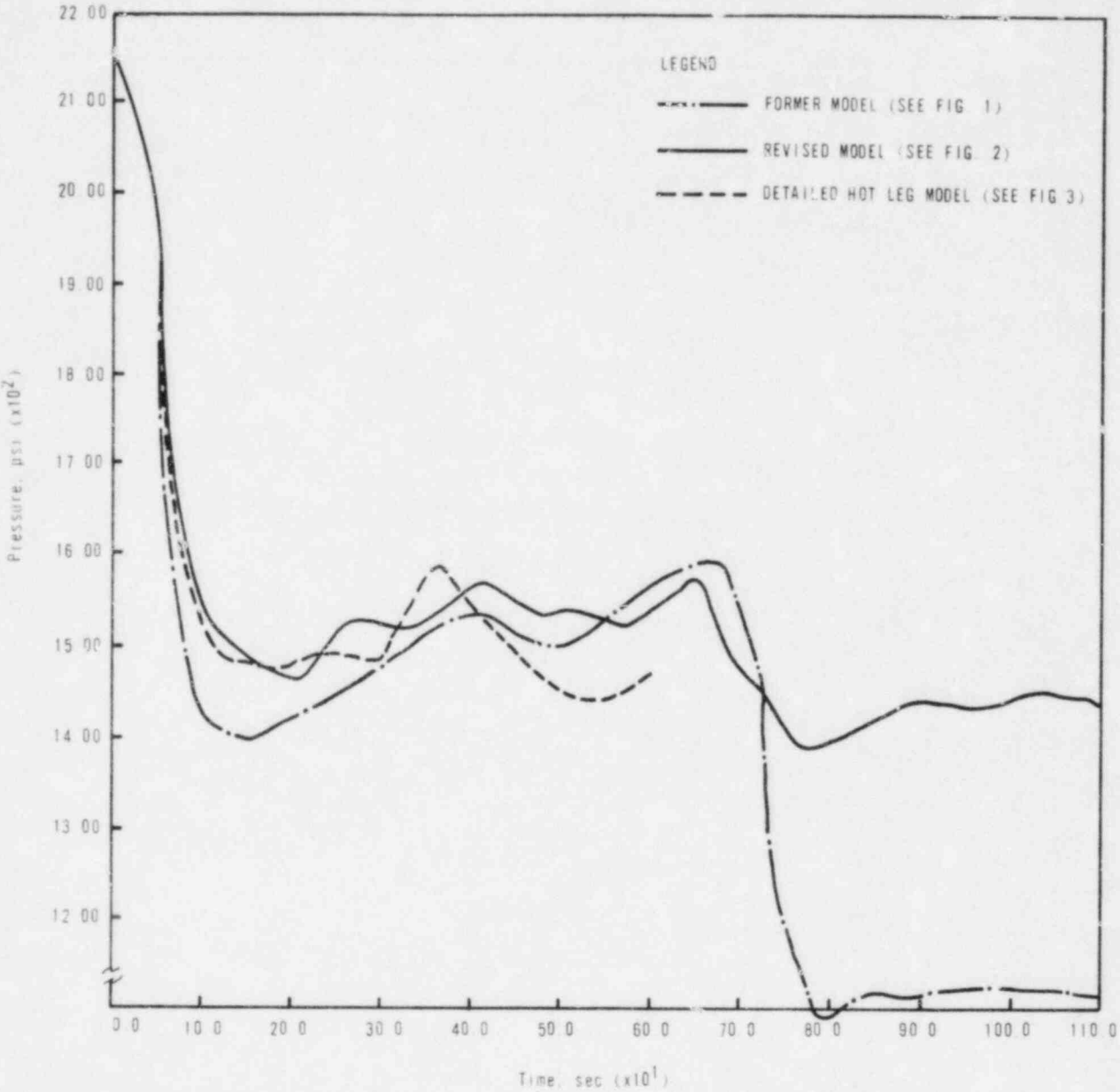

Figure F-5. Mixture Level Vs Time, Hot Leg Region

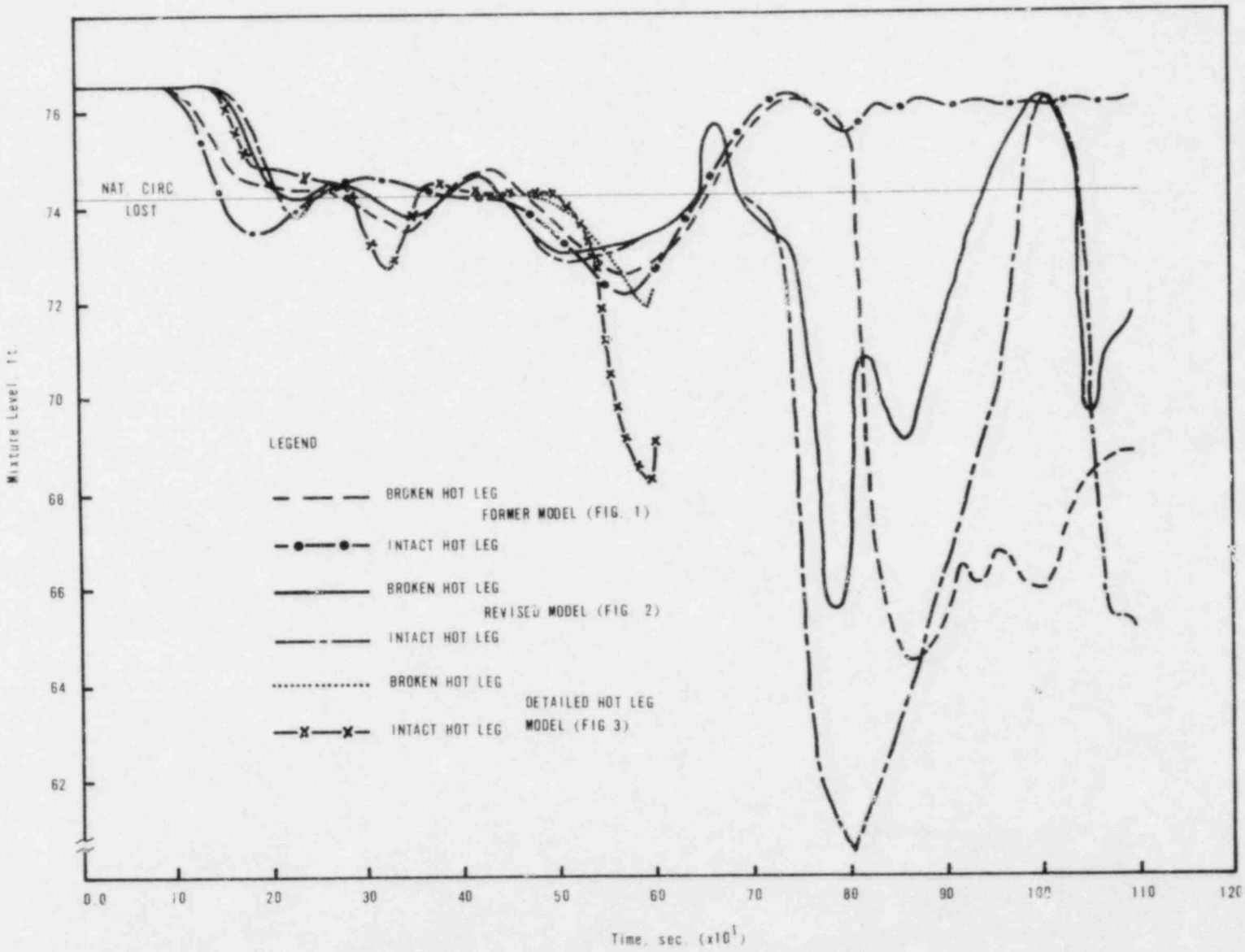

Figure F-6. Liquid Volume Vs Time, Hot Leg Region

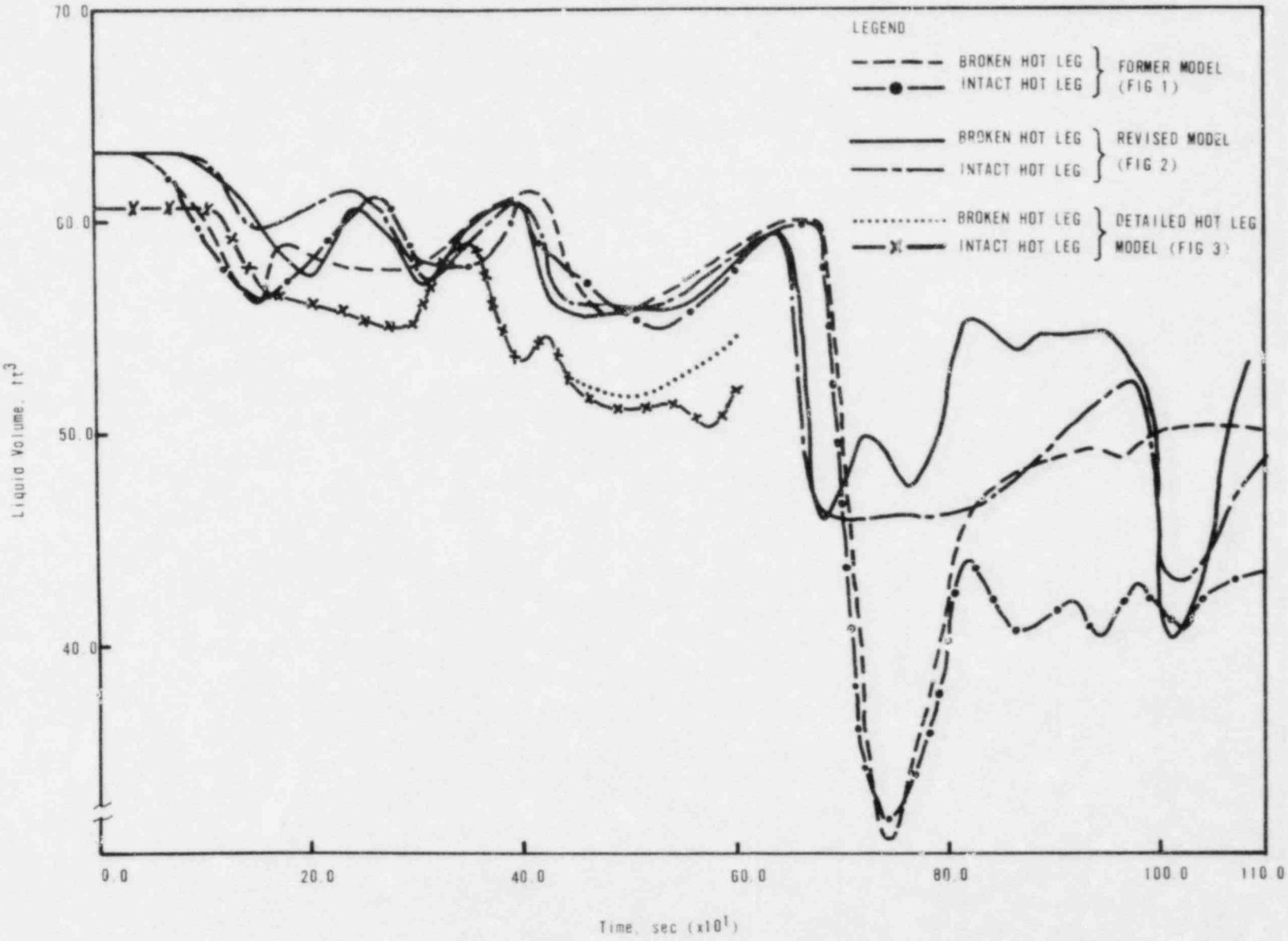

APPENDIX C

B&W's Natural Circulation Test Prediction of Semiscale Test S-NC-2

ABSTRACT

As part of the Small-Break LOCA Methods Program, the CRAFT2 computer code was benchmarked against the Semiscale natural circulation test S-NC-2 to demonstrate the analytical capability of the upgraded CRAFT2 code in tracking the various modes of natural circulation observed during a small-break LOCA. The results of the analysis show that the upgraded CRAFT2 code was capable of predicting the various modes of natural circulation reasonably well.

1. Introduction

In NUREG-0565, Section 4.1.1.1, paragraph 1, the NRC Staff questioned the ability of existing computer models to "correctly predict the various modes of natural circulation and the interruption of natural circulation, if it occurs." This concern has been addressed as part of the Small-Break LOCA Methods Program. This appendix describes the results of the post-test prediciton of the Semiscale Mod-2A natural circulation test S-NC-2. In response to the NRC questions, the CRAFT2 code was upgraded, particularly the steam generator model. This post-test analysis of test S-NC-2 was used to bechmark the capability of the upgraded CRAFT2 code to track the various modes of natural circulation observed during a small break.

Test S-NC-2 was a baseline natural circulation test involving one loop of the Mod-2A system. Three modes of natural circulation were observed during this experiment: single-phase, two-phase, and the reflux condenser mode. A characteristic of this test was that the predominant variable during the test was the liquid mass inventory of the system. As the liquid mass inventory was varied and the various modes of natural circulation were established, the loop-flow rates changed considerably.

Section 3 describes the Semiscale test facility Mod-2A and natural circulation test S-NC-2. The CRAFT2 modeling techniques and the assumptions used in predicting the test are discussed in section 4. The comparison of the test data to the CRAFT2 predictions is discussed in detail in section 5.

2. Summary and Conclusions

During this analysis only the single- and two-phase natural circulation modes were predicted. The reflux condenser mode of natural circulation was not considered here since the relevant phenomenon was not applicable to a B&W NSS. The single- and two-phase modes of natural circulation were obtained by draining discrete amounts of liquid out of the reactor vessel lower plenum, allowing sufficient time for steady-state conditions to be achieved between drains. The overall loop natural circulation mass flow rate varied considerably depending on system mass inventory. The variation in loop mass flow rate with inventory was a result of the transition from single-phase to two-phase natural circulation.

Initially, the draining simply lowered the vessel liquid level to the top of the hot leg with no significant voiding in the loop. Consequently, there was little change in loop mass flow rate. Further draining caused the loop mass flow rate to increase sharply and eventually peak. This increase in flow was caused by increased voiding in the upflow portion of the steam generator, which increased the overall loop density gradient. The peak in flow occurred as steam bubbles in the upflow side eventually spilled over into the downflow side of the steam generator, causing a reduction in overall loop density gradient between the upflow and downflow sides in the steam generator.

The results of the post-test predictions of test S-NC-2 show that the CRAFT2 computer code compared reasonably well with the data. CRAFT2 predicted the same general trends as were found in the test. For most of the data points, the results calculated by CRAFT2 were within the uncertainties of the measurements. This analysis demonstrates that the upgraded CRAFT2 code is capable of predicting the single- and two-phase natural circulation modes observed during the small-break LOCA transient.

3. Semiscale Test Facility

3.1. The Mod-2A System

The Semiscale Mod-2A system is part of the NRC's Water Reactor Safety Research effort. The Mod-2A system is a small-scale model of a four-loop, U-tube steam generating PWR plant (Figure G-1). All of the major components of a PWR are found in the system. The intact loop simulates the three intact loops of a PWR. The broken loop models the single loop in which the break occurs. The vessel contains a full-length, electrically heated core and a full-length upper head and upper plenum. The relative elevations of all the major components are maintained. To overcome the ambient heat loss problem, the Mod-2A system is equiped with external heaters to minimize net heating or cooling of the fluid.

3.2. S-NC-2 System Configuration and Test

Test S-NC-2 was a baseline natural circulation test involving one loop of the Mod-2A system as shown in Figure G-2. The broken loop and vessel upper head were removed and replaced with end caps. The intact loop pump was replaced with a spoolpiece scaled to the equivalent hydraulic resistance of a pump in

the locked-rotor condition. Initial conditions were established using the core as a heat source and the steam generator as a heat sink. Note that the pressurizer was valved into the system only until the initial steady-state conditions were achieved. When steady state was reached, the pressurizer was valved out of the system for the remainder of the transient. Throughout the test, the steam generator secondary pressure was maintained constant using a continuous feed-and-bleed process.

Test S-NC-2 measured three different nodes of natural circulation and the transition between them that resulted from varying the system mass inventory. The three modes of natural circulation observed were the single- and two-phase and the reflux mode. The predominant variable during the test was the liquid mass inventory of the system. As the liquid inventory was varied and the various modes of natural circulation were established, the loop flow rates changed considerably. To induce the various modes of natural circulation, discrete amounts of liquid were drained from the bottom of the RV lower plenum in 1% to 2% steps. After each step, the system was allowed enough time to stabilize before the next period of draining was started.

The test results can best be demonstrated using Figure G-12, "Mass Flow Rate Vs Percent Mass Inventory." The results of the test show that for liquid mass inventories down to roughly 94%, the system performance was similar to that for the single-phase values. Initial draining simply lowered the RV liquid level to the top of the hot leg with no significant voiding in the loop. Further draining caused the loop mass flow rate to increase sharply and eventually peak for inventories between 86 and 91%. This increase in flow rate was caused by increased voiding in the upflow portion of the steam generator, which resulted in a higher overall loop density gradient. The peak in the flow rate occurred as steam bubbles in the upflow side eventually spilled over into the downflow side of the steam generator, causing a reduction in overall loop density gradient. Decreasing the system inventory further resulted in a continuous two-phase flow with decreasing mass flow rate.

4. The CRAFT2 Semiscale Model

4.1. CRAFT2 Code, Version 26.0

The CRAFT2 program was developed to study the transient behavior of a nuclear steam system undergoing a loss-of-coolant accident (LOCA).[6] The program

solves the mass and energy conservation equations, the continuity equation, and the equation of state for water.

The CRAFT2 program permits the user to select the nodal representation that produces the best finite differencing of the fluid system to be analyzed. The program then solves the conservation equations for each node and the momentum equation for each flow path between nodes. CRAFT2 utilizes explicit solution techniques to analyze the transients. The nuclear steam system is simulated by a node and flow path representation. Components with different thermal-hydraulic characteristics must be simulated as different nodes.

CRAFT2 contains flexible models of all major nuclear steam system components. Various options as well as user input parameters enable the program to model the reactor core, RC pumps, steam generators, and connecting piping in any configuration and operation mode desired. The diversity of the models also allows the program to accurately model any thermal-hydraulic system containing similar components.

Version 26.0 of the CRAFT2 code was used because it contains all of the small-break LOCA upgrades and their modifications addressed in NUREG-0565. Included in this version are a non-equilibrium pressurizer model, an upgraded two-phase pump model, and a new upgraded steam generator model. During this analysis only the upgraded steam generator model and the homogeneous drift-flux model were used. For more information on the upgraded steam generator mode, see reference 6.

4.2. Assumption Made During the Analysis

The following major assumptions were used during this analysis:

1. The CRAFT2 model included 37 control volumes interconnected by 41 flow paths.
2. The flow regime-dependent (LAHEY and OHKAWA), homogeneous drift-flux model was used in the core and downcomer and the steam generator upflow and downflow sides. Dual flow paths were used in the hot leg to model any countercurrent flow. Single flow paths were used in the pump and cold leg piping.

3. The lower plenum was divided into two nodes, the bottom of which was representative of a stagnant pool or "dead node zone." Nodal conditions for the upper half of the lower plenum were set by the EG&G preliminary data: a pressure of approximately 1500 psia and a temperature of roughly 522F.

4. The secondary steam generator pressure was maintained at a constant pressure of 831 psia. This was different from the secondary pressure used in the test. For an explanation of this difference, see section 4.3.2 of this appendix.

5. Core power was maintained at a constant 60 kW throughout the transient.

6. The pressurizer was valved out of the system when equilibrium was reached and before draining commenced.

7. System fluid was drained from the bottom half of the vessel lower plenum using a leak path.

8. Natural circulation flow rates were measured across the pump and in the downcomer regions.

9. The system was assumed to be adiabatic throughout the transient.

4.3. Node and Flow Path Description

The CRAFT2 noding scheme used during this analysis is shown in Figure G-3. Table G-1 gives the nodal description of the CRAFT2 model. The CRAFT2 model consists of 37 nodes, or control volumes, and 41 flow paths. In all of the primary coolant flow paths, except the hot and cold legs, the drift flux slip model was used to allow for phase separation. Dual flow paths were used in the hot leg to allow for countercurrent flow. Single paths were used in the cold leg. The lower plenum was divided into two nodes, the lower of which represents a "dead zone" or stagnant pool.

4.3.1. Core Model

The core was represented by three nodes. The peaking factors were based on the core axial power profile for the Mod-2A core.[5] The maximum power peaking factor was 1.55. The maximum heat generation rate was 11.23 kW/ft. The core heat generation was maintained at a constant 60 kW of power throughout the analysis.

4.3.2. Steam Generator Model

The steam generator model used in this analysis was the new, upgraded steam generator model that will be used in the small-break version of the CRAFT2 code. The primary side of the steam generator was characterized by twelve nodes. The secondary side was represented by eight axial nodes and a downcomer region.

For this analysis, the steam generator level was held at an elevation corresponding to the top of the U-tubes. This was done by keeping the feedwater flow constant at the steady-state value and holding the secondary at a constant pressure.

The secondary pressure was held constant at approximately 830 psia. This was almost 40 psia lower than in the test. The difference in secondary pressures between the test and the post-test prediction was due to the assumptions regarding the primary side initial conditions. A pressure of 1500 psia and a temperature of 522.8F was assumed for the vessel lower plenum. These thermodynamic properties were taken from the preliminary data package for semiscale natural circulation test S-NC-2. The properties of all the other primary control volumes were based on this assumption. Assuming that there was no heat loss through the cold leg piping, the temperature at the steam generator exit should also be 522.8F. For an overly designed steam generator (as was the case in this test), the secondary temperature should be the same as the primary temperature at the steam generator exit, i.e., 522.8F. Since the secondary side in a U-tube steam generator was at saturated conditions, the corresponding pressure for a saturation temperature of 522.8F was input in the analysis. This value was approximately 830 psia and was almost 40 psia lower than in the test. This lower secondary pressure in the analysis was expected to predict a lower primary system pressure.

4.3.3. Pressurizer Model

The pressurizer was only used for the first few seconds of the analysis. It was used to allow the system to reach steady state. Once reached, the pressurizer was valved out of the system for the remaining transient.

4.3.4. Leak Model

To simulate the periods of draining, a leak path with a controllable discharge coefficient was modeled at the bottom of the lower plenum. Two computer runs were necessary to obtain data for a point. The first run was to drain the system, and the other was to stop the draining process and allow the system to stabilize. Typically, the draining process lasted for one second while stabilization took approximately 200 seconds.

5. Discussion of the Results

During the analysis, both single- and two-phase modes of natural circulation were predicted. No prediction of the reflux condenser mode of the natrual circulation was made since this method of natural circulation cooling is not applicable to B&W's once-through steam generators (OTSGs).

This section presents the results of the comparison of the natural circulation test data and the upgraded CRAFT2 predictions. The major variable during this analysis was the amount of liquid mass inventory in the primary system. All points of comparison between the test data and the post-test predictions were made with reference to this variable.

5.1. Test Measurement Uncertainties

The following measurement uncertainties existed during the test[11]:

1. Mass flow rates ± 0.11 lbm/s
2. Absolute system pressure ± 30 psia
3. System liquid mass inventory ± 5%

Most notable was the uncertainty in the measurement of the liquid mass inventory. According to Mr. G. G. Loomis of EG&G[11], a leak was discovered during the test S-NC-2. Leakage was calculated after the S-NC-2 results and it was estimated that the system liquid mass inventories were within + 5% during the test S-NC-2.

In order to better understand the uncertainties of the system mass inventory during the test, a quick comparison of the various tests (S-NC-2, S-NC-3, and S-NC-10) was performed. All of these tests were conducted at essentially the

the same power level and with a constant secondary pressure of approximately 870 psia. Figures G-4 through G-6 show the comparison between these tests. Since all the tests were at essentially the same initial conditions, they all should show the hot leg becoming saturated at basically the same system inventory. As can be seen from Figures G-4 through G-6, the hot leg became saturated at 92% system inventory for test S-NC-2, while tests S-NC-3 and S-NC-10 show that the hot leg reached saturation at 97% system inventory. Based on this, it appears that the S-NC-2 system mass inventory may have been higher than what was estimated during the test. This expectation was further enhanced by the fact that tests S-NC-3 and S-NC-10 were conducted after S-NC-2, and EG&G had a better understanding for making estimates of the leakage in the system. The RELAP5 pretest prediction of S-NC-2 also indicates that the system mass inventory may have been higher than that estimated during the test.

Based on the comparison and discussion above, it was concluded that the system mass inventory was more likely to be higher than what was calculated during the test. Hence, an upper error band of the liquid mass inventory due to measurement uncertainties was included on Figures G-7 through G-12.

5.2. Primary System Pressure Response

Figure G-7 compares the calculated primary system pressure with the test data. Once the pressurizer was valved out and draining commenced, the system pressure dropped rapidly to the hot leg fluid saturation pressure. The system pressure then decreased continuously as the coolant was drained from the system. The secondary pressure was maintained at a constant level of 830 psia throughout the test.

It is obvious from Figure G-7 that CRAFT2 is capable of predicting the trend of depressurization of the system. As explained in section 4.3.2, the 40-psia-lower secondary pressure assumption in the CRAFT2 analysis was expected to predict a lower system pressure. In addition, the accuracy of the measured absolute pressures was within +30 psia. By taking these facts into consideration, it was concluded that the system pressure response predicted by the upgraded CRAFT2 comptuer code was within the uncertainties of the measurements.

5.3. Temperature Response

The cold leg and hot leg temperatures calculated by CRAFT2 are shown in Figures G-8 and G-9. These temperatures were a function of the system pressure. Both hot and cold leg temperatures predicted by the code showed the same trends as observed in the test. The absolute temperature values were slightly lower because the system pressure was underpredicted (section 5.2).

The differential temperatures (ΔT) across the core and steam generator are shown on Figures G-10 and G-11. It is obvious from these figures that the ΔTs calculated by the code for most data points are within the error band.

5.4. System Mass Flow Rate

The system mass flow rate was compared to the amount of liquid inventory in Figure G-12. Single-phase natural circulation exists at 100% inventory. Two-phase natural circulation occupies the wide spectrum from practically full down to about 70%.

For liquid inventories above about 96 to 97%, the only significant voiding occurs in the upper head until the liquid level drops to the top of the hot leg. The overall density gradient changed only a little; thus, system natural circulation flows were not significantly affected.

The peak two-phase flow point occurred between 88 to 93% inventory. During this portion of the transient, saturated steam was being carried into the hot leg to just below the bend in the U-tubes. As the hot leg density decreased, the loop flow increased. Further draining of inventory resulted in lower loop flow because steam was carried over the bend and into the downside of the steam generator, decreasing the gravity imbalance.

As can be seen from Figure G-12, CRAFT2 predicted loop flow trends reasonably well. The comparison of calculated and measured flow rates was best at the higher system mass inventories. CRAFT2 did slightly overpredict the two-phase natural circulation flows.

This overprediction of the natural circulation flow rate was attributed to the rate at which phase-separation occurs in the vessel. Previous analyses have shown that the slip model available for use with the CRAFT2 code underestimates the rate at which phase-separation occurs at low system flow.[8] A faster phase-separation model would decrease the void fraction in the core and hot

leg. A lower void fraction in the hot leg and core regions would lower the density gradient, and thus the predicted system flow would be lower.

In general, calculated trends from the upgraded CRAFT2 calculations compared well with the data. There were slight differences between the calculated and measured results, which were due to the modeling assumptions. Most of the data points predicted were within the measurement uncertainties.

6. References

1. P. L. Thornhill, Post Test Prediction for Semiscale Test S-07-10D, B&W Document No. 86-1125888-01, June 1981.
2. J. H. Taylor (B&W) to R. P. Denise (NRC), "Analysis Prediction for Test S-07-10B," October 9, 1979.
3. System Design Description for the MOD-3 Semiscale System, Rev. B, EG&G Idaho, December 1980.
4. G. G. Loomis, et al., Quick Loop Report for Semiscale Mod-2A Test S-NC-2, EGG-SEMI-5507, EG&G Idaho, July 1981.
5. M. T. Leonard, RELAP5 Standard Model Description for the Semiscale Mod-2A System, EGG-SEMI-5692, EG&G Idaho, December 1981.
6. R. A. Hendrick, et al., CRAFT2 - Fortran Program for Digital Simulation of a Multinode Reactor Plant During Loss of Coolant, BAW-10092, Rev. 3, Babcock & Wilcox, November 1982.
7. G. G. Loomis, et al., Final Report for the Semiscale Mod-2A Test S-NC-2, EG&G Idaho.
8. J. R. Paljug, et al., TwoPhase Flow Model Evaluation, B&W Document No. 86-1134305-00, September 1982.
9. G. G. Loomis and K. Soda, Quick Look Report for Semiscale Mod-2A Test S-NC-3, EGG-SEMI-5522, EG&G Idaho, August 1981.
10. P. North to R. E. Tiller, Letter, "Transmittal of Selected Results From Semiscale Mod-2A Test S-NC-10," (PN-130-81), October 1981.
11. G. G. Loomis (EG&G Idaho) and N. K. Savani (B&W), telephone conservation, June 30, 1982.

Table G-1. Nodal Description

Node	Description	Node	Description
1	Downcomer annulus	20	SG front half of primary
2	Downcomer	21	SG front half of primary
3	Lower plenum	22	SG back half of primary
4	Core	23	SG back half of primary
5	Core	24	Containment
6	Core	25	SG secondary
7	Upper plenum	26	SG secondary
8	Hot leg	27	SG secondary
9	Pressurizer	28	SG secondary
10	SG inlet	29	SG secondary above SG pri.
11	SG front half of primary	30	SG secondary cont. flow sep'r
12	SG front half of primary	31	Lower plenum (dead zone)
13	SG back half of primary	32	SG front half of primary
14	SG back half of primary	33	SG front half of primary
15	SG outlet	34	SG back half of primary
16	SG secondary, downcomer	35	SG back half of primary
17	Cold leg	36	SG secondary
18	Pump suction	37	SG secondary
19	Pump discharge		

Figure G-1. Semiscale Mod-2A System Isometric
(Cold Leg Break Configuration)

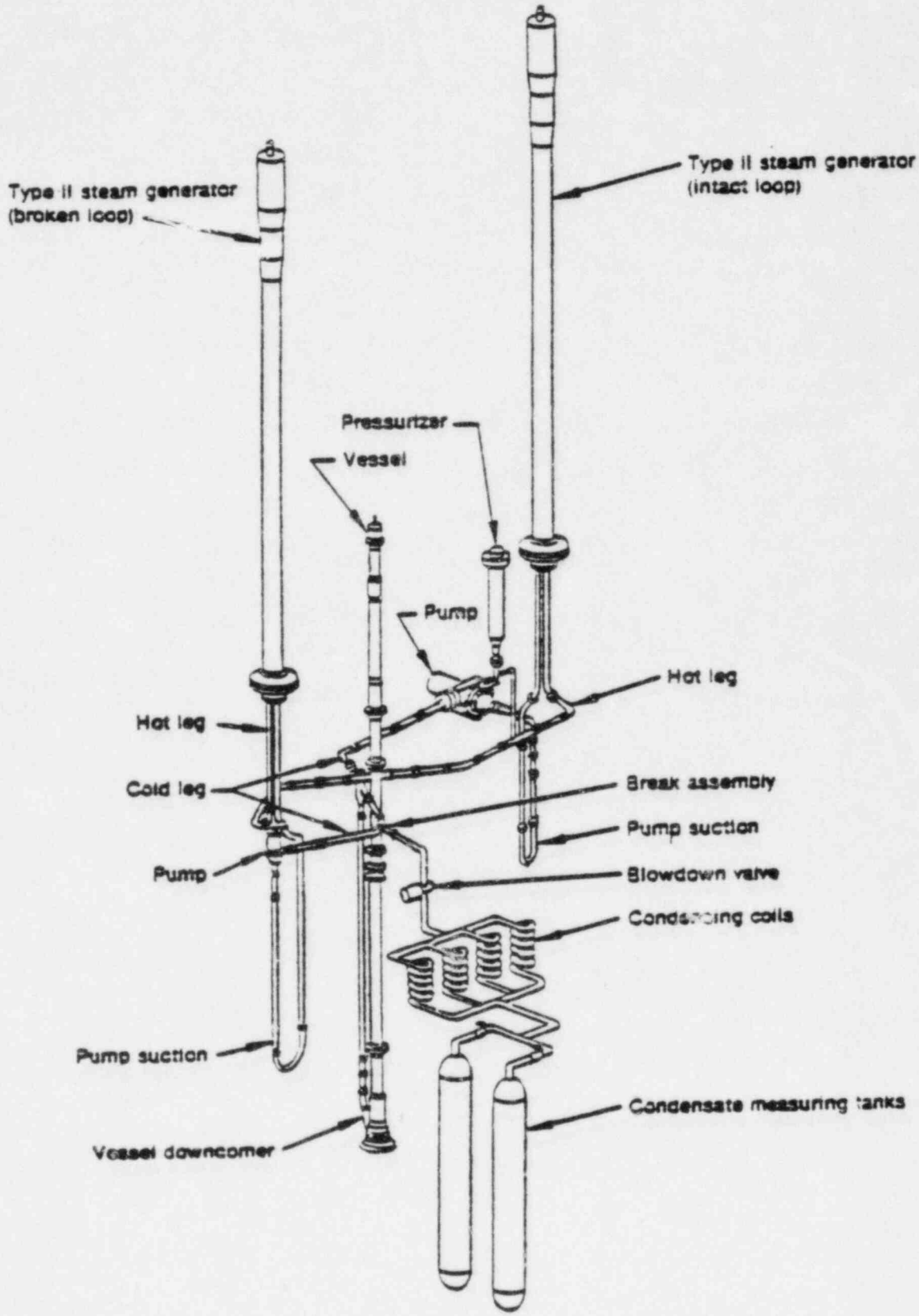

Figure G-2. Schematic of the System Configuration for Test S-NC-2

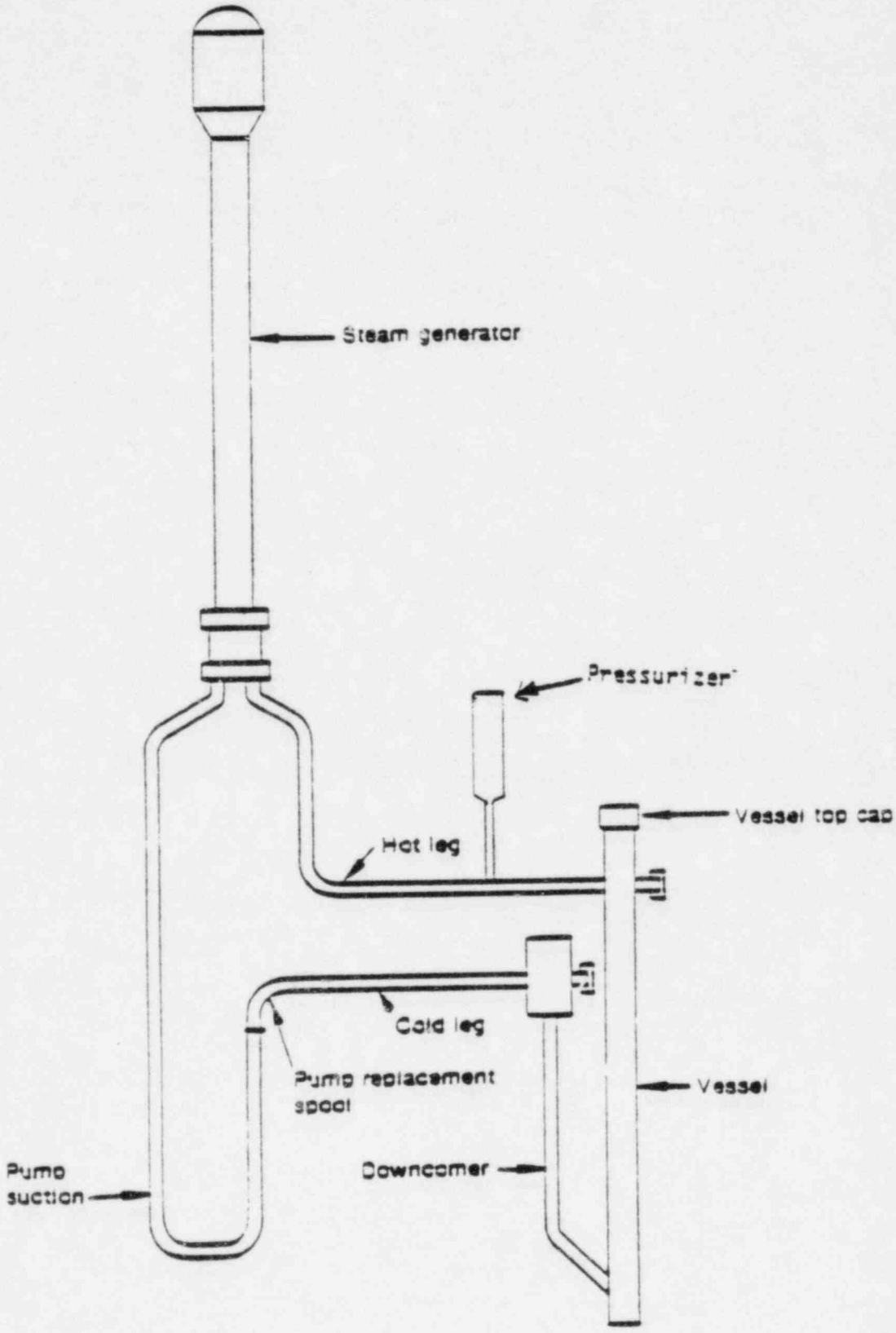

Figure G-3. CRAFT2 Noding Diagram

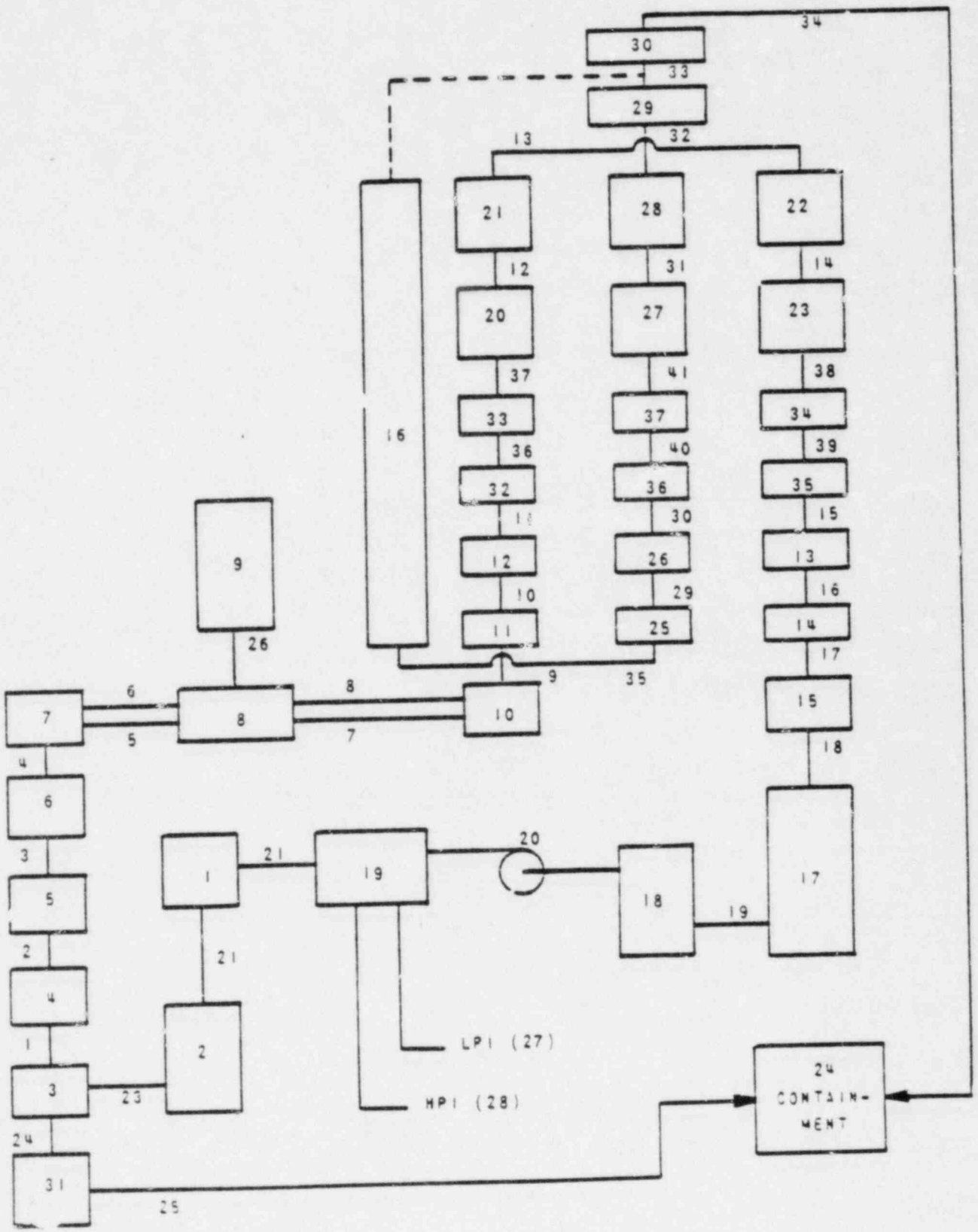

Figure G-4. System Pressure

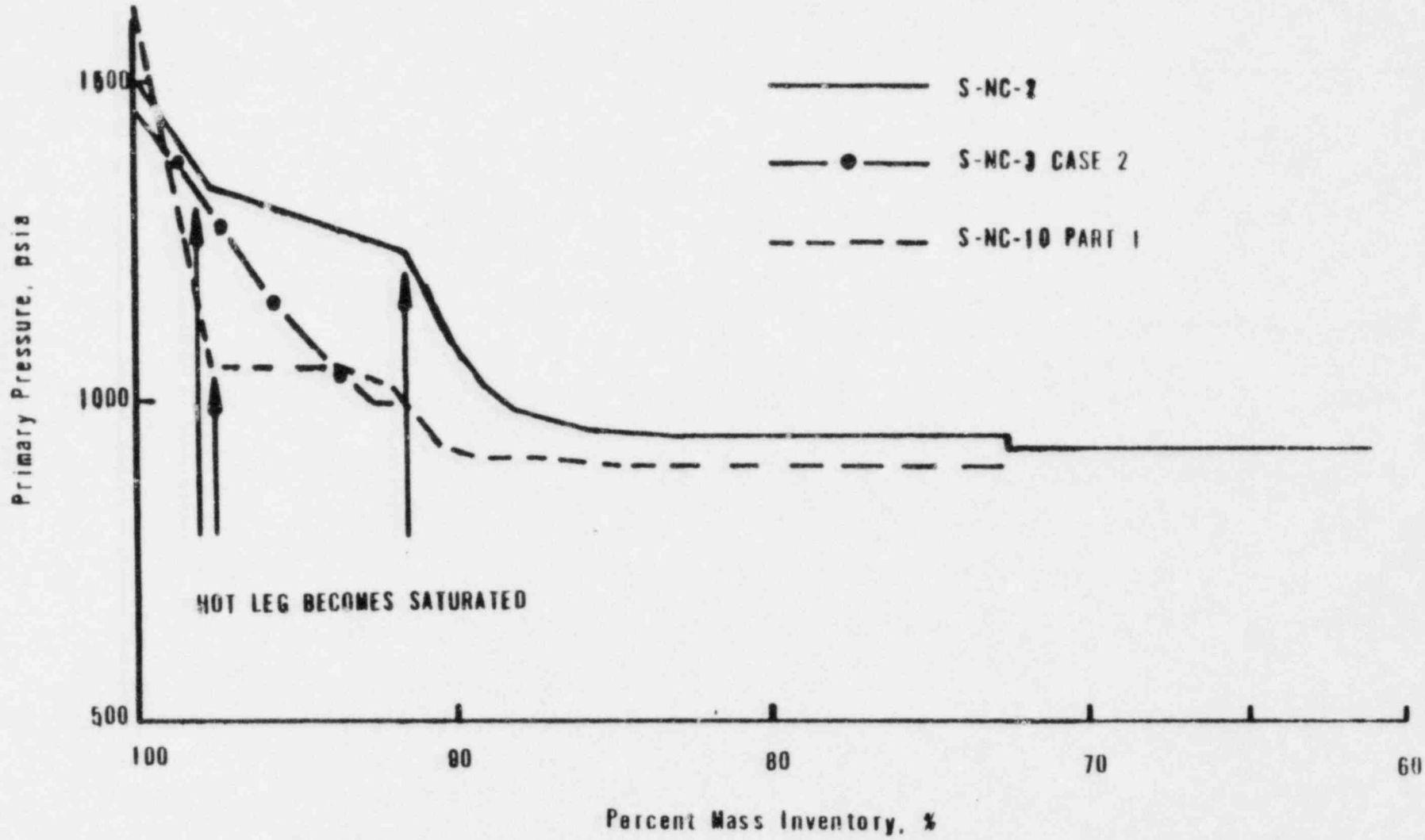

Figure G-5. Hot Leg Fluid Temperature

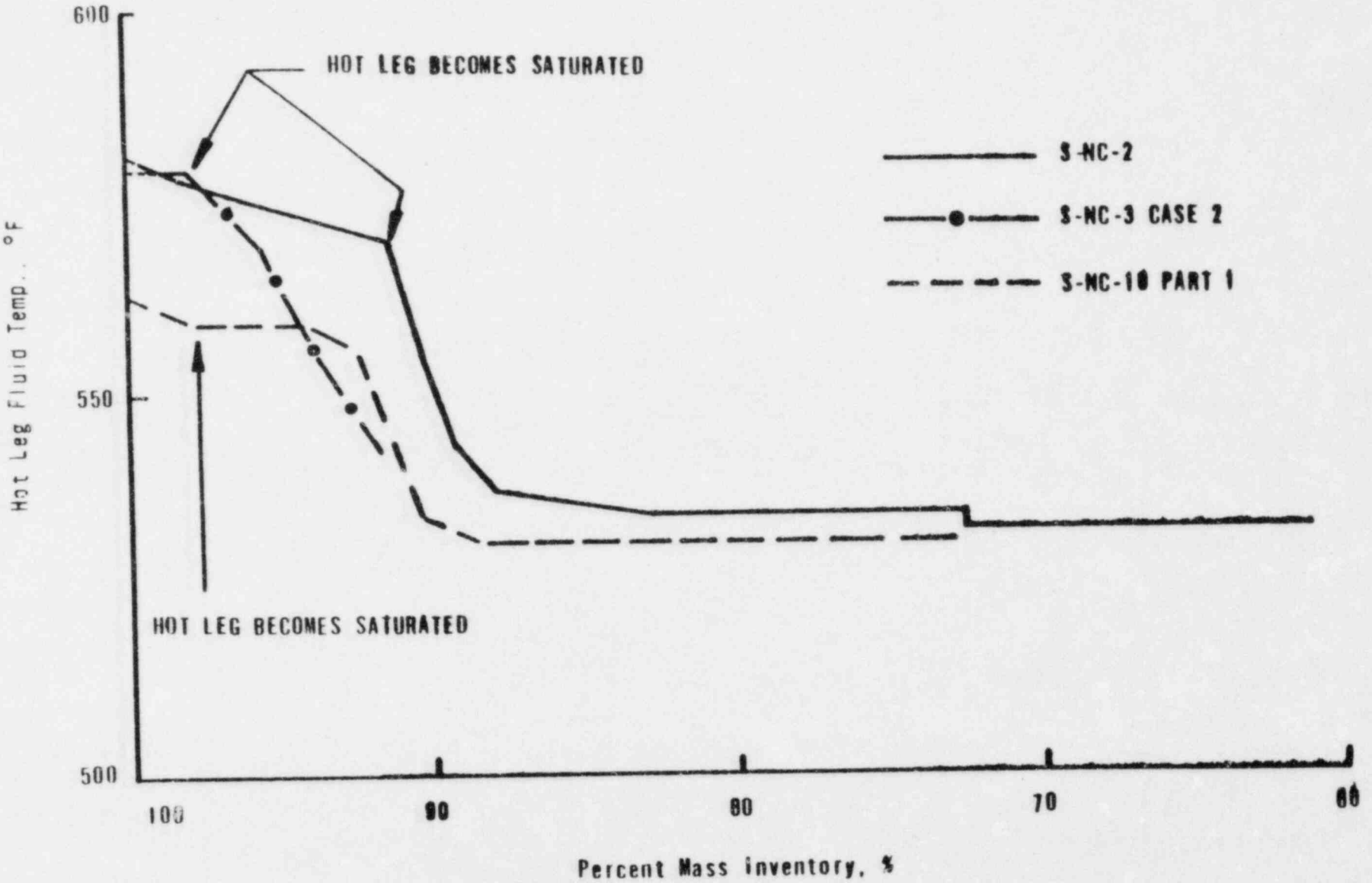

Figure G-6. Mass Flow Rate

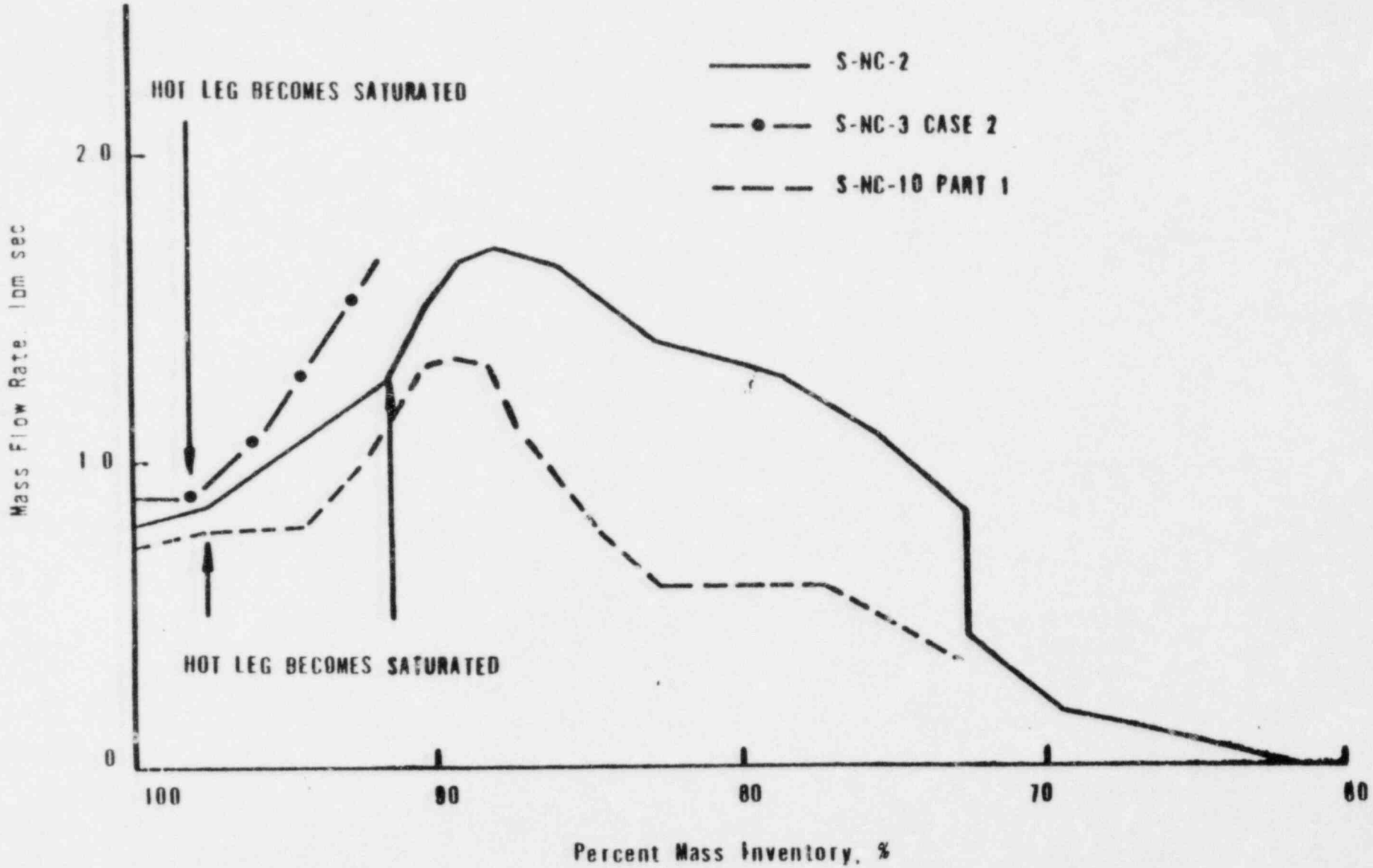

Figure G-7. Primary System Pressure

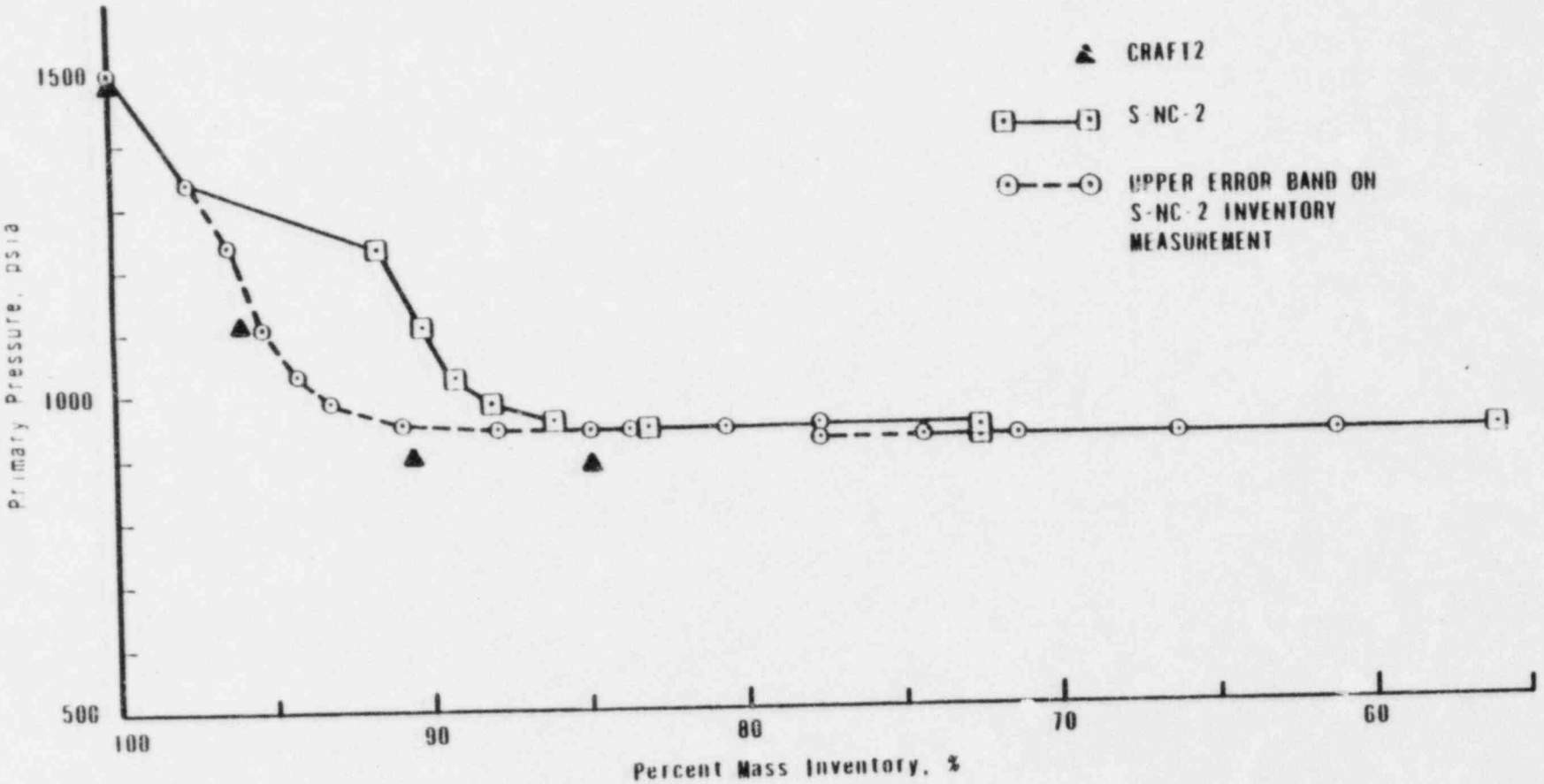

Figure G-8. Cold Leg Fluid Temperature

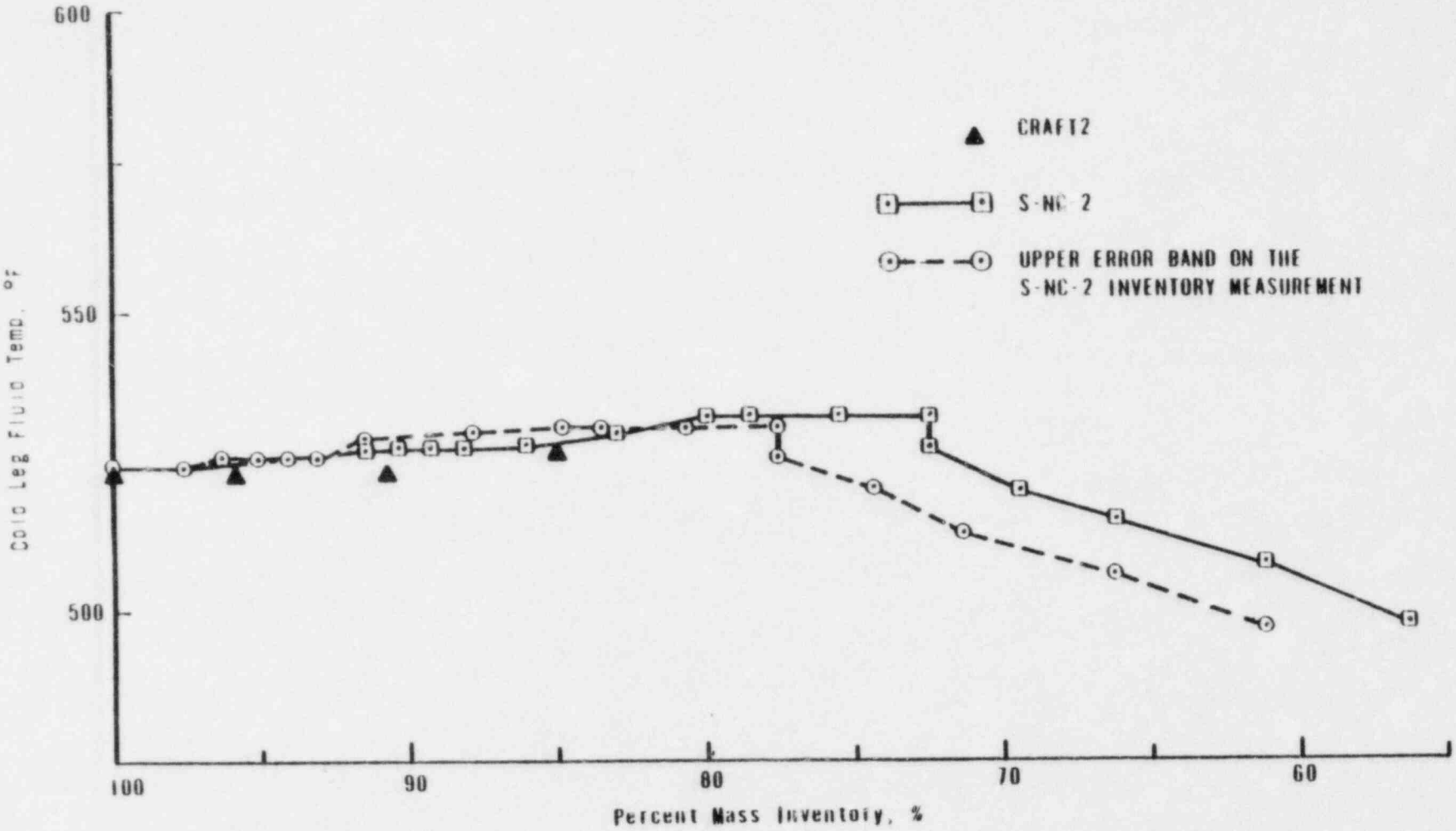

Figure G-9. Hot Leg Fluid Temperature

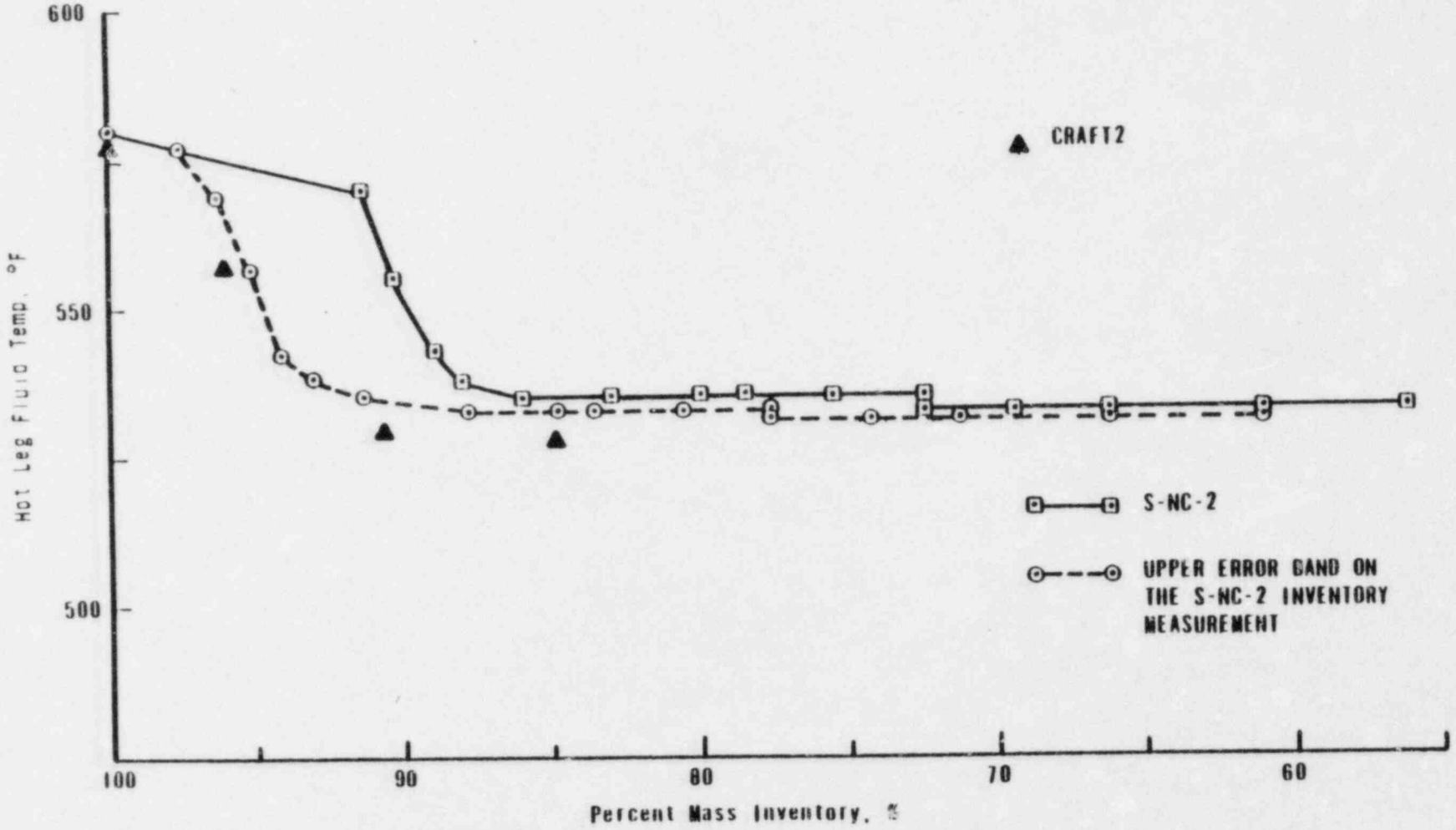

Figure G-10. Cor. Temperature Differential

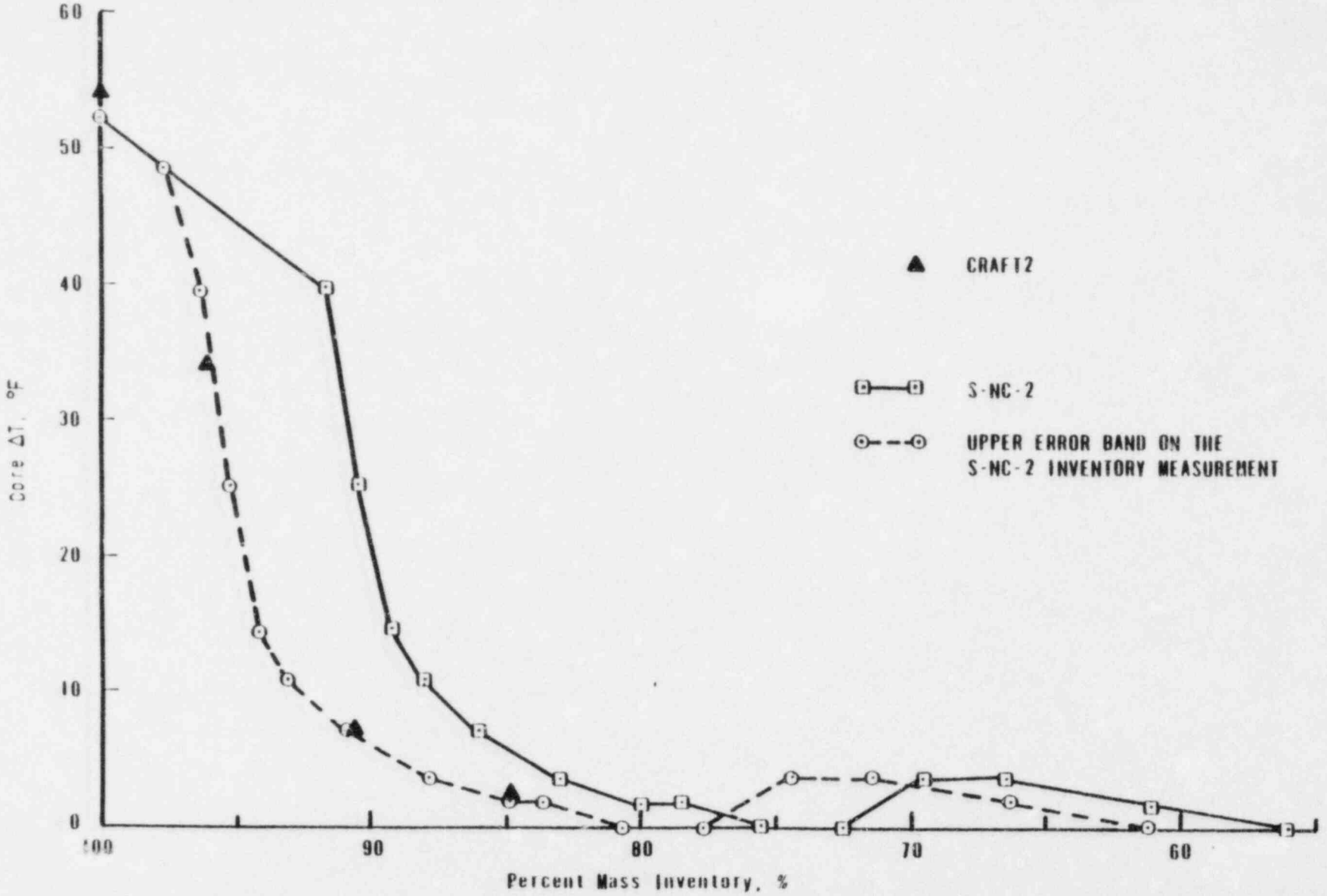

Figure G-11. Steam Generator Temperature Differential

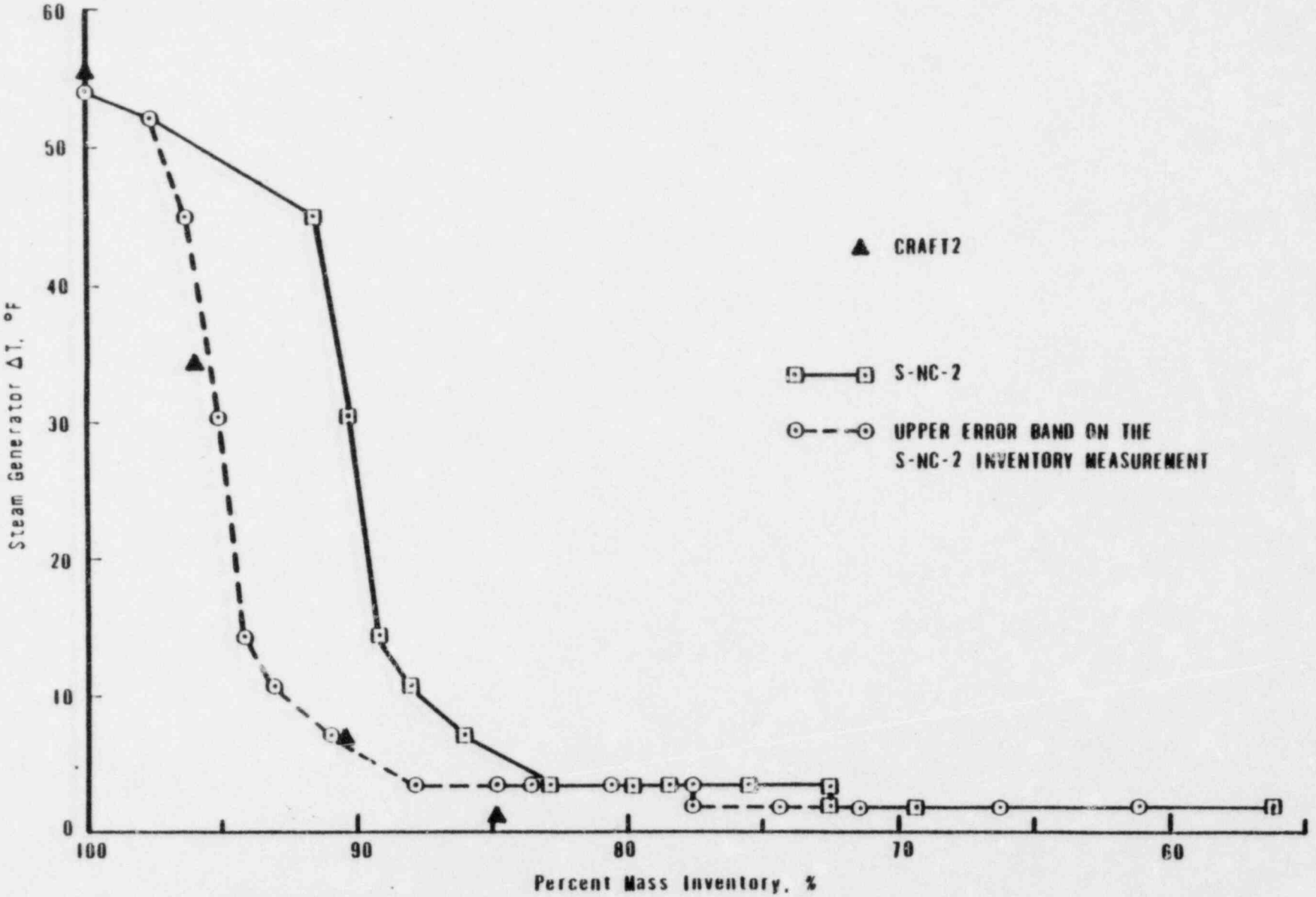

Figure G-12. Mass Flow Rate

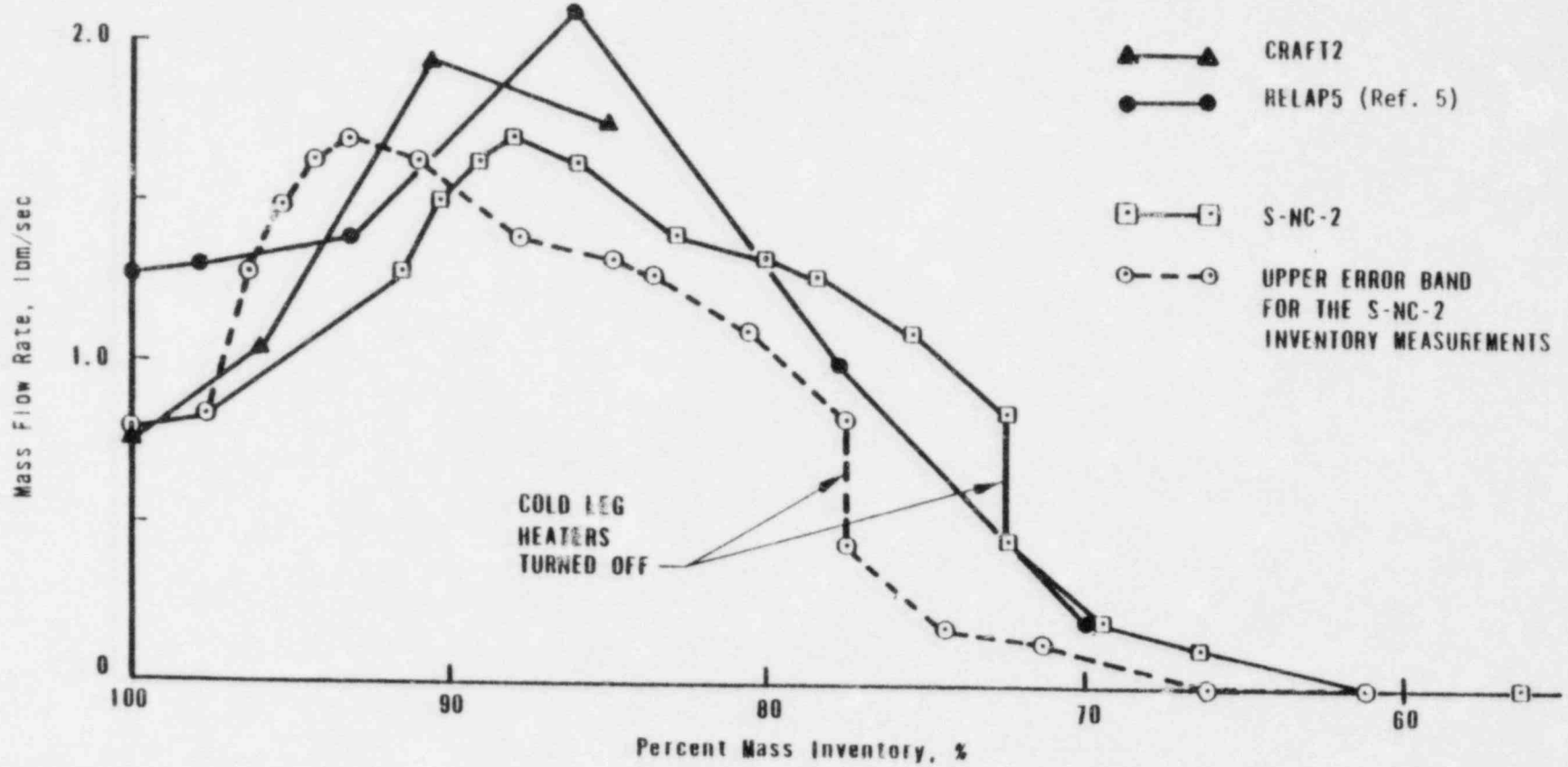

APPENDIX H

CRAFT2 - Loss of Offsite Power Plant Transient Prediction

ABSTRACT

The CRAFT2 computer code was benchmarked against a loss of offsite power (LOOP) transient at Arkansas Nuclear One, Unit 1. This analysis was performed, as part of the Small-Break LOCA Methods Program, to demonstrate the analytical capability of the upgraded CRAFT2 code to correctly predict the steam generator and pressurizer response during a B&W plant transient. The results show that the upgraded CRAFT2 computer model was quite capable of predicting the system response during the ANO-1 LOOP event.

1. Introduction

In NUREG-0565, Section 4.1.1.1, paragraph 1, the NRC Staff questioned the ability of existing computer models to "correctly predict the various modes of natural circulation and the interruption of natural circulation if it occurs." This concern has been addressed as part of B&W's Small-Break LOCA Methods Program. This appendix presents a benchmark of the upgraded CRAFT2 code with the post-trip transient response to a loss of offsite power (LOOP) at Unit 1 of the Arkansas Nuclear One site (ANO-1). This post-trip analysis of the ANO-1 high-pressure reactor trip is intended to benchmark the ability of the updated CRAFT2 code to correctly predict the steam generator and pressurizer responses during a B&W plant transient involving natural circulation and the use of the auxiliary feedwater system (AFWS).

The criteria related to selection of the B&W plant transient are provided in section 3. The initial conditions and the sequence of events of the ANO-1 reactor trip are discussed in section 4. The CRAFT2 modeling techniques and the assumptions used in predicting the post-trip responses are discussed in section 5. The transient data are compared to the CRAFT2 prediction in section 6.

2. Summary and Conclusions

A benchmark of the upgraded CRAFT2 computer model to a B&W plant transient has been completed. The selected transient was a loss of offsite power (LOOP) event that occurred at Arkansas Nuclear One, Unit 1, on June 24, 1980. Trees in the power lines caused the loss of power. This created a ground fault separating the plant from the grid. The turbine governor and intercept valves partially closed, creating a mismatch between steam production and steam demand. The reactor tripped shortly thereafter on the RPS high pressure signal. This transient was significant because the plant was cooled by natural circulation for one hour and 40 minutes.

The results of the benchmark between the calculated results and the ANO-1 data show that the upgraded CRAFT2 code data compared extremely well with the transient data. Both the steam generators and the pressurizer models correctly predicted their response to the LOOP event. This analysis demonstrated that the upgraded CRAFT2 code was capable of predicting the natural circulation mode observed during the small-break transients.

3. Selection of B&W Plant Transient

In order to select an appropriate transient against which to benchmark the upgraded CRAFT2 code, certain criteria were established. The following criteria were chosen for the post-trip analysis:

1. The transient must be from a 177-FA lowered-loop plant.
2. The plant must go through the transition from forced to natural circulation.
3. The auxiliary feedwater system must be used.
4. The transient should have initiated from a high power level.
5. The transient should have been benchmarked previously.
6. Sufficient data of good quality should exist.

Several plant transients were assessed according to these criteria. Table H-1 lists the B&W plant natural circulation transients. Of the transients that were considered, the ANO-1 reactor trip of June 24, 1980, was determined to best meet the specified criteria. The ANO-1 transient data are included in reference 3, and a benchmark of the ANO-1 high-pressure reactor trip is presented in reference 4.

4. The ANO-1 Transient

4.1. Discussion

On June 24, 1980, while operating at full power (2568 MWt), the ANO-1 plant experienced a partial loss of offsite power (LOOP). Trees in one power line caused three other lines to be tripped, separating the plant from the grid. The turbine intercept and governor valves closed slightly, reducing generator output to maintain frequency. This created a mismatch between reactor power production and steam generator demand. The surplus energy increased the RC pressure. A manual reactor runback was started just before the reactor/turbine trip on high RC pressure. The reactor coolant pumps were also tripped upon reactor/turbine trip. The transient was of particular interest because the plant was cooled by natural circulation for approximately one hour and 40 minutes, after which the RC pumps were restarted.

4.2. Plant Conditions Prior to Reactor Trip

The plant operating conditions at the time of the reactor/turbine trip were as follows[3]:

- 100% power/2568 MWt
- All reactor coolant pumps operating
- Total reactor coolant flow: 139.35×10^6 lbm/h
- Cold leg temperature: 556.9F
- Hot leg temperature: 600.9F
- Reactor coolant pressure: 2176.8 psia
- Steam generator outlet pressure: 923.64 psia
- Pressurizer level: 180 in.
- Main feedwater flow: 5.63×10^6 lbm/h (per loop)

4.3. Sequence of Events

The ANO-1 reactor had been operating at 100% power for approximately 15 days before the reactor/turbine trip. At 1540 hours on June 24, 1980, one 500-kV power line was isolated to the switchyard. A ground fault caused by trees in the lines tripped two other 500-kV lines and a 161-kV line, creating a partial LOOP event. Within a few seconds, the ANO-1 generator frequency reached the overspeed protection control setpoint. The intercept and governor valves began to close to maintain the generator frequency. This created a mismatch between the amount of steam produced and that demanded. A manual runback of the reactor was initiated. During the runback, the excess energy increased the RC pressure to the high-pressure setpoint, causing the reactor/turbine trip. A partial sequence of events is listed on the following page; a more detailed listing is provided in reference 3.

Time	Time into event, s	Event description
14:28:57	-680.0	Mayflower 500-kV line isolated to the switchyard.
15:40:16	-1.0	Mabelvale 500-kV lines tripped due to ground fault - trees in lines.
15:40:16.9	-0.1	161-kV Morrelton East line tripped.
15:40:17	0	ANO-1 generator reaches OPC setpoint, governor and interrupt values begine to close, manual runback initiated.
15:40:21.1	4.1	Reactor/turbine trip on high RC pressure.
15:40:38	21.0	Steam driven EFW pump trips on overspeed.
15:40:51.1	34.1	Makeup started (14 gpm per loop).
15:41:51.1	94.1	EFW started (450 gpm per loop).[4]
15:42:01		Two HPI trains started (one pump per loop).
17:20	5888.9	RC pump C started.
17:21	5948.9	RC pump B started.
17:24	6128.9	RC pump D started.
17:26	6248.9	RC pump A started.

The steam-driven emergency feedwater pump tripped on overspeed upon its initial start. However, it did start twice as needed after it was reset. No other problems were encountered during this transient.

4.4. RC System Response

The initial response of the system was a sharp pressurization of both the reactor coolant system (RCS) and the OTSGs. This corresponded to the closing of the governor and intercept valves on the turbine. The maximum pressure the RCS reached was 2325 psia. After the reactor tripped, the RCS depressurized to 1885 psia in approximately 65 seconds because of the decreasing amount of core energy. Emergency feedwater was injected into the OTSG at roughly 95 seconds. It was assumed that emergency feedwater flow was 450 gpm to each generator and held constant throughout the remainder of the transient. At this time the generators were effectively removing all of the decay heat.

In order to increase the RCS pressure to put the plant in a hot standby condition, two HPI trains were manually actuated. The increase in system mass from the HPI system began filling the pressurizer, compressing the steam bubble and raising the RCS pressure. Both the hot and cold leg temperature increased initially with the increase in pressure and then decreased. The cold leg temperature continued to decrease with the OTSG pressure while the hot leg temperature increased slightly during the repressurization period. The plant was stabilized within roughly 300 seconds with the following conditions:

- Hot standby
- T_{avg}: 545F
- RCS pressure: 2170 psia
- All RC pumps operating

E. CRAFT2 Plant Transient Model

E.1. CRAFT2 Code

The CRAFT2 computer program was developed to study the transient behavior of a nuclear steam system undergoing a loss-of-coolant accident (LOCA).[5] The program solves the conservation equations for mass and energy, the continuity equation, and the equation of state for water.

The CRAFT2 program permits the user to select the nodal representation that results in the best finite differencing of the fluid system to be analyzed. The program then solves the conservation equations for each node and the momentum equation for each flow path between nodes. CRAFT2 utilizes explicit solution techniques to analyze the transients. The nuclear steam system (NSS) is simulated by a node and flow path representation.

CRAFT2 contains flexible models of all major NSS components. Various options as well as user input parameters enable the program, to model the reactor core, RC pump, steam generators, and connecting piping in any configuration and operating mode desired. The diversity of the models also allows the program to accurately model any thermal-hydraulic system containing similar components.

The upgraded CRAFT2 code contains all of the small-break LOCA upgrades and their modifications that were addressed in NUREG-0565. Included in this code are a non-equilibrium pressurizer model, an upgraded two-phase pump model, and a new, upgraded steam generator model.

5.2. Model Description

The CRAFT2 noding scheme used in this analysis is shown in Figure H-1, and the nodal and flow path description is provided in Table H-2. The CRAFT2 model comprises 57 nodes and 79 flow paths. The model that was used in this analysis was the same as the one developed for the 177-FA lowered-loop plants.[6] The initial conditions of operation for the plant transient analysis were obtained from reference 3 and are shown in section 4.2.

5.2.1. Modeling the OTSG

The steam generator (OTSG) model used in this analysis was the new, upgraded model described in the CRAFT2 topical report.[5] Both steam generators were characterized by two radial and six axial regions on the primary side and six axial regions on the secondary side with a separate node for the downcomer. Also, both generators were treated alike with regard to OTSG pressure, main feedwater flow, and emergency feedwater (EFW) flow.

At the initiation of the ANO-1 transient, the turbine governor and intercept valves partially closed, causing a mismatch between the energy produced and the energy demanded. As a result, the RCS, along with the steam generator, repressurized. This caused the reactor to trip on high pressure. In the analysis, the reactor was tripped at 4.5 seconds.

During the transient, the steam-driven EFW pump tripped on overspeed and was restarted manually before the 100-second automatic time delay. From reference 4, the EFW pumps were started at 90 seconds after reactor trip. The EFW flow was held constant throughout the transient at 450 gpm to each OTSG.

5.2.2. Makeup Flow to the RCS

For the ANO-1 transient, the reactor reached the RPS high-pressure trip setpoint approximately 4.5 seconds into the transient. The initiation of the transient was the partial closing of the turbine governor and intercept valves. There was a 30-second time delay from reactor trip until makeup flow

was re-initiated to the RCS. This delay was based on 15 seconds for the diesels to become fully loaded and another 15 seconds for the makeup/HPI pumps to reach full speed. It was assumed during this analysis that all makeup and letdown flow was lost. The only liquid entering the RCS was the difference between seal injection flow and seal return. This amounted to a total makeup flow of 28 gpm.

The system needed to repressurize in order to return to hot standby conditions; to achieve this, two HPI trains were manually actuated at 100 seconds. The increase in mass flow into the RCS creates a constant insurge into the pressurizer, which begins to increase its level. As the level increases, it compresses the steam bubble in the top of the pressurizer and thus increases RCS pressure.

5.2.3. Pressurizer Heater

During a LOOP event, all power to the pressurizer heaters is lost until the diesels begin accepting loads. For ANO-1, the first two banks of heaters are the only ones loaded on the diesels.[7] Both heaters turn on at a pressure of 2150 psia and remain on until the pressure reaches 2170 psia. This is accounted for in this analysis.

6. Analytical Results

This section describes the comparisons of the results of the upgraded CRAFT2 code model and the LOOP event at ANO-1 on June 24, 1980. The RC system pressure, RC temperature, and pressurizer responses are discussed separately.

6.1. RCS Pressure Response

A comparison of the calculated primary system pressure to the ANO-1 data is shown in Figure H-2. As can be seen from the figure, the updated CRAFT2 code model results compare very well with the actual RC pressure response. The only difference between the ANO-1 test data and the CRAFT2 prediction was the overestimation of the peak pressure, which was due to the following: During the ANO-1 transient, the partial closing of the turbine intercept and governor valves was responsible for the repressurization and for the eventual reactor trip at 4.5 seconds. To simulate this with CRAFT2, the RCS had to be pressurized. This was achieved by completely closing the valves to the turbine

(since partial closing of the valves is not possible with the CRAFT2 code prior to the reactor trip). Because of the termination of the total steam flow to the turbine, the RCS is expected to pressurize to a higher value than for the ANO-1 transient.

The subsequent depressurization in RC pressure was caused by the decrease in fission power when the reactor trips. At roughly 20 seconds the steam generators start drying out, causing the RCS pressure to level out at 1900 psia. The RCS repressurization at 100 seconds was due to manual actuation of the two HPI trains. The mass added by the HPI system began filling the pressurizer, compressing the steam bubble in the top of the pressurizer and thus increasing the pressure. The pressure is expected to remain at roughly 2175 psia (hot standby pressure) for the remainder of the transient.

6.2. Temperature Response

The cold and hot leg temperatures calculated by the upgraded CRAFT2 code are shown in Figures H-4 and H-5, respectively. The cold leg temperature increased sharply at the beginning of the transient because of the pressurization of the OTSG. As the pressure increases, so does the steam temperature. The resulting temperature difference between the primary and secondary side was significantly smaller than that at the beginning of the transient. This caused the reduction in heat transfer, which resulted in a higher cold leg temperature. After the reactor trip, the cold leg temperature drops to 548.5F in approximately 80 seconds. The cold leg temperature decreased thereafter because of the decreasing decay heat. As can be seen in Figure H-4, the predicted cold leg temperature compared reasonably well with the transient data.

The hot leg temperature (Figure H-5), like that of the cold leg, increased slightly at the beginning of the transient. The hot leg temperature dropped to approximately 570°F in 80 seconds after the reactor trip. The hot leg temperature increased slightly at this time due to the drying out of the OTSGs. Shortly after EFW actuation, the hot leg temperature began to decrease. This was due to the constant EFW and decreasing decay heat. As can be seen in Figure H-5, the CRAFT2-predicted hot leg temperature compared reasonably well with the ANO-1 data.

Comparison of the hot and cold leg temperatures is difficult because of the following missing information:

1. Insufficient data concerning steam generator secondary side pressure.
2. Unavailability of the data regarding EFW flow and OTSG level.
3. Unknown makeup and HPI flows throughout the transient.

Despite these factors, the results calculated by the upgraded CRAFT2 code were in excellent agreement with the transient data.

6.3. Pressurizer Level

The predicted pressurizer level response is compared to the ANO-1 pressurizer level in Figure H-6. As can be seen in the figure, CRAFT2 predicted the level very well through the first 75 seconds of the transient. At this time the hot leg temperature, as predicted by CRAFT2 and shown in Figure H-5, was approximately 4°F higher than the ANO-1 data. The 4°F temperature difference accounts for the 14-inch-higher level and was due solely to the expansion of the liquid. As the steam generators began to dry out and the hot leg temperature began rising, the pressure level started to increase. At 100 seconds, two HPI trains were started. The additional mass entering the system continued filling the pressurizer, as can be seen in Figure H-6. Overall, the CRAFT2 nonequilibrium pressurizer model compared well with the transient data by showing the same trends and by calculating essentially the same level.

7. References

1. Generic Evaluation of Small Break Loss-of-Coolant Accident Behavior in Babcock & Wilcox Designed 177-FA Operating Plants, NUREG-0565, U.S. Nuclear Regulatory Commission, January 1980.
2. "Proposal to B&W Owners Group for Small-Break Methods Program," Babcock & Wilcox.
3. T. F. Scott, Reactor Trip - Loss of Offsite Power on 6/24/80, and Attachment, Document No. 13-008-0774-00, Babcock & Wilcox, July 26, 1980.
4. K. C. Heck, "EFW Level Rate Control Evaluation," Babcock & Wilcox, July 1981.

5. J. J. Cudlin, et al., CRAFT2 - Fortran Program for Digital Simulation of a Multinode Reactor Plant During Loss of Coolant, BAW-10092, Rev, 3, Babcock & Wilcox, October 1982.

6. M. Ferguson, et al., Small-Break 177-FA Lowered-Loop Steam Generator Noding Sensitivity Studies, Document No. 86-113782000, Babcock & Wilcox, October 1982.

7. R. S. Talley, Midland-2 Loss of Offsite/Onsite Power Transient Information, Document No. 86-1131520-00, Babcock & Wilcox, March 1, 1982.

8. "Evaluation of Transient Behavior and Small Reactor Coolant System Breaks in the 177-Fuel Assembly Plant," Vol II, Babcock & Wilcox, May 7, 1979.

Table H-1. Summary of Natural Circulation Tests[8]

Date	Plant	Power, %	Comments
5/1/73	Oconee	0	SG depress to induce natural circulation: unacceptable for analysis
5/1/73	Oconee	0	SG level increase to induce natural circulation: unacceptable for analysis
11/4/73	Oconee 1	--	Loss-of-offsite power (LOOP) test: insufficient data
5/2/74	Oconee 1	--	Natural circulation test: missing some data, possibility
1/4/74	Oconee 2	75	LOOP - AFW delayed 7 minutes: possible benchmark case
2/22/75	ANO-1	100	LOOP - RC pump start at 5 minutes: does not allow fully developed natural circulation flow, possible case
4/23/77	Crystal River	--	LOOP test: experience indicates data quality is poor
4/22/78	TMI-2	15	LOOP test: possible benchmark
11/29/77	Davis-Besse 1	--	LOOP: wrong plant type
1/15/79	Davis-Besse 1	--	LOOP test: wrong plant type
12/3/78	Davis-Besse 1	--	Natural circulation test: wrong plant type
6/24/80[4]	ANO-1	100	LOOP: previously benchmarked, possible case

Table H-2. Node and Path Identification, CRAFT2 Model

Node No.	Identification
1	Downcomer
2	Lower plenum
3	Core
4,14	Hot leg piping
5,6,30,32, 38,40,42,44, 46,48,50,52	SG No. 1
7,26,28,34, 36,65,56	SG No. 1 secondary
8	SG No. 1 lower head
9,11,19,10, 12,20	Cold leg
13	Upper downcomer
15,16,31,33, 39,41,43,45, 47,49,51,53	SG No. 2
17,27,29,35, 37,55,57	SG No. 2 secondary
18	SG No. 2 lower head
21	Pressurizer
22	Containment
23	Upper plenum
24,25	SG upper head

Path No.	Identification
1,2	Core
3,4,18,19	Hot leg piping
5,20,40,42	Hot leg, upper SG
6,41,50,52, 54,56,68,60, 62,64,68,70	SG No. 1 tubes
7,66	SG No. 1 lower head
8	Core bypass
9,13,24	Cold leg piping
10,14,25	Pumps
11,12,15,16, 26,27	Cold leg piping
17,31	Downcomer
21,43,51,53, 55,57,59,61, 63,65,69,71	SG No. 2 tubes
22,67	SG No. 2 lower head
23	Low-pressure injection
18,29	Upper downcomer
30	Pressurizer
32	Vent valve
33,34	Leak and return path
35,36	High-pressure injection
37	Containment spray (HPI-X)
38,39	Upper plenum
44,48,46,72, 74,76,78	SG No. 1 secondary
45,47,49,73, 75,77,79	SG No. 2 secondary

Figure H-1. CRAFT2 Nodal Diagram for Plant Transient Simulation

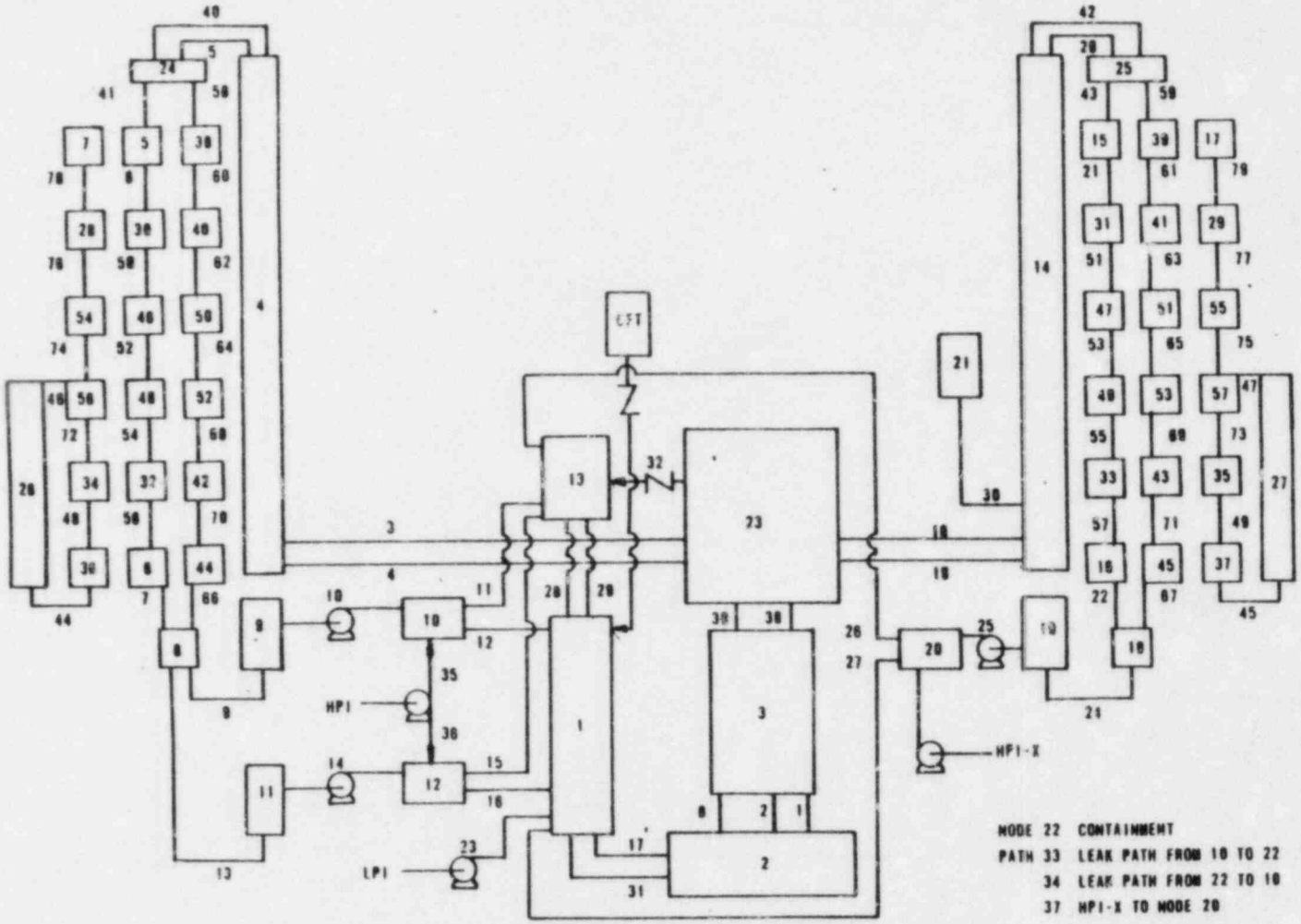

Figure H-2. RCS Pressure Vs Time Comparison

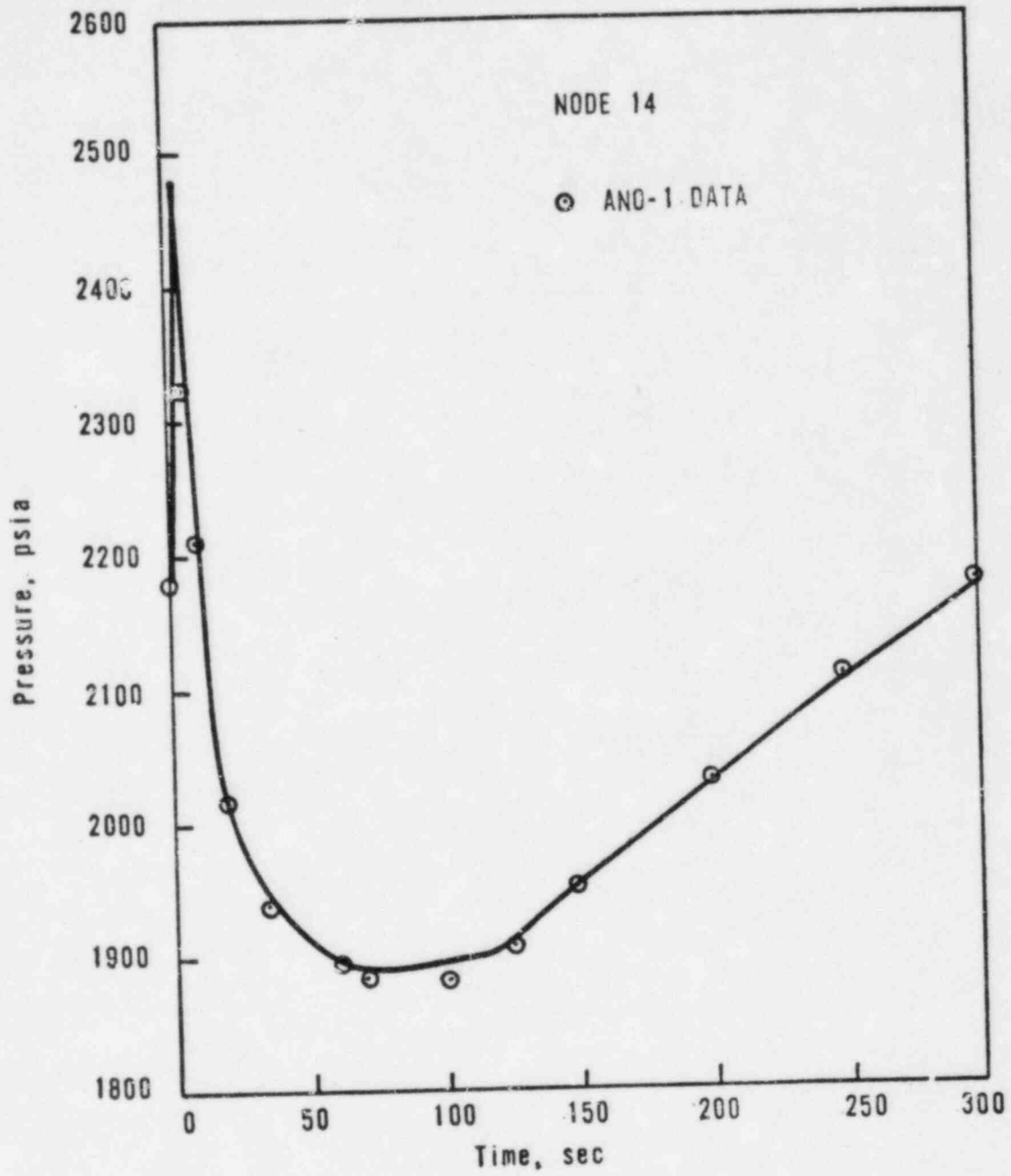

Figure H-3. Steam Generator Pressure Vs Time Comparison

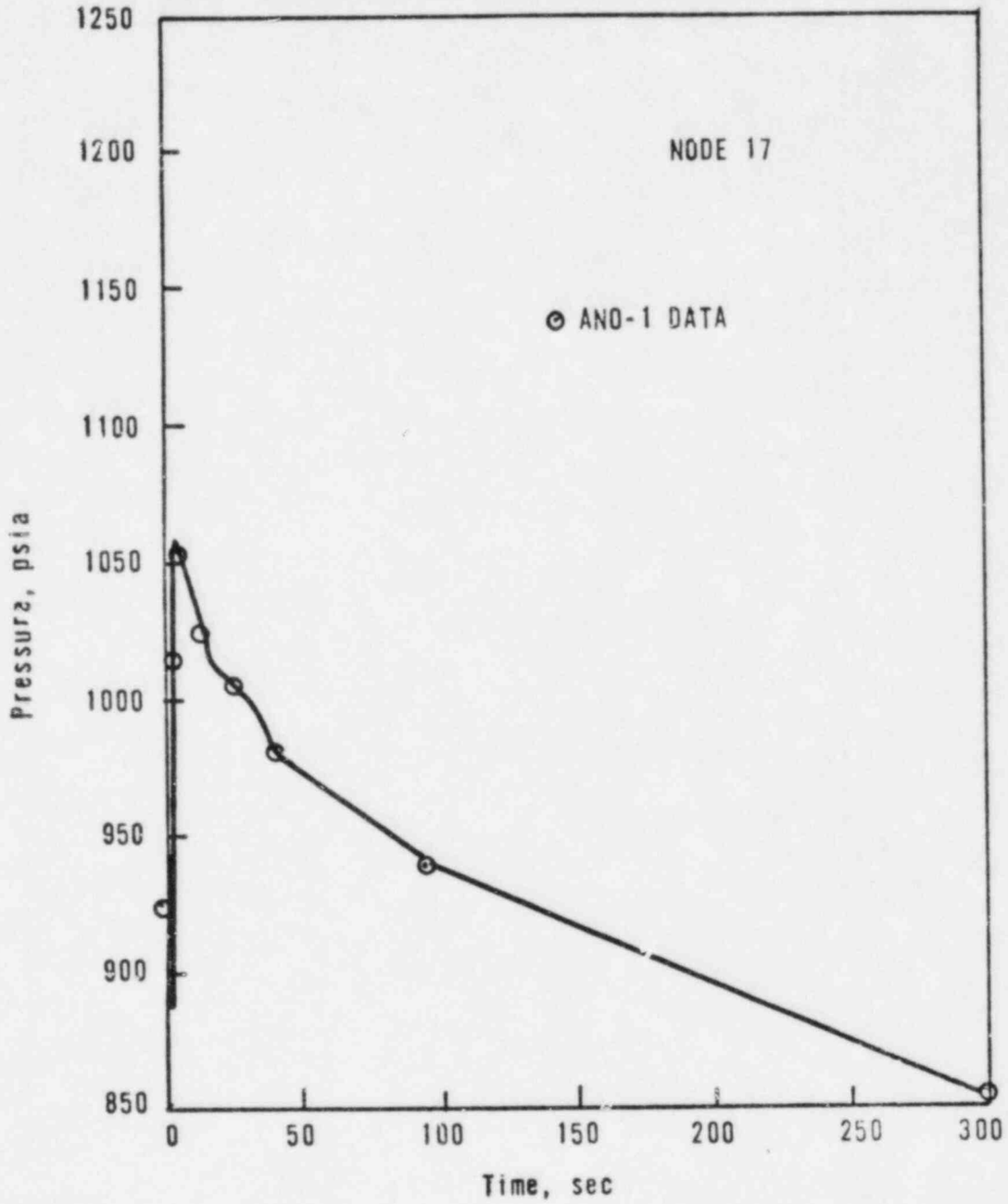

Figure H-4. Cold Leg Temperature Vs Time Comparison

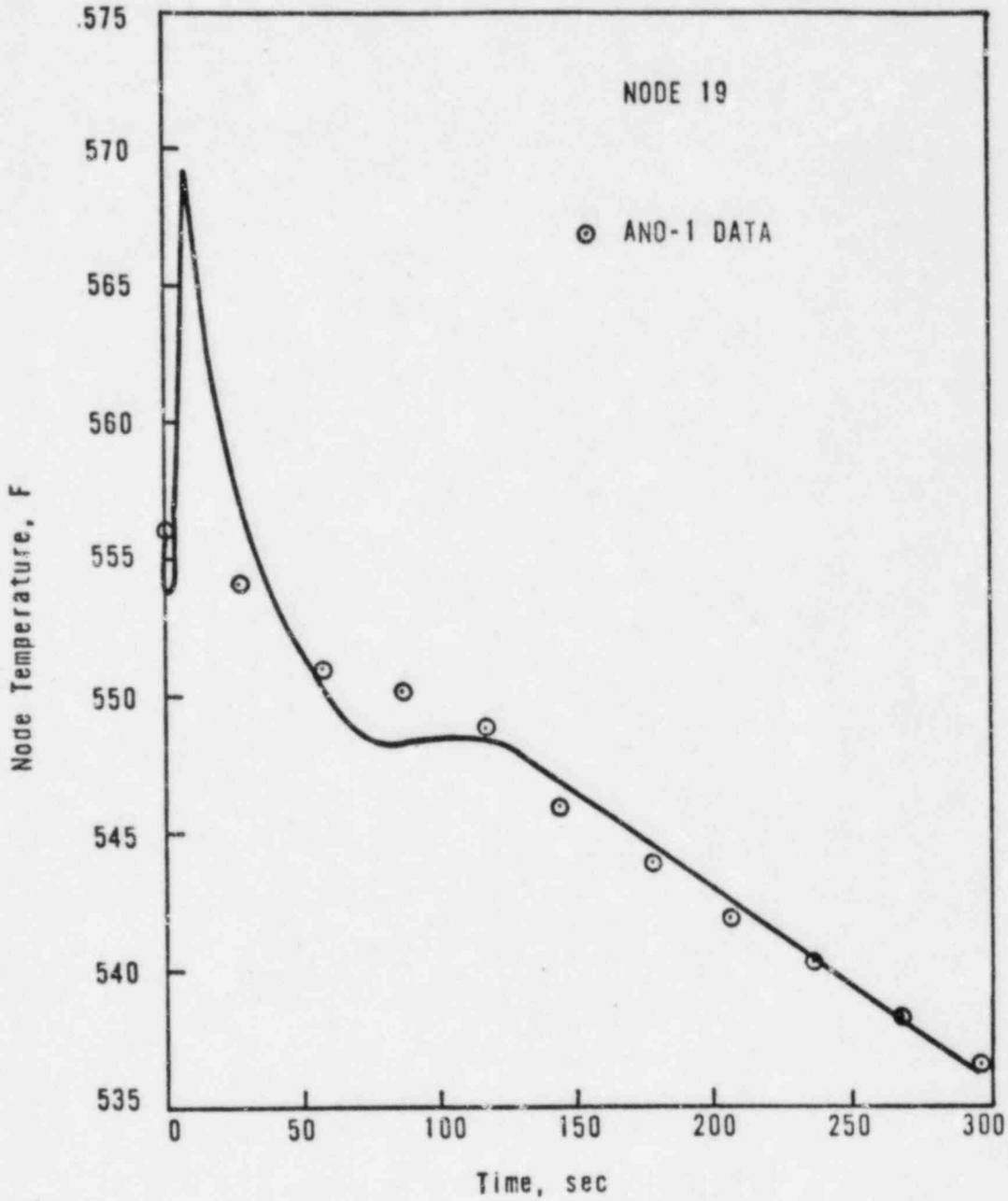

Figure H-5. Hot Leg Temperature Vs Time Comparison

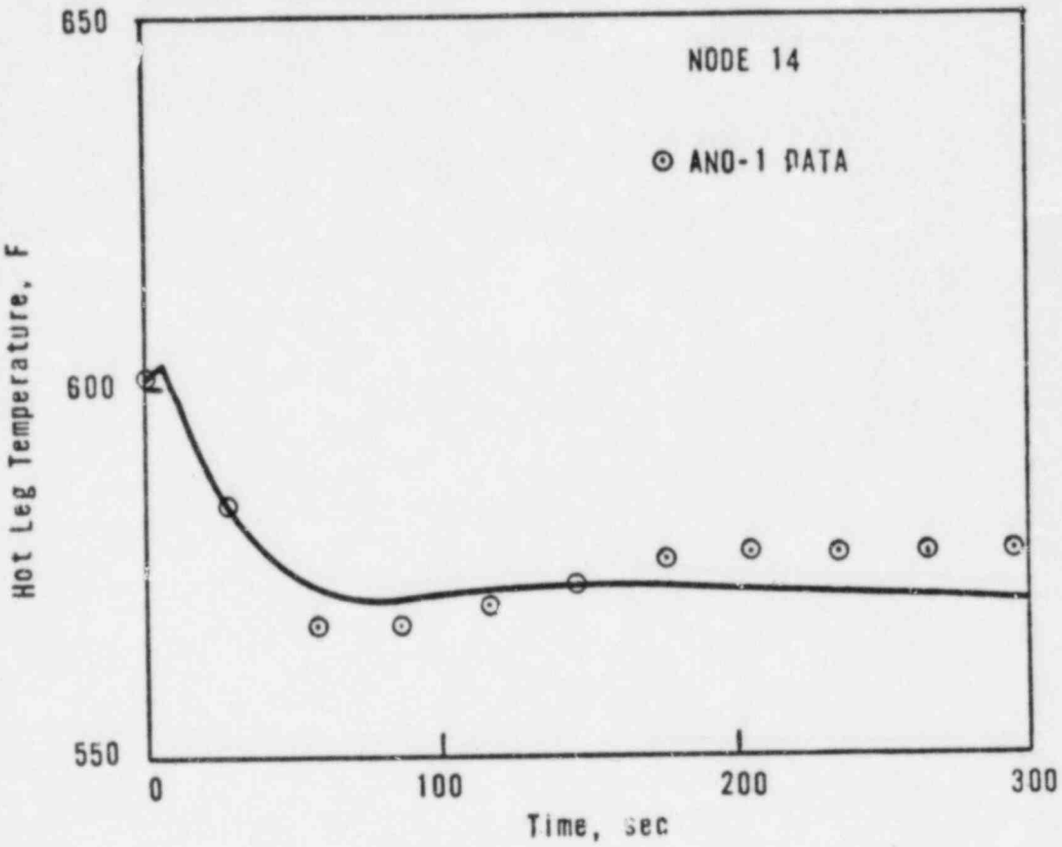

Figure H-6. Pressurizer Level Vs Time Comparison

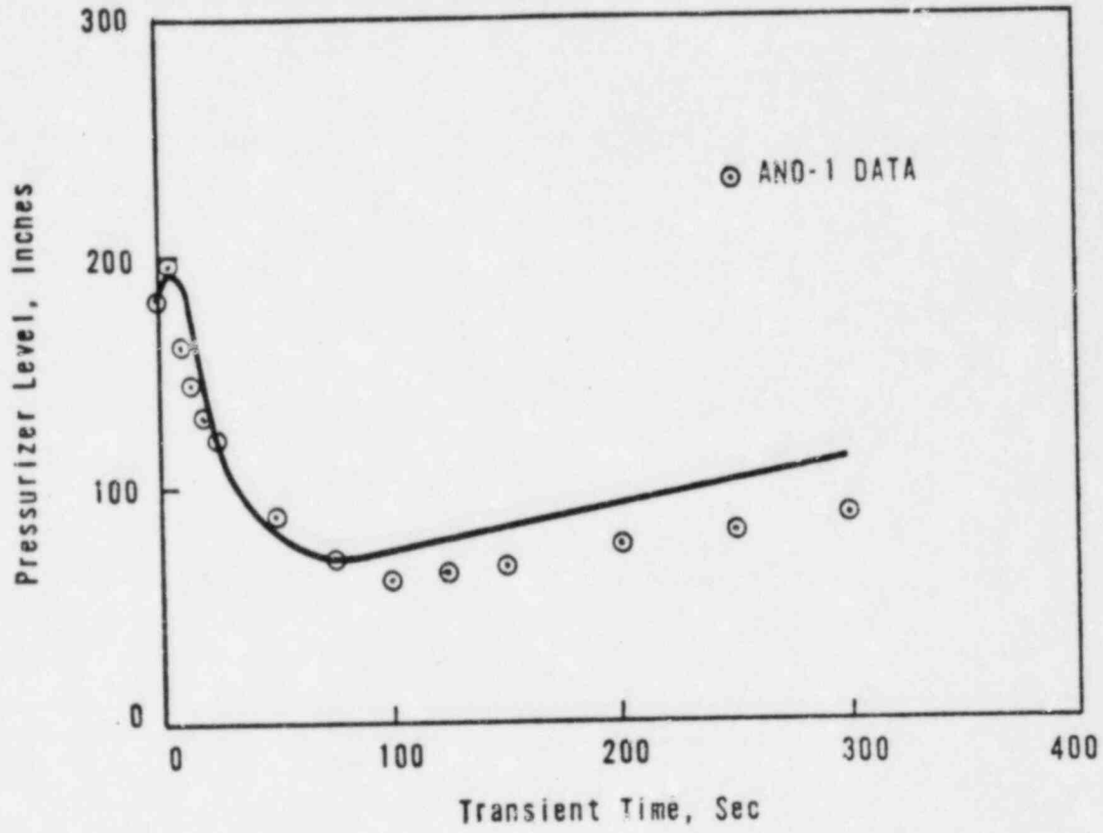

APPENDIX I

Noding Sensitivity Studies for 205-FA Plants

(TO BE PROVIDED DECEMBER 1, 1982)